

University of Windsor

Scholarship at UWindor

Electronic Theses and Dissertations

Theses, Dissertations, and Major Papers

10-30-2020

Weight Reduction in Electric Motors: Aluminum vs Copper Wires

Lucas Chauvin
University of Windsor

Follow this and additional works at: <https://scholar.uwindsor.ca/etd>

Recommended Citation

Chauvin, Lucas, "Weight Reduction in Electric Motors: Aluminum vs Copper Wires" (2020). *Electronic Theses and Dissertations*. 8440.
<https://scholar.uwindsor.ca/etd/8440>

This online database contains the full-text of PhD dissertations and Masters' theses of University of Windsor students from 1954 forward. These documents are made available for personal study and research purposes only, in accordance with the Canadian Copyright Act and the Creative Commons license—CC BY-NC-ND (Attribution, Non-Commercial, No Derivative Works). Under this license, works must always be attributed to the copyright holder (original author), cannot be used for any commercial purposes, and may not be altered. Any other use would require the permission of the copyright holder. Students may inquire about withdrawing their dissertation and/or thesis from this database. For additional inquiries, please contact the repository administrator via email (scholarship@uwindsor.ca) or by telephone at 519-253-3000ext. 3208.

Weight Reduction in Electric Motors: Aluminum vs Copper Wires

By

Lucas Chauvin

A Thesis
Submitted to the Faculty of Graduate Studies
through the Department of Mechanical, Automotive and Materials Engineering
in Partial Fulfillment of the Requirements for
the Degree of Master of Applied Science
at the University of Windsor

Windsor, Ontario, Canada

2020

© 2020 Lucas Chauvin

Weight Reduction in Electric Motors: Aluminum vs Copper Wires

by

Lucas Chauvin

APPROVED BY:

N.C. Kar

Department of Electrical and Computer Engineering

V. Stoilov

Department of Mechanical, Automotive, and Materials Engineering

A. Edrisy, Co-Advisor

Department of Mechanical, Automotive, and Materials Engineering

A.R. Riahi, Co-Advisor

Department of Mechanical, Automotive, and Materials Engineering

September 09, 2020

DECLARATION OF ORIGINALITY

I hereby certify that I am the sole author of this thesis and that no part of this thesis has been published or submitted for publication.

I certify that, to the best of my knowledge, my thesis does not infringe upon anyone's copyright nor violate any proprietary rights and that any ideas, techniques, quotations, or any other material from the work of other people included in my thesis, published or otherwise, are fully acknowledged in accordance with the standard referencing practices. Furthermore, to the extent that I have included copyrighted material that surpasses the bounds of fair dealing within the meaning of the Canada Copyright Act, I certify that I have obtained a written permission from the copyright owner(s) to include such material(s) in my thesis and have included copies of such copyright clearances to my appendix.

I declare that this is a true copy of my thesis, including any final revisions, as approved by my thesis committee and the Graduate Studies office, and that this thesis has not been submitted for a higher degree to any other University or Institution.

ABSTRACT

Environmental concerns driven by climate change have resulted in increased market demand for lightweight and inexpensive electric vehicles. This study examines the feasibility of replacing copper conductors with aluminum conductors in automotive scale electric motors to address this demand. A comprehensive review of the literature contrasting aluminum and copper conductors is included to create a unified source for future research. This study also contains a two-part formability and windability analysis of square cross section electrical conductor aluminum and rectangular electrolytic tough pitch copper. The first part of the analysis applies standardized testing from ASTM D1676 to characterize the formability and windability of both conductors. Aluminum saw formability and windability advantages over copper, especially regarding springback, accommodation of elongation during high speed winding, and repeated absorption of bends and twists during winding; however, insulation adhesion and delamination issues occurred for elongation beyond 10% due to incompatibility of properties between the polymer coating and aluminum wire. The second part of the analysis compares forming behaviour of aluminum to known results for copper using a novel wire bending simulator machine. The effects of normal load, wire travel speed, and forming angle on coefficient of friction (COF) are analyzed to determine the feasibility of using aluminum for hairpin windings. The analysis finds that COF increases with both wire travel speed and forming angle. COF versus normal load shows a spike in COF followed by a sharp decrease indicative of a deformation mechanism that copper did not experience. Macroscopic analysis reveals aluminum to be more susceptible to damage from the forming equipment when compared to copper. Microscopic analysis reveals shingles and a suspected near-surface deformed layer at the aluminum/insulation interface. Detachment of these imperfections was found to occur at peak COF loads and higher from crack propagation and insulation flow into said cracks. Overall, this study shows aluminum is a viable conductor that provides significant cost and weight savings in electric machines with similar performance to copper; however, further improvement to aluminum surface quality and insulation properties is required to effectively replace copper.

DEDICATION

I dedicate this work to my family,
for being by my side every step of the way,
no matter what,
always guiding me in the right direction,
to be the best version of myself I can be

ACKNOWLEDGEMENTS

Firstly, I would like to thank my supervisors, Dr. A. Edrisy and Dr. A.R. Riahi for the opportunity to conduct this research along with their guidance and supervision along the way. They pushed me to always present my best work possible, helped me troubleshoot stumbling blocks and provided me with the opportunity to present my work at a national conference in Vancouver B.C.

I would also like to thank Dr. N.C. Kar, Eunha Chu, Himavarsha Dhulipati, Dr. Shruthi Mukundan and the rest of the CHARGE lab team for the warm welcome into their team for fruitful collaborative work. They also provided me with the amazing opportunity to travel abroad for the first time and present the collaborative research at an international conference in South Korea.

Additionally, I would like to thank Dr. Olufisayo Gali and Sharon Lackie for their immense and instrumental help with microscopy and observational analysis.

Special thanks go to Matt St. Louis and Jerome Finnerty for helping me with my tensile testing.

Special thanks also go to the CEI Technologists Andrew Jenner, Keven Harkai, Dean Poublon, Bruce Durfy and Dave McKenzie for all their assistance with troubleshooting, fabrication, and keeping my research on track.

Further acknowledgements and thanks to everyone from the EECOMOBILITY (ORF) and HEVPD&D CREATE project for the opportunity to conduct my research as well as learn, network, and present at annual conferences.

TABLE OF CONTENTS

DECLARATION OF ORIGINALITY	iii
ABSTRACT	iv
DEDICATION	v
ACKNOWLEDGEMENTS	vi
LIST OF TABLES	xi
LIST OF FIGURES	xii
LIST OF ABBREVIATIONS	xxiii
NOMENCLATURE	xxiv
Chapter 1 INTRODUCTION.....	1
1.1 Organization of Thesis	5
Chapter 2 ALUMINUM VS COPPER: ADVANTAGES & DISADVANTAGES.....	6
2.1 Electrical Conductor History	6
2.1.1 Aluminum Housing Wire Crisis.....	8
2.1.2 Common uses of Aluminum and Copper.....	9
2.2 Electrical Conductor Alloys.....	10
2.2.1 Aluminum Alloys.....	11
2.2.2 Copper Alloys	12
2.3 Material Properties of Aluminum and Copper	14
2.4 Fabrication	16
2.5 Cost.....	17
2.6 Recyclability	19
2.6.1 Environmental Impact	20
2.7 Weight and Mass	21
2.8 Mechanical Performance	23
2.8.1 Equivalent Conductor Strength	23
2.8.2 Cold Workability	23
2.8.3 Influence on Formability and Windability	24
2.9 Electrical Performance.....	25
2.9.1 AC vs DC Performance.....	26
2.10 Thermal Performance	27
2.10.1 Melting Point and Annealing Behaviour.....	27
2.10.2 Thermal Conductivity.....	28
2.10.3 Thermal Expansion	29
2.10.4 Specific Heat and Heat Capacity.....	29
2.10.5 High Temperature Use	30

2.11 Corrosion	31
2.12 Connections and Terminations	32
2.12.1 Problems with Aluminum Connections	32
2.12.2 Aluminum Joining Techniques	33
2.13 Insulation Performance	34
2.14 Alternative Conductors	36
2.14.1 Induction Motor Rotors	36
2.14.2 Aluminum Strip Conductor	38
2.14.3 Copper Clad Aluminum	39
2.14.4 Carbon Nanotubes	40
2.14.5 Improving Aluminum Electrical Conductivity.....	42
2.14.5.1 Improved Boron Treatment.....	42
2.14.5.2 Addition of Graphene and CNT to Aluminum	42
2.14.5.3 Simultaneous High Strength and High Conductivity.....	43
2.15 Replacing Copper with Aluminum: Case Studies	45
2.15.1 Utilization of Aluminum Strip and Anodized Conductors.....	45
2.15.1.1 Anodized Round Aluminum Magnet Wire.....	45
2.15.1.2 Cheap Wind Turbine Generator.....	47
2.15.1.3 Small Hand Tool Motor	47
2.15.1.4 Movie Projector Application.....	48
2.15.1.5 Linear Actuators.....	48
2.15.1.6 Accelerator Magnets	49
2.15.1.7 Transformer Windings	49
2.15.2 Hydroelectric Generators	52
2.15.3 AC vs DC Operation	52
2.15.3.1 Traction Motor Applications.....	54
2.15.4 Precompressed Aluminum Windings	56
2.15.5 Induction Motors	58
2.15.6 Elevator motor.....	59
2.15.7 Appliance Motors	59
2.15.8 Rectangular Windings	60
2.16 Important Takeaways.....	61
Chapter 3 LITERATURE REVIEW.....	64
3.1 Hairpin Style Conductors.....	64
3.1.1 Advantages and Disadvantages of Hairpin Windings	64
3.1.2 Utilization of Hairpin Conductors: Case Studies	66
3.1.3 Hairpin Conductor Manufacturing	68
3.1.3.1 Hairpin Formation Damage Analysis	71

3.2 Conductor Failure Modes	71
3.2.1 Insulation Contact Deformation	72
3.3 Aluminum Surface Defects.....	74
Chapter 4 METHODOLOGY.....	77
4.1 Research Objectives.....	77
4.2 Magnet Wire Samples Used	78
4.2.1 Aluminum Insulation Characterization	78
4.3 Formability and Windability Testing Procedures.....	80
4.3.1 Tensile Testing Procedure	80
4.3.2 Elongation Testing Procedure	84
4.3.3 Film Adherence and Flexibility Testing Procedure.....	84
4.3.4 Elastic Ratio Method Procedure.....	86
4.3.5 Low Stress Elongation Testing Procedure	87
4.3.6 Springback Testing Procedure.....	88
4.4 Wire Bending Simulation Testing Procedures.....	90
4.4.1 Wire Bending Simulator Machine.....	90
4.4.2 Coefficient of Friction Measurement Testing Procedures.....	92
4.4.2.1 COF vs Normal Load Testing Procedure.....	94
4.4.2.2 COF vs Speed Testing Procedure	95
4.4.2.3 COF vs Forming Angle Testing Procedure.....	95
4.5 Sample Observation Methods.....	96
4.5.1 Sample Cross Section Preparation	96
Chapter 5 RESULTS.....	97
5.1 Formability and Windability Testing Results.....	97
5.1.1 Elongation Testing Results.....	97
5.1.1.1 Stress vs Strain Curve Stress Drop Observations	99
5.1.1.2 Aluminum Film Insulation Delamination Observation.....	100
5.1.1.3 Aluminum Film Insulation Delamination Peel Test	101
5.1.1.4 Copper Film Insulation Peel Test	104
5.1.1.5 Elongation Sample Texture Change Observations	106
5.1.2 Film Adherence and Flexibility Testing Results	109
5.1.2.1 Film Adherence Peel Testing Observations.....	110
5.1.2.2 Delamination Investigation.....	115
5.1.2.3 Insulation Damage Observations	121
5.1.3 Elastic Ratio Testing Results.....	124
5.1.4 Low Stress Elongation Testing Results.....	125
5.1.5 Springback Testing Results	126
5.2 Wire Bending Simulation Testing Results.....	128

5.2.1 COF vs Normal Load Testing Results	128
5.2.2 COF vs Travel Speed Testing Results.....	141
5.2.3 COF vs Forming Angle Testing Results	147
5.3 Wire Bending Simulator Testing Observations	153
5.3.1 Thermal Imaging.....	153
5.3.2 Counterface Contact Area Observations	156
5.3.2.1 Aluminum vs Copper Contact Transfer.....	159
5.3.3 Wire Contact Surface Observations	162
5.3.3.1 End of Test Bump Analysis	167
5.4 Aluminum and Copper Cross-Sectional Analysis	169
5.4.1 Fresh Aluminum and Copper Surface Features.....	169
5.4.2 Tested Wire Cross Section Observation.....	174
5.4.2.1 Delamination Observation	183
Chapter 6 DISCUSSION	187
6.1 Formability and Windability of Aluminum and Copper	187
6.2 Die Forming Simulation of Aluminum and Copper	190
6.3 Aluminum Insulation Performance.....	192
6.3.1 Aluminum Insulation Flexibility	192
6.3.2 Aluminum Insulation Adherence	194
6.3.3 Aluminum Insulation Long Term Performance	195
Chapter 7 SUMMARY AND CONCLUSIONS.....	197
7.1 Suggestions for Future Research	199
REFERENCES	201
VITA AUCTORIS	212

LIST OF TABLES

Table 2.1. Comparison of properties for copper and aluminum conductors used in this study.....	14
Table 2.2. Corrosion rates (average mils per year) for solid metals in various environments [13], [24, pp. 17-1 - 17-8].	32
Table 3.1. Pictorial representation of polymer deformation in each deformation regime [124]......	73
Table 5.1. Elongation testing results for aluminum and copper wire samples.	98
Table 5.2. Elastic ratio testing results for aluminum and copper magnet wire samples.	124
Table 5.3. Low stress elongation testing results for aluminum and copper magnet wire samples.....	125
Table 5.4. Springback testing results for aluminum magnet wire samples.	127
Table 5.5. Springback testing results for copper magnet wire samples.....	127
Table 5.6. COF vs normal load testing results for 3 mm radius support roller.	131
Table 5.7. COF vs normal load testing results for 24 mm radius support roller.	132
Table 5.8. COF vs aluminum wire travel speed testing results for 3 mm radius support roller.....	142
Table 5.9. COF vs aluminum wire forming angle testing results for 3mm radius support roller.....	148
Table 5.10. COF vs aluminum wire forming angle testing results for 24mm radius support roller.....	148

LIST OF FIGURES

Figure 1.1. 2010 global greenhouse gas emissions by economic sector [1].	1
Figure 1.2. Long term projection of global passenger vehicle sales by drivetrain (left) and share of sales (right) [2].	2
Figure 1.3. Aluminum and copper commodity price from 2000 to 2008 [11].	3
Figure 2.1. Timeline for the first use of common metals [15].	6
Figure 2.2. Thermal life comparison between various insulations applied to aluminum and copper where aluminum is represented with grey bars and sees longer life for all insulation types [24, pp. 14-1 - 14-13].	34
Figure 2.3. Relative breakdown stress versus aging time for aluminum and copper magnet wire at 230°C aging temperature [65].	35
Figure 2.4. Cross section highlighting copper oxide growth of thermally aged sample at 240°C for 1500 hours and resulting oxide fracture causing enamel delamination [29].	36
Figure 2.5. Copper Clad Aluminum wire [77].	39
Figure 2.6. Motor size comparison between copper, copper litz, aluminum and CNT stator coils [80].	42
Figure 2.7. Electron interaction with vertical and horizontal grain boundaries in cold drawn microstructure at a) 24.6% b) 83.1% and c) 90.2% area reduction [86].	45
Figure 2.8. Power generation comparison between aluminum foil windings in prototype wind turbine and baseline copper design [89].	47
Figure 2.9. Coil temperature comparison of aluminum versus copper as frequency increases (left) and motorette winding power loss versus frequency highlighting cross over point where aluminum sees lower losses (right) [56].	53
Figure 2.10. Precompressed aluminum windings along with cross section view (upper left) highlighting high slot fill capability and minimal air gap between conductors [9].	57
Figure 3.1. Hairpin style conductors (left) and example of individual insertion into stator slots (right) [108], [114].	65
Figure 3.2. General Motors permanent magnet motor package utilizing hairpin style conductors [111].	65
Figure 3.3. Slot fill comparison between round wire windings (left) and hairpin windings (right) [108].	65

Figure 3.4. Hairpin wound stator manufacturing process path [116].	69
Figure 3.5. Hairpin die forming process (a) and step by step in process bending (b) [119].	70
Figure 3.6. Hairpin conductor insertion into stator and subsequent bending/twisting of ends for joining [108]......	70
Figure 3.7. Map of deformation regimes for polymers as a function of contact angle and normal load [124]......	73
Figure 3.8. Delamination of brittle near-surface deformed layer from crack initiation and propagation resulting in flakes delaminating from the aluminum surface [126]......	75
Figure 3.9. Shingle on deformed aluminum surface (left) and cross section view highlighting shingle is detached from the bulk material (right) [127]......	76
Figure 4.1. Magnet wire samples tested in this study: insulated aluminum (top), bare aluminum (middle), insulated copper (bottom).	78
Figure 4.2. Backscattered electron SEM image of Aluminum magnet wire cross section consisting of aluminum substrate with apparent surface shingles, 31 μm insulation base layer, 12 μm insulation top coat, and mounting material.	79
Figure 4.3. (Left) Tensile testing clamp patent design to maximize clamping pressure on magnet wire and mitigate breakage where 1 is the magnet wire, 2 is the clamp body, and 3 is the clamping member to secure the magnet wire over a large area [129]. (Right) Fabricated tensile testing clamp from [14] designed for use with rectangular cross section copper magnet wire and used for aluminum magnet wire in this study.	81
Figure 4.4. Alternate clamping method for aluminum and copper wires using only the clamping member of the tensile testing clamp to accommodate the shorter copper wires used in this study as well as to mitigate stress concentrations on aluminum wire at grip exit when used as intended.	82
Figure 4.5. Clamping method for testing copper wires to failure using self-tightening tensile testing wedge grips and folded wire ends to increase clamping pressure area.	83
Figure 4.6. Example of peel test procedure on aluminum magnet wire where a knife is used to separate the insulation from the base conductor to create a pull tab for attempted insulation removal.....	86
Figure 4.7. Low stress elongation testing process path.	87
Figure 4.8. Springback testing apparatus design specifications from [128]......	88
Figure 4.9. Custom built springback testing apparatus used for copper and aluminum magnet wire samples in this study.	89

Figure 4.10. Custom built wire bending/forming simulator from [14]. Forming angle is controlled by positioning the arms supporting the linear actuators to preset angles where the support roller is the focal point. Wire motion and tension are controlled using two linear actuators in tandem. 91

Figure 4.11. Close up of wire bending/forming simulator from [14]. The magnet wire is fixed to both linear actuators using clamps fixed to tension sensors used for wire tension control. A steel support roller controls contact area as well as strain experienced on the wire surface along with forming angle. Pressure exerted on the wire surface is controlled by placing weights on the friction arm which imparts a normal load through a load sensor and counterface made of desired contact material. Friction force is measured through elastic deflection of the friction arm in the direction of wire travel. 92

Figure 4.12. 24 mm steel support roller used for testing. 94

Figure 4.13. 3 mm steel support roller used for testing. 94

Figure 5.1. Stress vs strain curves for aluminum and copper magnet wire elongation testing samples..... 98

Figure 5.2. Stress drops in copper stress vs strain curves throughout plastic zone (left) and example of insulation fracture associated with each stress drop (right) from [14]..... 99

Figure 5.3. Stress drop in aluminum magnet wire stress vs strain curve at the onset of failure (left) and example of insulation fracture and delamination responsible for the stress drop at the necking region (right)..... 100

Figure 5.4. Fracture ends of aluminum wire elongated to failure highlighting a tube of delaminated insulation starting at the red circles and ending at the fracture end. Shrinkage of the insulation away from the aluminum wire fracture ends is also highlighted. Copper wire insulation does not see the same problem, remaining adhered up to the fracture end. 101

Figure 5.5. Illustration of aluminum elongation sample peel test. (a) An incision was made at the start of the delamination zone resulting in complete removal of the delaminated tube (b-c). Performing the peel test on the remaining adhered insulation adjacent to the delamination zone resulting in easy insulation removal (d-e). Second peel test attempt at base of wire with same results (f). Overall peel test results showing total insulation removal of aluminum elongation sample (g). 103

Figure 5.6. Copper elongation sample peel test results showing good adhesion at the fracture end with only small pieces of insulation able to be removed (a-c) and the same behaviour at the base of the wire (d-e) with resulting flakes of removed insulation (f). 105

Figure 5.7. Orange peel texture change observed post elongation testing on insulated copper wire (a), bare aluminum wire (b), insulated aluminum wire (c) and underlying surface of peeled insulated wire (d). 106

Figure 5.8. Keyence laser microscope image (left) and secondary electron SEM micrograph (right) of untested bare aluminum sample highlighting smooth surface features with manufacturing rolling mark imperfections. 107

Figure 5.9. Keyence laser microscope image (left) secondary electron SEM micrograph (right) and topographical map (bottom) illustrating significant surface texture change on bare aluminum sample elongated to failure. Original surface features are almost completely replaced by orange peel texture. 108

Figure 5.10. Keyence laser microscope image (left) and secondary electron SEM micrograph (right) of underlying surface of peeled insulated aluminum elongated to failure revealing less prominent orange peel texture compared to bare aluminum sample elongated to failure. Original surface features are still easily discernable. 108

Figure 5.11. Film adherence and flexibility testing stress vs strain curves for insulated aluminum magnet wire tested to 5%, 10%, 15% and 20% elongation. 110

Figure 5.12. Peel test results for fresh, untested, insulated aluminum wire establishing baseline insulation adhesion. (a) A pull tab was able to be created with significant effort and damage to underlying aluminum. (b-c) Insulation adhesion was too strong to remove any significant amount of insulation with only small pieces breaking off (d)..... 111

Figure 5.13. Peel test results for fresh, untested, insulated copper wire establishing baseline insulation adhesion. (a-e) Small pull tabs could be created but resulted in significant damage to underlying conductor and only small pieces of insulation breaking off (f). . 112

Figure 5.14. Peel test results for 5% (a-b) and 10% (c-e) film adherence samples. Insulation adhesion was almost identical to the fresh wire for both samples. Creating pull tabs was slightly easier for the 10% sample and larger pieces of insulation were able to be removed (e). 114

Figure 5.15. Peel test results for 15% film adherence sample. (a-b) Large pull tabs were easily created..... 115

Figure 5.16. Secondary electron (left) and backscattered electron (right) SEM micrographs of underside of delaminated insulation tube highlighting suspected aluminum particles removed from the wire surface during delamination. 116

Figure 5.17. Higher magnification view of suspected aluminum particles imbedded in the underside of delaminated insulation. 116

Figure 5.18. EDS mapping results of backscattered SEM image from Figure 5.16. The distribution of (a) carbon, (b) aluminum, (c) carbon & aluminum, (d) nitrogen and (e) oxygen establish imbedded particles in the underside of delaminated insulation are aluminum. 117

Figure 5.19. Secondary electron (left) and backscattered electron (right) SEM images of aluminum wire surface which experienced insulation delamination during elongation

testing. SE image shows suspected insulation particles adhered to the surface left behind from delamination while the BSE image confirms they are of different composition to aluminum. Example of an aluminum shingle like those seen on the underside of delaminated insulation is also highlighted. 119

Figure 5.20. Higher magnification view of suspected insulation particle left behind on aluminum surface post insulation delamination. 119

Figure 5.21. EDS mapping results of backscattered SEM image from Figure 5.20. The distribution of (a) aluminum, (b) carbon, (c) carbon & aluminum, (d) nitrogen and (e) oxygen establish adhered particle is insulation left behind post delamination. The carbon and nitrogen maps also reveal insulation remnants in the aluminum surface crevices. . 120

Figure 5.22. Copper insulation damage sustained during elongation to failure. (a) Small pin holes and splits in the insulation. (b) Larger, less common split in insulation with side view in (c). 122

Figure 5.23. Aluminum insulation damage sustained during elongation to failure. (a) Small pinhole failure of insulation. (b) Less common, large split revealing the underlying conductor. (c) Example of gross insulation failure consisting of insulation split the width of the conductor and delamination zone around the fracture. 123

Figure 5.24. Low stress elongation stress vs strain curves for aluminum and copper wire samples. 126

Figure 5.25. Bending direction for aluminum and copper magnet wire samples for springback testing. 127

Figure 5.26. Average COF vs normal load testing results for aluminum and copper magnet wires. (a) Uses trend line to highlight change in COF for aluminum wire samples as normal load increases. (b) Highlights COF standard deviation for each testing condition. 133

Figure 5.27. Variation of COF with aluminum wire travel length for normal load testing at 7 lbs with 3 mm radius support roller. 134

Figure 5.28. Variation of COF with aluminum wire travel length for normal load testing at 7 lbs with 24 mm radius support roller. 134

Figure 5.29. Variation of COF with aluminum wire travel length for normal load testing at 12 lbs with 3 mm radius support roller. 134

Figure 5.30. Variation of COF with aluminum wire travel length for normal load testing at 12 lbs with 24 mm radius support roller. 135

Figure 5.31. Variation of COF with aluminum wire travel length for normal load testing at 17 lbs with 3 mm radius support roller. 135

Figure 5.32. Variation of COF with aluminum wire travel length for normal load testing at 17 lbs with 24 mm radius support roller.	135
Figure 5.33. Variation of COF with aluminum wire travel length for normal load testing at 22 lbs with 3 mm radius support roller.	136
Figure 5.34. Variation of COF with aluminum wire travel length for normal load testing at 22 lbs with 24 mm radius support roller.	136
Figure 5.35. Variation of COF with aluminum wire travel length for normal load testing at 27 lbs with 3 mm radius support roller.	136
Figure 5.36. Variation of COF with aluminum wire travel length for normal load testing at 27 lbs with 24 mm radius support roller.	137
Figure 5.37. Variation of COF with aluminum wire travel length for normal load testing at 32 lbs with 3 mm radius support roller.	137
Figure 5.38. Variation of COF with aluminum wire travel length for normal load testing at 32 lbs with 24 mm radius support roller.	137
Figure 5.39. Variation of COF with aluminum wire travel length for normal load testing at 37 lbs with 3 mm radius support roller.	138
Figure 5.40. Variation of COF with aluminum wire travel length for normal load testing at 37 lbs with 24 mm radius support roller.	138
Figure 5.41. Variation of COF with aluminum wire travel length for normal load testing at 42 lbs with 3 mm radius support roller.	138
Figure 5.42. Variation of COF with aluminum wire travel length for normal load testing at 42 lbs with 24 mm radius support roller.	139
Figure 5.43. Variation of COF with copper wire travel length for normal load testing at 22 lbs with 3 mm radius support roller.	139
Figure 5.44. Variation of COF with copper wire travel length for normal load testing at 22 lbs with 24 mm radius support roller.	139
Figure 5.45. Variation of COF with copper wire travel length for normal load testing at 42 lbs with 3 mm radius support roller.	140
Figure 5.46. Variation of COF with copper wire travel length for normal load testing at 42 lbs with 24 mm radius support roller.	140
Figure 5.47. Average COF vs aluminum wire travel speed testing results. (a) Uses trend line to highlight change in COF as travel speed increases. (b) Highlights COF standard deviation for each wire speed.	143

Figure 5.48. Variation of COF with aluminum wire travel length for travel speed testing at 5 mm/s.....	144
Figure 5.49. Variation of COF with aluminum wire travel length for travel speed testing at 10 mm/s.....	144
Figure 5.50. Variation of COF with aluminum wire travel length for travel speed testing at 15 mm/s.....	144
Figure 5.51. Variation of COF with aluminum wire travel length for travel speed testing at 20 mm/s.....	145
Figure 5.52. Variation of COF with aluminum wire travel length for travel speed testing at 25 mm/s.....	145
Figure 5.53. Variation of COF with aluminum wire travel length for travel speed testing at 30 mm/s.....	145
Figure 5.54. Variation of COF with aluminum wire travel length for travel speed testing at 35 mm/s.....	146
Figure 5.55. Variation of COF with aluminum wire travel length for travel speed testing at 40 mm/s.....	146
Figure 5.56. Average COF vs aluminum wire forming angle testing results. (a) Uses trend line to highlight change in COF for 24 mm radius support roller as forming angle increases. (b) Highlights COF standard deviation for each testing condition and better compares COF between support rollers for each forming angle.	149
Figure 5.57. Variation of COF with aluminum wire travel length for forming angle testing at 10° with 3 mm radius support roller.....	150
Figure 5.58. Variation of COF with aluminum wire travel length for forming angle testing at 10° with 24 mm radius support roller.....	150
Figure 5.59. Variation of COF with aluminum wire travel length for forming angle testing at 30° with 3 mm radius support roller.....	150
Figure 5.60. Variation of COF with aluminum wire travel length for forming angle testing at 30° with 24 mm radius support roller.....	151
Figure 5.61. Variation of COF with aluminum wire travel length for forming angle testing at 60° with 3 mm radius support roller.....	151
Figure 5.62. Variation of COF with aluminum wire travel length for forming angle testing at 60° with 24 mm radius support roller.....	151

Figure 5.63. Variation of COF with aluminum wire travel length for forming angle testing at 90° with 24 mm radius support roller.....	152
Figure 5.64. Thermal images of aluminum magnet wire tested at 12 lbs normal load. (a) Pre-test reference temperatures. (b) End of test temperatures.	154
Figure 5.65. Thermal images of aluminum magnet wire tested at 27 lbs normal load. (a) Pre-test reference temperatures. (b) End of test temperatures.	154
Figure 5.66. Thermal images of aluminum magnet wire tested at 37 lbs normal load. (a) Pre-test reference temperatures. (b) End of test temperatures.	154
Figure 5.67. Thermal images of copper magnet wire tested at 22 lbs normal load. (a) Pre-test reference temperatures. (b) End of test temperatures.....	155
Figure 5.68. Counterface contact from testing aluminum at 12 lbs normal load with 3 mm radius support roller. (a) Macroscopic view of scratch contact at edge of counterface surface. (b) Higher magnification optical microscope image of scratch contact.....	157
Figure 5.69. Counterface contact from testing aluminum at 27 lbs normal load with 24 mm radius support roller. (a) Macroscopic view of scratch contact and large amount of material transfer and smearing on counterface surface. (b) Higher magnification optical microscope image showing decreasing size particle transfer and smearing over scratching.....	157
Figure 5.70. Counterface contact from testing aluminum at 37 lbs normal load with 3 mm radius support roller. (a) Macroscopic view of scratch contact and large amount of material transfer on counterface surface. (b) Higher magnification optical microscope image showing small particle transfer at counterface edge followed by larger particles over scratching. (c) Higher magnification optical microscope image of highlighted region showing small and large particle transfer on counterface surface.	158
Figure 5.71. Counterface contact from testing copper at 42 lbs normal load with 3 mm radius support roller. (a) Macroscopic view of dual contact regions with light scratching and dense material transfer and smearing on counterface surface. (b) Higher magnification optical microscope image of larger particle transfer over light scratching at edge of counterface. (c) Higher magnification optical microscope image of very fine, dense, and layered material transfer making up most of the contact path.	159
Figure 5.72. Counterfaces used to evaluate differing transfer mechanisms between aluminum wire (left) and copper wire (right). (left) Aluminum wire contact region from 27 lbs normal load on counterface consisting of scratching, material transfer, and smearing. (right) Copper wire contact region from 42 lbs normal load on counterface consisting of two contact regions from edges of the wire with light scratching and dense material transfer.	160
Figure 5.73. Secondary electron SEM images of aluminum (left) and copper (right) contact regions depicted in Figure 5.72. (left) Aluminum wire contact sees prominent scratching and decreasing size particle transfer from counterface edge (top) to middle. (right) Copper	

wire contact on counterface sees layered material transfer with larger particles on top of a dense film of fine particles..... 160

Figure 5.74. Secondary electron and backscattered electron SEM images of copper wire contact region on counterface with associated iron and carbon EDS maps for elemental analysis. SE image along with the iron map reveal varying levels of material transfer thickness while the carbon map indicates material transfer is copper wire electrical insulation..... 161

Figure 5.75. Secondary electron and backscattered electron SEM images of aluminum wire contact region on counterface with associated iron and carbon EDS maps for elemental analysis. Images reveal distinct particle transfer rather than layering as seen with copper transfer while iron and carbon maps indicate transfer is aluminum wire electrical insulation. 162

Figure 5.76. Top and bottom surface contact for aluminum magnet wire tested at 12 lbs normal load with 3 mm radius support roller..... 164

Figure 5.77. Top and bottom surface contact for aluminum wire tested at 27 lbs normal load with 24 mm radius support roller..... 164

Figure 5.78. Top and bottom surface contact for aluminum wire tested at 37 lbs normal load with 3 mm radius support roller..... 164

Figure 5.79. Representative top and bottom surface contact for copper wire tested at both 22 and 42 lbs with both support rollers..... 165

Figure 5.80. Macroscopic image (left) and Keyence laser microscope image (right) of damaged inflicted to aluminum and copper wire surface from smooth 3 mm radius support roller and 24 mm radius support roller with machined surface. (a) Aluminum against 3 mm radius support roller which causes ironing and light scratching. (b-c) Aluminum and copper against 24 mm radius support roller which caused gauging and associated cracking around gauge lines. 166

Figure 5.81. Aluminum wire top contact end of test transition between depressed and ironed insulation and fresh wire surface tested at 12 lbs normal load. (a) Keyence laser microscope image of transition zone. (b) Topography map highlighting raised region at bump peak. (c) End of test bump profile from line scan across transition zone..... 168

Figure 5.82. Mounted wire samples with both edgewise and lengthwise cross-sections for SEM analysis. 169

Figure 5.83. Backscattered electron SEM images of fresh insulated aluminum wire cross section. (a) Lengthwise and (b) edgewise cross section view showing complete insulation penetration into voids between and around aluminum shingles. (c) Numerous shingles a few microns in thickness populating the aluminum wire surface. (d) Darker lines between shingles and bulk aluminum suggesting different elemental composition or cracks..... 171

Figure 5.84. Backscattered electron SEM image of aluminum shingle and dark area at shingle/bulk aluminum boundary used for EDS mapping. Distribution of (b) aluminum, (c) carbon, (d) oxygen, with phase map (e) and phase composition (f). Oxygen map suggests shingle/bulk aluminum boundary contains oxides as no presence of elements composing electrical insulation were detected. 172

Figure 5.85. Secondary electron images of fresh insulated copper wire cross section. (a-c) Generally featureless, very smooth, and high-quality copper surface. (d) Example of surface defect consisting of bumps or craters a few microns in height and width..... 173

Figure 5.86. Surface features of aluminum sample tested at 27 lbs normal load. (a) Edgewise cross section showing deeper penetration of insulation into aluminum surface than seen on the fresh sample. (b) Lengthwise cross section highlighting formation of subsurface cracks from testing. (c) Higher magnification secondary electron SEM image of subsurface crack with backscattered electron SEM image (d) showing different elemental composition inside crack. 175

Figure 5.87. Secondary electron and associated backscattered electron SEM images of edgewise aluminum wire cross section tested at 37 lbs normal load. (a-f) Shows crack propagation around shingles, detaching or nearly detaching them from the bulk aluminum. (e-h) Show crack propagation deeper into the bulk aluminum surface than that seen for testing at 27 lbs normal load. 177

Figure 5.88. Secondary electron and associated backscattered electron SEM images of lengthwise aluminum wire cross section tested at 37 lbs normal load. Cracks propagate around and underneath shingles, detaching them and pushing them away from the bulk aluminum. 178

Figure 5.89. Secondary electron (top) and backscattered electron (bottom) SEM images of lengthwise aluminum wire cross section tested at 37 lbs normal load. Very long subsurface cracks suggest crack initiation and propagation at a suspected near-surface deformed layer, detaching it from the bulk aluminum. BSE images shows dark voids in subsurface cracks suggesting different elemental composition suspected to be electrical insulation. 179

Figure 5.90. Higher magnification secondary electron SEM images of subsurface cracks in lengthwise aluminum wire cross section tested at 37 lbs normal load. Crack initiation and propagation along suspected near-surface deformed layer/bulk aluminum interface is highlighted resulting in separation of near surface layer from bulk aluminum..... 180

Figure 5.91. Backscattered electron SEM image of subsurface crack used for EDS mapping. Distribution of (b) aluminum, (c) carbon, (d) Nitrogen, with phase map (e) and phase composition (f). Carbon and nitrogen maps along with phase maps suggest subsurface crack is filled with electrical insulation. 182

Figure 5.92. Secondary electron SEM images of edgewise copper wire cross section tested at 42 lbs normal load. Copper surface remains mostly featureless and smooth (left) with only surface defects being small bumps or craters a few microns in height and width (right). 183

Figure 5.93. Secondary electron and associated backscattered electron SEM images of void formation in insulation surrounding and penetrating aluminum shingles from testing at 37 lbs normal load. (a-b) Void formation underneath shingle suggesting onset of delamination from bulk aluminum. (c-d) Void formation in insulation region between neighboring aluminum shingles. 184

Figure 5.94. Backscattered electron SEM images of insulation delamination from bulk conductor at very edge of aluminum sample tested at 37 lbs normal load where it was sectioned from the larger wire sample. (c-e) Highlight crack propagation around aluminum shingles with some left imbedded in insulation accounting for observations made in Section 5.1.2.2..... 186

Figure 6.1. Effect of applied strain on LSE of copper wire [29]. 188

LIST OF ABBREVIATIONS

EV	Electric Vehicle
IACS	International Annealed Copper Standard
AWG	American Wire Gauge
Al	Aluminum
EC	Electrical Conductor grade aluminum
ACSR	Aluminum Conductor Steel Reinforced
AAAC	All Aluminum Alloy Conductor
Cu	Copper
ETP	Electrolytic Tough Pitch grade copper
OF	Oxygen Free grade copper
OFE	Oxygen Free Electronic grade copper
CCA	Copper Clad Aluminum
CNT	Carbon Nanotubes
DC	Direct Current
AC	Alternating Current
LCA	Life Cycle Assessment
TOC	Total Owning Cost
CLPU	Cold Load Pick Up
COP	Coefficient of Performance
EER	Energy Efficiency Ratio
QA	Quality Assurance
SEM	Scanning Electron Microscope
EDS	Energy Dispersive X-ray Spectroscopy
SE	Secondary Electron
BSE	Backscattered Electron
LSE	Low Stress Elongation
PM	Permanent Magnet
PMSM	Permanent Magnet Synchronous Machine

NOMENCLATURE

E	Elastic Modulus
G	Shear Modulus
SFE	Stacking Fault Energy
COF	Coefficient of Friction
STD/STDEV	Standard Deviation
HRB	Rockwell B Hardness
wt%	Weight Percent
ppm	Parts per Million
rpm	Revolutions per Minute
P	Total Winding Cost
<i>c</i>	Commodity Price
<i>m</i>	Conductor Mass
g	Gram
kg	Kilogram
lbs	Pounds
L	Conductor Length
A	Conductor Cross-Sectional Area
m	Metre
mm	Millimetres
cm	Centimetre
in	Inches
GPa	Gigapascal
MPa	Megapascal
psi	Pounds per Square Inch
N	Newton
Nm	Newton Metre
K	Kelvin
°C	Degrees Celsius

° / deg	Degrees
s / sec	Seconds
h	Hour
min	Minutes
erg	Energy Unit Equal to 10^{-7} Joules
W	Watt
kWh	Kilowatt hour
J	Joule
Ω	Ohm
A	Ampere
V	Volt
Hz	Hertz
ρ	Electrical Resistivity
S	Siemens (Electrical Conductivity)
R	Electrical Resistance
R_{ac}/R_{dc}	AC to DC Resistance Ratio

Chapter 1

INTRODUCTION

Global warming and humanity's impact on the health of the planet has been a topic of discussion for many years now. Greenhouse gas emissions are continually rising, and the effects of global warming cannot be ignored any longer. This has been pushing society towards implementing more ecofriendly solutions to our daily activities. Looking at the global greenhouse gas emissions from 2010 in Figure 1.1, 14% of all emissions came from transportation [1]. As more nations industrialize and their economies grow, there will be an increasing need for commercial and passenger vehicles which will increase their share of global emissions. One solution to combat this is to electrify said vehicles.

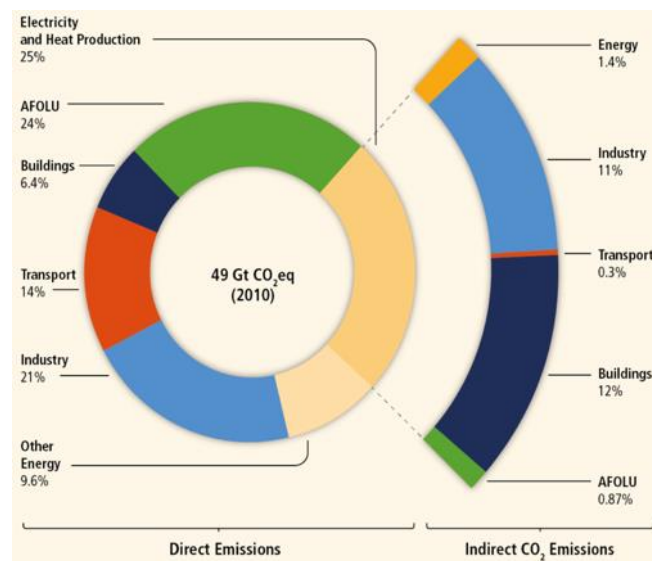


Figure 1.1. 2010 global greenhouse gas emissions by economic sector [1].

Electric passenger vehicles are still a fairly new technology but Figure 1.2 projects a large increase in their popularity over the next 20 years [2]. Combustion vehicles remain dominant however because of a few main problems associated with the slow growth of electric vehicle (EV) market share. They are still quite expensive, and their mileage is not on par with combustion vehicles yet. There is also the issue of small charging networks and long charging times. Tesla, Inc. has done a great job pushing passenger EV's into the market along with plans to enter the long-haul cargo transport market. They have also

pushed the entire automotive industry towards vehicle electrification with many new models from major manufactures coming to market over the next few years. This is a step in the right direction, but the main problems associated with their limited growth still needs to be addressed. Therefore, further research is required to reduce EV cost, decrease their weight and improve their efficiency so they can better compete with gasoline vehicles and become a viable option for the average consumer.

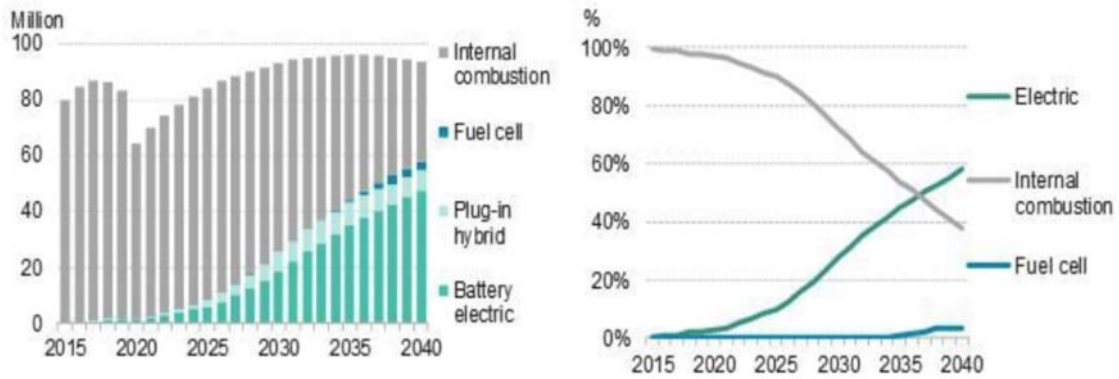


Figure 1.2. Long term projection of global passenger vehicle sales by drivetrain (left) and share of sales (right) [2].

The question then becomes, how can the cost and weight of an electric vehicle be reduced and in turn, increase overall vehicle efficiency? One approach is to look at the electric motor and the materials involved with its construction and operation. Specifically, the electrical conductors used to convert electrical energy into mechanical force are analyzed. Electrical conductors have been used for well over a century with the most common materials used being silver, copper, gold, and aluminum. Silver has the highest conductivity of all metals, but it is very expensive and has low strength making it only suitable for specialty applications [3]. Gold also has high conductivity, but it is a precious metal with high cost also making it unsuitable for bulk application. This leaves copper and aluminum as the only suitable metals for industrial scale application due to their acceptable price and desirable mechanical properties [4].

Copper has the best electrical and thermal conductivity of all industrial scale metals [5] due to its large mean free path, around 100 atomic spacings, allowing free electrons to flow with less resistance from matrix atoms and lattice imperfections [6], [7]. The mechanical properties of copper allow it to be easily drawn into small diameter wire, coated with electrical insulation, and connected or terminated with a myriad of techniques [5].

Copper is such a prevalent conductor material that the electrical conductivity for a commercially pure, annealed sample was established as a standard unit of measure in 1914 which is known as the International Annealed Copper Standard (IACS) [8]. The conductivity of all other metals was then expressed as a percentage of commercially pure annealed copper with it having a conductivity of 100% [8]. These are the reasons it has been the material of choice for the vast majority of electrical applications which is especially true for high performance motors like those used for automotive applications, where copper is almost exclusively used [9].

However, copper is a heavy metal, and its price has been rising since as early as the 1940's where a noticeable price gap started forming between it and aluminum, the next best conductor [10]. Since the early 2000's, copper's rising price has been dramatic, especially compared to aluminum which has remained more stable, as illustrated in Figure 1.3. This trend is expected to continue, with future copper prices projected to be high and volatile [11] due to demand and scarcity [3]. For this reason, aluminum, which is a less common conductor but has successfully been used in various applications for over 100 years [12], [13], is now being considered as a replacement to copper for high performance motor applications.

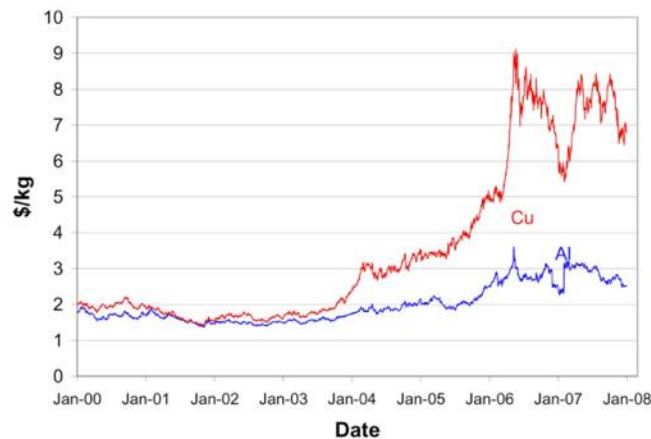


Figure 1.3. Aluminum and copper commodity price from 2000 to 2008 [11].

It is evident that aluminum has a substantial price advantage over copper, with raw material prices per kilogram as of July 2020 seeing aluminum 75% cheaper than copper. Aluminum also has a density 30% that of copper which is highly attractive for weight

savings. However, electrical conductor grade aluminum only has 61.8% the electrical conductivity of copper. This means an aluminum wire with equivalent current carrying capacity to a copper wire will require a cross-sectional area/volume increase of 1.6x. This has been one of the main factors limiting the growth of aluminum as a conductor in high performance applications, especially where motor size is a design constraint. Considering this disadvantage though, an equivalent aluminum conductor will still see a weight reduction of 50% over the copper wire which is substantial when weight and overall vehicle efficiency have become more important design considerations for the automotive sector. Even though the conductivity of aluminum is nearly 40% lower than copper, dramatic weight and cost savings can still be achieved on an equivalent conductor basis which could translate to more affordable, lighter, and more efficient electric vehicles to increase their growth in the automotive market.

Based on these market trends and the shift of the automotive industry towards vehicle electrification, it is the appropriate time to rekindle the century old aluminum versus copper conductor debate. Therefore, this work performs a feasibility study on the replacement of copper with aluminum conductors in high performance electric motors targeted for electric vehicle application. This involves a comprehensive analysis of advantages and disadvantages of replacing copper with aluminum conductors as seen in literature since the inception of the aluminum versus copper conductor debate. The results of this comprehensive review will serve as a unified source to better aid research on the use of aluminum conductors moving forward.

This work also seeks to add knowledge to the field from a metallurgical standpoint rather than the common electrical one. This involves a formability and windability study of square cross section aluminum and copper conductors coated with a general purpose, high temperature, polymer based insulative coating. The formability and windability of both magnet wires is characterized according to ASTM D1676. A novel wire bending simulator machine is also used to characterize these properties as well as damage behaviour and deformation mechanisms of both conductors during die forming simulation; a procedure used for hairpin style conductors. Results for aluminum will be directly compared to those found for copper in a previous study [14].

1.1 Organization of Thesis

Chapter 1 - Introduces the motivation and scope of this thesis.

Chapter 2 - Covers an extensive literature review of aluminum versus copper conductors covering more than 100 years of research. This involves looking at the advantages and disadvantages of replacing copper with aluminum in terms of cost, mechanical, electrical, and thermal properties, insulation performance, corrosion and electrical connections. A case study-based analysis is also performed to illustrate where aluminum is being implemented into electrical applications and how it compares to copper.

Chapter 3 - Performs a literature review pertaining to the metallurgical-based formability and windability study of square cross section aluminum and copper magnet wires. This includes the unique manufacturing processes of hairpin style conductors and associated forces responsible for damage during formation. Common conductor failure modes involved with manufacturing and shaping operations as well as surface defects specific to aluminum wires are also reviewed.

Chapter 4 - Outlines the methodology used for formability and windability testing of both copper and aluminum magnet wires. Standardized testing methods from ASTM D1676 are covered as well as testing procedures with a novel wire bending simulator debuted by A. Demiri in [14].

Chapter 5 - Details the results of this testing as well as optical and scanning electron microscope observations on the deformation behaviour and damage mechanisms experienced by both conductors during testing.

Chapter 6 - Discusses results in association with observations made and their implications for the future of aluminum conductors.

Chapter 7 - Summarizes the key findings of this study as well as recommends topics for future study.

Chapter 2

ALUMINUM VS COPPER: ADVANTAGES & DISADVANTAGES

This chapter performs an exhaustive literature review on aluminum versus copper conductors as its been debated for over 100 years. It serves as a unified source of information to better aid the aluminum versus copper debate for future research.

2.1 Electrical Conductor History

Copper was the first real metal to be utilized for tools and weapons and it was likely discovered by the Egyptians around 9000BC [15]. It was very easy to work with due to its excellent malleability [15]. Around 5000 years ago, its use accelerated in the Bronze Age where it and its alloys were produced in much more significant quantities for use in a myriad of applications [13]. From this point forward, copper and its alloys were extensively used and produced in large quantities [13]. Aluminum is found in Bauxite ore and was not isolated into a pure form until 1827 [13]. This was a difficult process however, so aluminum was initially viewed as a precious metal with a cost greater than platinum, gold, or silver [13]. It was not until 1886 that electrolytic reduction was discovered, allowing aluminum to be produced in large quantities [13]. A timeline marking the first use of common metals is presented in Figure 2.1 highlighting how established copper is in society and how new aluminum is comparatively.

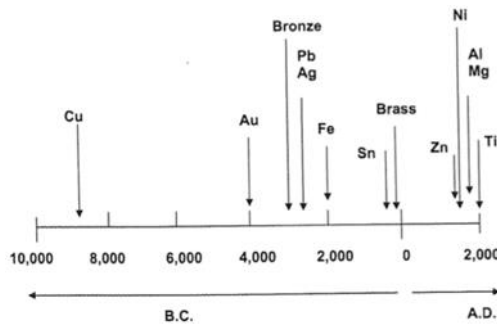


Figure 2.1. Timeline for the first use of common metals [15].

The electrical industry effectively started in September 1882 where the Pearl Street Station in Lower Manhattan was built as the first commercial electricity generation station

[13]. This was before large-scale production capability of aluminum and its realization as a conductor were established. Therefore, copper was used as the first electrical conductor due to its familiarity and prevalence in society and has evolved with the electrical industry since [13]. This left the world slow to respond to using aluminum in the early 1900's resulting in an initially high cost [13]. This was despite early research by Lord Kelvin who improved the conductivity of pure aluminum to 68.5% that of pure copper at the time [16]. Coupled with the dramatically lower weight compared to copper, an equivalent aluminum wire would be highly advantageous for overhead conductors with only a modest increase in diameter needed and a weight less than 50% that of copper wire [16]. With the electrolysis process already significantly reducing the price of aluminum [16] the debate between its use over copper began.

A news article was published in 1899 comparing aluminum vs copper conductors. It highlighted the increasing demand for copper exceeded its supply, quickly increasing its price [17]. The main disadvantages of aluminum were the 60% increase in cross-sectional area required for equivalent conductivity to copper, and its natural oxide layer causing connection problems [17]. Although a 50% weight reduction for equivalent conductors was still realized [17]. At this time there were also reports of aluminum being successfully used for several applications by the Pittsburgh Reduction Company, Niagara Falls power generation and Bell Telephone Company [17]. Despite its cost, as much as 5x higher than copper, it was also being adopted for overhead power lines [4]. Another article from 1911 notes the strength advantages of equivalent aluminum conductors due to their increased cross section [18]. By this point, fine insulated aluminum wire was much more expensive than copper, but in larger gauges, it started to see cost advantages [18].

During World War II and post war, the aluminum versus copper debate started to see a significant shift as world copper shortages pushed aluminum to become a much more prevalent conductor [12], [13]. Production was dramatically increased for the war effort, mainly to produce aircraft, but it remained high post war as aluminum found use in more industries [13]. In 1954, the US Underwriters Laboratory listed circuit size electrical conductor (EC) aluminum cable for wiring buildings [19]. Around this time, there were still copper shortages, so transformer designers looked to aluminum for its use in dry type transformers to ease the burden on copper supplies and leave it for more critical

applications [20]. One hundred aluminum transformers were built and implemented and over their 3-4 years of service at the time of publication, they experienced no issues compared to copper counterparts [20]. However, more steel material was required in the transformer core resulting in slightly larger dimensions and 3% greater weight compared to the copper transformers [20]. They were also 1.3x more expensive due to increased costs of aluminum wire fabrication and joining along with higher insulated wire costs compared to copper [20].

By 1957, new aluminum overhead power line alloys were being tested in north America after successful use for years in Europe [21]. Convention up to this point was to use EC aluminum conductor with a conductivity of 61% IACS around a steel wire core known as aluminum conductor steel reinforced (ACSR) [21]. Instead, all aluminum alloy conductors (AAAC) were being tested with a 53% IACS rating, and strength on par with hard drawn copper at the time at only half the weight [21]. At this time, Reynolds Metal Company introduced aluminum strip conductors for use in transformer coils [22]. They allowed for extremely compact coils since an anodic aluminum oxide film could be used for electrical insulation rather than conventional polymer or tape films [22]. They also allowed for significantly increased operating temperatures since the melting point of aluminum oxide far exceeds that of aluminum [22]. The coil shape was advantageous for heat dissipation and the resulting coil weight was 50% less than a conventional copper coil [22].

2.1.1 Aluminum Housing Wire Crisis

Moving forward to the 60's and 70's, aluminum became increasingly popular in housing and building wire as a replacement to copper. In 1974, aluminum saw its peak usage accounting for 31% of the market [12]. However, its use came with a multitude of failures and in the worst cases, catastrophic failure resulting in fires. As a result, by 1991 its market share dropped to just 8% [12] and it still has a bad reputation to this day. It is a misconception that aluminum itself was the problem here though. The culprit was bad connections and terminations as a result of ignorance on how to properly terminate aluminum as well as lack of regulated connectors that compensated for its differing mechanical and thermal properties from steel and copper. The coefficient of thermal

expansion for steel is 50% lower than aluminum which resulted in loosening of connections [3], [12]. Temperature cycling during normal use would cause this loosening and result in reduced contact area and increased contact resistance [12], [23]. As cycling continued, temperature would increase further, slowly degrading the electrical contact and eventually cause insulation and connection failure and fires [3], [12], [23].

Since then, new 8XXX series aluminum alloys have been introduced and manufacturers have developed code compliant connections specifically designed for aluminum to mitigate these problems so it can safely be used as building wire [13], [24, pp. 7-1 - 7-6]. However, its first impression in the copper dominant building wire market was poor [4], resulting in an unjustified bad reputation which still stands today. The familiarity of copper as the first metal humans utilized, and the lack of communication on appropriate technology and education required to properly implement aluminum resulted in its slow adoption into other electrical markets where copper is dominant [4].

2.1.2 Common uses of Aluminum and Copper

Despite its reputation and lower conductivity compared to copper, aluminum wire has successfully been used in many electrical applications for decades. Its first main debut was in power distribution as overhead power lines. In the 1950's, aluminum started actively replacing copper transmission lines [24, pp. 14-1 - 14-13] and by 1966 it made up 97% of high voltage transmission lines and 75% of distribution cables [25]. By 1971, aluminum had established itself as a viable and economic electrical conductor with widespread use in power transmission and distribution [26]. Today, aluminum is almost exclusively used in the whole power transmission network from the power plant to point of use meters and entrance lines into buildings [12], [13], [24, pp. 11-1 - 11-27]. Aluminum was quickly adopted for use in distribution transformers due to their simplicity [27]. Aluminum can be used in both dry and oil type transformers but Al-Al windings are more common and successful in distribution transformers while Cu-Cu windings are almost exclusively used for power transformers [3], [28].

Aside from power distribution, there are two types of electrical equipment aluminum can successfully be used in: bus bars (busway, switchboards, switch gear and motor control centres) and magnet wire (motors and transformers) [12], [13]. Copper is the

conductor of choice for bus bars but aluminum, being half the weight for equivalent conductivity, is a popular choice when weight is a concern for large scale operations using millions of pounds of conductor [24, pp. 13-1 - 13-70]. Aluminum magnet wire can also be used in hydroelectric generators since they are specifically made for each application, allowing for more design freedom to accommodate it [27]. Additionally, it is used in small, fractional horsepower motors like those in washers and dryers [24, pp. 14-1 - 14-13]. Aluminum windings are popular in higher temperature applications like nuclear reactors, missiles and supersonic aircraft since it is stable without rapid oxidation or flaking like seen with copper [25].

Aluminum strip conductor, either anodized or used with conventional insulation methods is used in many applications. This includes large lifting electromagnets where the reduced weight of aluminum allows for greater payloads, and magnetic levitation coils where operating temperatures are high [25]. Strip or foil coils can also be downsized and used in small motors like those of hand tools [5]. Aluminum is very popular in induction machines where its advantages with casting technology allow for single piece rotors to be made resulting in lower weight for reduced inertia, and more economical and balanced design [24, pp. 16-1 - 16-6]. These motors are popular for both household appliances and large industrial equipment [24, pp. 16-1 - 16-6].

Copper is the conductor of choice for most other electrical applications. As a general rule of thumb, when a design has a size or efficiency constraint, copper is used since a larger volume of aluminum is required for equivalent performance [7], [12], [13], [23], [29]. Conversely, when weight savings and cost reduction are the goal, aluminum is the better option [7], [12], [13], [23]. This is generally why copper is almost exclusively used in high performance motors since maximizing efficiency and reducing machine size have been design criteria [9].

2.2 Electrical Conductor Alloys

Conventional strengthening mechanisms like work hardening, solid solution strengthening and age hardening along with alloying elements reduce the conductivity of metals and can also result in thermodynamically unstable alloys which is problematic for manufacturing and use of enameled wires [19]. Maximizing conductivity is a must for

achieving the highest efficiency in electrical applications which is why aluminum and copper conductors are generally preferred to be used in a pure and annealed state. However, there are certain alloying elements which improve electrical conductivity, like boron for aluminum and oxygen for copper. Therefore, it is desirable to use low alloyed aluminum and copper to maximize mechanical properties for manufacturing and use, while mitigating the impact on electrical conductivity as much as possible. In this case, alloying elements used should have very low solubilities in the base metal so they can form stable precipitates which are unlikely to dissolve back into the matrix or coarsen during wire processing [19]. Precipitates, or second phases, are desired because they have much less impact on conductivity than do alloying elements or impurities dissolved in solid solution [6].

2.2.1 Aluminum Alloys

Pure aluminum has the highest conductivity of its alloys but is far too soft for reliable use as an electrical conductor [3]. For this reason, multiple alloys have been developed over the years to improve its strength while minimizing impact to electrical conductivity. Aluminum is generally alloyed with small amounts of boron and iron. Boron is used to tie up impurities (V, Ti, Zr, Cr, Ca) as borides which sink to the bottom of the melt during casting where they can be removed [6], [29], [30]. Otherwise they dissolve in solid solution, decreasing electrical conductivity [6], [30]. Iron has very low solubility in aluminum, so it mainly forms second phases which do not affect conductivity as much [6]. For example, iron in solution increases electrical resistivity by $2.56 \mu\Omega\text{cm/wt\%}$ iron compared to an increase of $0.058 \mu\Omega\text{cm/wt\%}$ iron as a precipitate [19]. Therefore, it appreciably increases strength, which is highly desirable in aluminum, while minimally affecting conductivity [31]. If higher iron contents are used (0.5-1%), elongation is improved for the annealed wire and recrystallization temperature and strength are increased at medium temperatures (300°C) [5]. Magnesium can also be added to improve creep resistance, which is essential for reliable connections and resisting centrifugal forces in rotational operation, as well as strength at medium temperatures [5].

The most common, cheapest, and readily available aluminum alloy conductor used is Electrical Conductor (EC) aluminum or A1350 in an annealed state [10]. It has a purity

of 99.5% with a 61.8% IACS conductivity [32]. It is mainly used as an insulated or covered wire or cable and especially prominent in overhead power lines [24, pp. 7-1 - 7-6]. For use in the building wire industry, 8XXX series aluminum alloys were developed with excellent thermal stability and creep resistance [24, pp. 7-1 - 7-6] to mitigate problems seen with connection failures and fires in the 60's and 70's. These alloys have about the same conductivity as A1350 but they are generally alloyed with higher contents of iron with a more detailed breakdown of alloying elements found in [29]. To improve upon the strength of aluminum for applications where it is essential, heat treatable 6XXX series alloys were developed and used which see an increase in conductivity as precipitation hardening occurs [10]. After WWII, A6101 at 55% IACS was developed with significantly higher yield strength and better creep resistance than A1350 due to additions of magnesium and silicon at the expense of conductivity [13], [24, pp. 13-1 - 13-70]. It is mainly used for bus bars and other applications where high conductivity is required as well as good mechanical properties [3], [13]. A6063 was also used as a high strength option mainly for high voltage, outdoor substation buses [24, pp. 13-1 - 13-70]. Where strength is more important than conductivity, A6061 with a T6 temper is used [24, pp. 13-1 - 13-70].

2.2.2 Copper Alloys

Pure copper already has superior mechanical properties to aluminum so little alloying has been needed for its successful use. The main alloying element used is oxygen, which behaves the same for copper as boron does for aluminum. In small amounts, up to 200 ppm, it ties up impurities (Se, Fe, Bi, Pb) as oxides, removing them from solid solution and increasing conductivity [6], [29], [33]. Above this amount, conductivity starts to decrease [33]. This alloy is known as electrolytic tough pitch (ETP) copper and has a purity of 99.9% with a standard electrical conductivity of 100% IACS but generally higher at 101% [6], [7]. However, ETP copper is not suitable for high temperature applications or where long term exposure to hydrogen is required due to hydrogen embrittlement [6], [7]. For resistance to hydrogen embrittlement, oxygen free (OF) or oxygen free electronic (OFE) with lower oxygen contents, 10 ppm and 5 ppm respectively, can be used [7], [33]. OF copper has better ductility than ETP so it is more suitable for deep drawing operations [33] but has a higher annealing temperature making it unsuitable for magnet wire

application where lower annealing temperatures are better for manufacturability [7], [29], [33]. Silver bearing copper alloys offer 100% conductivity but better creep strength, stress to rupture and resistance to softening at high temperatures which are important for power transformers where more strength and rigidity is required to resist forces from surge and overload [6], [7], [29].

2.3 Material Properties of Aluminum and Copper

To properly analyze the advantages and disadvantages of replacing copper with aluminum conductors, their relevant properties need to be compared. Table 2.1 provides these properties for the most common alloys of copper and aluminum used for magnet wire and electric motor applications. The third column provides the ratio of aluminum to copper for easier illustration of where it is advantageous and disadvantageous to use. Moving forward with the comparative analysis of replacing copper with aluminum, these alloys and associated properties will be used unless otherwise stated.

Table 2.1. Comparison of properties for copper and aluminum conductors used in this study.

Properties (20°C) (Annealed)	ETP Copper	EC Aluminum	Al/Cu Ratio
Cost (July 13/20) (\$US/Kg) [34] [35]	6.54508	1.66449	0.25
Abundance (Mass %) [13]	0.0001	8	
Recyclability with Motor [36]	Poor	Good	
Density (Kg/m ³) [32] [37]	8890	2705	0.30
Electrical Conductivity (IACS) [8] [32] [37]	100%	61.8%	
Volume Resistivity ($\Omega\text{mm}^2/\text{m}$) [8] [32] [38] [37]	0.017241	0.027899	1.618
Weight Resistivity ($\Omega\text{g}/\text{m}^2$) [38]	0.15328	0.07541	0.49
Temperature Coefficient (/K) [37] [38]	0.00393	0.00408	1.04
Equivalent Cross-Sectional Area	1	1.62	
Equivalent Mass	1	0.49	
Elastic Modulus (GPa) [32] [37]	115	69	0.60
Tensile Strength (MPa) [38]	248 - 276	62 - 96.5	0.25 - 0.35
Equivalent Tensile Strength (MPa)	248 - 276	100 - 156	0.40 - 0.57
Yield Strength (MPa) [38]	62 - 83	27.5 - 48	0.44 - 0.58
Equivalent Yield Strength (MPa)	62 - 83	44.5 - 77.5	0.72 - 0.93
Elongation (%) [32] [37]	35	23	0.66
Stacking Fault Energy (erg/cm ²) [39] [40]	80-90	200-250	
Strain Hardening Exponent [40]	0.30	0.15	
Melting Point (°C) [8] [32] [37]	1083	657	0.61
Thermal Conductivity (W/mK) [32] [37]	388	234	0.60
Thermal Expansion (/°C) (20-300°C) [32] [37]	17.7	25.5	1.44
Specific Heat (J/KgK) [32] [37]	386	900	2.33
Equivalent Heat Capacity (J/K)	386	443	1.15
Oxidation (>200°C) [6] [41] [42] [26]	Continuous	Stable	

The conductivity of EC aluminum is 61.8% that of ETP copper. To form an equivalent resistance aluminum conductor, its cross-sectional area needs to increase according to the following equations:

$$\text{Resistivity} = \rho = \frac{RA}{L} \quad (1)$$

$$\text{Resistance}_{Cu} = \text{Resistance}_{Al}$$

$$\text{Length}_{Cu} = \text{Length}_{Al}$$

$$R_{Al} = \frac{\rho_{Al}L_{Al}}{A_{Al}} \quad \& \quad R_{Cu} = \frac{\rho_{Cu}L_{Cu}}{A_{Cu}} \quad (2)$$

$$A_{Al} = \frac{\rho_{Al}}{\rho_{Cu}} A_{Cu} = \frac{0.027899}{0.017241} A_{Cu}$$

$$\text{Area}_{Al} = \mathbf{1.6181} \text{Area}_{Cu} \quad (3)$$

Where R is wire resistance, A is wire cross-sectional area and L is wire length. Electrical resistivities from Table 2.1 were used resulting in aluminum requiring 1.62x the cross-sectional area/volume for equal conductivity to the same length copper wire. Actual dimensional increase differs for each conductor profile: round, square, rectangular, or strip.

Using this ratio, the mass relationship between an aluminum and copper wire of equal resistance and length can be determined according to the following equations:

$$\text{Density} = \frac{m}{LA} \quad (4)$$

$$\text{Length}_{Cu} = \frac{\text{mass}_{Cu}}{\text{Density}_{Cu} \text{Area}_{Cu}} \quad \& \quad \text{Length}_{Al} = \frac{\text{mass}_{Al}}{\text{Density}_{Al} \text{Area}_{Al}}$$

$$m_{Cu} = \frac{A_{Cu} D_{Cu}}{A_{Al} D_{Al}} m_{Al} = \frac{8890}{1.6181 \times 2705} m_{Al} \quad (5)$$

$$\mathbf{m_{Cu} = 2.0311 m_{Al}} \quad (6)$$

Where m is conductor mass and densities are taken from Table 2.1 resulting in a copper conductor being 2.03x heavier than an equivalent resistance aluminum one.

2.4 Fabrication

Modern aluminum and copper magnet wire processing methods are quite similar. They are most often formed from continuous casting in an in-line process where round conductors are cold drawn and square or profile conductors are cold rolled with intermediate annealing around 90% area reduction [6], [7]. Both materials can be drawn to very fine sizes without requiring intermediate annealing [6], [7], [29]. Drawing dies are either polycrystalline or, for finishing sizes, single crystal diamonds [7]. When switching between copper and aluminum, dies need to be thoroughly cleaned to avoid cross contamination from fines [10]. Aluminum also uses mineral based drawing lubricants instead of the soap type materials used for copper [10]. More precise and detailed information on the steps of magnet wire manufacturing can be found in [6], [7], [15] and [24, pp. 1-1 - 1-7].

The biggest difference between aluminum and copper manufacturing is the much lower tensile strength of aluminum. This requires slight modification of the forming and winding process techniques and parameters since tension control can be more difficult, but aluminum can still be handled easily and quickly [24, pp. 14-1 - 14-13], [43], [44]. Tensile strength of the formed wire is also an important consideration for the insulation application process (enamelling) [10]. For this reason, aluminum alloys with higher strength may be desirable but high temperatures can be reached during drawing and enamelling which are problematic for their final properties [19], [45]. During drawing, high speeds and highly cold worked wire coupled with insufficient cooling from the lubricant can result in temperatures up to 232°C which can initiate static recrystallization. This leads to inhomogeneous properties from the hot wire cooling at different rates as it is wound on the spool [19]. During the insulation curing process, the elevated temperatures can reduce the strength of alloyed aluminum wire to almost the same level as annealed EC aluminum, effectively mitigating the benefits of alloying [45]. Tape type insulations do not require a curing process so this problem can be avoided [45] but final wire strength after manufacturing is important to consider when deciding between insulated copper and aluminum conductors.

During fabrication, specifically the drawing stage, it is also important to consider texture changes in both metals with large cross section reductions. Copper is elastically

anisotropic meaning elastic modulus (E) and shear modulus (G) both change with texture [6], [29], [31]. E is maximum in the <111> direction where G is minimum [6], [29]. Changes to texture and these properties are most prevalent around 90% area reduction or greater [6], [29]. Therefore, it is best practise, to anneal before 90% reduction to avoid undesired changes to mechanical properties [6], [29]. Aluminum on the other hand, is very isotropic so it does not experience the same property changes with texture change at high area reduction [6], [29], [31]. Although, it is still a good idea to anneal aluminum prior to 90% reduction since grain size reduces above this level, affecting mechanical properties and in particular, increases flow stress [29], [31].

2.5 Cost

Since the 1940's, there has been a growing gap in cost between raw aluminum and copper [10]. In the early 2000's, copper started to see drastic increases in price as illustrated in Figure 1.3, especially compared to aluminum [11]. Looking at present day material costs in Table 2.1, aluminum is 25% the price of copper per kilogram. Considering the lower conductivity of aluminum, Equation (6) gives the mass ratio required for equivalent resistance conductors which can be used to determine a more realistic cost comparison of the two metals according to the following equations:

$$P = mc \quad (7)$$

$$P_{Cu} = m_{Cu} \times c_{Cu} \quad \& \quad P_{Al} = m_{Al} \times c_{Al}$$

$$P_{Cu} = \frac{m_{Cu}c_{Cu}}{m_{Al}c_{Al}} P_{Al} = 2.0311 \frac{6.54508}{1.66449} P_{Al} \quad (8)$$

$$P_{Cu} = 8P_{Al} \quad (9)$$

Where P is the total winding cost in (\$), c is commodity price in (\$/kg) and the resulting cost of an equivalent aluminum winding is 12.5% that of the copper winding. This is a substantial difference that makes the 38% lower conductivity of EC aluminum much more acceptable [11]. The substantial cost differential also has a trickle-down effect to the consumer where it is now starting to affect their buying decisions [3].

The rising and volatile price of copper is not expected to stop anytime soon as commodity price is closely tied with abundance [11]. Aluminum is the most abundant metal on earth making up about 8% of the earth's crust while copper only comprises about 0.0001% [13], [24, pp. 1-1 - 1-7]. This is the reason aluminum prices have historically been a lot less volatile than those of copper [12], [13], [28]. Attempting to predict future pricing trends, [11] estimated how many years of supply are left for each conductor based on 2008 consumption data and predicted reserves. Copper was calculated to have 31 years of supply left while aluminum has 141 years of supply left [11]. As the copper supply dwindles though, reserves that were previously deemed uneconomical and therefore left out of calculations may be usable, but regardless, the price advantage for aluminum is expected to continue or increase into the future [11].

Raw material price is only one part of the story however, and many other costs are associated with electric motor fabrication. Finished magnet wire price and commercial demand and availability also play a big role in overall magnet wire cost. There is little data available on finished magnet wire pricing but by 1989, magnet wire sizes in the range of 8-24 American wire gauge (AWG) were cheaper per unit length for aluminum with cost savings of 15-25%, or more for larger gauges over copper [24, pp. 14-1 - 14-13]. Regarding magnet wire appropriate for high frequency machines, litz or stranded aluminum wire commercial availability is low resulting in finished copper and aluminum prices being similar [11]. There is also the fact that high frequency designs use less wire, so potential cost savings from switching to aluminum would be reduced [11]. There would be extra cost and hassle associated with connecting aluminum windings to copper wire used throughout the rest of the electrical system [11].

The real issue comes from the bad reputation of aluminum touched on earlier. Aluminum used to be a very prevalent conductor in many electrical applications but the housing market crisis sparked reduced usage [3], [13]. In an attempt for manufacturers to save money on a low demand product, they started limiting available aluminum options and reducing inventory, further reinforcing the unjust reputation of aluminum being an inferior conductor [13]. Even though the problems have been solved and aluminum is just as reliable as copper, old habits and its prevailing reputation continue to limit aluminum supply [3], especially in high performance and high frequency applications.

Modification of electrical equipment also needs to be considered in overall cost. Using aluminum requires an increase in cross-sectional area to operate on an equivalent basis to copper which may require increased motor core size, more conductor interleaving, or a greater number of parallel strands [11]. However, the cost savings from switching to aluminum can offset these additional modification costs [11]. In general, cost savings by switching to aluminum based electrical equipment with identical performance to the copper counterpart are expected to be between 15-45% [3], [12], [13].

There is also the factor of electricity costs and how that impacts manufacturing and operational costs over electrical equipment life. Aluminum is produced by electrolysis, a purely electricity-based process, while copper can also be produced by electrolysis but it is not the primary production method [28]. With rising energy costs, this needs to be considered, as well as the impact generation of electricity has on global warming [11]. The argument here is that trying to save money by switching to aluminum may decrease efficiency and therefore increase lifetime operation costs and carbon footprint [11]. In which case, it may be better to optimize electrical equipment design to minimize copper use without compromising efficiency [11].

With all factors considered, the replacement of copper with aluminum wires is not purely based on raw material price, but on technological change [4]. This accounts for the lack of aluminum in high performance machinery even though it has been significantly cheaper for a long time. Address the technological disadvantages of switching to aluminum and the argument changes from simply saving money to saving money for identical performance to copper.

2.6 Recyclability

Electric motors are mainly made up of electrical steel ($\approx 40\%$), aluminum in the form of the casing or frame ($\approx 17\%$), copper or aluminum windings ($\approx 12\%$) with the remainder being insulation material, auxiliary components and permanent magnets [46], [47]. There are two main options for recycling of electric motors: shredding or disassembly and re-use [46], [47]. Shredding is mainly performed for motors under 10 kW since larger than this can damage the shredder [48]. Shredding does not allow the re-use or repair of motors/motor components that may still be good [36], [46], [47] which is why researchers

in [36] proposed an automated robot to disassemble and better recycle motors around or below 1 kW. The other main problem with shredding is contamination of electrical steel from copper. Shredding automatically sorts the multitude of motor pieces but it is an imperfect process and the amount of copper left in steel scrap is around 0.25-0.3% [36]. This is highly problematic since if copper concentrations exceed 0.02% in steel scrap, it becomes unusable for sheet steel reproduction [36]. Aluminum does not see this same problem where much higher quantities can be present in the steel scrap without affecting its quality for re-use as sheet steel [48].

Disassembly and separation of windings from the steel core requires significant effort and cost [36], [46], [47]. It does allow the re-use of still functional machine components and the separation of windings for re-melting and re-use but is quite labour intensive [46], [47]. This makes the future of recycling motors, especially small-scale motors that are being shredded, a big concern because it essentially comes down to cheap shredding with contamination of electrical steel from copper windings or costly disassembly to improve overall recyclability of the motor. The use of aluminum windings may be a solution to help mitigate this problem particularly for smaller scale motors.

2.6.1 Environmental Impact

Another important consideration when discussing aluminum versus copper conductors is their impact on the environment during manufacturing and operation over the life of the component. An environmental impact study was performed in [11], comparing aluminum and copper conductors. They found that copper had an environmental impact of 12.5 mpt/cm³ (milipoint) compared to aluminum with an impact of 2.1 mpt/cm³ [11]. Accounting for the volume increase required for aluminum, it still had 30% the environmental impact compared to copper [11].

A. Allanore in [49] conducted a more in-depth analysis of environmental impact associated with metal extraction and refinement into usable raw material. Since aluminum is produced entirely by electrolysis it has a very high specific energy (kWh per ton) for production compared to copper which is mainly produced by chemical extraction from sulfides. Results found aluminum used 18 000 kWh/t to produce where 13 000 kWh/t was used to make aluminum and 5 000 kWh/t was used to make the carbon anode required for

production which also directly produces CO₂ emissions. This is compared to copper with a specific energy of 3 600 kWh/t. [49]

Another study conducted a life cycle assessment (LCA) for equivalent copper and aluminum underground insulated and armoured cables in the Chinese market [50]. The study looked at life cycle environmental impacts for both conductors from global warming potential, acidification potential, eutrophication potential, human toxicity potential and energy consumption. Over the life of the conductor, the bulk of the environmental impact, 98%, came from losses during power transmission. Key results saw 4124 kg of copper had a power consumption of 2.1 million kWh while 1995 kg of aluminum (50% for equivalent conductors) had a power consumption of 2.2 million kWh. Equivalent aluminum and copper cables had comparable power consumption but reducing it during transmission is important to consider when comparing aluminum and copper to reduce life cycle environmental impact. Regarding the other environmental impact factors studied: copper had a consistently higher impact for transportation, 7x the human toxicity potential for the raw material, and 2.5-3x the impact for discarding and recycling with regards to acidification potential and energy consumption. [50]

2.7 Weight and Mass

One of the biggest advantages of aluminum over many metals, especially copper, is its very low density. Table 2.1 highlights the density of aluminum being 30% that of copper. However, as discussed previously, the volume of aluminum needed to make an equivalent conductor to copper must increase. Accounting for this, Equation (6) demonstrates that aluminum wires will still see a significant weight savings of 50% which is highly advantageous when lightweight design criteria are becoming more prevalent. Another way to view this is by reviewing the electrical resistivity by weight for both conductors in Table 2.1. Here aluminum sees a 49% lower resistivity. This can be better understood as 1 kg of aluminum has twice the conductivity as 1 kg of copper or the same conductivity as 2 kg of copper [3], [12], [13], [24, pp. 2-1 - 2-4].

The significant weight savings provided by aluminum was the main driving factor for its nearly exclusive use in power delivery. Aluminum started being introduced into overhead power lines as early as the 1890's and at this time it was significantly more

expensive than copper [4]. However, the weight savings allowed for longer spans between support towers, less robust support equipment, and easier handling and labour which resulted in reduced capital and installation costs [3], [4], [24, pp. 2-1 - 2-4]. This also made aluminum a popular choice for power and distribution transformers as well as bus conductor where 50% weight savings is substantial when millions of pounds of conductor is used which results in labour and support equipment robustness being reduced [3], [24, pp. 13-1 - 13-70], [24, pp. 14-1 - 14-13]. Aluminum wire in duct work or conduit also sees advantages where fewer pull in points are required, longer spans can be used vertically, and pulling drag is reduced since it is proportional to weight [3], [4].

Reduced weight of aluminum windings can be advantageous in portable equipment or where maximum payload capacity is desired like in lifting electromagnets, or aerospace applications [24, pp. 14-1 - 14-13] [25]. This can transfer to the automotive industry in which the benefits of weight reduction are crucial [51]. A 4m long 12 V battery cable was replaced with aluminum in [51] which resulted in 1.4 kg overall vehicle weight savings. Accounting for the increased cross section of aluminum, and in turn, greater amount of insulation used, 30-40% weight savings could be had for wires longer than 300 mm [51]. Rotating machinery can also see significant advantages from the reduced weight offered by aluminum due to reduced inertia, easier dynamic balancing, reduced vibration and in turn, increased machine life [4], [24, pp. 14-1 - 14-13].

In general, for identical performance, equipment utilizing aluminum will be cheaper, and lighter [3]. In most situations, equipment size will remain the same for both conductors but certain applications like dry type transformers, conduit, and bus bars will see a size increase that needs to be considered carefully [3]. In these instances, larger conduit and more space may be required for machinery as well as larger magnetic circuits which could mitigate weight savings [3], [25]. However, the much higher density of copper may increase its carbon footprint resulting in overall lifetime efficiency being reduced [52]. There is also the factor of advantages to labour and install with aluminum as well as less costly and robust supporting equipment when aluminum is used [3]. At the end of the day, if weight is a design concern, aluminum should be considered but if size is constrained, copper may be the better choice [3], [7], [12], [13], [23], [29].

2.8 Mechanical Performance

The following subsection relates the mechanical properties of aluminum and copper to their performance in manufacturing and windings processes as well as operational use.

2.8.1 Equivalent Conductor Strength

In general, looking at the mechanical properties for aluminum and copper in Table 2.1, annealed EC aluminum has lower properties than ETP copper across the board. EC aluminum is a softer and weaker metal compared to ETP copper, but this does not consider equivalent sized wires. Aluminum requires a larger cross-sectional area by 62%. Accounting for this, the strength of an equivalent conductivity aluminum wire increases by the same area ratio from Equation (3) resulting in the following relationship:

$$Strength_{Equivalent\ Al} = 1.6181Strength_{Al} \quad (10)$$

The results of this equation are found in the 4th column (Al/Cu Ratio) of Table 2.1 in the equivalent tensile and yield strength rows. Equivalent annealed EC aluminum sees a tensile strength increase from 35% that of copper to 57% while yield strength increases from 58% that of copper to 93%. Depending on the aluminum alloy used and what type of hardened state it is in, the equivalent resistance aluminum wire will be nearly as strong as copper, effectively making its lower strength properties a non-issue [3], [4], [12], [13].

2.8.2 Cold Workability

From Table 2.1, aluminum and copper have stacking fault energies (SFE) of 200-250 erg/cm² and 80-90 erg/cm² respectively [39], [40]. Conversely, their strain hardening exponents are 0.15 and 0.30 for aluminum and copper respectively [40]. This means that aluminum, with a much higher stacking fault energy, will have shorter spacing between partial dislocations resulting in lower stacking fault probability, less force required for partial recombination, and easier cross slip at lower stresses [39], [40]. This means it will not strain harden easily or to a great extent since dislocations are harder to pin down [39],

[40]. The opposite is true for copper which strain hardens more quickly and to a greater extent [39], [40].

Plastic deformation occurs locally at the weakest part of the material or gauge length. This causes the material to strain harden, increasing resistance to further plastic deformation. Applied stress then increases and concentrates at the next weakest part where it strain hardens as well. The cycle continues as the gauge length increases and cross section reduces until the strain hardening capacity of the material is reached. Necking then occurs followed by material failure. This means the higher stacking fault energy of aluminum makes it harder to form than copper in processes which require excessive deformation. Copper will strain harden easier and to a greater extent, spreading the strain out over the work piece. Aluminum is not as effective at spreading out the strain, instead localizing it. This results in aluminum experiencing plastic instability/necking sooner than copper, making it a less viable option for excessive deformation processes like deep drawing. [39], [40]

2.8.3 Influence on Formability and Windability

The higher SFE of aluminum is one of the reasons it has lower tensile and yield strength as well as lower elongation compared to copper. As illustrated above, its higher SFE is disadvantageous for processes like deep drawing but it can be advantageous in electrical conductor manufacturing and coil winding. Both aluminum and copper have good formability and can be easily drawn to very fine wire sizes, and up to 90% area reduction before requiring intermediate annealing [6], [29]. In terms of **Workability** (ability of a wire to withstand single or repeated bending and ability of bus bar to be bent to a specific radius in either dimension), aluminum compares well with other metals allowing it to be drawn, extruded and rolled with excellent bend quality [24, pp. 2-1 - 2-4]. Coil winding typically sees wire elongation up to 10% [53], [54] so the higher SFE of aluminum will not be problematic here either.

The lower yield strength of aluminum means less strain energy is required to form it and will better conform to an arbour during manufacturing and winding [24, pp. 14-1 - 14-13]. Machines working with aluminum can run faster and with wire sizes 4x larger than the largest acceptable copper wire [24, pp. 14-1 - 14-13]. In the case of hand winding,

operator fatigue will be reduced from lower yield strength since it is much easier to handle compared to copper [24, pp. 14-1 - 14-13]. However, yield strength is responsible for resistance to deformation from mechanical and electrical forces, like centrifugal, surge, overload, and short circuit forces which can impose extreme stress on windings [10], [26], [45]. The lower yield strength of annealed EC aluminum means it will be less resistant to these forces. This is why copper is almost exclusively used in large power transformers [28] and why there is such a big emphasis on improving the strength of aluminum alloys without altering electrical conductivity.

Tensile strength is responsible for determining winding tension and travel speed during manufacturing [26], [45]. Aluminum, having a lower tensile strength than copper, requires lower winding tensions [11]. This coupled with its lower yield strength and stiffness actually makes aluminum easier to wind than copper [10], [55]. This also relates to springback, and **Conformability** (ability of a magnet wire to maintain its shape during forming or winding with minimal springback [7], [29]). Aluminum's lower elasticity and strength mean it can better retain deformation [9] which then results in less springback compared to copper [24, pp. 14-1 - 14-13]. Springback directly impacts coil winding space, mean turn length, ease of manufacturing, in service performance, and product costs [45]. Since aluminum experiences lower springback, less winding tension is required to form coils that better conform to coil shape, are more compact, have shorter end turns and more efficiently use available space which also helps compensate for its lower conductivity [10], [24, pp. 14-1 - 14-13], [55]. The overall motor package could then be reduced since end windings are shorter resulting in reduced motor costs. This also means that rectangular aluminum coils will experience less side bow [24, pp. 14-1 - 14-13]. When higher strength aluminum conductors are required, either by strain hardening or alloying, the benefits it sees with lower springback and better conformability will be reduced or negated [45].

2.9 Electrical Performance

As highlighted in Table 2.1, the electrical conductivity of EC aluminum is 61.8% that of copper. According to Equation (3), aluminum requires a cross-sectional area 62% larger than copper to form an equal resistance wire. It was also demonstrated in Section 2.7 that copper has a weight resistivity 49% that of copper meaning it has twice the

conductivity on a per pound/kilogram basis. In general, a 2 gauge size increase is required for aluminum to replace copper [24, pp. 14-1 - 14-13]. With regards to electric motors, aluminum generally cannot be implemented in a machine designed for copper at the larger size required [24, pp. 14-1 - 14-13]. However, some motors, like high frequency machines which frequently use less copper than available space in the winding window, or induction machines, could accommodate aluminum without modification [11], [24, pp. 14-1 - 14-13] thanks to the advantages illustrated in the previous section. In transformers, aluminum cross-sectional area needs to increase to accommodate both its lower conductivity and strength. This may also be achieved with increased stack length or larger laminations but can result in a size increase to the transformer container and more oil used in the case of oil type transformers [24, pp. 14-1 - 14-13], [4]. In general, when looking to replace copper with aluminum windings in electric machines without changing machine geometry and keeping ohmic winding losses the same, all variables become equal except conductivity and slot fill factor [9]. Therefore, either the conductivity of aluminum or the slot fill needs to be increased for effective replacement in this scenario [9].

2.9.1 AC vs DC Performance

The most common comparison of electrical conductivity between aluminum and copper is direct current (DC) resistance where EC aluminum has 61.8% IACS [4]. However, this is not suitable for technologies that use alternating current (AC) like high performance motors [4]. Therefore, it is better to compare the AC resistance of both conductors, but this is difficult since it depends on the system operating parameters and type and size of wire used [4]. There is still a DC resistance component in these electric motors though so overall machine loss depends on both AC and DC components [56].

AC losses for motor windings are generally broken down into skin effects (inversely proportional to the square of conductivity) and proximity effects (proportional to conductivity) [11], [57]. Therefore, higher electrical resistivity (lower electrical conductivity) in AC applications reduces AC losses giving an advantage to aluminum [11], [56]. Regarding losses involving skin effect, the skin depth in aluminum is 1.28x that of copper due to its lower conductivity [57]. Accounting for the larger cross section of aluminum required gives it further advantages since more outer surface area is available to

accommodate skin effect which results in more efficient conductor utilization [12], [13]. Regarding proximity losses, for the same size conductors, aluminum will see 61% the losses of copper, but for equivalent conductors, where aluminum surface area increases, it actually sees greater losses by 64% but using stranded conductors could help mitigate this increase [57]. Since aluminum sees reduced AC losses, higher slot fill can be accommodated which results in lower DC losses, further compensating for its lower conductivity compared to copper [58], [59].

Authors from [11] performed an analysis of AC losses between aluminum and copper with optimization formulas for three winding types: standard, foil, and litz. They found that optimal standard windings saw 18% higher losses for aluminum that required a 39% increase in volume but cost 35% that of the copper winding based on raw material price [11]. The optimal foil winding saw a smaller volume increase of 28% but even cheaper windings at 15% the cost of copper. Optimal litz wire had the same losses for both metals but aluminum was 19.5% the cost of copper [11]. However, aluminum litz wire is not widely available so once the increased cost of manufacturing and supply is incorporated, the cost benefit of aluminum may be reduced [11]. More detail on the advantages and disadvantages of aluminum in AC and high frequency applications is found in Sections 2.15.1.7, 2.15.3 and 2.15.4.

2.10 Thermal Performance

The following subsection relates the thermal properties of aluminum and copper to their performance in various electrical applications.

2.10.1 Melting Point and Annealing Behaviour

Looking at thermal properties in Table 2.1, aluminum has a 39% lower melting temperature at 657°C compared to copper at 1083°C. As discussed in Section 2.4, magnet wire is most often made by an in-line process. This means annealing and enamel curing occur in line creating a bottleneck in the process to accommodate the time necessary to properly anneal the wires and cure the insulation [6]. In an effort to maximize production speed, furnace times are kept short making conductors with low recrystallization

temperatures more desirable [6] so they can achieve the required level of annealing quickly. Aluminum has a lower melting temperature and therefore a lower recrystallization temperature allowing for the possibility of more rapid in-line manufacturing. This can also be disadvantageous however, since enamel curing temperatures are generally high enough to anneal aluminum wire [10]. This can also be problematic for aluminum when soldering or during temperature spikes from faults in operation causing softening if not already in an annealed state [4].

2.10.2 Thermal Conductivity

From Table 2.1, the thermal conductivity of EC aluminum is 60% that of ETP copper at 234 W/mK and 388 W/mK respectively. It can also be seen that the temperature coefficient of resistance for aluminum and copper is almost the same at 0.00408/K and 0.00393/K respectively. This means that the conductivity ratio between aluminum and copper will remain pretty much the same over a wide range of temperatures [9]. Due to its lower thermal conductivity, aluminum dissipates heat from hot spots less quickly than other metals [24, pp. 2-1 - 2-4]. However, for equivalent fill factors, the cross slot thermal conductivity of aluminum is only slightly lower than that of copper [57]. Similar results were found in [60] where little difference in thermal conductivity was observed between equivalent aluminum and copper windings. This is beneficial for aluminum since it performs similarly to copper despite its much lower thermal conductivity. Regarding the necessary volume increase for equivalent aluminum, bus bars can increase in width by 27% or thickness by 50% [24, pp. 13-1 - 13-70]. The former reduces resistance heating and increases thermal heat transfer area resulting in increased heat dissipation [24, pp. 13-1 - 13-70].

In general, it is a misconception that aluminum runs hotter than copper [12], [13]. Manufacturers build machines to satisfy performance criteria or temperature rise standards so if designed properly, the temperature rise for both conductors will be similar [3], [12], [13].

2.10.3 Thermal Expansion

Thermal expansion needs to be carefully considered when replacing copper with aluminum as it has a 44% higher expansion coefficient at 25.5/°C compared to copper at 17.7/°C over a temperature range of 20-300°C, as seen in Table 2.1. This can be problematic for electrical connections, especially those with stronger, dissimilar metals, causing reliability concerns over time from thermal cycling [3]. These problems became painfully clear in the 1960's and 70's as discussed in Section 2.1.1. For wire used in conduit, ducts, or underground, thermal expansion generally translates into lateral motion known as “snaking” rather than overall movement of the wire [4], [24, pp. 2-1 - 2-4]. This means more room is required in these scenarios to accommodate the switch to aluminum [4]. As the main discussion of this study is the replacement of copper with aluminum in high performance electric motors, the larger volume of aluminum required for equivalent resistance needs to factor in thermal expansion. This is especially important when trying to maintain overall machine geometry or increasing the slot fill with aluminum conductors.

2.10.4 Specific Heat and Heat Capacity

Having a high thermal capacity is very important for conductors that experience temporary short circuits, surge or overload conditions where the associated abrupt temperature rise needs to be absorbed to mitigate the extent of overall wire temperature increase and damage inflicted to its insulation [4], [9]. These scenarios are often found in power delivery systems like overhead power lines and transformers, or in solar aircraft during take-off [9], [24, pp. 6-1 - 6-16]. From Table 2.1, aluminum has 2.33x the specific heat of copper. This is highly advantageous for aluminum, giving it the ability to better withstand short circuit, surge and overload conditions [12]. However, the mass difference between equivalent aluminum and copper conductors needs to be considered to properly compare their performance. Using the mass relationship from Equation (6), specific heat values from Table 2.1, and the mass of a copper as 1 kg, the heat capacity for an equivalent aluminum conductor is calculated according to the following equations:

$$C = mc \quad (11)$$

$$C_{Equivalent\ Al} = \frac{m_{Al}}{m_{Cu}} c_{Al} \quad (12)$$

$$Heat\ Capacity_{Equivalent\ Al} = 443.13\ J/K \quad (13)$$

Where C is the heat capacity (J/K) of the wire, m is the mass of the wire and c is the specific heat (J/kgK) of aluminum or copper resulting in aluminum having a 15% higher heat capacity than copper. Therefore, equivalent conductivity aluminum is still a good option for the above-mentioned scenarios compared to copper [13].

2.10.5 High Temperature Use

Current electric machines have maximum ambient temperatures of 130-150°C which corresponds to maximum internal temperatures of 180-200°C [61]. Magnet technology exists to operate at temperatures higher than this, so the current limiting factor is conventional organic based electrical insulations [61]. High temperature operation also poses a problem to conductor strength, especially for strain hardened wires. At operating temperatures between 80-100°C, low temperature annealing can reduce aluminum strength by 5-10% over the long term [26]. This is accelerated at higher temperatures like those seen in short circuit, surge, or overload conditions where temperatures can reach 250-300°C resulting in strain hardened wire reducing to annealed conductor strength levels over time [26].

This was a concern for high strength aluminum alloys in overhead power lines where a **Thermal Limit** (maximum continuous operating temperature which maintains minimum tensile properties) [24, pp. 6-1 - 6-16] was set to mitigate strength loss over the long conductor life [24, pp. 3-1 - 3-26]. This also ties in with overload figure of merit discussed in [44] where aluminum was found to be higher than copper, even under strained conditions meaning aluminum is more stable at high temperatures [44]. In general, aluminum can withstand higher operating temperatures since copper is susceptible to flaking and rapid oxidation above 200°C where aluminum does not experience the same problems, even up to melting temperature [25]. However, there are concerns over the ability of aluminum conductors to maintain their shape above 150°C operating

temperatures [9]. There are also the advantages anodized or insulated aluminum strip conductor can provide in high temperature applications, but these will be discussed further in Section 2.15.1.

2.11 Corrosion

Aluminum is more prone to oxidation with a valence of +3 compared to copper with a valence of +1 which explains why it is not found in nature as a pure element but as a combination of elements [24, pp. 1-1 - 1-7], [28]. In its processed form, aluminum is always covered by a tenacious thin film of aluminum oxide which forms almost immediately in the presence of air and does not continuously grow [12], [13], [24, pp. 1-1 - 1-7], [24, pp. 2-1 - 2-4]. This gives it excellent natural corrosion resistance that can be further improved with anodizing [24, pp. 2-1 - 2-4]. If the oxide layer is broken in the presence of air, it will quickly reform to protect the underlying aluminum [12], [13]. However, if it is broken in a moist environment with limited or no exposure to air, it will corrode [13]. Copper on the other hand, has good corrosion resistance and is covered by an oxide layer but it will continuously grow over the life of the conductor [12], [13].

Looking at corrosion rates in various environments for aluminum and copper in Table 2.2, it is clear that aluminum has good corrosion resistance compared to copper [13], [24, pp. 17-1 - 17-8]. Weather tests performed for 30 years in simulated industrial environments which include hydrogen sulfide, ammonia, and sulfur dioxide have also highlighted the good corrosion resistance of aluminum [10]. This allows it to better compete against copper in industrial and coastal environments for use as overhead power lines and bus bars, especially since copper wire and silver coatings are very susceptible to corrosion from hydrogen sulfide [3], [24, pp. 13-1 - 13-70]. Copper can still be used here but it requires tin plating instead, where silver and nickel plating can help with corrosion resistance in other environments [29]. Where better corrosion resistance is required for aluminum and its connections, nickel plating can be used [10]. Aluminum also has better corrosion resistance when used with rubber type insulations since they contain sulphur which corrodes copper [4].

The focus has been on environmental corrosion but with regards to electrical connections between aluminum and copper, galvanic corrosion can occur [10]. When connected together, aluminum is more susceptible to corrosion in the presence of an electrolyte since the two metals form a galvanic cell where aluminum is anodic to copper [4], [51]. This means aluminum to copper connections need to be waterproofed to avoid corrosion [4]. Rapid and secure connection techniques which encapsulate the joint are available to combat this issue [10]. The use of hermetic motors can also help mitigate this problem since no electrolyte is present to cause galvanic corrosion [62].

Table 2.2. Corrosion rates (average mils per year) for solid metals in various environments [13], [24, pp. 17-1 - 17-8].

ATMOSPHERIC CORROSION OF SOLID METALS OVER A 10 YEAR PERIOD					
Atmos- phere	Location	Al	Cu	Zn	Pb
Desert	Phoenix, AZ	0.000	0.005	0.010	0.009
Rural	State College, PA	0.001	0.023	0.042	0.019
Coastal	Key West, Florida	0.004	0.020	0.021	0.022
Coastal	La Jolla, CA	0.028	0.052	0.068	0.016
Industrial	New York, New York	0.031	0.047	0.190	0.017
Industrial	Altoona, PA	0.025	0.046	0.190	0.027

2.12 Connections and Terminations

2.12.1 Problems with Aluminum Connections

Connections and terminations with aluminum conductors were one of the biggest hurdles to its wide spread use [4] and the biggest factor in its bad reputation developed during the housing wire crisis of the 60's and 70's. The differing mechanical properties of aluminum, especially its thermal expansion, did not allow easy and reliable use of preexisting connection technologies developed for copper. The main factors that affect the stability, quality, and reliability of aluminum connections are: aluminum's natural oxide layer is electrically insulative, differing thermal expansion coefficients, galvanic corrosion

with dissimilar metals, stress relaxation, cold flow, intermetallic compound formation, and fretting [55], [63]. All these factors lead to deterioration of the connection and a resulting increase in contact resistance leading to failure [11], [63]. Today, connection concerns are a thing of the past as many new techniques optimized for aluminum have been developed, even automated ones, that when used according to regulation, provide connections and terminations as reliable as copper [11], [12], [24, pp. 14-1 - 14-13].

Copper oxides, chlorides, and sulfides are more conductive than those for aluminum which means without removal of aluminum oxide, contact resistance increases and a poor connections result [3]. Where connections loosen from thermal cycling, oxidation of the joint can occur forming an electrically resistive layer that further degrades the connection [11]. Away from connection points though, as discussed in the previous section, aluminum oxide is advantageous and protects the conductor from corrosion [3]. To combat aluminum oxide, many modern solutions exist but one is to plate the aluminum connection with silver, tin or nickel to form reliable connections [3], [24, pp. 11-1 - 11-27], [63]. Welding, brazing, and staking break the aluminum oxide so it is not problematic for these techniques [12]. High pressure crimp or compression connections also work to break and pierce the aluminum oxide and form an air tight seal to prevent further oxidation [10], [23], [24, pp. 2-1 - 2-4], [24, pp. 11-1 - 11-27]. Oxide inhibiting compound is used to remove present oxide and prevent future growth [24, pp. 2-1 - 2-4].

Connection problems with thermal expansion have been discussed previously in Section 2.1.1. Aluminum has high stress relaxation compared to copper, experiences cold flow at moderate stresses, has a higher creep rate and is more prone to fatigue compared to copper [4], [12], [13], [20], [29]. These all gradually decrease connection clamping pressure during thermal cycling which increases contact resistance, ultimately leading to connection failure [20], [51]. Modern solutions incorporate Belleville spring washers to maintain clamping pressure and longer connections to distribute clamping force to accommodate creep [4], [12], [13], [20], [24, pp. 11-1 - 11-27].

2.12.2 Aluminum Joining Techniques

Modern connection technologies and techniques solve the problems of the past providing electrical connections as reliable as those made for copper. Screw type

connectors are a viable option but only aluminum bolts should be used for aluminum wire [11], [24, pp. 11-1 - 11-27]. Conventional soldering is effective with the same tools and techniques used for copper but special procedures, solder, and flux are required [24, pp. 14-1 - 14-13]. Ultrasonic soldering can also be used which breaks up aluminum oxide allowing the solder to wet the aluminum surface [10]. Multiple welding techniques provide easy and reliable connections, often with minimal to no surface preparation including: shielded inert arc welding, spot welding, cold welding and cold pressure welding, [11], [24, pp. 13-1 - 13-70], [24, pp. 14-1 - 14-13], [25], [64].

2.13 Insulation Performance

In general, insulation applied to aluminum can operate one IEEE temperature class higher than copper with the same lifespan or for a longer lifespan when operated at the same temperature [24, pp. 14-1 - 14-13]. The advantages aluminum sees with regards to thermal aging are illustrated in Figure 2.2. The residual breakdown stress for a polyesterimide insulation applied to both aluminum and copper in [65] shows the same behaviour where copper accelerates degradation of insulation while aluminum has little to no affect. Results from this study are shown in Figure 2.3. At a 230°C aging temperature, copper saw an increase followed by a drastic decrease in breakdown stress past 1000 hours while aluminum gradually decreased [65]. The reasons for this are explained by the differing behaviour of the natural oxide layers present on both aluminum and copper.

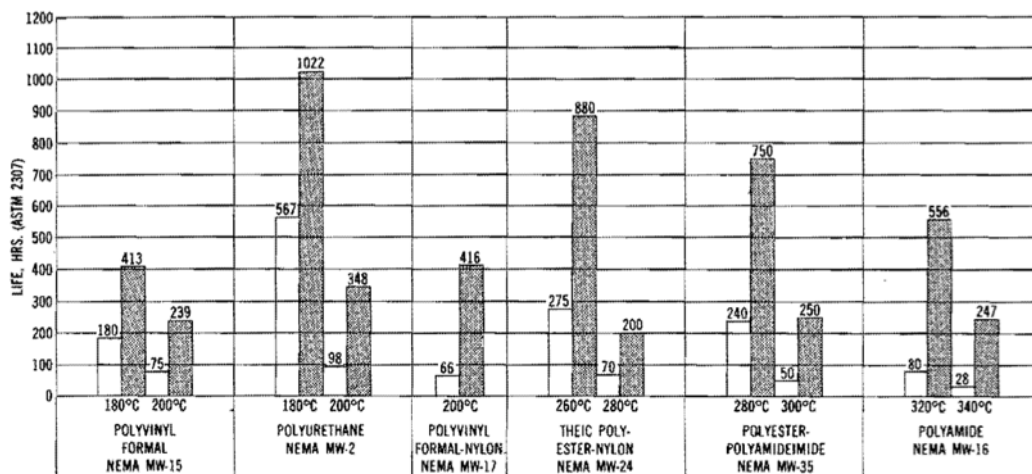


Figure 2.2. Thermal life comparison between various insulations applied to aluminum and copper where aluminum is represented with grey bars and sees longer life for all insulation types [24, pp. 14-1 - 14-13].

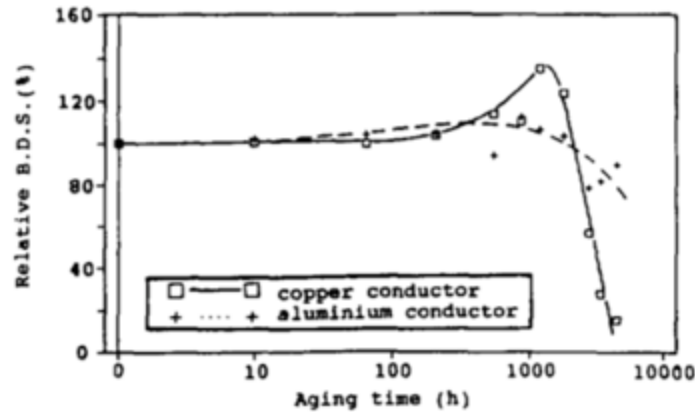


Figure 2.3. Relative breakdown stress versus aging time for aluminum and copper magnet wire at 230°C aging temperature [65].

It is known that copper will oxidize continuously over time while aluminum has a thin and stable oxide layer that protects it from further oxidation [12], [13], [26], [65], [66]. Above 200°C, copper oxidation becomes rapid with its rate and severity being dependent on temperature and insulation oxygen permeability [42]. During thermal aging, this copper oxide layer grows unstably into the underlying conductor [26], [42], [66]. As a result, the effective conductor cross section reduces, increasing electrical resistance, and further intensifying heating and oxidation rate [42]. This can lead to ultimate conductor failure, but the insulation usually fails before this occurs [42]. Copper oxide will also grow into the insulation layer, thinning and degrading it, leading to premature failure [29], [65]. Copper oxide bonds very well to insulation material, but as it grows and becomes thicker, its brittle nature results in fracture and delamination from the copper substrate [6], [26], [41], [42], [66]. These localized delamination zones experience stress concentrations from mechanical and electrical forces during operation, ultimately leading to enamel failure [42]. An illustration of this phenomenon is found in Figure 2.4 where the oxide is seen growing into both the conductor and enamel along with a crack between the two where delamination occurred [29].

Therefore, above 200°C, copper acts as a catalyst to insulation degradation due to unstable copper oxide growth while aluminum oxide remains stable with excellent adhesion to the base metal, showing overall better stability at high temperatures [6], [10], [26], [42], [66]. This allows aluminum to have better resistance to long term aging and a higher thermal index for some insulations, operating 10-20°C higher than copper [6], [26].

In general, for the same insulation, thermal life of the copper magnet wire will be a percentage that of the aluminum one but below 200°C or in reduced oxygen environments, where the copper oxide is more stable, performance differences between the two metals will be less significant [42], [67].

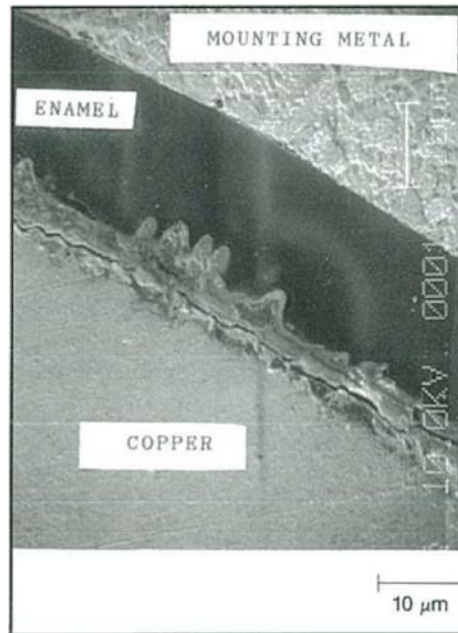


Figure 2.4. Cross section highlighting copper oxide growth of thermally aged sample at 240°C for 1500 hours and resulting oxide fracture causing enamel delamination [29].

2.14 Alternative Conductors

This subsection looks at alternative conductor materials instead of conventionally used round or square EC aluminum wires to compete with copper. This includes induction motor rotors, anodized aluminum strip conductor, copper clad aluminum, carbon nano tubes, and new alloys and processing techniques to create simultaneously high strength and high conductivity aluminum conductors.

2.14.1 Induction Motor Rotors

The topic of aluminum versus copper used in induction machines is substantial enough to result in its own literature review. As the main concern of this study is the use of aluminum magnet wires in high performance motors, only a brief review of some advantages and disadvantages between aluminum and copper rotor bars is given below.

Squirrel cage induction machines are one of the most popular motors used in household appliances, heavy industrial equipment, and recently in the Tesla Model S [24, pp. 16-1 - 16-6], [68]. The introduction of aluminum casting technology in induction machines to make rotors, end rings, and cooling vanes in one piece dramatically improved the economics of their manufacture [24, pp. 16-1 - 16-6]. Aluminum cast rotors also improved reliability and rotor balance for less vibration during operation, especially at high speeds [24, pp. 16-1 - 16-6], [69]. The lower weight of aluminum reduced centrifugal forces and their effects on motor components [24, pp. 16-1 - 16-6], [69]. Rotors make up a large part of overall motor mass so the reduced weight provided by aluminum reduced inertia which if too high can limit motor capabilities [24, pp. 16-1 - 16-6], [70]. When copper rotor bars are used, they need to be placed deeper in the rotor core so there is extra steel lamination thickness above them to better retain the bars and resist the extra centrifugal forces associated with their heavier weight [69].

The lower conductivity of aluminum decreases overall machine efficiency compared to copper slightly but it does improve starting torque [24, pp. 16-1 - 16-6], [70]. In general, using copper instead leads to improved motor efficiency but since the rotor only accounts for about 20% of overall machine losses, efficiency increase is small [70], [71], [72]. However, even with a small efficiency increase, the reduced losses and therefore operating costs over machine life could compensate for the increased initial costs of using copper instead [71].

Copper can be implemented in two ways, as a cast rotor to directly compete with cast aluminum rotors, or as fabricated bar rotors [69]. The high melting temperature of copper means conventional die materials do not work so exotic materials are required to make special high temperature dies [70]. This makes casting copper rotors extremely expensive due to the much higher tooling cost and very short lifespans of casting dies [70], [72]. The higher temperatures seen during casting copper can also negatively affect the electrical steel laminations [72]. This results in low availability of cast copper rotors worldwide, limiting their use to special purposes like high speed electric vehicle motors [72]. Instead, fabricated copper rotors can be used which are more popular for large motors while aluminum cast rotors are very popular and more economical for small motors [69]. One advantage of fabricated copper rotors is their repairability due to easy access to rotor

components and re-baring being a simple operation [69]. It is generally more economical for an aluminum rotor to be re-cast but the manufacturer would be required to do this, adding to the service time [69].

2.14.2 Aluminum Strip Conductor

A 1955 article discussed a new type of aluminum conductor in the form of a very thin strip insulated with anodic aluminum oxide rather than conventional insulation methods which was introduced by the Reynolds Metals Company [22]. Coils of this new aluminum strip could be made very compact without conventional insulation layers to accommodate the 60% increase in volume needed for aluminum without increasing equipment size [22]. These new aluminum coils were 50% lighter than conventional round conductor copper coils, saw excellent heat transfer, no hot spots formation since every conductor was exposed, resisted burnout since they could operate up to the melting point of aluminum and easily accommodated automation for reduced costs [22]. There was also the advantage of anodic aluminum being integral to the conductor with excellent adhesion to the base metal rather than an external layer bonded to the wire with a varnish.

Aluminum strip conductor was able to take advantage of the superior properties of anodic aluminum oxide insulation where round conductors could not. Aluminum oxide is extremely hard, inelastic, and brittle so it worked well on straight conductors but during winding, cracking of the insulation occurred making them unsuitable for use [24, pp. 14-1 - 14-13], [73]. However, it could successfully be used on aluminum foil around 0.1mm thick with around 5um of oxide insulation. The one issue with strip conductor is the weakness of the insulation at the edges where mechanical stress are high from tight bending radii, friction, and external wear making it more susceptible to breakdown and failure [74], [75]. Natural porosity of aluminum oxide is also an issue which requires sealing to prevent problems associated with moisture during use [64], [76].

The biggest advantage of anodized aluminum strip is seen in high temperature operation where it can effectively be used up to the melting point of aluminum (657°C) since aluminum oxide starts to melt above 2000°C [25], [64], [73]. This is especially important today since high temperature machines like those used as air extractor fans for fires or actuator motors for plane landing gear are becoming more popular, necessitating

the demand for higher temperature insulations [76]. As it stands, commercially viable high temperature motors do not yet exist [74] so anodized aluminum strip seems like a promising option. Aluminum foil, although it has lower thermal conductivity than copper, also sees very good heat transfer [25], [64]. Heat from the centre of the coil is transferred to the edge and motor casing faster than conventional round wire coils allowing it to withstand larger surges, reducing required safety factors [25], [73]. Aluminum foil coils also see smaller inter turn voltages, eliminating the need for extra and expensive insulation required for conventional round copper wires [25], [73].

2.14.3 Copper Clad Aluminum

Copper clad aluminum (CCA), pictured in Figure 2.5 [77], is a bimetallic compound conductor made of an aluminum core, generally EC aluminum, with a copper cladding that makes up either 10% or 15% of the wires cross-sectional area [11], [78], [79]. It combines optimal properties of both conductor materials in one package [11], [78], [79]. This includes the significant weight savings of aluminum along with the high conductivity of copper and its excellent solderability and connection advantages since aluminum and its electrically resistive oxide are not on the surface [11], [78], [79]. Density, conductivity, and strength are slightly higher than that of pure EC aluminum [78], [79].

CCA is generally meant for special purpose, high frequency applications [11] where the current resides mostly on the skin of the conductor, hence the copper cladding for the highest conductivity where the current concentrates. Generally, for high frequency AC applications one would use a wire diameter smaller than the skin depth of the application to essentially negate losses from skin effect all together [11]. However, some



Figure 2.5. Copper Clad Aluminum wire [77].

high frequency applications also have significant DC current such as in single layer windings or motors that operate at both low and high speeds; making CCA conductors more advantageous to use than conventional small diameter stranded or litz wires [11]. Copper clad aluminum would also be advantageous in these scenarios where it would be difficult to make connections with aluminum since CCA shares all of the connection advantages of copper [11]. CCA can be used in many applications but some notable ones are in regular and high performance audio applications, wireless power delivery, extreme temperature sensors and even residential power conductors as a substitute to aluminum [78], [79].

2.14.4 Carbon Nanotubes

Carbon nanotubes (CNT) are a newer technology being explored as an alternative to both copper and aluminum with a host of advantages over both, although a lot of work is still required to create an effective conductor “wire” to use in electrical applications. Carbon nanotubes have very high electrical conductivity since electric charge can travel through the CNT with virtually no scattering [52]. This results in a theoretical current density of 100 MA/cm² which is roughly 1000x that of conventional conductor metals like copper [52]. A CNT has an electrical conductivity of 100 MS/m compared to 59.6 MS/m and 35 MS/m for copper and aluminum respectively [52]. However, carbon nanotubes are used in a macroscopic yarn, which has a dramatically lower conductivity, around 3.4 MS/m, but at the time of writing [52], it was improved to 10 MS/m. This is substantially lower than both copper and aluminum, requiring a large volume increase for equivalent performance [52], [80].

The mechanical and electrical properties of carbon nanotube yarn can help compensate for its low conductivity. Firstly, it has a density of 1500 kg/m³, 17% that of copper and 55% that of aluminum giving it an advantage where weight is a design constraint and volume is not [52], [80]. They also have good flexibility, high bending fatigue resistance, good corrosion resistance, and high strength and elastic modulus [52]. Regarding electrical performance, the carbon nanotubes in the macroscopic yarn act as individual conductors, effectively acting as a litz wire and eliminating any impact from skin effect [52], [80]. Proximity effects can also be all but eliminated if processed as

multifibres which can be transposed [52]. Temperature coefficient of resistance for CNT yarn is negative, or very close to zero, meaning there will be no increase in joule loss or reduction in conductivity as temperature increases [52], [80]. For example, at a 150°C operating temperature and accounting for eddy current and circulating current losses, a copper conductor will see its conductivity drop from 59.6 MS/m to around 32 MS/m while the CNT yarn will have the same conductivity as it did at room temperature [52]. Therefore, carbon nanotubes have a lot of advantages in AC and high frequency application compared to aluminum and copper conductors [52].

Both [52] and [80] illustrate these advantages by testing CNT yarn in a high-speed permanent magnet synchronous machine and a coreless multidisc axial flux permanent magnet machine respectively. Test results from [52] found merit to using CNT and with further advancements of its macroscopic yarn conductivity, it will catch up or surpass copper making it a viable alternative. Researchers in [80] compared CNT yarn to standard and litz copper wire as well as aluminum wire. The size difference of all 4 motors and the associated volume increase necessary for aluminum and CNT is illustrated very well in Figure 2.6 for equivalent produced torque and loss per dissipation area [80]. Although the CNT machine was the largest, its weight was only slightly higher than that of the aluminum machine while both copper machines were significantly heavier due to the much higher density of copper [80]. Power density per unit volume and unit mass were compared for each machine with aluminum and CNT having the higher power density per unit mass at all speeds tested [80]. Past 7000 rpm however, the CNT machine had the highest power density by mass meaning it is already competitive to both copper and aluminum at the significantly lower 6 MS/m conductivity used in this study [80].

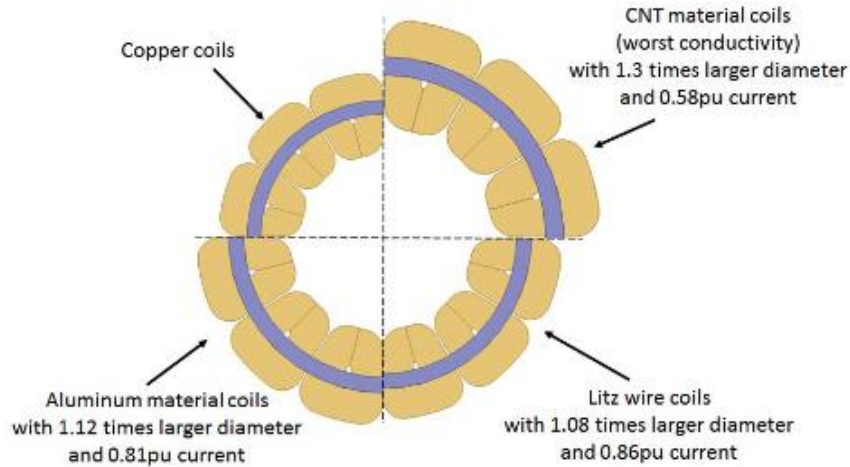


Figure 2.6. Motor size comparison between copper, copper litz, aluminum and CNT stator coils [80].

2.14.5 Improving Aluminum Electrical Conductivity

2.14.5.1 Improved Boron Treatment

It was discussed in Section 2.2.1 how the addition of boron in aluminum improves its electrical conductivity by tying up impurities as borides, removing them from solid solution where they do the most harm to electrical conductivity. Researchers in [30] took this a step further by trying to improve the conductivity of AA1070 with a modified boron treatment. Titanium is normally an impurity boron helps remove but the study tried adding Ti to the boron treatment process to improve its efficiency at tying up impurities [30]. Their findings saw boron treatment efficiency increase from 77.7% to 93.3% resulting in an electrical conductivity increase from 64.6% to 65.3% since it was able to remove more impurities from solid solution [30].

2.14.5.2 Addition of Graphene and CNT to Aluminum

Another new method being explored to improve the electrical conductivity of aluminum is alloying with graphene and carbon nanotubes which are known to have excellent electrical properties. High quality graphene added to copper in [81] saw a successful increase of electrical conductivity compared to another reduced graphene oxide composite and pure aluminum. The highest conductivity was achieved at 1 wt% high

quality graphene but with higher percentages, conductivity decreased due to agglomeration of the graphene and resulting poor wettability leading to cavity formation [81].

A metal matrix composite of aluminum and 0.2 wt% graphene nanoplatelets was studied in [82]. Researchers found the graphene formed into fibres in the rolling direction of the rod creating a lamellar structure well bonded to the aluminum matrix but with the presence of some microcracks at the interface [82]. This reduced the composite ductility, but ultimate tensile strength was increased 36.8% over a pure aluminum sample with the same casting and rolling process as the composite [82]. However, electrical conductivity of the composite was 0.7% IACS lower than the pure aluminum sample but still resulted in both a high strength and high conductivity conductor [82]. A carbon nanotube aluminum composite was also studied in [83] which was formed by cold pressing multiwall CNT and pure aluminum powder at room temperature followed by hot extrusion. Results saw the aluminum powder/CNT composite formed at a compressive stress of 561 MPa had the highest conductivity of all samples with 64.21% IACS [83]. This was 5% higher than a hot extruded sample of pure aluminum formed at the same pressure and 1% higher than the as-cast pure aluminum sample [83]. Yield strength and tensile strength of the aluminum powder/CNT composite were also about 2x higher than the annealed cast pure aluminum sample [83]. Overall, this new technology proved promising for both conductivity and strength improvement of aluminum conductors so they can better compete with copper.

2.14.5.3 Simultaneous High Strength and High Conductivity

One of the biggest drawbacks of aluminum aside from its lower electrical conductivity compared to copper is its low strength which limits its use in certain applications. For this reason, much work was done in the later 1990's to produce high strength aluminum alloys to better compete against copper with minimal sacrifice to electrical conductivity. This proved challenging since conductivity and strength are contradictory [84], just like the strength versus ductility relationship. This is because conventional strengthening mechanisms such as solid solution alloying, second phase additions, cold working, and grain refinement introduce defects into the lattice which block dislocations, improving strength, but also blocking and scattering electrons, decreasing electrical conductivity [84]. However, [84] discussed how twin boundaries have a much

lower impact on electrical conductivity while still improving strength. They then tested this observation with nano growth twins in high purity copper foil finding a drastic improvement in strength, at least one order of magnitude higher than coarse grained copper, and an electrical resistivity of $96.9 \pm 1.1\%$ [84]. Although this study looked at the improvement of copper, the technology shows promise and could be considered in future for aluminum.

Artificial aging is commonly used to improve the strength of aluminum alloys but for AA-6201 commonly used in overhead power lines, over aging is required to achieve desired electrical performance at the expense of alloy strength [85]. For all aluminum alloy conductors, a strength minimum of 295 MPa and conductivity minimum of 52.5-53% is required. Conventional AA-6201 achieves the required conductivity but with a lower tensile strength of 250 MPa due to over aging and resulting incoherent precipitates [85]. Research in [85] modified the AA-6201 alloy by incorporating AlB_2 in hopes to satisfy the required conductivity without sacrificing strength for both high conductivity and extremely high conductivity variants of the aged alloy. With optimal aging times and temperatures, they achieved a minimum conductivity of 55% as well as a minimum tensile strength of 295 MPa without incoherent boundaries at precipitates [85].

Researchers from [86] also found simultaneous strength and conductivity increase in commercially pure aluminum wires cold drawn to area reductions greater than 83.1%. This occurred for two reasons: 1) the $\langle 001 \rangle$ texture transformed into the $\langle 111 \rangle$ texture, which is harder, resulting in increased strength, 2) vertical grain boundaries were decreased while parallel/horizontal grain boundaries increased. This is best illustrated with Figure 2.7 where grains elongate during cold forming to a point above 83.1% area reduction where vertical grain boundaries that oppose the flow of electrons and increase scattering are reduced while grain boundaries parallel to electron flow are increased. This resulted in a 1% IACS increase where the cold drawn sample had a yield strength of 160 MPa and 63% conductivity compared to a conventional aluminum sample with a required yield strength of 160 MPa and conductivity of 62%. [86]

Results from these papers show promise for the increase of both electrical conductivity and strength for aluminum and its alloys, two of aluminum's biggest drawbacks, so it can better compete with copper.

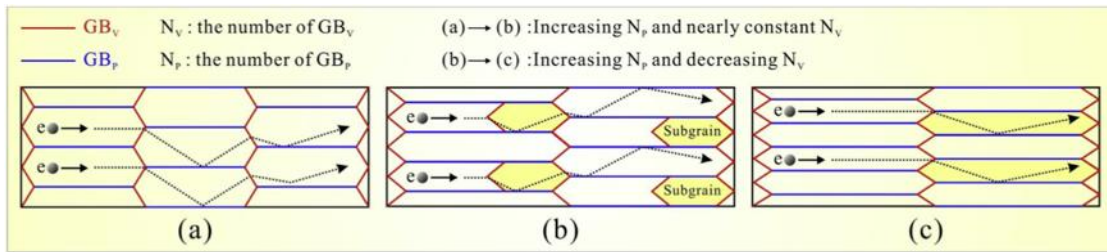


Figure 2.7. Electron interaction with vertical and horizontal grain boundaries in cold drawn microstructure at a) 24.6% b) 83.1% and c) 90.2% area reduction [86].

2.15 Replacing Copper with Aluminum: Case Studies

The following section summarizes specific instances where aluminum conductors have replaced copper in current research along with the advantages and disadvantages of doing so. It serves to better the understanding of where aluminum has been successfully and unsuccessfully used as well as the areas of study still left to explore in the aluminum versus copper debate.

2.15.1 Utilization of Aluminum Strip and Anodized Conductors

2.15.1.1 Anodized Round Aluminum Magnet Wire

A 1959 study looked at magnet wire options for 600°C operation including nickel clad copper, silver, and anodized aluminum wire. Overall, the round anodized aluminum wire did not perform as well as the insulated silver and nickel clad copper wires, but its insulation was much thinner at 0.7 circular mils, compared to the other two at 7.5 circular mils giving it better performance on a volt/mil basis. The insulation resistance of the anodized aluminum wire was initially lower up to around 300°C due to the porous nature of the oxide but once it dried out, it had the highest resistance of the conductors tested. The dielectric breakdown of the aluminum wire also saw advantages of being more constant over the whole temperature range while the silver and nickel clad copper saw significant decrease. Observing the conductors post testing, the glass serving insulation protecting the silver and copper saw the silicone burn out, easily being scraped off but remained intact enough to protect the conductors. On the other hand, anodized aluminum saw no deterioration of the aluminum oxide insulation but did see some light corrosion believed to be from residual corrosive electrolyte from manufacturing. [87]

Another study looked at round aluminum stranded wires with a 1-2 μm thick anodized coating as a low-cost alternative to the very expensive copper litz wire [88]. The natural oxide coating on aluminum wires, around 1-2 ηm thick, was also looked at and compared to uninsulated copper [88]. The problem with very small diameter stranded or litz aluminum wire at the time of publication, 2007, is the process was not very well developed for aluminum meaning initial overhead cost would be very high but the anodizing process is well established and would not add greatly to manufacturing cost [88]. Results saw the uninsulated aluminum wire with the natural oxide layer had an interstrand resistance up to 6x higher than that of the uninsulated copper wires [88], highlighting the advantages aluminum oxide has as an electrical insulation, even without modification of its thickness.

The stranded aluminum wire bundle was anodized and wrapped in an insulated tape and compared against copper litz wire for eddy current losses, relative losses in a transformer, and power loss in a 1kW scaled down prototype starter/alternator axial flux permanent magnet (PM) machine [88]. For eddy current losses, the aluminum anodized wire performed similar to copper litz and even better past 7 kHz with half the number of conductors as the litz wire [88]. For the transformer windings, litz performed better from 0-10 kHz where joule losses were more prominent, but the aluminum wire performed very similar above this frequency range. Up to 1500 Hz, copper litz wire performed better in the starter/alternator but this marked a cross over point where aluminum saw dramatically lower power loss instead [88]. However, the motor was designed for 800 Hz operation so the advantages of aluminum were not useful in this case but could be beneficial for higher frequency machines [88]. Overall, the anodized stranded aluminum wire performed very similar to copper litz wire, allowing it to offer manufacturing cost advantages if implemented into industry [88]. However, it is known that aluminum oxide is quite brittle and previous work saw issues with the oxide on round conductors so further work analyzing the formability and windability of these conductors and their impact on electrical performance would be beneficial.

2.15.1.2 Cheap Wind Turbine Generator

A new design for a human scale wind turbine meant for rural areas to provide quick and affordable energy was proposed in [89]. The goal was to use readily available and ultra-cheap materials leading to the design choice of aluminum foil windings and recycled VHS tape for insulation [89]. The study compared 3 prototype designs against a conventional copper wound generator with 0.8 mm insulated conductors [89]. Copper performed the best but as seen in Figure 2.8, the aluminum foil prototype A2-2 generated close to the same power [89]. The key findings of this study highlight how effective aluminum can be at providing extremely cheap power generation to rural areas that do not have access to and/or cannot afford conventional copper wound generators.

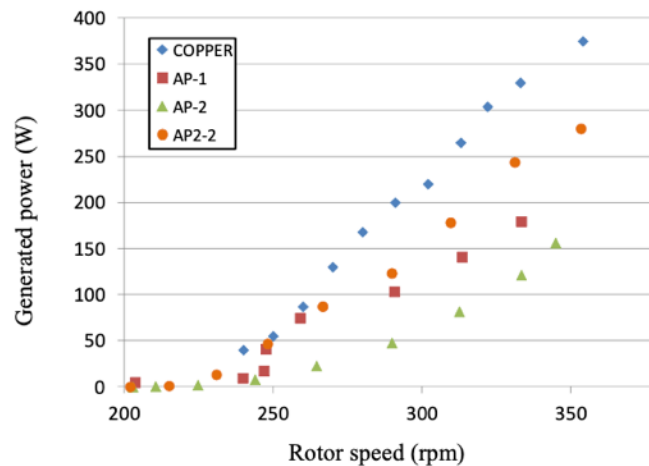


Figure 2.8. Power generation comparison between aluminum foil windings in prototype wind turbine and baseline copper design [89].

2.15.1.3 Small Hand Tool Motor

Two stators designed for small motors in hand tools were compared using 0.48 mm diameter copper wire and 0.25 mm x 10 mm aluminum strip interleaved with polyester film insulation on the basis of manufacturing time/cost and thermal performance [5]. The copper coils could be wound at 2100 rpm resulting in a stator fabrication time of 2 min 56 sec versus 1500 rpm for aluminum coils [5]. However, with slight modification of stator design to better accommodate aluminum strip, winding speed would be expected to considerably increase [5]. At rated output, the copper stator saw a temperature rise of 72°C

while the aluminum stator rose 68°C [5]. Overall, the aluminum foil wound motors were cheaper to produce, and had better thermal performance [5].

2.15.1.4 Movie Projector Application

The same paper above also analyzed the use of aluminum strip for the transformer winding responsible for the low voltage lamp of a movie projector while the film travel motor remained copper. The transformer switched from 2 mm diameter copper wire to 0.13 mm x 38 mm aluminum foil interleaved with polyester film insulation. The aluminum coil saw better cooling performance resulting in 40% lower voltage drop after 1 hour as well as 5% cost savings and 240 g weight savings for whole movie projector. [5]

2.15.1.5 Linear Actuators

Round, rectangular, and foil windings in both type 1 grade insulated copper and anodized aluminum variants were compared for use in a linear actuator based on thermal performance. The copper foil conductor used an insulation thickness of 12 µm while all aluminum conductors used an anodized insulation thickness of 3 µm. Aluminum oxide is 140x more thermally conductivity than the epoxy insulation used for copper with conductivities of 28 W/mK and 0.2 W/mK respectively. Initial thermal measurements saw the rectangular and foil copper conductors performing better than aluminum though they saw greater temperature distribution. With the addition of a thermally conductive foil between the coil bundle and actuator housing, all aluminum variants saw a dramatic improvement in thermal performance where only the rectangular copper coil saw a thermal performance increase. With better thermal performance, the aluminum windings had better current carrying capability resulting in a higher actuating force. Overall, equivalent force and thermal behaviour actuators could be made with anodized aluminum conductors while the higher thermal conductivity of the anodized insulation allowed for better heat dissipation from the extra losses it experiences due to lower conductivity. [90]

2.15.1.6 Accelerator Magnets

In 1981, anodized aluminum strip was used for the quadruple and sextuple magnets for LEP at CERN. Magnet coils were about 50% of the unit cost so using cheaper materials was very desirable. Winding speed of anodized aluminum coils was increased since there were no conductor crossovers. Very high slot fills of 82% and 74% were achieved due to the very thin anodized coating as electrical insulation along with very good heat transfer. Coil weight was also reduced 50% compared to an equivalent copper coil. However, there were two problems associated with the wire: the anodized layer was porous, so it needed to be sealed to avoid problems with moisture, and the supplied coil from the manufacturer had a fault nearly every 60 meters which required patching with polyimide film. [64]

Aluminum wire was also considered for CERN accelerator magnets much earlier in 1967 although it was more of a cost-based analysis. At the time, copper and aluminum were about the same price but there were still cost advantages to using aluminum in specific scenarios. These included: when the magnet system could be fully optimized for aluminum and there was no space constraint, when the magnet system was large, when an aluminum specific cooling system could be used since bimetallic systems should be avoided and where electricity costs were high and operating costs were a design constraint. [91]

2.15.1.7 Transformer Windings

Two identical transformers, one with copper windings and the other with the same size and configuration aluminum windings, were compared in [11] on the basis of AC resistance. At low frequencies, around 1-80 kHz, copper saw much lower AC resistance since eddy currents were negligible and DC resistance mattered most where aluminum has 1.64x the DC resistance of copper [11]. At intermediate frequencies, around 80-120 kHz, aluminum and copper performed almost equal since eddy current losses became significant, offsetting the higher DC resistance of aluminum [11]. For frequencies above this, proximity losses became substantial meaning copper again saw lower AC resistance, although the performance gap with aluminum was half what it was at low frequencies [11]. This shows there is an upper limit to which aluminum sees lower AC resistance compared to copper. With the raw material price of aluminum being much lower, there is already cost

advantages in this application at low frequencies without increasing its volume [11]. Greater advantages could be seen at high frequencies where its higher resistance becomes advantageous [11], but this only applies up to a certain point.

In 1951, aluminum started being used for dry type transformers to relieve the stress on already short supplies of copper [20]. One hundred dry type aluminum transformers were built and evaluated after 3 to 4 years of service with no issues found [20]. Aluminum did not suffer from its low tensile properties at the elevated 250°C operating temperature since its strength increased with the required conductor volume increase [20]. It also had 78% the watt density compared to copper since its resistance was the same but surface area was greater, allowing for more heat dissipation [20]. Connections with aluminum proved more costly and difficult but with silver coating, anti-corrosive additives, and Belleville spring washers, good connections were made [20]. The aluminum transformers ended up being slightly larger in all dimensions and required more core steel material but were only 3% heavier than their copper counterparts [20]. Although, their cost was 1.3x higher due to low raw material price difference, and higher fabrication and joining costs of aluminum [20]. This proved early on that aluminum could be a viable replacement to copper in dry type transformers and with technology improvements they could start to see equivalent or lower unit costs compared to copper.

The aluminum versus copper debate for transformers has been active for decades in North America but is now picking up traction in India where they predominantly use copper but are looking to switch to aluminum. For large distribution transformers, 950 kVA, it was found that with proper design and optimization, the performance, reliability and lifespan will be nearly identical between copper and aluminum windings. Short circuit withstand capability should be similar as well since the 66% cross-sectional area increase for aluminum results in nearly the same strength as copper wires. Aluminum transformers would be slightly larger due to more conductor volume required but they would weight and cost less for the same performance. This research also highlighted the preference of aluminum for dry type, cast resin transformers since the thermal expansion of aluminum is closer to that of the resin than copper resulting in a lower risk of resin cracking and failing during operation. [92]

Further research in [93] and [94] looked at distribution transformers in India but utilized in non-ideal power grid situations. Repeated energization occurs in these grids leading to cold load pick up (CLPU) where high stress and temperature are induced in the windings from current several times higher than normal levels which persists for several hours [93], [94]. With these operating conditions, they found 30% higher failure rates in aluminum transformers compared to copper [93], [94]. The poor creep life of aluminum was found to be the issue which caused elongation and loosening of conductors in the windings between spacers resulting in an air gap which caused short circuit failure [93], [94].

Moving away from the new challenges faced by India, further cost analysis and more specifically, total owning cost (TOC) were evaluated between copper and aluminum transformers in [28] and [95]. Optimization formulas were used to determine when it was better to use each conductor in [28]. Results from the 2010 study found that below a power rating of 190 kVA, aluminum windings provided a cheaper overall unit cost [28]. Above this power rating, and copper windings resulted in cheaper transformers over their lifetime [28]. This was because in general, aluminum transformers require more core material, insulation, steel for the oil tank and more oil which negates the cost benefits of aluminum being significantly cheaper [28]. This is one of the reasons aluminum is such a popular choice for dry type transformers since oil is not used [28]. Another potential disadvantage was that transformer size increase may be too large for shipping or larger than standards specify [28]. Accounting for anodized aluminum coils and its associated advantages could potentially elevate the power rating where aluminum becomes less cost effective.

Research in [95] also looked at TOC but for dual copper/aluminum wound transformers. Conventional transformers with both conductors see the low voltage winding made of aluminum strip as the inner winding with the high voltage winding made of copper wire as the outer winding [95]. This study proposed the opposite configuration in hopes to reduce total owning cost of the transformer given that aluminum is much cheaper than copper and more winding material is required for the outer winding [95]. The new design saw 39% less copper and 48% more aluminum used by weight resulting in 29% lower material cost and 6-10% lower TOC for power ratings from 20-112.5 kVA [95]. This

highlights that the significantly lower cost of aluminum allows for abstract and unconventional designs to be tested which can lead to reduced overall machine costs.

2.15.2 Hydroelectric Generators

A 1967 paper performed a theoretical and mathematical analysis to determine the feasibility of replacing copper with aluminum windings in medium and low speed hydroelectric generators. The generators compared had the same rating, short circuit ratio and temperature rise leaving the independent variables to be machine gap diameter and the price of copper over aluminum assuming aluminum price stays the same. For the medium speed generator and conductor prices of the time, aluminum was not an economic option. However, if the aluminum coil could increase in both height and depth by 10% it became economic if the price of copper increased 20%. If the gap diameter was increased by 10% (the highest practical increase) the aluminum machine became economic with no copper price increase but also up to a £50/kW capitalization of losses for a 20% copper price increase. For the low speed generator, aluminum was also not economic at present conductor prices without modification. For the same aluminum coil size increase, it became economic if the price of copper increased by 10%. Allowing for a 10% increased gap diameter, the aluminum generator was also economic and if copper price increased by 5%, it was economic up to a £50/kW capitalization of losses. These results suggest a high-speed generator at the time was out of the question for substitution of aluminum windings. The paper concluded that at present conductor pricing, aluminum could be a viable option for low speed generators and even more so if the price of copper increased. [27]

2.15.3 AC vs DC Operation

Aluminum and copper coil exemplars and motorette assemblies were compared in [56] on the basis of thermal life and electrical performance in AC applications. The motorettes were designed to represent a 2 kW/kg high efficiency (97%), high frequency (800 Hz) PM motor. Results of note from this study are shown in Figure 2.9. The left figure illustrates the temperature difference decrease between conductors as frequency increases. This is because net power loss and resulting temperature increase are different for AC and

DC resistance and aluminum sees lower AC losses meaning it experiences less temperature increase at high frequencies compared to copper. To further illustrate the lower AC losses experienced by aluminum, the right chart in Figure 2.9 shows a cross over point, around 500 Hz, where the winding losses for aluminum become equal to, and lower than those of the copper motorette windings. R_{ac}/R_{dc} ratios versus frequency were also presented where aluminum saw much lower ratios, again highlighting its lower AC losses compared to copper. The results of this study suggest that if the same size aluminum wire were to replace copper it could result in higher efficiency at high speeds with the trade-off of lower efficiency at low speeds. [56]

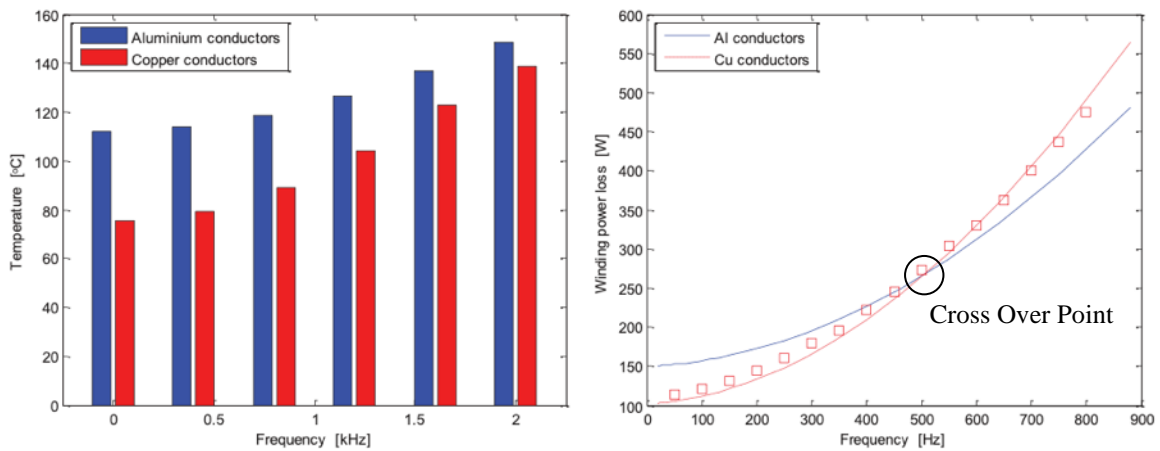


Figure 2.9. Coil temperature comparison of aluminum versus copper as frequency increases (left) and motorette winding power loss versus frequency highlighting cross over point where aluminum sees lower losses (right) [56].

Aluminum windings were also considered in a surface PM turbocharger designed with copper windings for use in electric vehicle range extender applications. The peak power of the turbocharger was 20 kW with a max torque of 1.7 Nm and a max speed of 150 000 rpm. The copper machine was compared against an identical with aluminum windings, finding both to have the same max efficiency of 97% although the high efficiency region for aluminum started at higher speeds and existed over a shorter torque range. At very high speeds, there was a small operating range where aluminum saw 0.5% higher efficiency due to its lower AC losses. Overall, there was not a significant difference between the performance of both machines aside from aluminum providing a 20% reduction in machine weight. This is substantial but without any real performance advantages to using aluminum the authors deemed it impractical to use. [96]

2.15.3.1 Traction Motor Applications

Researches in [96] looked at implementing aluminum in a spoke PM machine designed with copper windings for fully electric motorsport application. The machine had a peak power of 200 kW, max torque of 480 Nm and base and max speeds of 4000 and 12000 rpm respectively. Again, aluminum was directly substituted in for copper windings and both machines saw the same maximum efficiency of 97% with aluminum seeing it in a smaller area. However, due to the reduced AC losses provided by aluminum, it saw higher efficiency at speeds above 7000 rpm, comparable performance at medium speeds and lower efficiency than copper at speeds below 2000 rpm due to elevated DC resistance. [96]

To better quantify the advantages of the aluminum machine in AC operation, both motors were compared in a real racetrack driving cycle [96]. With most operating points residing in the medium to high speed region, aluminum saw a slightly higher average efficiency over the driving cycle of 94.28% compared to copper at 93.58% [96]. It was also found that for the same motoring energy through the cycle, the copper machine required 20.7 Wh more energy per lap [96]. This meant the vehicle would require more battery capacity to compensate which could increase vehicle weight further, reducing overall vehicle efficiency. Regarding thermal performance, the reduced AC losses of the aluminum machine resulted in less heat production since most of the operating points were in the high-speed region of the motor [96]. Considering a 15 lap drive cycle, copper saw winding temperature vary between 140-180°C with an average of 155°C and maximum magnet temperature of 100°C compared to aluminum with winding temperatures between 130-140°C with an average of 135°C and a maximum magnet temperature of 85°C [96]. This would allow a less robust cooling system to be used for the aluminum motor, reducing vehicle weight, on top of the 1.3 kg already saved in motor weight [96].

In [97] a spoke type high speed ferrite magnet motor with distributed aluminum windings intended for electric vehicle application was reviewed for its feasibility. Peak performance of the aluminum wound motor was theoretically compared to an identical machine with copper wires of the same size and configuration. Both machines had similar peak performance, but the copper machine saw about 25% higher continuous performance due to lower resistivity and losses. Aluminum to copper connections were also experimentally tested for reliability with cyclic thermal loading. No change in electrical

performance was detected and no physical degradation of the windings or connections was observed confirming reliable aluminum to copper connections. [97]

This same full-scale prototype motor underwent dynamic performance analysis in [58] for comparison against project requirements and the 2010 Nissan Leaf motor which uses rare earth magnets and copper windings. Compared to using copper windings, the prototype aluminum wound motor saw 70% winding mass reduction and 90% reduction in winding cost according to raw material price. Compared to project requirements, it provided max torque 20 sec longer than required. Peak torque was 10% lower than required but the machine saw 24% more peak power at a higher base speed. Continuous power was lower than required at low speeds but up to 28% higher above 6500 rpm. Compared to the 2010 Nissan Leaf motor, it had the same volume but provided 15% lower max torque, 10% higher power density, and 25% lower maximum continuous power density. Overall, the aluminum prototype machine achieved competitive intermittent and continuous performance to a state-of-the-art electric vehicle motor without the use of rare earth magnets or copper conductors. [58]

The performance of aluminum in both low speed and high speed permanent magnet synchronous machines (PMSM) designed for automotive traction application was also analyzed in [98] and [99] respectively. The low speed motor in [98] was designed with copper windings for direct drive application and theoretically compared against an identical motor with the same size and configuration aluminum windings. For the same output torque of both machines at a base speed of 405 rpm, copper had a peak current of 9 A with ohmic losses of 156 W while aluminum required 13 A with ohmic losses of 225 W resulting in 4.15% lower efficiency compared to the copper machine [98]. For the same ohmic loss of 156 W instead, the aluminum machine saw an 18% reduction in torque [98]. Regarding thermal performance from 20-100°C, the copper machine saw an efficiency reduction of 2.65% while the aluminum machine saw a 3.8% drop [98]. Comparing the machines for both urban and highway driving cycles with the performance parameters of the 2018 Ford Focus, they both satisfied all torque speed points. However, at maximum energy density points, the aluminum machine saw 1.17% and 1.7% reduced efficiency compared to copper for the urban and highway drive cycles respectively [98]. This may seem like an acceptable performance drop considering a 14.7% reduced motor mass and 67% reduced winding cost

based on material price for the aluminum machine, but the majority of losses for low speed operation come from the winding, so it makes a big impact [98].

The high speed PMSM was also theoretically compared against an identical motor with the same size and configuration aluminum windings. For the same input power of 400 V and 78 A, the rated efficiency of the copper motor was 1.71% higher than aluminum which saw a winding loss 1.53x higher. For the same winding loss of 807 W, the aluminum machine saw reduced current density of 63.14 A compared to 78 A for copper resulting in 24% lower torque and reduced rated output power. The constant power speed range of the aluminum machine was also reduced from 3000-10000 rpm to 3000-7000 rpm accordingly. Regarding thermal performance for the same output torque from 20-100°C, the copper and aluminum machines saw 0.94% and 1.5% reduction respectively. A drive cycle analysis using the vehicle performance parameters of the 2018 Ford Focus was also performed for both machines for urban, highway, and worldwide lightweight test cycles. For equivalent input power, the copper machine saw 1% higher efficiency for the urban cycle and 0.6% higher efficiency for the other two. For equivalent peak winding losses, the aluminum machine had lower torque but both machines still satisfied all torque speed points for urban and highway drive cycles. For the worldwide lightweight test cycle, aluminum did not satisfy a few points at base speed where torque was high, but both failed to satisfy some points at high speed. Very similar drive cycle performance coupled with a 12% reduction in weight for the aluminum machine and resulting 90% winding cost reduction based on raw material price means aluminum conductors are a viable option for this high-speed traction motor. If the design was further optimized for aluminum, the disadvantages seen could be compensated for. [99]

2.15.4 Precompressed Aluminum Windings

It was discussed at the beginning of Section 2.9 that electrical conductivity and slot fill factor are the only independent variables when considering replacing copper with aluminum for unchanged machine geometry and equivalent winding losses [9]. Improvement of electrical conductivity is extremely challenging as has been seen in previous sections but improving slot fill factor is a viable option. This approach was taken

by [9] when designing a prototype motor for a solar plane and [57] for stranded windings to be used in an automotive traction motor.

Motor design requirements for a solar plane are low weight, extremely high efficiency while cruising, extensive overload capability during take-off and very good reliability for multi-year, continuous operation. To satisfy these design requirements, aluminum and copper windings were compared but the aluminum windings were pre-compressed, as seen in Figure 2.10, to achieve extremely high slot fill percentage and compensate for its lower conductivity while maintaining machine geometry. The aluminum winding required 74% slot fill which is unattainable by conventional winding technology, but a pre-compression process was previously successful with copper windings up to 80% slot fill, so the same method was used in this study. The previously compressed copper windings required 400 MPa to compress completely and saw a springback of 2-3% while aluminum only needed 250 MPa and saw a lower springback of 0.5-1%. The compression process needed extra tooling but required less skill than hand winding and took much less time. [9]

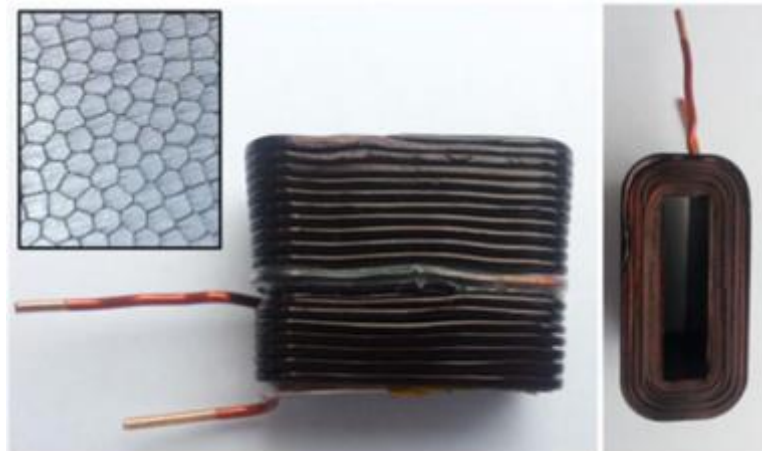


Figure 2.10. Precompressed aluminum windings along with cross section view (upper left) highlighting high slot fill capability and minimal air gap between conductors [9].

Compared to a conventionally wound copper coil with 43% slot fill, steady state temperature for the aluminum coil was lower despite its lower thermal conductivity due to the very high slot fill and near complete elimination of air gaps between conductors [9]. Aluminum also saw a 17% lower phase resistance and the copper winding saw 30% higher losses due to it running hotter [9]. The aluminum machine was 9% lighter with up to 85%

winding cost reduction based on raw material price [9]. Therefore, for equivalent electrical performance, precompression of aluminum coils proved to be a viable option with reduced weight and cost and improved thermal performance. However, it is also important to consider precompressed copper windings could be used instead [9] which would be much harder for aluminum to compete against but would not result in cost or weight advantages.

Research in [100] also looked at precompressed aluminum coils for solar aircraft applications. The study reviewed three permanent magnet motor topologies and their optimization with use of compressed aluminum windings for high efficiency, low mass, and reduced diameter [100]. Copper windings were not considered in this study which is a big step in the right direction for trying to take full advantage of aluminum conductors rather than substituting them into a design optimized for copper use.

Precompressed stranded aluminum windings were considered for an automotive segmental rotor switched reluctance machine meant to perform the same as the Nissan leaf interior permanent magnet motor. Compressed stranded aluminum windings with a slot fill of 77% were compared against bobbin wound and precompressed copper windings with a slot fill of 39% and 77% respectively. At maximum speed and power, the aluminum coil saw 18% lower DC losses, significantly higher AC losses due to larger size conductors used, and total winding loss only 7% higher than the conventionally wound copper coil. The aluminum coil was also 1.8x lighter and 6x cheaper based on raw material price. The precompressed copper coil had 40% lower DC losses but higher AC losses resulting in the aluminum coil only having 10% increased total winding loss. However, the copper coil was 3.3x heavier and 11x more expensive since much more copper was used. Compared to the Nissan leaf motor, the precompressed aluminum wound motor had a larger volume but similar mass and performance without the use of copper or rare earth permanent magnets allowing for significantly reduced material costs. [57]

2.15.5 Induction Motors

Aluminum and copper conductors were compared for use in an induction machine using aluminum rotor bars [101]. For both aluminum and copper wound machines to have the same efficiency and performance, aluminum winding volume needed to increase [101]. This resulted in a total machine volume increase of 47% including an increase to the rotor

and stator diameters, and slot area [101]. Aluminum windings were 85% cheaper than copper windings but the motor volume increase resulted in an overall price increase of 19% [101]. This demonstrates that for specific machines, accommodating conventionally wound aluminum can result in larger machinery and an overall increase in costs.

2.15.6 Elevator motor

Aluminum and copper windings were compared in a direct drive permanent magnet elevator motor [102]. Aluminum conductor volume increased to be equal resistance to copper resulting in increased stator slot area and outer diameter [102]. Stator core weight increased by 1.7 kg and core losses increased accordingly but total machine weight reduced by 2.3 kg even though volume increased by 9% [102]. Both machines had very similar efficiencies and winding losses, but the overall machine cost only reduced by 12% for the aluminum windings due to increased cost of the larger stator core [102]. Where size is not a design concern and the extra volume of aluminum can be accommodated, a similar performance motor to its copper counterpart that weights and costs less can be implemented.

2.15.7 Appliance Motors

Aluminum and copper were compared for use in a single-phase fractional horsepower asynchronous induction motor to be used in a hermetic compressor of a refrigerator [103]. The coefficient of performance (COP) and energy efficiency ratio (EER) of both motors was similar but the aluminum machine had 5% lower efficiency [103]. The required aluminum conductor volume increase resulted in 17% increased electrical steel costs and 12% weight increase, but winding cost and weight reduced 76% and 62% respectively with overall motor cost decreasing 46% [103]. Manufacturing the aluminum wound motor initially saw challenges with its low strength resulting in wire breakage but once this was overcome, 50 prototype motors were made and validated with quality assurance (QA) testing revealing no issues [103]. Another home appliance motor was tested with aluminum in [104] with similar performance to the copper alternative. The

aluminum motor ran about 10°C hotter but was slightly quieter and weighed 40% less than the copper motor [104].

Single phase induction fan motors for air conditioners also saw manufacturing difficulties when switching to aluminum conductors [105]. Initially, defects and failures from galvanic corrosion of aluminum winding to copper lead wire connections as well as problems associated with winding and coil insertion caused increased manufacturing costs [105]. Overall, the aluminum motor was still significantly cheaper than the copper counterpart [105]. However, after 3 years of service, the aluminum wound motors started experiencing a lot of failures [103]. They were found to result from partial discharge occurring at air gaps formed in the end winding caused by separation of aluminum from the insulation due to mechanical and electrical forces during handling and aging [103]. Since the same QA testing used for copper motors was used for aluminum and the problem was aluminum specific, it was not detected [103]. This meant new QA testing needed to be added to the manufacturing process resulting in further increase to costs [103].

Although these studies reveal aluminum winding result in significantly cheaper appliance motors, the extra costs associated with switching to aluminum need to be considered. Accounting for extra manufacturing costs from experienced difficulties, additional QA testing, and potential failure analysis could reduce or mitigate cost savings offered by aluminum making it much less enticing to switch to.

2.15.8 Rectangular Windings

Research in [59] looked at both aluminum and copper rectangular conductors in multiple configurations for use in a prototype modular wound, segmental stator radial flux interior permanent magnet machine. The rectangular wires offer highly repeatable and economic manufacturing with well-defined thermal performance [59]. The paper compared 3 winding variants for each conductor type but in general, copper motors saw higher continuous torque as well as higher torque at low speeds due to their lower DC losses [59]. Aluminum had a much longer continuous torque region giving it higher torque at higher speeds where the torque of the copper motor already started decreasing [59]. Aluminum windings were confirmed to be less susceptible to AC effects allowing it to utilize greater fill factors which in turn reduced their DC resistance giving them better efficiency at lower

speeds than they would otherwise see [59]. The motors were also compared in an extra urban driving cycle where the copper machines saw up to 2.9% higher efficiency [59]. Although, the aluminum windings reduced overall motor weight by up to 3.6 kg and winding costs were around 10x lower [59] making aluminum a competitive option where design goals favour weight and cost reduction and allow for a slight decrease in efficiency.

Research in [106] also looked to implement aluminum windings with the design requirements of low cost and manufacturability in a PM starter generator. Three winding variants were tested: edge wound rectangular wires, multi strand round wire, and compressed multistrand round wire. The edge wound rectangular wire provided the highest fill factor allowing for more volume of aluminum to be used to compensate for its lower DC resistance. The resulting aluminum motor satisfied design requirements and provided comparable electrical loading to a conventionally wound copper machine. [106]

2.16 Important Takeaways

- EC aluminum requires a 62% increase to cross-sectional area for equivalent conductivity to copper, but this still results in a 50% reduction in winding weight.
- Aluminum has 49% the electrical resistivity of copper by weight meaning 1 kg of aluminum has equivalent conductivity to 2 kg of copper.
- The cost of an equivalent aluminum winding is 12.5% that of a copper winding based on current raw material prices.
- Aluminum can offer significant cost advantages based on its much lower raw material price. However, all costs associated with machine manufacture and operation need to be considered. These include finished magnet wire cost, manufacturing challenges and modifications, QA testing, failure analysis and cost of electricity for the extra losses incurred due to its lower conductivity. All these combined can reduce or eliminate the cost advantage seen by aluminum.
- Aluminum conductors would be more advantageous to use from a recyclability point of view for small motors destined for shredding as their recycling process. Very small percentages of copper contaminate recycled electrical steel prohibiting its re-use as a sheet steel where aluminum does not see the same problem.

- The environmental impact of manufacturing and using aluminum can be higher than copper since it is fabricated solely by electrolysis and incurs more losses over its operational life due to lower conductivity.
- Lower yield strength of aluminum is advantageous for manufacturing since less strain energy is required to form it. This also makes the springback of aluminum lower than copper which has a host of advantages including more compact coils, higher slot fill factors, shorter end turns and overall more compact motors and reduced costs.
- For equivalent conductors, the lower strength of aluminum becomes less problematic and close to that of copper due to strength increasing with the same area/volume ratio required for equivalent conductivity.
- Thermal conductivity of aluminum is lower than copper but for equivalent conductors inside a motor, it has been shown that thermal conductivity is similar for both conductors since the larger volume of aluminum increases heat dissipation area.
- An equivalent aluminum wire also has a 15% higher thermal heat capacity compared to copper which is critical for short circuit and surge conditions as well as overload scenarios like those seen in solar plane takeoff.
- In general, aluminum can withstand higher operating temperatures than copper which experiences flaking and rapid oxidation that leads to degradation of electrical insulation and premature failure.
- Connections and terminations were a big problem for aluminum in the past, but all problems have since been solved allowing for electrical connections as reliable as those used for copper. However, the inherent problems of high thermal expansion, stress relaxation, cold flow, creep and fatigue still need to be carefully considered. This is especially true when considering aluminum for use in high performance automotive motors where copper has been exclusively used and is not as susceptible to these problems. When bimetallic connections are used, these issues also need to be carefully considered since corrosion can become a concern as well.
- Anodized aluminum strip has proven to be highly advantageous in high temperature operation since aluminum is more stable at high temperatures compared to copper and aluminum oxide electrical insulation has a melting temperature far exceeding that of

aluminum. Aluminum foil conductors also offer significant thermal performance advantages.

- Aluminum foil associated with other low cost or recycled components can offer economical approaches to supply power to rural areas that cannot afford or access conventional and expensive machinery.
- If weight is a design constraint, aluminum wire should be considered. If machine size is a design constraint, copper should be considered. If the machine volume increase can be accommodated from using aluminum, it could result in machines that are cheaper and lighter despite the size increase.
- Without change to machine geometry and for equivalent winding loss; either aluminum conductivity needs to increase, or its slot fill percentage needs to increase.
- Precompressed windings with extremely high slot fill percentages offer a unique approach to maintain machine geometry while achieving similar electrical performance, improved thermal performance, and reduced cost and weight.
- Directly substituting the same size aluminum wire in machines designed for copper can lead to overall similar performance thanks to the reduced AC effects experienced by aluminum which helps compensate for the elevated DC losses it sees compared to copper. Depending on the machine, aluminum could see lower efficiency at low speed operation but higher efficiency at high speed operation. However, this advantage at high frequencies only extends to a certain point, where copper would again start to see lower losses and greater efficiency.
- Where performance of the aluminum machine is slightly lower, the few percent efficiency loss may be an acceptable tradeoff for reduced weight and machine cost now.
- With further optimization of aluminum windings in electric machines to maximize their advantages, especially for high frequency operation, the loss of efficiency may not be necessary in the future.
- The significantly lower cost of aluminum allows for abstract and unconventional designs to be studied and implemented which can lead to overall machine cost reduction. This changes the question of aluminum versus copper conductors, to how can both be simultaneously and effectively used in novel machine designs?

Chapter 3

LITERATURE REVIEW

The previous section looked at the advantages and disadvantages of switching from copper to aluminum conductors from a wide variety of angles. However, there has been little work done from a metallurgical point of view on the windability and formability of these conductor materials. This is particularly true for hairpin style magnet wires which are gaining increased popularity due to their good performance and mass producibility catering to full autonomy. The following sections provided background literature on these conductors and their manufacturing as well as common modes of failure experienced with their unique forming operations. Surface defects specific to aluminum are also reviewed for better understanding of the feasibility of using them as hairpin conductors.

3.1 Hairpin Style Conductors

Conventional coil windings can be made of round, rectangular, or strip conductors that are either pre-formed and inserted into the stator slots or wound into the stator slots directly. Hairpin style conductors differ from this convention in that they are generally larger gauge rectangular or square individual wires that are precision formed into a 3D hairpin shape as can be seen in Figure 3.1 (left). These individual wires are then axially inserted into the stator slots as seen in Figure 3.1 (right) where a complete coil is formed by joining the ends of the individual wires together [107], [108]. These types of windings have been successfully used for decades in alternators and starters [109] but have recently become more popular in the automotive sector since they cater well to mass production and fully automated manufacturing [110]. An example of a complete motor package with hairpin windings can be seen in Figure 3.2 [111].

3.1.1 Advantages and Disadvantages of Hairpin Windings

Hairpin windings offer a myriad of advantages over conventional coils with the first major one being much higher slot fills, around 73% compared to around 40% for conventional windings [108], [109], [110]. The slot fill difference between both types of

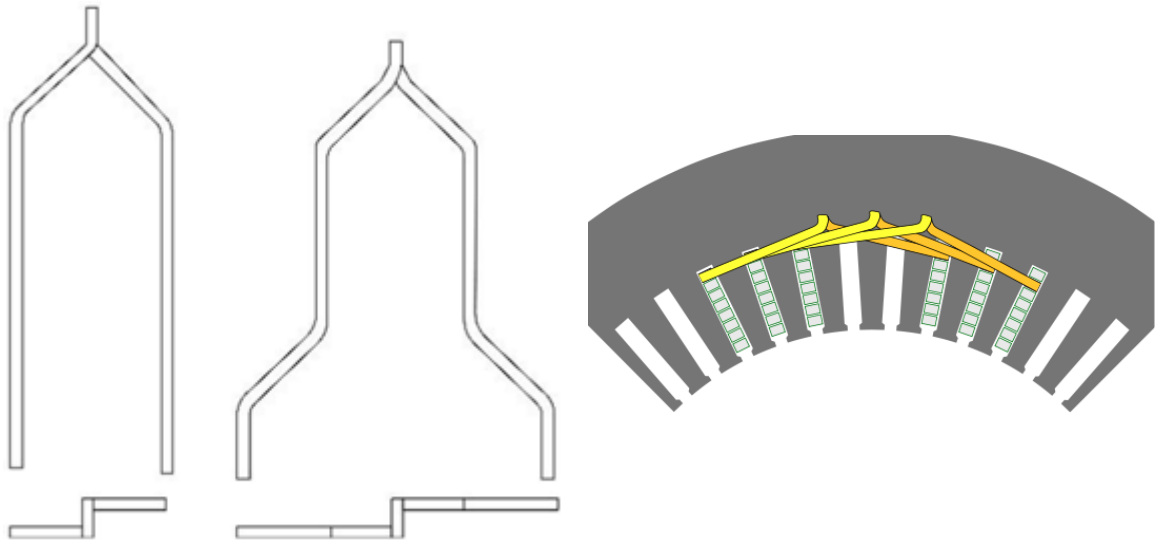


Figure 3.1. Hairpin style conductors (left) and example of individual insertion into stator slots (right) [108], [114].

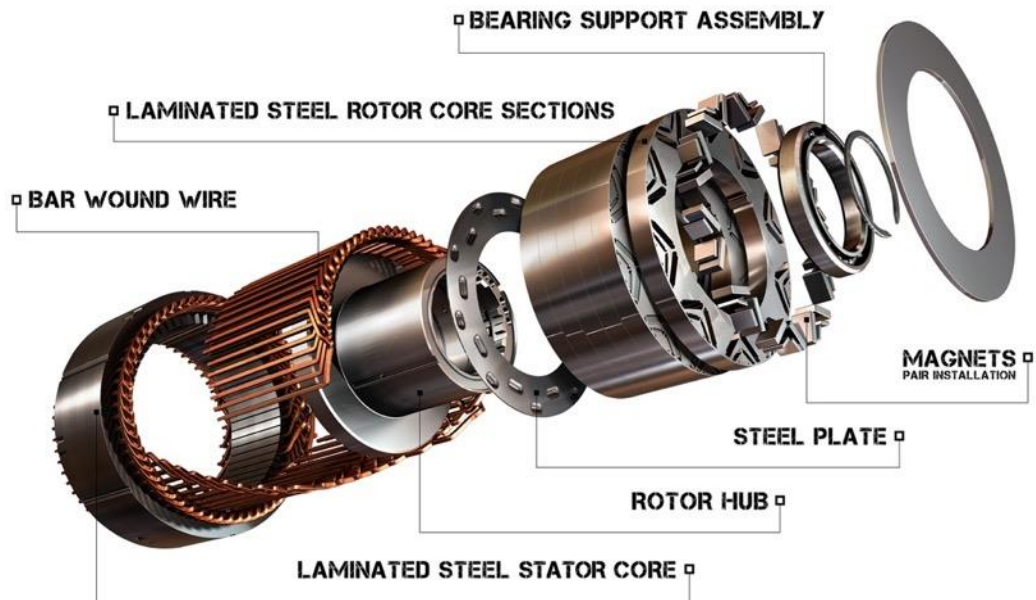


Figure 3.2. General Motors permanent magnet motor package utilizing hairpin style conductors [111].

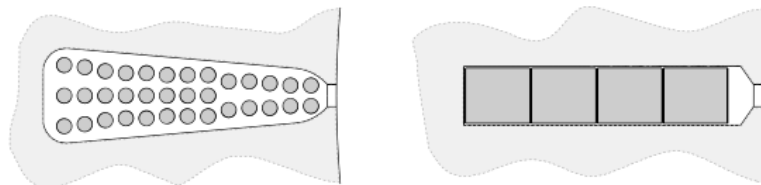


Figure 3.3. Slot fill comparison between round wire windings (left) and hairpin windings (right) [108].

windings can be seen in Figure 3.3 where there is a lot of air gaps and unused space in the round wire stator slot while the hairpin conductors use up virtually the entire rectangular slot area. The higher slot fill achieved reduces DC resistance, increasing current and power density and improving motor performance at high torque and low speed [108], [110]. However, the larger conductors used make the winding more susceptible to AC effects since current distribution is non uniform at high speeds increasing losses from skin and proximity effects [68], [108], [110], [112]. Stranded and litz conductors perform much better in these applications but hairpin conductors can be transposed across each winding layer to equalize current density differences across all conductor paths to effectively combat elevated AC losses [108], [112].

Hairpin windings also allow for shorter and tighter end turns, increasing active conductor length for the motor package, and reducing end winding losses and excess heat generation [109], [110]. Thermal performance of hairpin windings is also improved over conventional windings since the higher slot fills allows for better heat transfer to the stator teeth [108] - [110]. The end windings also have increased surface area due to the larger conductors making them well suited for liquid cooling [109], [110]. This allows for lower temperature operation and therefore more efficient performance and extended insulation life [109], [110]. Better thermal performance also allows for operation at higher continuous power levels that would be peak power at the thermal limit for conventionally wound motors [109].

3.1.2 Utilization of Hairpin Conductors: Case Studies

Rectangular hairpin windings were implemented into a golf cart motor design in [107] with its performance compared to that of a commercially available conventionally wound motor. The rectangular hairpin wires used increased slot fill to 70-75% and catered better to mass production design considerations than high slot fill hand wound coils with round wires. One big advantage the hairpin conductors saw in this study was the minimized stator slot opening. Cogging torque is responsible for creating vibration and noise and results from interaction of rotor magnets with stator slots but can be severely reduced with minimized slot opening size. Round conductors require slot openings at least slightly larger than one wire diameter so they can be wound into the slot, but hairpin conductors are

axially inserted so no slot opening is required. Motor efficiency and torque decrease with slot opening size, so hairpin conductors allow both to be maximized compared to conventional windings. With this advantage and those known for hairpin conductors, the motor in this study saw similar efficiency and variable speed range to the commercially available round wire motor but with 120% the power density per volume. [107]

Research in [68] compared the use of conventional stranded windings and rectangular hairpin windings in pre-existing electric vehicle traction motors. Induction motors saw the greatest benefit from using hairpin windings compared to the other motor topologies analyzed in this study. Both induction machines saw similar peak torque, but the hairpin windings provided lower DC resistance at low speeds due to higher slot fill which improved motor efficiency. Hairpin windings also saw significantly improved continuous torque and power along with better heat extraction. However, at high speeds, AC losses became dominant and the hairpin windings saw a rapid decrease in performance due to the large conductor size. The higher slot fill achieved did come with the disadvantage of more copper used however which resulted in a 4 kg winding weight gain, increasing cost and overall weight of the machine. [68]

Hairpin windings have also been used in the 1st and 2nd generation Chevy Volt motors [110], [113]. All the advantages of using hairpin conductors discussed in the previous section apply to the Chevy Volt motors. The higher slot fill and tighter end turns achieved with hairpin conductors reduced phase resistance by 30-40% compared to a similar torque and power motor using conventional windings [110]. The increased AC losses and resulting decreased performance were also not seen with this motor [110]. Testing revealed the hairpin windings were advantageous below 8000 rpm where the motor mainly operated below 5000 rpm, so the increased AC losses were not a concern [110]. This resulted in improved efficiency and thermal performance over the operating range compared to conventional windings [110]. This study highlights the necessity of determining the performance of hairpin windings in the operating range of the desired motor before writing it off due to comparatively poor performance at high speed operation.

To further combat AC winding loss in hairpin windings, a novel approach was taken in [112] where both aluminum and copper windings were used simultaneously. Relatively large variable fields are present near the slot opening due to interaction of the

magnets and armature with the stator slots [112]. This means AC affects are higher near the slot opening and reduce as depth increases into the slot [112]. Conventional windings can be organized to avoid this high AC loss area but as seen in Figure 3.3, hairpin conductors take up almost the entire slot area and removing some to avoid the opening would not be a feasible option. Therefore, this study proposed using aluminum hairpin conductors near the slot opening since it will have reduced AC losses from its higher electrical resistivity and switching back to copper windings in the outer layers of the slot where its higher conductivity is more advantageous [112]. The use of aluminum can reduce the weight and material cost of the motor but bimetallic connections between the copper and aluminum hairpins could pose corrosion problems [112]. Comparing the performance of this novel winding design to an all copper design saw slightly increased losses at low speed/high load due to increased resistance of aluminum but at high speed/low load total winding losses were reduced [112]. This study proposes a very interesting approach to the aluminum versus copper debate where the question may no longer be one or the other but how to effectively utilize both in a specialized and novel machine designs.

3.1.3 Hairpin Conductor Manufacturing

Hairpin windings differ from conventional windings in that the individual conductors are formed outside of the motor and then inserted into the stator for subsequent joining to form a complete coil [110]. The winding and manufacturing techniques for conventional windings are not covered in this work since the focus is on hairpin style windings but detailed information can be found in references [114] and [115]. The process of manufacturing a hairpin wound stator is illustrated in Figure 3.4 [116]. The square or rectangular cross section wires are first straightened, which can be done with a series of progressively larger diameter rollers, measured, and cut to length [117], [118]. The ends of the wires are then stripped chemically, mechanically, or by laser to prepare them for joining together after insertion into the stator [117], [118]. Bending of the wires into the characteristic horseshoe/hairpin shape can then done by three point bending, die bending, swivel or in process bending around a mandrel or die, CNC free form bending with a complex machine or any combination of the four [117].

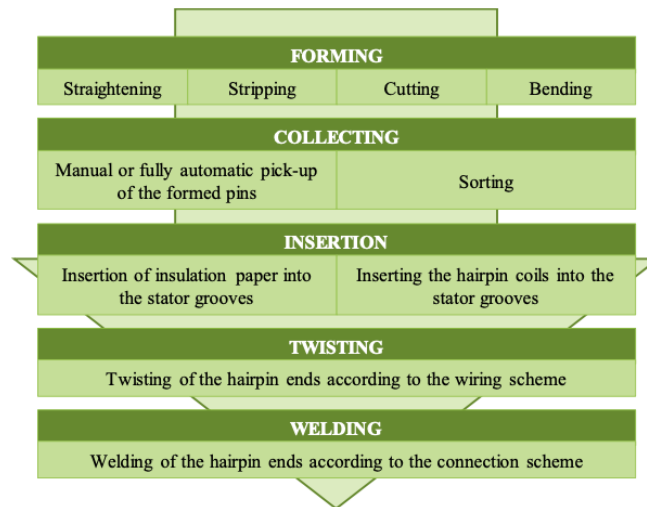


Figure 3.4. Hairpin wound stator manufacturing process path [116].

Die bending or three point bending is a multistage process depicted in Figure 3.5 (a) where the wire is first pressed into the “U” shape with a die or three point bending setup [117], [118], [119]. A second die is then used for 3D shaping of the “U” shaped wire to give it the “S” bend required for shifting between layers of different stator slots [117], [118], [119]. Swivel, or in process bending is depicted in Figure 3.5 (b) where the wire is bent into the “U” shape around a mandrel or die and the 3D “S” shape is formed by die pressing the same as before [117], [119]. An excellent example of CNC free form bending is found in [120] which is a video of BMW’s prototype E-drivetrain production using a complex machine like those used for wire or spring bending to form hairpin conductors. This process involves wire being continuously fed through a nozzle while the CNC machine first strips the end, then bends it into the 3D shape with a multi-axis tool, strips the other end and cuts the wire at the final length forming a completed hairpin conductor [116], [120]. The advantage of this process over the others is it allows for the formation of any size or shape hairpin winding without the long lead times and extra costs of making dies resulting in more efficient manufacturing where windings are continuously being optimized and refined [117].

The completed windings are then collected, sorted, and arranged into their final configuration before being inserted into the stator as a complete coil [116], [117]. This is a highly meticulous process that has zero tolerance for error since if even one conductor is out of place it could have devastating effects on motor functionality [117]. During insertion

into the stator, due to extremely high slot fills, exact precision is required to mitigate damage to the slot liner or conductors themselves [117]. After successful insertion, individual conductor ends are paired together by twisting or bending [117]. The paired ends are then connected, generally using resistance, laser, or ultrasonic welding or soldering if appropriate [117]. The process from insertion to joining is illustrated in Figure 3.6 with the final step being quality assurance testing [117].

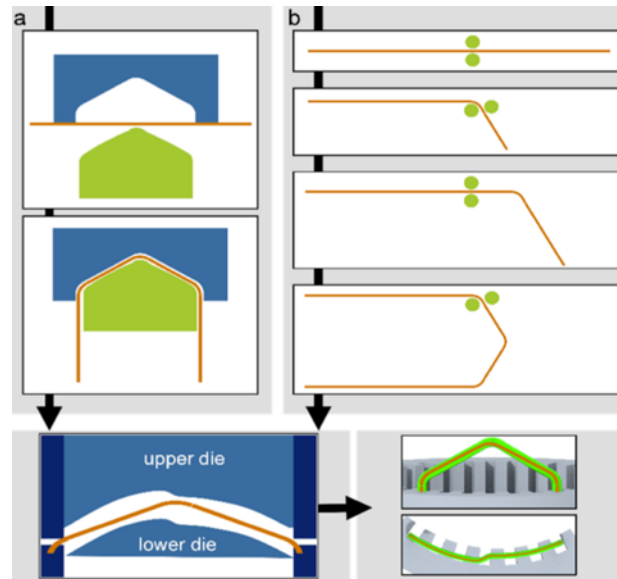


Figure 3.5. Hairpin die forming process (a) and step by step in process bending (b) [119].

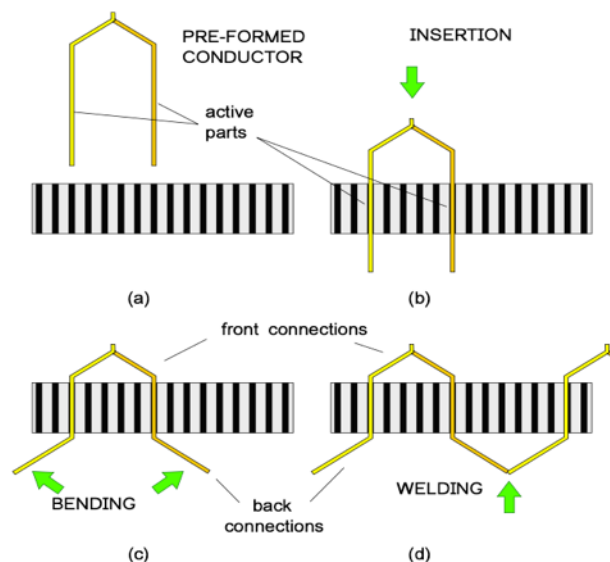


Figure 3.6. Hairpin conductor insertion into stator and subsequent bending/twisting of ends for joining [108].

3.1.3.1 Hairpin Formation Damage Analysis

Conventional winding mainly involves tensile stresses inflicted on the wire resulting in stretching [119]. This is not the case for hairpin windings which experience tensile, bending and compressive forces during formation [118], [119]. For this reason, damage free processing techniques for hairpin style conductors are still largely undefined; requiring a lot more work to analyze these forces and how they contribute to winding damage [118]. Research in [118] looked to characterize these forces and the associated damage to build FEA models for more rapid prototyping of new hairpin windings in the future. One of the main issues found was insulation thickness change where the wire is bent [118]. The inner radius sees thickening of the insulation, while the outer radius sees thinning which reduces strain resistance of the insulation that can lead to further thinning [118]. This can lead to decreased electrical resistance and dielectric strength, or in the event of failure, delamination or insulation fracture [118]. This insulation thinning needs to be carefully considered when looking to determine conductor reliability post forming operations [118].

Electrical properties of the hairpin conductor post forming also need to be considered and were analyzed in [119]. A hairpin wire was analyzed for change in resistance post insertion and twisting [119]. The formed conductor contained six 45° bends and one 90° bend which resulted in an increase in resistance of 2.34 $\mu\Omega$ where a straight wire had a resistance of 89-96 $\mu\Omega$. Accounting for this increase in resistance per conductor and per joint across the whole phase saw a very minimal impact to machine performance but there was noticeable impact at high torque where the current is highest [119].

3.2 Conductor Failure Modes

With little information available on the damage sustained by hairpin style conductors during their unique forming process, this section looks at failure modes for conductors in general.

During the manufacturing of windings, they experience deformation, bending, abrasion, high tensions and associated frictional forces to achieve tightly wound coils with high slot fill factors [54], [121]. These can lead to insulation damage and poor reliability

during operation [121]. There is also the issue of voltage gradients that can be formed, especially in end turns, from non-uniform elongation and cross-sectional area change leading to problems [54]. Improper insulation cure can also be problematic as under cured insulation is softer and will sustain damage easier or even flow at high temperatures leading to unprotected wires and short circuiting [122]. Over cured insulation will be hard and brittle resulting in cracking and flaking during bending or when experiencing abrasion forces [122].

During manufacturing, the most common defect for magnet wire is the formation of slivers or fines [6], [7], [29]. These can extend into the insulation during the enameling process and cause current leakage or potential sites for dielectric or continuity failures [6], [29]. The largest source of damage sustained by conductors during manufacturing and forming is mechanical damage during drawing in the form of die marks, gouges, slivers or fines [7]. Slivers or fines are partial delaminations of material that can break off during subsequent forming or can be pressed back into the wire surface along with other contaminants like oxides or intermetallics [123]. Surface pores or voids may also form from improper processing or corrosion [123]. These imperfections can act as stress concentration sites resulting in wire breakage during forming as well as cause adhesion issues between the conductor and electrical insulation [7], [29], [123]. Illustrations of some of these surface defects and imperfections, especially those found in drawn aluminum wire, can be found in [123].

3.2.1 Insulation Contact Deformation

Research in [124] overviews some of the tribology of contact stress effect on polymers as a function of contact angle and normal load. The main variables involved with polymer tribology are contact angle, applied normal load, associated depth of load applicator penetration, surface lubrication, and relative sliding velocity. Figure 3.7 provides a map of deformation regimes for polymers as a function of contact angle and normal load while Table 3.1 illustrates the surface damage associated with each regime. As attack angle decreases from 180° (flat on flat), damage transforms accordingly: firstly, elastic deformation results in no permanent deformation, followed by ironing which irons asperities smooth, and ductile ploughing which permanently moves material out of the path

of the indenter. Further decrease in attack angle coupled with increase in normal load or increase in friction results in destructive plastic deformation, firstly with ductile machining and cracking which ploughs material while leaving behind cracks, lesions, and surface tears. Brittle machining follows as the most extreme deformation at 0° contact angle where plastically deformed material breaks away from the surface in a brittle manner. [124]

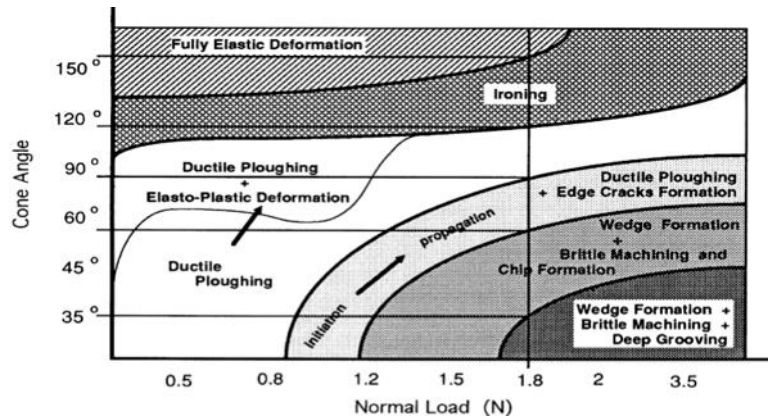


Figure 3.7. Map of deformation regimes for polymers as a function of contact angle and normal load [124].

Table 3.1. Pictorial representation of polymer deformation in each deformation regime [124].

Response (Pictorial)	Generic	α
	Elastic	180°
	Ironing	150°
	Ductile Ploughing	120°
	Ductile Machining + Cracking	90°
	↕	60°
	Brittle Machining	30°
		0°

When discussing insulation deformation, it is important to consider wire windability. Damage resistance of a magnet wire during high speed and high tension winding mainly depends on lubricity and scrape resistance of the insulation surface but adhesion between the insulation and conductor is also very important. To improve magnet wire windability, and in turn damage resistance, one method is to improve the strength of the insulation to make it more abrasion resistant. Another is to improve surface condition by decreasing COF to avoid damage from abrasive surfaces in the first place. Lastly, when abrasion resistance and surface condition have been maximized, or contact loads overcome these properties, improving adhesion strength between conductor and insulation will help to mitigate sustained damage. [121]

3.3 Aluminum Surface Defects

Aluminum is known to form a near-surface deformed layer during hot and cold rolling with a thickness ranging from hundreds of nanometers to a few micrometers [125]. This layer is formed due to shear stresses during deformation as well as interaction with the tooling [125]. The microstructure of these near-surface deformed layers are different from the bulk material, being characterized by nano-sized, fine and equiaxed grains along with grain boundaries that may or may not be populated with oxide particles [125]. These layers also have many voids and microcracks which when coupled with the fine grain structure and oxides at grain boundaries severely reduces the layers ductility compared to the bulk material [126]. The near-surface deformed layer then becomes a favorable location for crack initiation and propagation which results in flakes of this layer delaminating during subsequent forming operations [126]. An illustration of this layer and the resulting crack propagation and flake delamination are presented in Figure 3.8.

During rolling, thin layers of aluminum, including the delaminated flakes, transfer to the roller surface where they experience oxidation and are subsequently transferred back to the aluminum surface [127]. Surface metal can also be pushed backwards on itself and smeared across the bulk material surface leading to the formation of a shingle as seen in Figure 3.9 (left) [127]. A thin layer of oxide would have been present on the surface material and once pushed back on itself, now sees an aluminum oxide layer between the detached shingle and bulk material as see in Figure 3.9 (right) [125]. As rolling continues,

both the delaminated material and shingles can be pressed back into surface and bonded with the parent material resulting in buried oxide layers that may lie beneath both the near-surface deformed layer and a layer of normal bulk material [125]. High aspect ratio rolling coupled with high speed and worn tool surfaces results in increased interaction between the aluminum surface and roller leading to increased shingle formation and thicker near-surface deformed layers [127]. Both the near-surface deformed layer and shingle formation lead to poor surface quality that may lead to the issues discussed in Section 3.2 regarding magnet wire breakage and poor insulation adhesion.

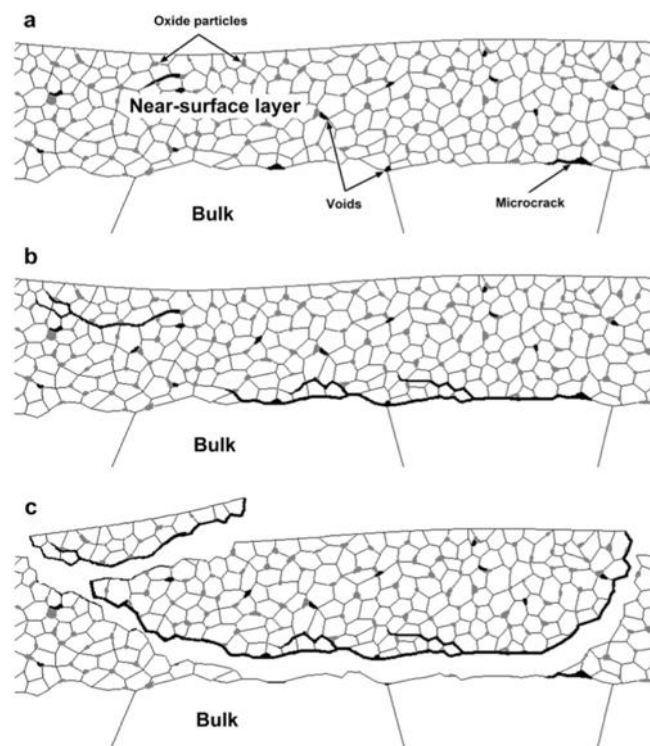


Figure 3.8. Delamination of brittle near-surface deformed layer from crack initiation and propagation resulting in flakes delaminating from the aluminum surface [126].

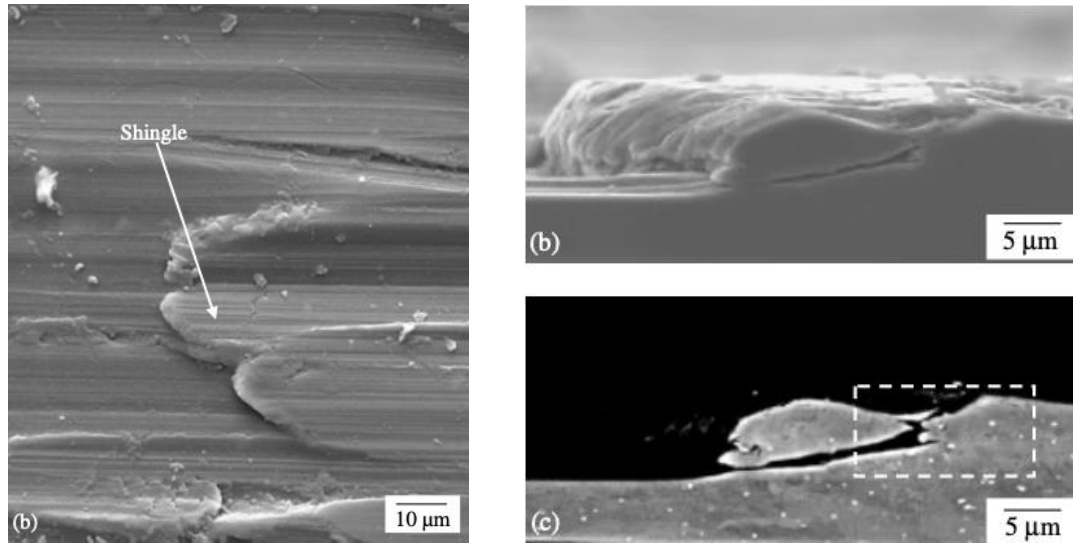


Figure 3.9. Shingle on deformed aluminum surface (left) and cross section view highlighting shingle is detached from the bulk material (right) [127].

Chapter 4

METHODOLOGY

4.1 Research Objectives

Post review of available literature, two main gaps in knowledge were discovered. Firstly, current research mainly focuses on simulation-based analysis of aluminum versus copper magnet wires in electric machines. These studies typically perform surface level performance analysis on lab scale motors focusing on conductivity, weight and conductor cost. This ignores some important motor performance parameters gleaned from drive cycle analysis or prototype/full-scale machine analysis. Secondly, there is a lack of metallurgical based analysis of aluminum conductor performance in manufacturing, winding and motor operation. This is especially true for hairpin windings and their unique formation processes where aluminum has seen very little use and study.

From these gaps in knowledge, 4 objectives were established to accomplish the main research goal of determining the feasibility of effectively replacing copper conductors with aluminum, specifically for use in automotive scale electric motors. The 4 objectives are:

- Perform a comprehensive literature review of aluminum versus copper electrical conductors to create a unified source of information to better aid future research.
- Compare the advantages and disadvantages of replacing copper with aluminum magnet wire with emphasis on its use in high performance, automotive scale electric motors.
- Characterize and compare the formability and windability of shaped aluminum and copper conductors regarding manufacturing, winding, and hairpin winding formation processes.
- Characterize deformation behaviour and damage mechanisms for the aluminum and copper conductors studied.

4.2 Magnet Wire Samples Used

Both aluminum and copper magnet wires were utilized in this study. The copper wires are the same as those seen in [14], Section 3.1. They are a 3.5 x 3.7 mm shaped wire with a cross-sectional area of 12.94 mm² from Hitachi Cable designated as KMKED-22A. The wires came pre-straightened and pre-cut to a length of 14 inches (355 mm). The conductor alloy used is electrolytic tough pitch copper with 99.9% purity. The electrical insulation is a polyamide-imide base coat and polyamide-imide topcoat rated at a temperature class of 220°C.

Studied aluminum wires were used in both an insulated and bare variant. The conductor alloy is A1350, or electrical conductor (EC) aluminum with a purity of 99.5%. Samples are 7 AWG square (3.665 x 3.665 mm) with a cross-sectional area of 12.9 mm². Both aluminum variants came pre-wound on a spool. The film insulation is a modified polyester basecoat and polyamide-imide topcoat also rated at a temperature class of 220°C. All wire samples used can be seen in Figure 4.1 below.



Figure 4.1. Magnet wire samples tested in this study: insulated aluminum (top), bare aluminum (middle), insulated copper (bottom).

4.2.1 Aluminum Insulation Characterization

The film insulation on the aluminum magnet wires differs slightly from the copper wires used in this study which were characterized in [14], Section 3.1. Copper uses polyamide-imide for both the base and top coats while aluminum uses a modified polyester

basecoat and polyamide-imide topcoat. However, both conductors are designed for the same use cases and temperature class of 220°C. To properly compare these two insulated conductors, a fresh piece of aluminum was sectioned, mounted, polished and observed under scanning electron microscope (SEM). The cross section can be seen in Figure 4.2 where the backscattered electron (BSE) image clearly defines two distinct polymer layers. The base coat, adjacent to the aluminum substrate, is roughly 31 μm and is deposited on the conductor in layers during manufacturing although they cannot be seen like they can on the copper conductor in [14], Figure 56. The top coat is thinner than the base coat at roughly 12 μm resulting in a total insulation thickness of 43 μm . Insulation thickness varies slightly across the square conductor cross section, especially around the corners where it is moderately thicker. Compared to the copper insulation, which was measured as 48 μm thick [14], the insulation on aluminum is marginally thinner.

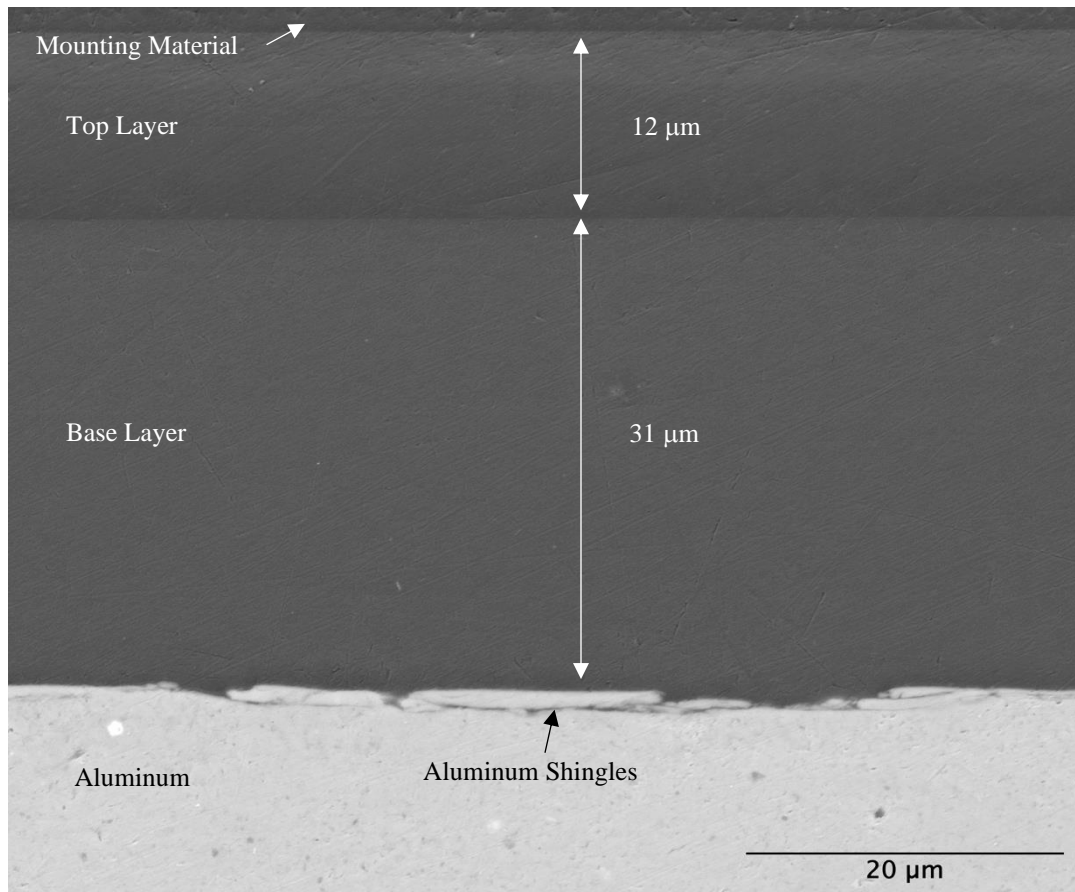


Figure 4.2. Backscattered electron SEM image of Aluminum magnet wire cross section consisting of aluminum substrate with apparent surface shingles, 31 μm insulation base layer, 12 μm insulation top coat, and mounting material.

4.3 Formability and Windability Testing Procedures

Electrical conductors and associated electrically insulative films require a certain amount of malleability and damage resistance during manufacturing and subsequent winding into coils for use in electrical machines. When designing a new electrical insulation, or comparing the capabilities of multiple conductors, it is important to be able to characterize their performance during manufacturing and winding operations. *ASTM D1676-17: Standard Test Methods for Film-Insulated Magnet Wire* does this with many test methods primarily designed to evaluate the electrical insulation on aluminum or copper conductors. Although, several test methods specifically characterize the formability and windability of these magnet wires which are the most important properties relating to manufacture and winding.

Formability is defined as the ability of a magnet wire to be formed into and maintain a desired shape. **Windability** is defined as the ability of a magnet wire to be made into a coil with maximum formability and compaction while minimizing sustained physical and electrical damage. It is desired to maximize these properties to yield faster production times with minimized wire breakage and form more compact coils that maintain their shape. [128]

ASTM D1676-17 outlines 5 specific tests to characterize formability and windability of aluminum and copper magnet wires:

- Elongation
- Film adherence and flexibility
- Elastic ratio method
- Low stress elongation
- Springback

4.3.1 Tensile Testing Procedure

All tests mentioned above, except springback testing, require the use of a tensile testing machine and a gripping solution that inhibits slippage and promotes failure in the gauge length. A 50 kN MTS Criterion Universal Testing Machine was used with standard wedge grips as well as a custom gripping solution. Conventional tensile testing requires

the manufacturing of standardized samples that conform well to standard gripping devices for universal testing machines. However, to test magnet wire, the entire cross section needs to be used so it cannot be altered to accommodate standard grips. The aluminum and copper being tested is also a large gauge and square and rectangular in cross section respectively; making the use of capstan or bollard gripping solutions difficult. These issues were addressed in [14], where a custom tensile testing clamp, seen in Figure 4.3, was designed and fabricated based on U.S. patent #3528283 for the 3.5 x 3.7 mm copper wire used in that study. The clamp was designed to spread clamping pressure over a large area to mitigate stress concentration and promote fracture in the gauge length [129]. Results from [14] show successful use of this clamp to perform elongation testing for rectangular cross section copper wires.

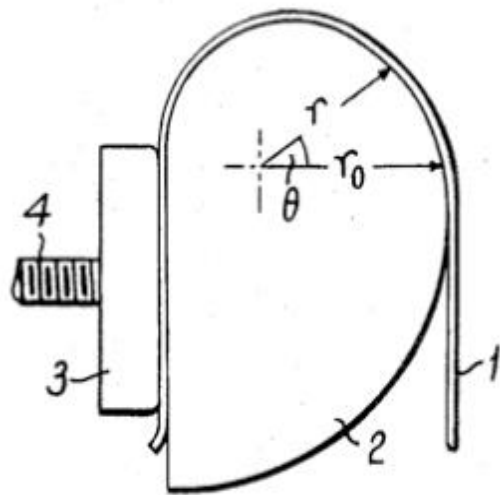


Figure 4.3. (Left) Tensile testing clamp patent design to maximize clamping pressure on magnet wire and mitigate breakage where 1 is the magnet wire, 2 is the clamp body, and 3 is the clamping member to secure the magnet wire over a large area [129]. (Right) Fabricated tensile testing clamp from [14] designed for use with rectangular cross section copper magnet wire and used for aluminum magnet wire in this study.

The copper magnet wire tested in this study differs from [14] in that the samples are 14 inches long instead of 24 inches so they are not long enough to wrap around both custom clamps for testing. The solution for this was to not wrap the wire around the clamp but instead use only the clamping member, seen as number 3 in Figure 4.3 (left), to hold the wire for testing. Using the clamps in this way still spread the clamping pressure over the 2 inch long clamping member while also providing a smooth exit from the clamp to

mitigate stress concentrations. This was especially important for the aluminum since it is much softer and weaker than copper. Wrapping the aluminum wire around the clamp as intended, coupled with the softness of annealed A1350, resulted in stress concentrations since it would conform to the clamp under tension, reducing the cross-sectional area and ultimately lead to failure at wire exit from the clamp. Utilizing the custom clamps as described can be seen in Figure 4.4.



Figure 4.4. Alternate clamping method for aluminum and copper wires using only the clamping member of the tensile testing clamp to accommodate the shorter copper wires used in this study as well as to mitigate stress concentrations on aluminum wire at grip exit when used as intended.

This clamping method mitigated the problems discussed for copper and aluminum resulting in successful tests and fracture within the wire gauge. However, elongating copper samples to failure with this alternate clamping method resulted in a loss of clamping pressure and wire slippage due to its greater elongation than aluminum. An alternate solution was to fold the ends of the copper wire on itself and use the standard wedge grips of the tensile testing machine. These wedge grips self-tighten as the wire elongates which helps maintain enough clamping pressure to run the test to wire failure. Folding the wire on itself effectively doubled the cross-sectional area under clamping pressure and reduced stress concentrations at wire exit from the grips, promoting failure inside the gauge length. This reduced the gauge length of the copper wire due to samples being a fixed length but did not affect the results in terms of comparing them to aluminum. This alternate copper wire clamping method for testing to failure can be seen in Figure 4.5.

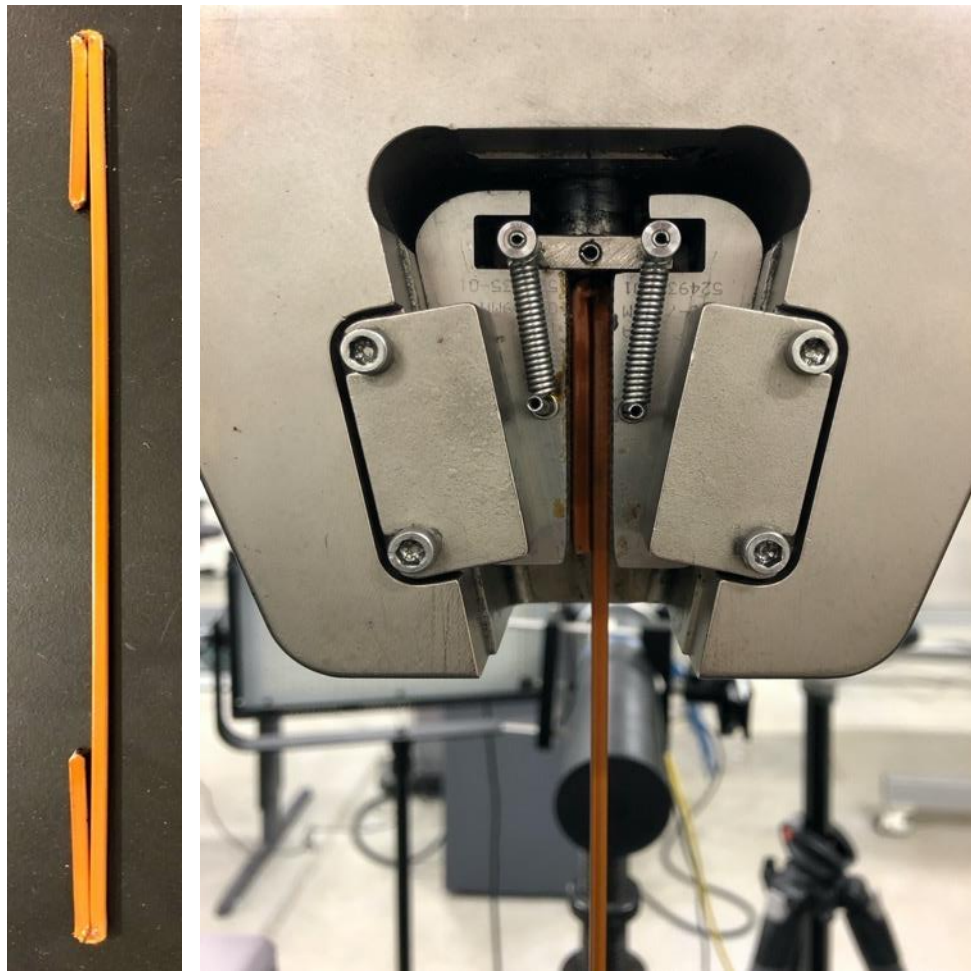


Figure 4.5. Clamping method for testing copper wires to failure using self-tightening tensile testing wedge grips and folded wire ends to increase clamping pressure area.

4.3.2 Elongation Testing Procedure

Elongation testing is used to determine the general ductility of materials. With regards to film-insulated magnet wire, it also measures the flexibility and adherence of the electrical insulation [128]. Elongation testing can also illustrate how a conductor material cold works which is an important factor for improving production efficiency and maximizing electrical conductivity.

Testing was conducted according to ASTM D1676-17, Sections 122-129. Aluminum wire samples were tested with the clamping method seen in Figure 4.4 with a gauge length of 10 inches (254 mm). Copper wire samples were tested using the clamping method from Figure 4.5 with a gauge length of approximately 145 mm. The standard requires a gauge length of 10 ± 0.1 inches (250 ± 2.5 mm) but the fixed length of the copper wires along with folding the ends to ensure successful testing meant this could not be met. Therefore, copper samples were estimated to elongate slightly less than expected for a wire of proper gauge length meaning elongation percentages could not be directly compared to aluminum. However, results on insulation film flexibility and adherence as well as cold workability were still directly comparable and more relevant to magnet wire formability and windability characterization.

Both wire samples were tested at an extension rate of 300 mm/min until failure within the gauge length. Strain induced in the wire was measured using the crosshead displacement of the universal testing machine grips. Elongation of all samples was calculated as a percentage according to Equation (14), where A is the length of the wire at break and B is the original gauge length. The average of three tests for each conductor type was taken.

$$\text{Elongation (\%)} = [(A - B)/B] \times 100 \quad (14)$$

4.3.3 Film Adherence and Flexibility Testing Procedure

Film adherence and flexibility testing is used to determine the level of stress required to produce visible cracks or loss of adhesion in the magnet wire film insulation. During winding operations, it is important for the insulation to remain properly adhered

while being flexible enough to accommodate minor elongation and bending to maintain magnet wire integrity during use. [128]

Elongation testing gives a good idea on the adherence and flexibility of the film insulation, but it is limited to evaluating these properties only after the wire has failed. Film adherence and flexibility testing according to ASTM D1676-17, Sections 141-148, specifically looks at these properties at elongation levels below that of fracture. The test also has the versatility to evaluate adherence and flexibility at various levels of elongation to determine the degree of adherence at each level.

Testing was only conducted on aluminum wires using the clamping method from Figure 4.4. Samples with a gauge length of 10 inches (254 mm) were elongated to the specified percentage at a rate of 300 mm/min. For the 7 AWG square aluminum wire tested, the standard called for elongation to a minimum of 15%. However, to test the level of film insulation adherence over a range of wire elongation, it was tested at 5%, 10%, 15%, and 20%. Since the test is based on a pass or fail rating, one wire sample was tested at each elongation level. Post testing, each wire was inspected for complete or partial delamination sustained from testing or by using slight pressure and lateral motion with the thumb and finger on the wire surface. The insulation was also inspected for cracks or failures which expose the underlying conductor.

These observation methods do not provide a quantitative measure for the level of adherence the film insulation has with the conductor at various levels of strain. Therefore, outside the scope of the standard, a peel test was performed on tested samples along with a fresh piece of aluminum and a sample elongation to failure for insulation adhesion comparison. The peel test involves using a utility knife blade to make an incision between the film insulation and conductor to try and remove the insulation. If a pull tab can be created, an attempt is made to peel the insulation off the conductor. The ability to create a pull tab of insulation, along with the success or difficulty of using it to remove the insulation from the conductor gives a rough measure of the level of film adherence at each percentage of elongation tested. An example of this test can be seen in Figure 4.6 where an incision was made, and a pull tab created, at the end of a cut piece of aluminum wire where the insulation was already partially delaminated from cutting.



Figure 4.6. Example of peel test procedure on aluminum magnet wire where a knife is used to separate the insulation from the base conductor to create a pull tab for attempted insulation removal.

4.3.4 Elastic Ratio Method Procedure

Elastic ratio testing is used to measure a magnet wires ability to elongate during high speed winding [128]. During winding operations, it is common to see elongation of the magnet wire up to 10% [53], [54], [128]. Therefore, it is important that the elastic ratio be a minimum for wires to best accommodate winding at high speeds [128]. Elastic ratio is determined by elongating the wire to failure and taking the ratio of load at 5% elongation by the load at fracture [128].

Testing was conducted according to ASTM D1676-17, Section 152 but the same procedure and wires were used from elongation testing in Section 4.3.2. This means wires were tested at an extension rate of 300 mm/min instead of the 250 mm/min outlined in the standard and the copper wire gauge length was 145 mm instead of the required 254 mm. The elastic ratio was calculated from an average of three tests for each conductor according to Equation (15).

$$\text{Elastic Ratio (\%)} = \left(\frac{\text{Load at 5\% Elongation}}{\text{Load at break}} \right) \times 100 \quad (15)$$

4.3.5 Low Stress Elongation Testing Procedure

The low stress elongation (LSE) test gives a measure of a magnet wires ability to absorb bends and twists during winding operations [128] by simulating bending strains usually experienced during the process [29]. It is one of the best criterion to use for evaluating conductor conformability or shape retention [7], [29]. LSE is determined by measuring the permanent, unstressed elongation of a wire during elongation to a specified stress associated with each conductor type [128]. Better formability is attributed to the wire that experiences greater permanent elongation [128].

Testing was conducted according to ASTM D1676-17, Section 153. Both aluminum and copper magnet wires were tested using the clamping method seen in Figure 4.4 with a gauge length of 10 inches (254 mm). Samples were elongated slowly, at a rate of 5 mm/min. The test began by applying an initial stress to straighten the wire followed by setting the elongation measurement device to zero. Aluminum and copper were pre-stressed to 27.6 MPa and 51.7 MPa, equating to a pre-load of 356 N and 669 N respectively. Both conductors were then elongated to a specified stress, which was held constant for 30 seconds, followed by a return to the initial stress where the resulting permanent elongation was recorded. The specified stress for aluminum and copper was 55.2 MPa and 103.4 MPa equating to a load of 712 N and 1338 N respectively. This testing procedure is represented graphically in Figure 4.7. Low stress elongation for each conductor was then calculated from an average of three tests according to Equation (16).

$$LSE (\%) = (Permanent\ Elongation \div Original\ Gauge\ Length) \times 100 \quad (16)$$

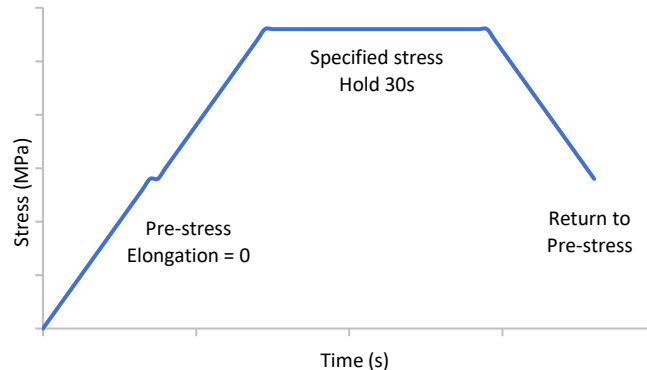


Figure 4.7. Low stress elongation testing process path.

4.3.6 Springback Testing Procedure

Springback testing measures the wires ability to maintain its shape after bending [128]. This is important for winding the wire into coils. Generally speaking, both low yield strength and high elastic modulus indicate minimal springback for a metal [7], [29]. Lower springback and in turn, greater formability, allows the wound coils to be more compact so they can achieve greater slot fill, shorter end turns as well as reduce material use, cost and overall machine size [10], [24, pp. 14-1 - 14-13], [45], [55].

Testing was conducted according to ASTM D1676-17, Section 155, with a custom built springback testing apparatus designed according to specifications in the same section. The standardized design can be seen in Figure 4.8 with the custom built springback tester seen in Figure 4.9. The magnet wire being tested was fixed between two jaws with a chamfered exit to limit stress concentrations induced on the wire as it was bent. The slider, with a knife edge in the middle, was set to a calculated position along the lever arm based on the diameter of the wire being tested. A gauge pointer was fixed to the end of the lever arm, positioned in line with the middle plane of the wire, to give an accurate measure of bending angle according to the graduated sector.

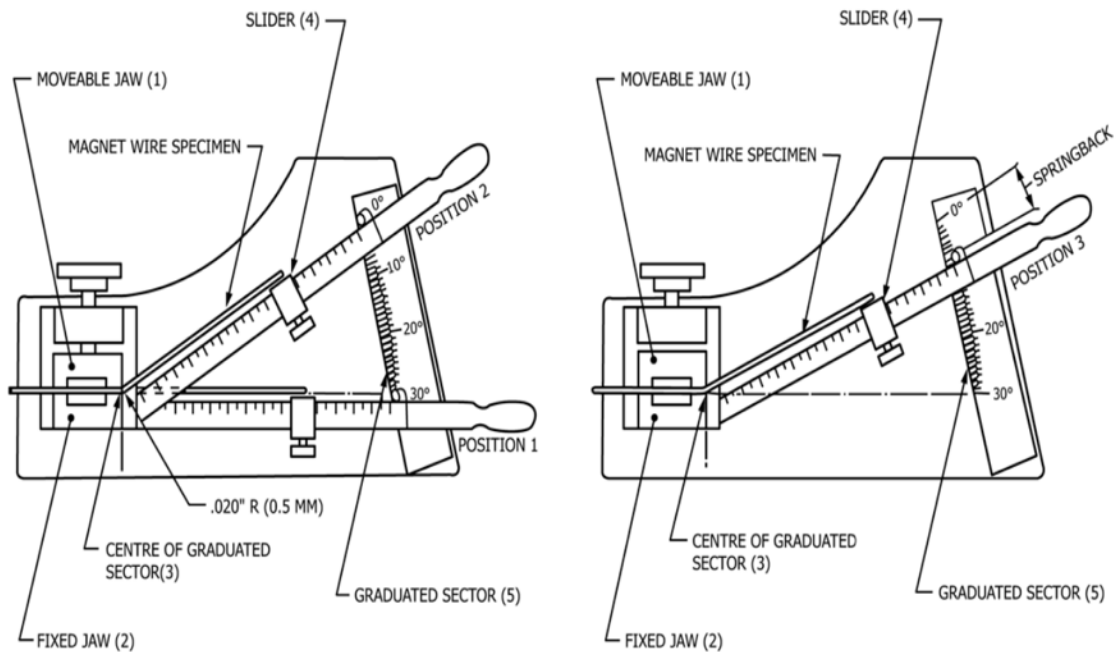


Figure 4.8. Springback testing apparatus design specifications from [128].

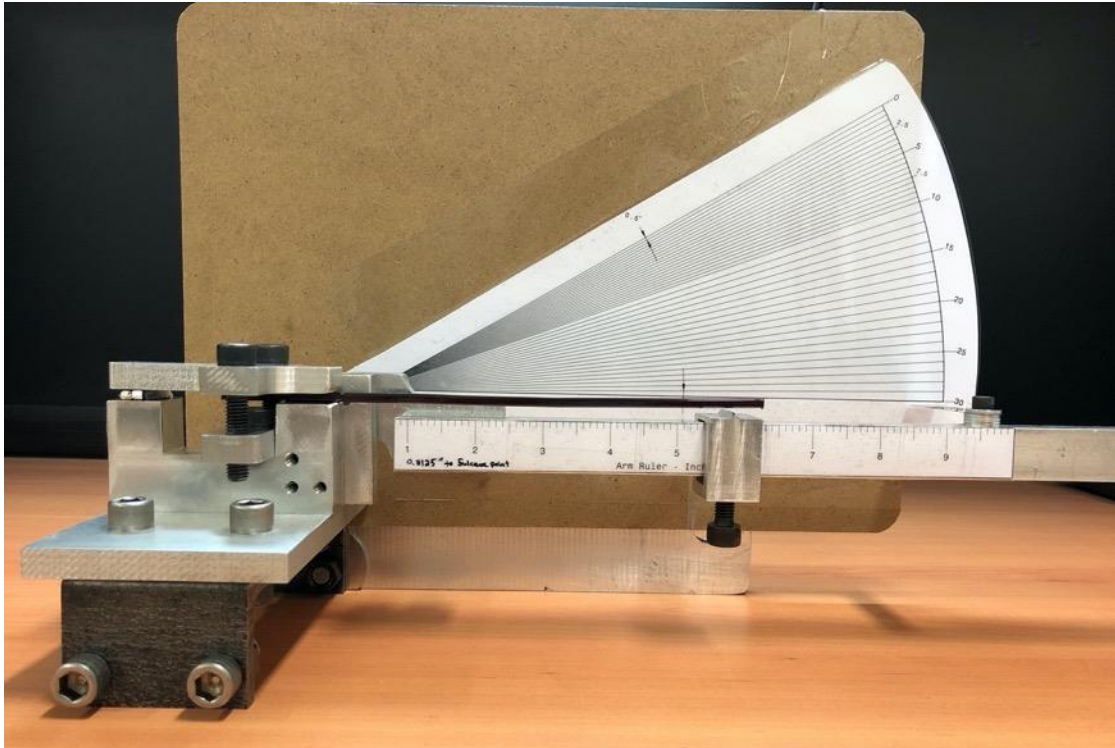


Figure 4.9. Custom built springback testing apparatus used for copper and aluminum magnet wire samples in this study.

Both bare and insulated aluminum were tested to see if the insulation process or the insulation itself would affect the springback of the conductor. Insulated copper was also tested across both rectangular dimensions to see the impact it would have on springback. For the square aluminum wire, having a thickness of 3.665 mm, the slider was positioned at 5.8 inches (147.5 mm). For the rectangular copper wire samples bent across the 3.7 mm dimension, the slider was positioned at 5.8 inches as well. Samples bent across the 3.5 mm dimension had the slider positioned at 5.5 inches (140 mm).

The testing procedure involved gently bending all wire samples from the resting 30° position to 0° at an angular rate between 2 and 5 seconds. The samples were then held at the 0° position for no more than 2 seconds where the lever arm was then slowly returned to its resting position at the same angular rate as initial bending. Springback was directly measured and recorded by bringing the lever arm back up to the now bent and relaxed wire, just touching it with the knife edge of the slider and reading the angle on the graduated sector using the gauge pointer. An average springback was taken from 3 samples for each aluminum and copper wire tested.

4.4 Wire Bending Simulation Testing Procedures

Round magnet wires are conventionally wound directly into the motor stator or into coils by hand, or machine to be inserted into the stator later. Shaped magnet wires like those used in this study are generally used as hairpin style conductors. The winding method for these conductors is entirely different, as discussed in Section 3.1.3, mainly consisting of die pressing and shaping conductors individually followed by axial insertion into the stator slots. This die forming procedure can see pressures up to 500 MPa applied to copper wire as well as speeds up to 20 mm/s from the wire sliding against the die [14]. This means coefficient of friction between the die and wire plays a critical role with regards to formability and windability during manufacturing. Therefore, simply characterizing both properties with the standardized methods seen in Section 4.3 is not enough to understand wire performance during this unique forming operation.

4.4.1 Wire Bending Simulator Machine

A. Demiri in [14] outlined 5 key variables involved with calculating the coefficient of friction between the wire and die:

- Material composition of contacting surfaces
- Condition of the contacting surfaces
- Pressure between moving contact surfaces
- Relative speed and acceleration between surfaces
- Percentage strain experienced on the wire surface

He then designed and built a testing machine to control these variables and replicate the conditions a shaped magnet wire experiences during die forming. The completed wire forming / wire bending simulator allowed for proper characterization of formability and windability for square or rectangular cross section wire. Details, design methodology, specifications, and instructional use of the machine can be found in [14]. Elements of the die forming process are found in [14], Section 3.3.2. Design and fabrication considerations along with how the machine controls sample motion, imparts pressure and surface strain on the wire, measures and outputs the controlled forces experienced by the wire can be

found in [14], Section 3.3.1. Detailed instructions on machine set up, use, and testing procedure can be found in [14], Appendix A.

The wire bending simulator is pictured in Figure 4.10. It controls the speed, acceleration and motion of the magnet wire using two actuators mounted on movable arms. Both actuators work in conjunction with each other to impart a desired tension on the wire while simultaneously moving it across the contacting surfaces with a precise speed and acceleration. Each arm can be positioned in 5° increments from 0° to 45° resulting in 0° to 90° forming angles experienced by the wire. Induced tension combined with forming angle allows for precise control of strain experienced on the wire surface.

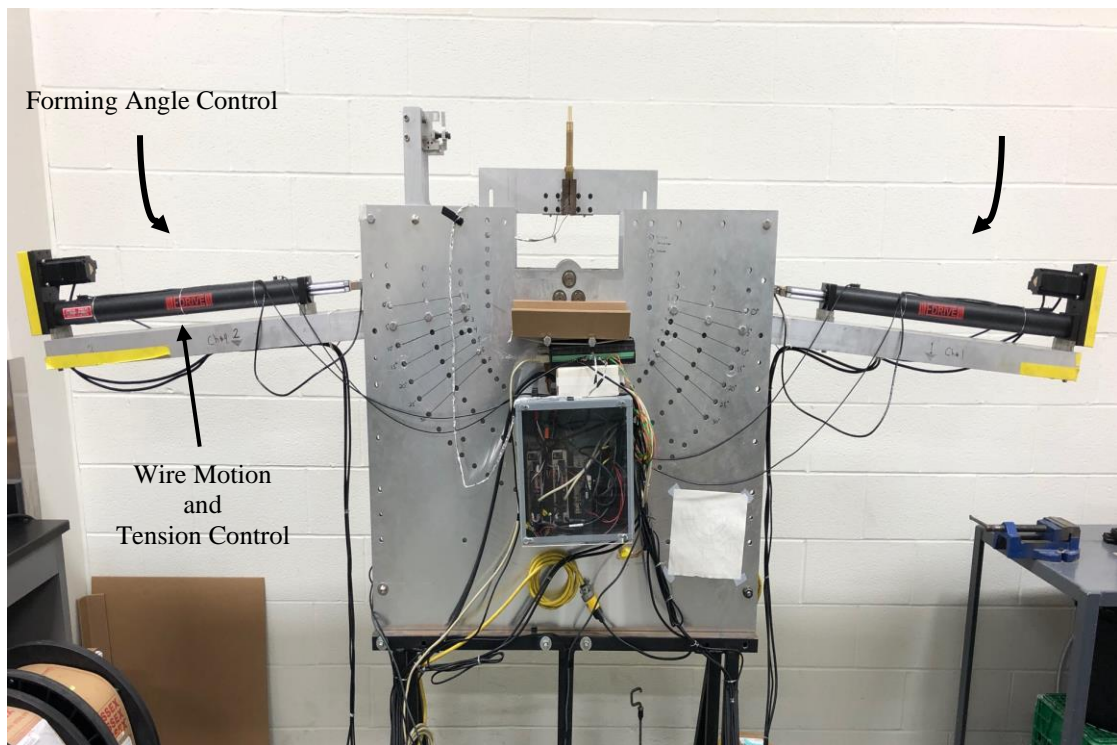


Figure 4.10. Custom built wire bending/forming simulator from [14]. Forming angle is controlled by positioning the arms supporting the linear actuators to preset angles where the support roller is the focal point. Wire motion and tension are controlled using two linear actuators in tandem.

A detailed view of how the machine controls contacting surfaces, imparts pressure on the wire surface and measure resulting friction force during testing can be seen in Figure 4.11. The wire is fixed to the ends of both actuators with a clamp and a tension sensor. The bottom surface of the wire is supported by a steel roller with a desired radius. Changing the radius of the roller along with the forming angle controls strain experienced on the wire

surface. Pressure is exerted on the wire surface by loading weights on top of the die material counterface in contact with the top of the wire.

During testing, the wire is moved from left to right, as seen in Figure 4.11, between the support roller and counterface. This causes the friction arm, which holds the counterface, normal load weights, and force measuring sensors, to elastically deflect, allowing friction force experienced by the wire to be directly measured. Further details on exactly how the wire bending machine controls forces exerted on the wire and measures friction force can be found in [14], Sections 3.1.1.1 and 3.1.1.2.

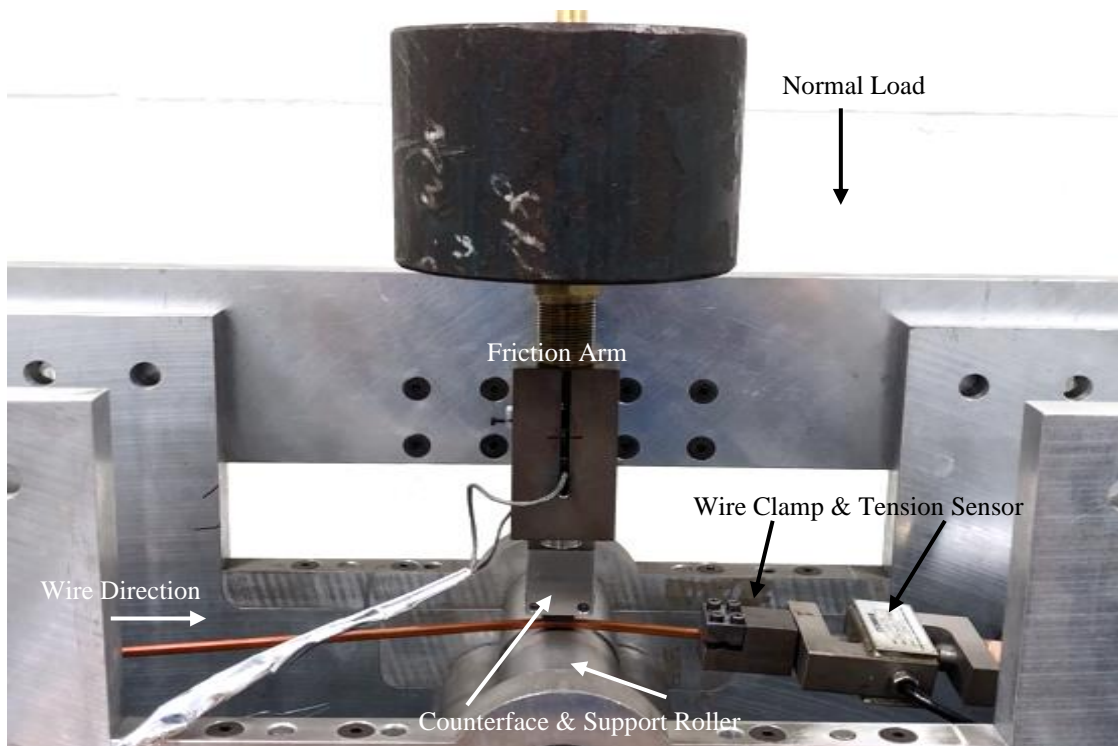


Figure 4.11. Close up of wire bending/forming simulator from [14]. The magnet wire is fixed to both linear actuators using clamps fixed to tension sensors used for wire tension control. A steel support roller controls contact area as well as strain experienced on the wire surface along with forming angle. Pressure exerted on the wire surface is controlled by placing weights on the friction arm which imparts a normal load through a load sensor and counterface made of desired contact material. Friction force is measured through elastic deflection of the friction arm in the direction of wire travel.

4.4.2 Coefficient of Friction Measurement Testing Procedures

A. Demiri extensively covered the effect of various testing parameters on the coefficient of friction between a steel die material and copper magnet wire in [14]. The objective of this research is to perform similar testing with aluminum magnet wire and

compare the results to those for copper. This will give a good idea how effectively aluminum can replace copper in the same die forming process and determine the feasibility of using it as a hairpin style conductor. The most notable copper results to compare aluminum to are COF versus wire travel speed and forming angle. Copper has established operating parameters for die forming which includes forming pressure. Aluminum does not, and since its material properties differ so much from copper, COF versus normal load testing was also performed to evaluate performance under various loads and establish an appropriate pressure for the procedure.

Wire samples tested were typically 350 mm long with an effective contact length of 220 mm. Prior to testing, wires were cleaned with a glass cleaner to remove any residual oils or contaminants left behind from manufacturing and handling. During testing, wires were only handled by their ends to avoid contaminating the contact surface. The die material used for the counterface was a pre-heat treated 4140 steel with a contact area of 12.7 x 8 mm. Counterfaces were polished to a 1 μm diamond finished prior to each test. Two support rollers were used to further control the strain experienced on the wire surface. A 24 mm radius roller with a machined surface seen in Figure 4.12 and a 3 mm radius roller with a smooth surface seen in Figure 4.13.

The standard wire speed and acceleration used for testing was 20 mm/s and 20 mm/s² respectively to remain consistent with copper testing done in [14]. The standard normal load used for testing was 12 lbs as determined by the analysis of coefficient of friction versus normal load results which is discussed in more detail in Section 5.2.1. Wire pre-tension used for aluminum was determined from recommended winding tensions in the Superior Essex magnet wire engineering data handbook [38], as well as trial testing at various preloads to measure the level of permanent elongation experienced. The maximum recommended winding tension for 7 AWG square aluminum wire according to [38] was roughly 125 lbs based on a yield strength of 6400 psi (44 MPa). Using the minimum yield strength for aluminum of 4000 psi (27.5 MPa) instead, gives a minimum winding tension of 80 lbs. Testing to preloads between 80 and 120 lbs saw no permanent elongation for 80 lbs and increasing permanent elongation above that. Therefore, the pre-tension used for aluminum wires was set to 80 lbs while that for copper was kept at 200 lbs, the same used for testing in [14].

The average COF and standard deviation were calculated from the portion of the test with constant speed. Acceleration phases of the test were discarded from the data range. Further details on test set up, precise testing procedures, software used, and data acquisition and analysis can be found in [14], Section 3.3.3 and Appendix A.

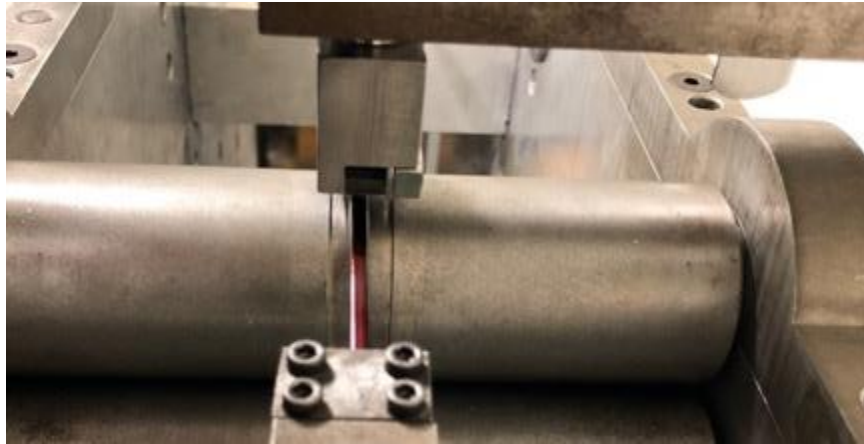


Figure 4.12. 24 mm steel support roller used for testing.

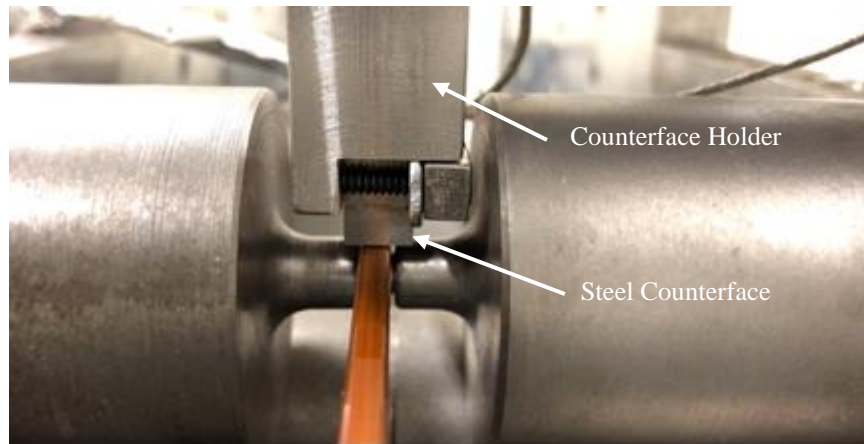


Figure 4.13. 3 mm steel support roller used for testing.

4.4.2.1 COF vs Normal Load Testing Procedure

All copper wire samples tested in [14] were done so with a normal load of 40 lbs since the die forming process had established operating parameters for copper. This was not the case for aluminum magnet wire, so a study was done to determine the effect pressure has on coefficient of friction.

Testing was conducted with normal loads of 7, 12, 22, 27, 32, 37 and 42 lbs for aluminum wires. Copper was also tested at 22 and 42 lbs for updated results using the

machine set up, materials, and procedures outlined in this study. Both support rollers were also used for each normal load tested. All other variables were kept constant. Speed and acceleration of the wire were set to 20 mm/s and 20 mm/s² respectively. Forming angle was set to 10° to eliminate damage caused to the wire by the edges of the steel counterface if the wire was tested at 0°. A minimum of three wire samples were tested at each normal load and support roller radius combination.

4.4.2.2 COF vs Speed Testing Procedure

Once the results of COF versus normal load were analyzed, a standard normal load to use for speed and forming angle testing was established. It was found in Section 5.2.1 that a normal load of 12 lbs saw minimal influence on COF and wire surface damage keeping the focus on the impact to COF from wire travel speed.

Testing was conducted at speeds of 5-40 mm/s in 5 mm/s increments for aluminum magnet wire. Forming angle was set to 10° and wire acceleration was kept constant at 20 mm/s². Only the 3 mm radius support roller was used for testing since both were not required to get the general trend of COF versus speed. Three samples were tested at each speed and the results were compared to those for copper from [14] which tested wires at 1, 5, 10, 15 and 20 mm/s.

4.4.2.3 COF vs Forming Angle Testing Procedure

Changing the forming angle, along with the support roller radius, alters the strain experienced on the surface of the wire. Copper wire samples from [14] were tested at forming angles of 0°, 30° and 60° along with contact surface strains of 2%, 5%, 10%, 15% and 20%. This research looks at the effect forming angle and in turn, surface strain, has on the coefficient of friction for aluminum wires and how the results compare to those for copper.

Testing was conducted at forming angles of 10°, 30°, 60° and 90° for aluminum wire samples. The applied normal load was kept constant at 12 lbs. Speed and acceleration of the wires were set to 20 mm/s and 20 mm/s² respectively. Both the 3 mm radius and 24 mm radius support rollers were used for testing at each forming angle. However, the 3 mm

radius roller was not used for 90° tests due to geometry limitations of the machine. Three samples were tested at each angle and support roller radius combination.

4.5 Sample Observation Methods

Post testing, deformation behaviour and damage mechanisms were observed for wire samples and steel counterfaces. Steel counterface and film insulation surfaces were first observed with a stereomicroscope to get a macroscopic view of the contact region. More detailed observation of material transfer, scratching and insulation damage was done with optical microscopy. A Keyence laser microscope was used to gather topographical information on the counterface and insulation contact regions as well as for elongated wire sample surfaces. Final observation on counterface material transfer regions, elongated wire sample surfaces and mounted cross-sections of fresh and tested wire samples was performed with a scanning electron microscope (SEM) along with energy dispersive X-ray spectroscopy (EDS) for composition analysis.

4.5.1 Sample Cross Section Preparation

Tested samples required further and more detailed analysis to determine the behaviour of the conductor and film insulation under various testing conditions. This required samples to be cut, mounted, and polished in preparation for observation with SEM. Samples were mounted in both the edge wise and length wise cross-sections to get a full picture view of the effect testing conditions had on the wire and insulation. Mounting was done with Buehler EpoThin 2 Epoxy resin and hardener. Grinding was performed with silicon carbide papers at P120, P180, P320, P400, P800 and P1200. This was followed by polishing with 9 µm and 1 µm alumina solution. Final polishing was done with 1 µm diamond solution. Samples were thoroughly cleaned with distilled water and a clean polishing cloth between polishing phases as well as after final polishing.

Chapter 5

RESULTS

This chapter covers results from the testing procedures outlined in Chapter 4 along with observations characterizing deformation behaviour and damage mechanisms for the samples tested.

5.1 Formability and Windability Testing Results

The following section outlines results from standardized magnet wire formability and windability testing found in *ASTM D1676-17: Standard Test Methods for Film-Insulated Magnet Wire*.

5.1.1 Elongation Testing Results

Three insulated aluminum samples and three insulated copper samples were tested according to the procedure outlined in Section 4.3.2 with the average elongation percentage and standard deviation reported. Standard elongation values from Table 2.1 are 23% for aluminum and 35% for copper. These can be compared to the testing results found in Table 5.1. Aluminum was found to have an average elongation of 32.80% with a standard deviation of 0.30%. Copper saw an average elongation of 62.48% with a standard deviation of 0.64%. Copper elongated nearly twice as much as aluminum even with a shorter gauge length which reduces the total elongation expected from a proper 10 inch long sample. Both conductors saw far greater elongation than typical values because they are large gauge wires.

The stress versus strain curves for both wires are found in Figure 5.1. The graph further illustrates the much greater elongation of copper compared to aluminum. This is attributed to aluminum having a higher stacking fault energy and lower strain hardening exponent compared to copper as discussed in Section 2.8.2. This results in a much greater level of cold working experienced for copper and therefore greater elongation compared to aluminum. Stress versus strain curves illustrate this as a very flat curve for aluminum and an increasing curve for copper. Although copper experiences greater elongation, overall

formability and windability of magnet wire is closely tied with material stacking fault energy and strain hardening exponent. This could give advantages to aluminum during manufacturing and winding operations since it requires less energy to form.

Table 5.1. Elongation testing results for aluminum and copper wire samples.

Aluminum			
Test #	Elongation (%)	AVG	STDEV
1	33.06	32.80	0.30
2	32.48		
3	32.87		
Copper			
Test #	Elongation (%)	AVG	STDEV
1	61.75	62.48	0.64
2	62.90		
3	62.79		

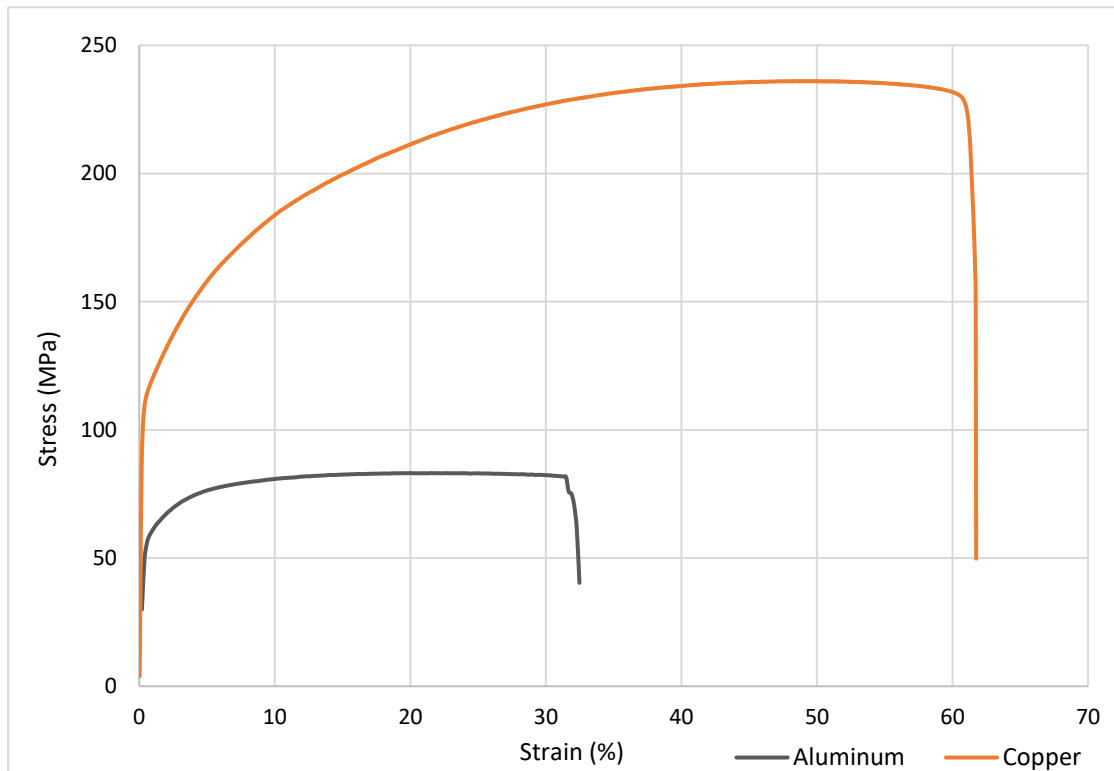


Figure 5.1. Stress vs strain curves for aluminum and copper magnet wire elongation testing samples.

5.1.1.1 Stress vs Strain Curve Stress Drop Observations

A. Demiri reported drops in stress during tensile testing in [14], Section 4.9.1. These drops in stress are highlighted in Figure 5.2 and were found to directly correspond to fracturing of the copper insulation. Copper samples tested according to the testing conditions used in this study did not see the same large fractures in insulation and corresponding stress drops. Aluminum experienced similar behaviour, but at the onset of necking and failure as seen in Figure 5.3. This sharp stress drop prior to wire fracture is associated with insulation fracture and delamination, exposing the bare aluminum conductor at the necking region. Where the insulation failed, it also experienced shrinkage, leaving the fractured ends of the aluminum wire exposed suggesting the insulation has a lower elongation limit than that of aluminum. This coupled with the delamination of insulation around the fracture point suggested there were adhesion and flexibility issues with the aluminum film insulation which required further investigation.

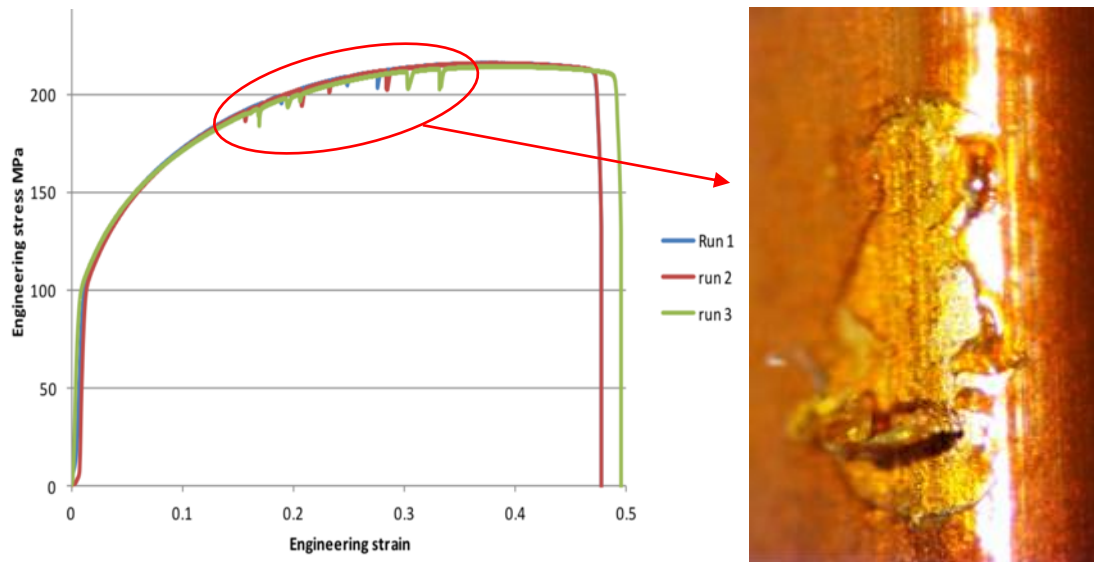


Figure 5.2. Stress drops in copper stress vs strain curves throughout plastic zone (left) and example of insulation fracture associated with each stress drop (right) from [14].

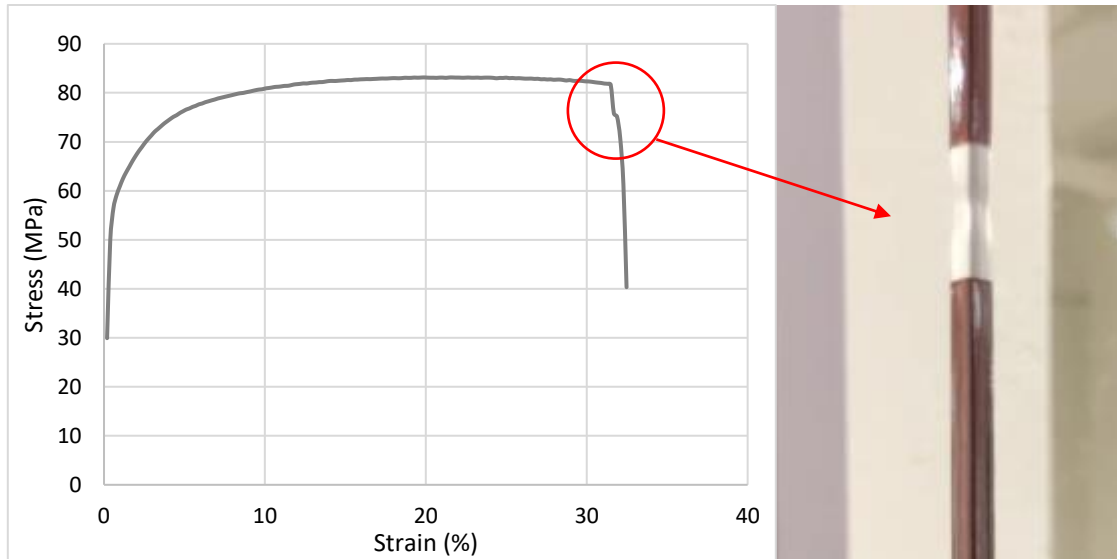


Figure 5.3. Stress drop in aluminum magnet wire stress vs strain curve at the onset of failure (left) and example of insulation fracture and delamination responsible for the stress drop at the necking region (right).

5.1.1.2 Aluminum Film Insulation Delamination Observation

Elongation testing measures the elongation of magnet wire, but it also evaluates the flexibility and adherence of the film insulation. Observing the fracture ends and insulation of both copper and aluminum wire samples tested showed a marked difference in deformation behaviour, as seen in Figure 5.4. A change in the light reflecting off the aluminum insulation can be seen highlighted by the red circles. This marks the start of the delamination zone where there is a long tube of delaminated insulation moving towards the fracture end. The insulation away from this point, towards the base of the wire, remained adhered to the conductor. Across all aluminum samples tested, the delamination tube ranged in size from 80-100 mm and the exposed end of the conductor, as a result of insulation shrinkage, ranged in length from 10-15 mm. Copper samples did not see this same behaviour and instead saw the insulation remain well adhered to the wire all the way to the fracture end.



Figure 5.4. Fracture ends of aluminum wire elongated to failure highlighting a tube of delaminated insulation starting at the red circles and ending at the fracture end. Shrinkage of the insulation away from the aluminum wire fracture ends is also highlighted. Copper wire insulation does not see the same problem, remaining adhered up to the fracture end.

5.1.1.3 Aluminum Film Insulation Delamination Peel Test

As described in Section 4.3.3 and Figure 4.6, peel testing was used to determine the level of insulation adherence remaining on both aluminum and copper samples elongated to failure. Studying the aluminum wire first, peel testing was performed on the tube of delaminated insulation as well as the remaining adhered insulation with the results shown in Figure 5.5. Firstly, an incision was made at the start of the delamination zone where the tube of delaminated insulation could be easily removed as a solid piece, Figure 5.5 (a-c). Interesting to note is the insulation would not slide back onto the conductor past its initiation point where the incision was made. This suggests the cross-sectional area of the delaminated tube of insulation reduced along with the necking region of the wire but reached its flexibility limit before aluminum did, resulting in delamination and shrinkage.

Next, the utility knife was used to attempt removal of the insulation still adhered to the rest of the wire sample. A pull tab of insulation was easily created since there was still some delaminated insulation the knife could easily get under, Figure 5.5 (d). The pull tab was then used to pull the insulation off the conductor in a spiral pattern around it. This operation was surprisingly easy as very little effort was required to remove the seemingly adhered insulation, suggesting film adherence was severely compromised during testing, Figure 5.5 (e). Since the pull tab was created from already delaminated insulation, the peel

test was attempted again but at the base of the sample where the wire exited the grips. Another incision was made around the wire and the knife was used to separate the insulation from conductor to create a pull tab. This again proved easy even though it was not initiated from the delamination zone. The pull tab was again used to peel the insulation off the conductor in a spiral pattern with the behaviour being the same as the first attempt, Figure 5.5 (f).

Overall peel test results are seen in Figure 5.5 (g) where all insulation was able to be removed from the conductor with ease. The delamination zone came off as a solid tube of insulation and the rest of the insulation remaining on the sample, which appeared adhered, came off very easily with the peel test. This demonstrates that for aluminum wires elongated to failure, there is a definite issue with film adherence and flexibility which results in significant loss of adhesion strength.

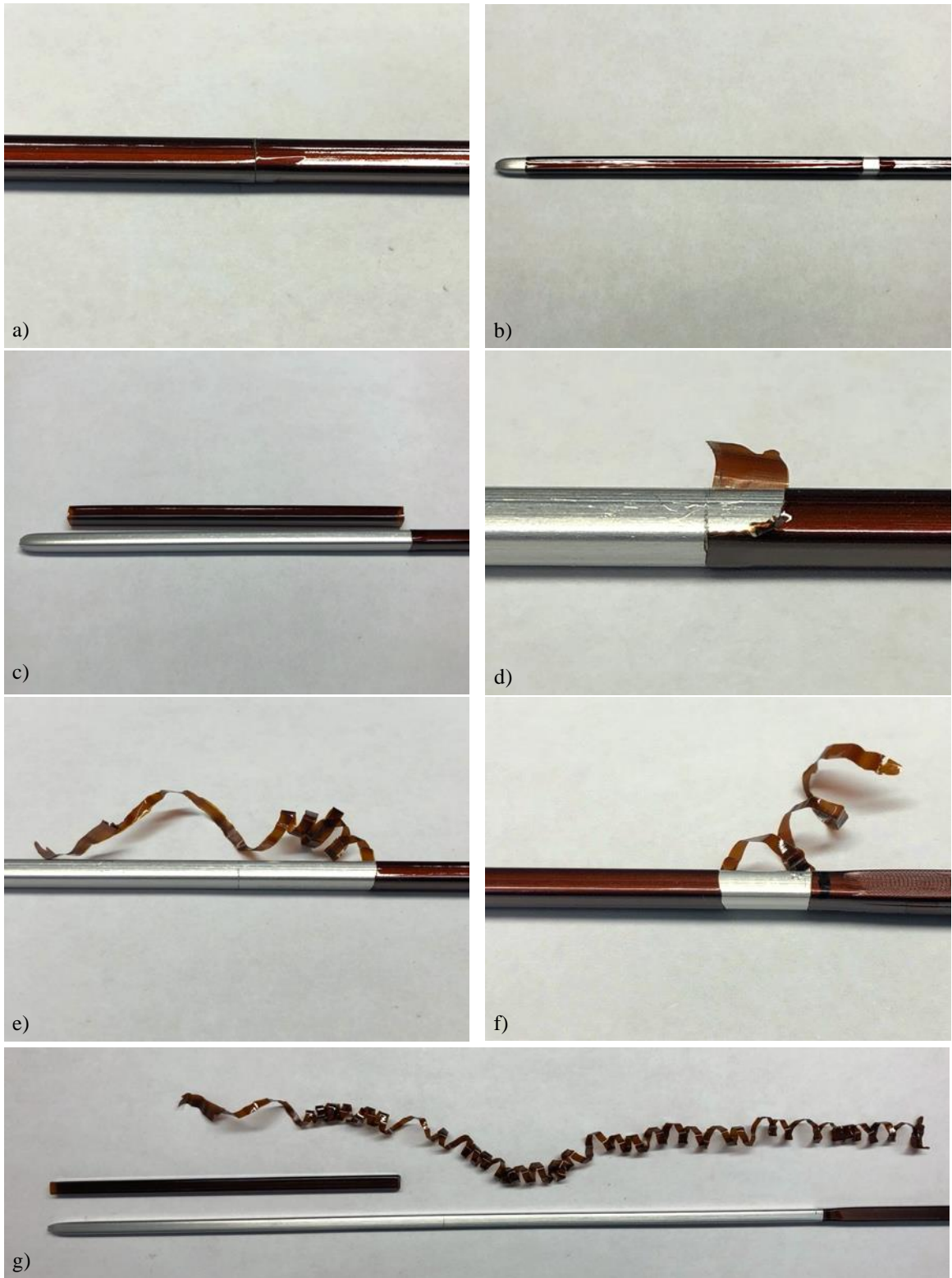


Figure 5.5. Illustration of aluminum elongation sample peel test. (a) An incision was made at the start of the delamination zone resulting in complete removal of the delaminated tube (b-c). Performing the peel test on the remaining adhered insulation adjacent to the delamination zone resulting in easy insulation removal (d-e). Second peel test attempt at base of wire with same results (f). Overall peel test results showing total insulation removal of aluminum elongation sample (g).

5.1.1.4 Copper Film Insulation Peel Test

Copper did not show any signs of delamination in [14] and the same held true for elongation testing in this study as can be seen by the fracture ends in Figure 5.4. However, aluminum insulation appeared to have good adhesion and the peel test revealed otherwise so the same test was done on a copper sample elongated to failure. Results of this test can be seen in Figure 5.6. The first peel test was done at the fracture end of the wire where a very small section of delaminated insulation already existed. A pull tab was able to be created from this, but the insulation was still very well adhered to the conductor and quickly broke off in small pieces, Figure 5.6 (a-c, f). The copper insulation was not able to be peeled off the wire from the fracture end like seen with the aluminum wire elongated to failure.

A second attempt was made at the base of the wire, but this resulted in the same behaviour. It was very difficult to get the knife between the insulation and conductor to create a pull tab which resulted in gouging and scratching of the underlying conductor surface, Figure 5.6 (d-e). If a pull tab was able to be created, it would not remove from the conductor in a solid piece of insulation past the corners of the cross section. Resulting flakes of broken insulation can be seen in Figure 5.6 (f). Adhesion between insulation layers and the conductor was too great to allow any appreciable amount of insulation to be removed. Portions of the base layer would often be left adhered to the wire during attempted insulation removal as well. Peel test results show excellent adhesion remaining between insulation and copper wire elongated to failure.

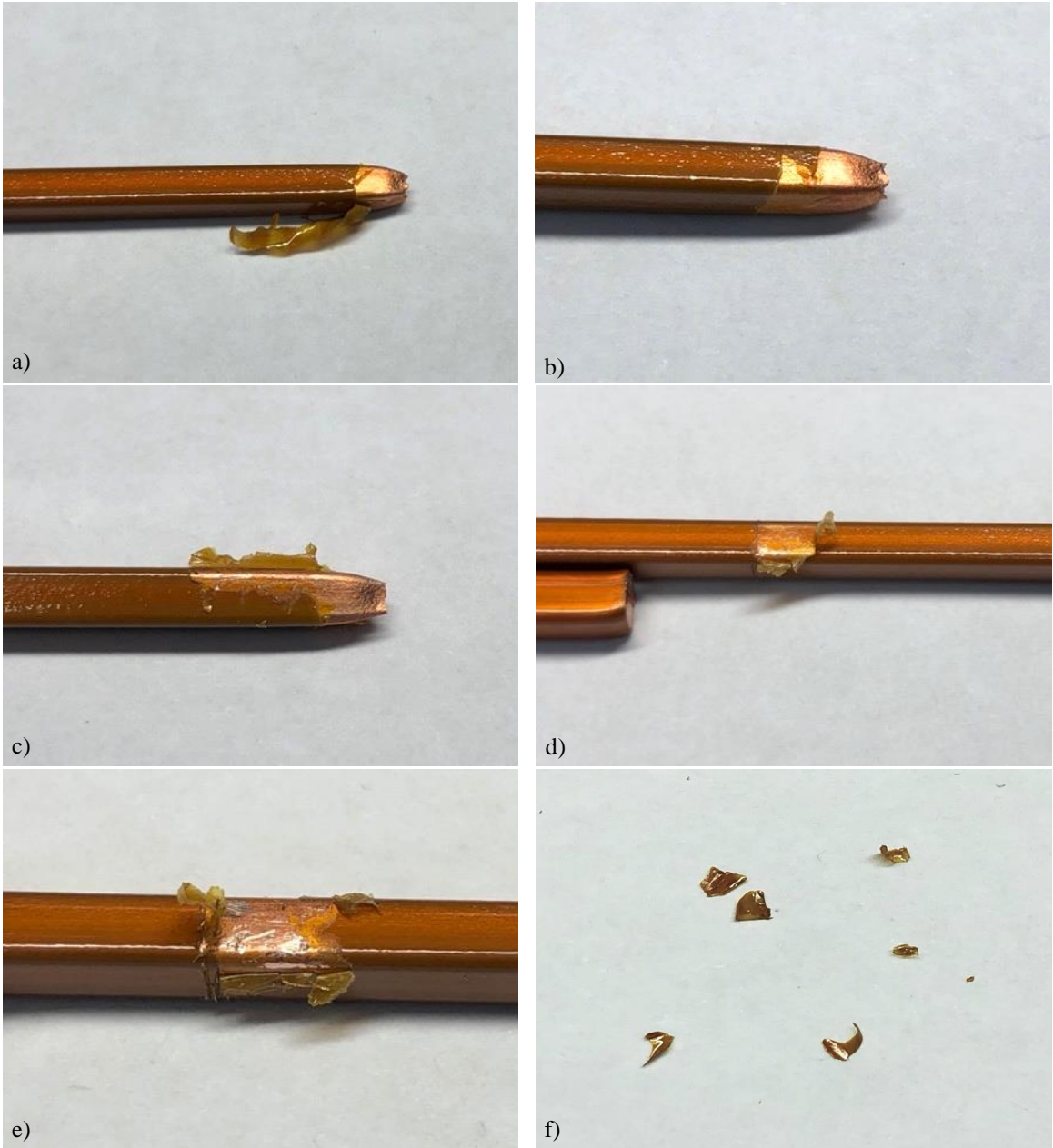


Figure 5.6. Copper elongation sample peel test results showing good adhesion at the fracture end with only small pieces of insulation able to be removed (a-c) and the same behaviour at the base of the wire (d-e) with resulting flakes of removed insulation (f).

5.1.1.5 Elongation Sample Texture Change Observations

A. Demiri noticed a texture change in copper wires samples that underwent tensile testing in [14], Figure 187, commonly known as orange peel and occurs due to excessive strain. Both copper and aluminum elongation samples in this study experienced the same texture change. However, the bare aluminum wires tested for reference experienced far more pronounced orange peel than the insulated aluminum sample. According to Figure 5.7, the bare aluminum wire (b) appears to have a very similar level of texture change as the copper sample (a). The insulated aluminum (c) shows little texture change through the insulation layer. Removing the insulation by the same method used for peel testing shows the underlying conductor experienced less texture change than the bare aluminum for the same experienced strain.

To further analyze this difference in behaviour between bare and insulated aluminum, a Keyence laser microscope was used to look at topography as well as SEM for a more detailed view of the texture. Observations were compared to the surface of a fresh piece of bare aluminum seen in Figure 5.8 which has a very smooth surface with marks and rolling lines left over from manufacturing and spooling. Comparing this to the bare aluminum sample elongated to failure in Figure 5.9, which displayed a similar level of texture change to the copper wire, there is a dramatic difference in texture. The orange peel

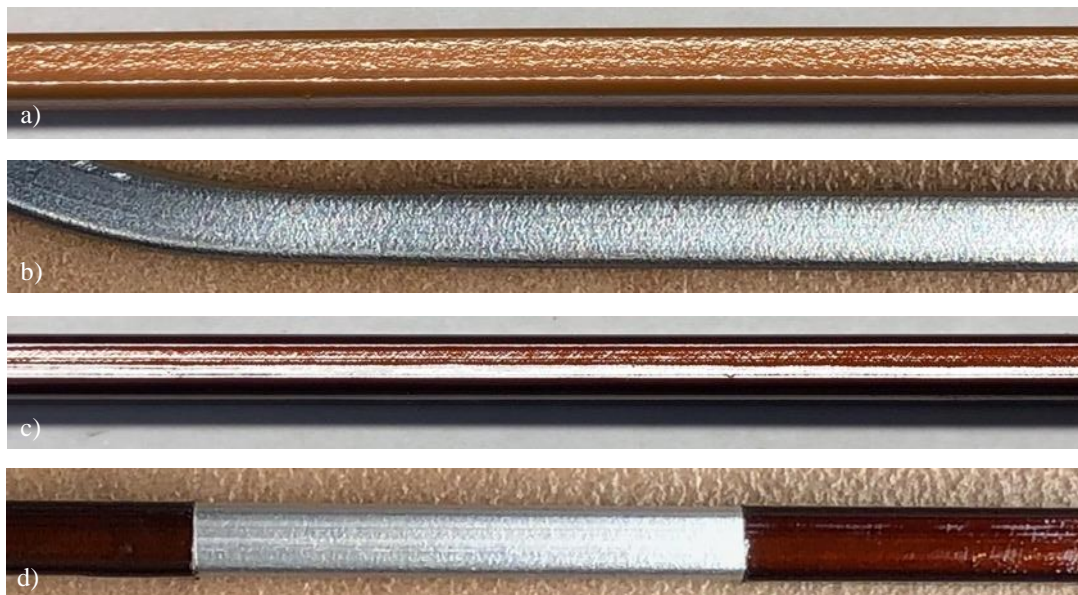


Figure 5.7. Orange peel texture change observed post elongation testing on insulated copper wire (a), bare aluminum wire (b), insulated aluminum wire (c) and underlying surface of peeled insulated wire (d).

texture covers the entire wire surface and almost completely removes marks and rolling lines left over from manufacturing. There are also striation lines at the peak of the texture bumps at roughly 45 degrees to the elongation direction. The texture map in Figure 5.9 further illustrates the degree of texture change. The insulated aluminum wire elongated to failure depicted in Figure 5.10 clearly shows a texture change took place but not to the same extent as the bare aluminum wire. Its texture is about halfway between the fresh aluminum and bare aluminum sample elongated to failure.

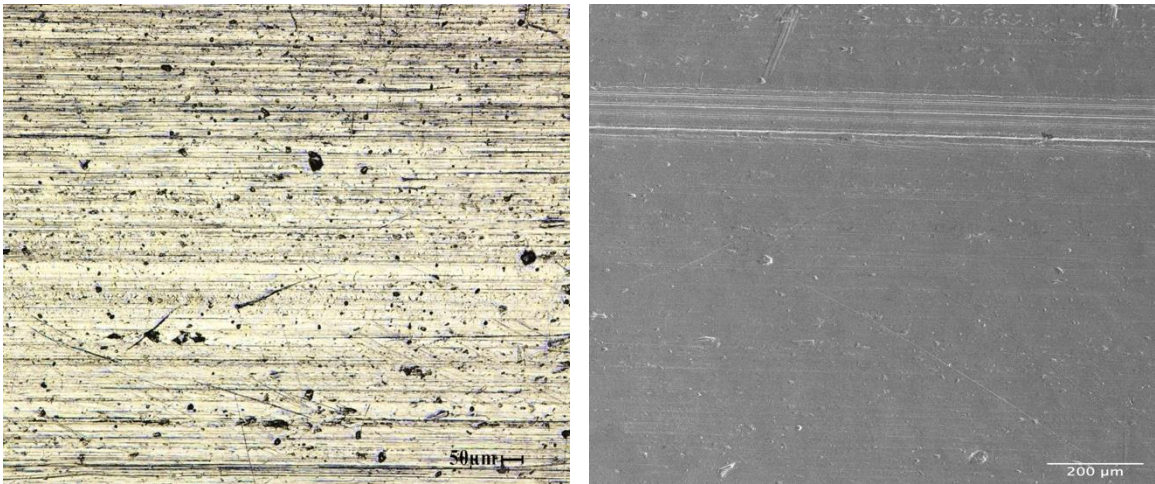


Figure 5.8. Keyence laser microscope image (left) and secondary electron SEM micrograph (right) of untested bare aluminum sample highlighting smooth surface features with manufacturing rolling mark imperfections.

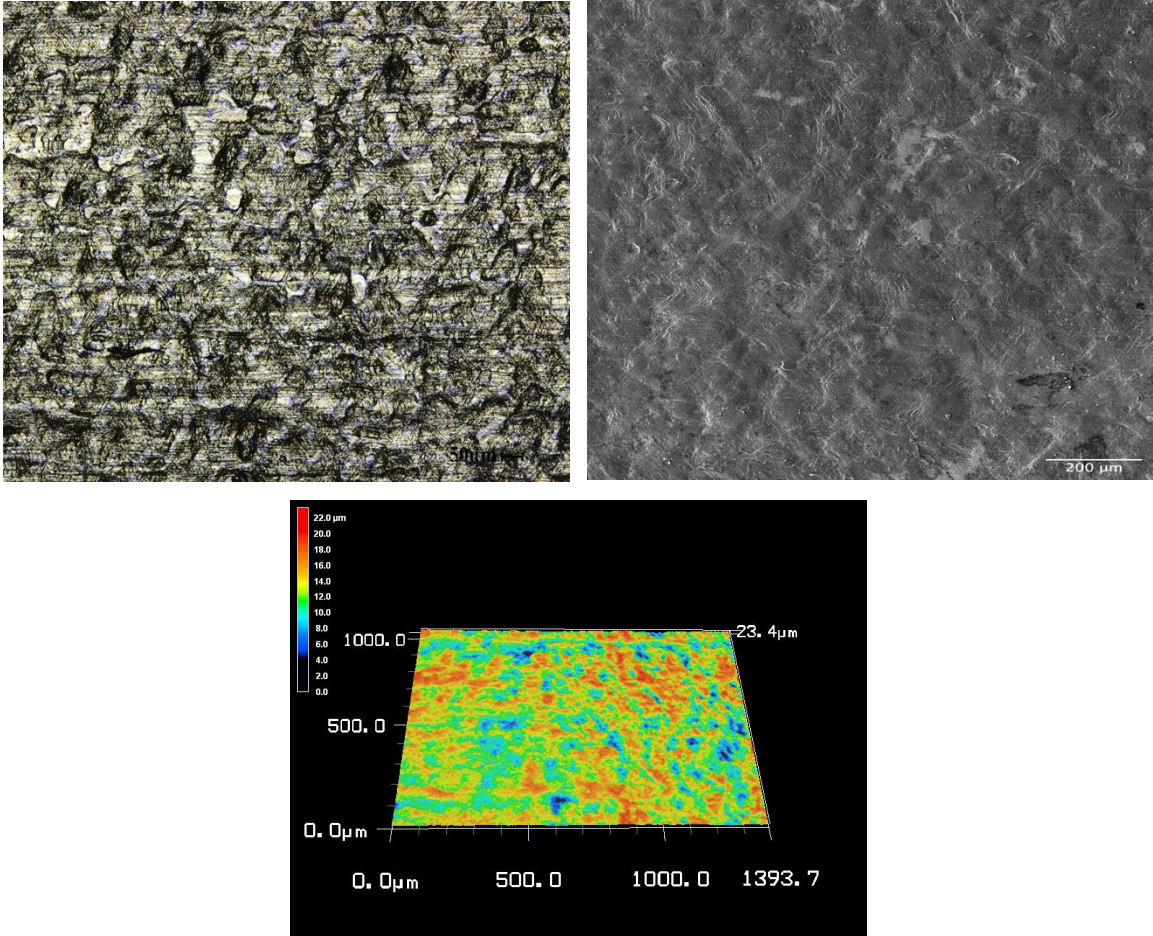


Figure 5.9. Keyence laser microscope image (left) secondary electron SEM micrograph (right) and topographical map (bottom) illustrating significant surface texture change on bare aluminum sample elongated to failure. Original surface features are almost completely replaced by orange peel texture.

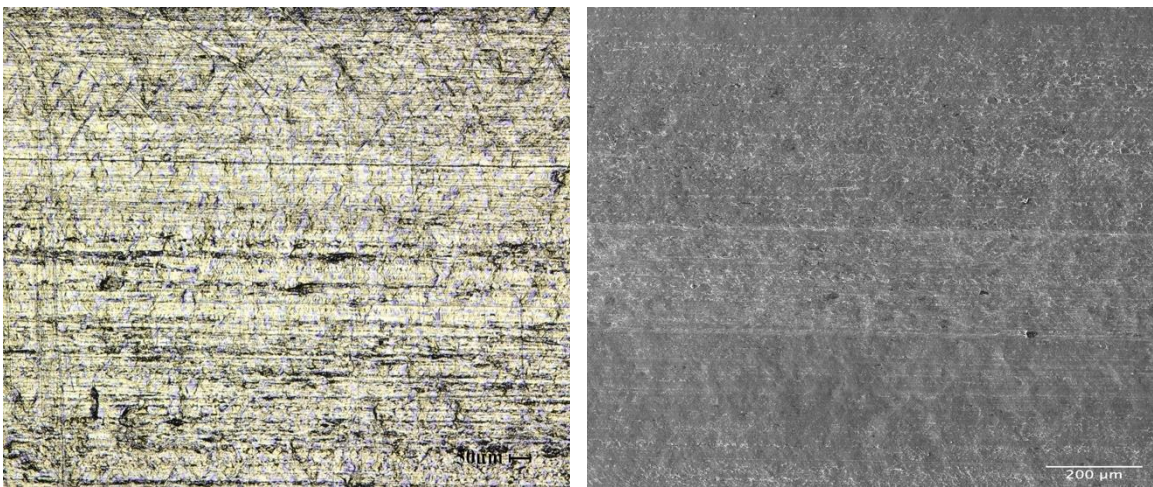


Figure 5.10. Keyence laser microscope image (left) and secondary electron SEM micrograph (right) of underlying surface of peeled insulated aluminum elongated to failure revealing less prominent orange peel texture compared to bare aluminum sample elongated to failure. Original surface features are still easily discernable.

5.1.2 Film Adherence and Flexibility Testing Results

To further investigate and understand the delamination issues observed post elongation testing, insulated aluminum wire samples were analyzed using standardized film adherence testing according to the procedure outlined in Section 4.3.3. The seemingly adhered insulation on aluminum elongation samples saw significant loss of adhesion strength so the same peel test was also performed on film adherence samples to determine the level of insulation adherence remaining for each strain level tested.

Insulated aluminum samples were tested at elongations of 5%, 10%, 15%, and 20% where they were subsequently analyzed for delamination and insulation fractures. Outside the scope of the standard, the peel test was performed on each sample as well as fresh pieces of insulated aluminum and copper for comparison. Stress versus strain curves for the samples tested can be seen in Figure 5.11 where each sample was elongated to and stopped at the designated strain. According to the standard, all samples passed the test as no delamination occurred. Applying pressure to the insulation with the thumb and forefinger did not reveal any delamination either. With the naked eye, no fractures or failures of the insulation were observed. Therefore, according to ASTM D1676, the insulation on aluminum wires tested has more than acceptable adherence and flexibility. However, a peel test was still performed to verify the level of adhesion remaining was still acceptable.

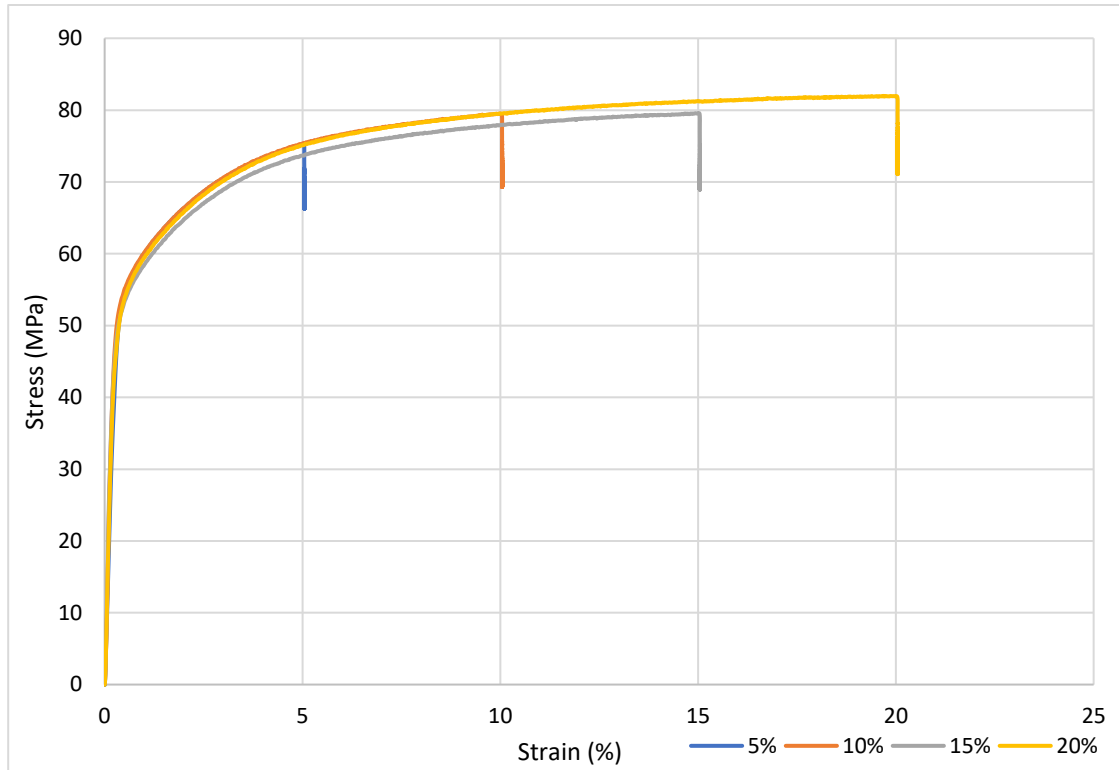


Figure 5.11. Film adherence and flexibility testing stress vs strain curves for insulated aluminum magnet wire tested to 5%, 10%, 15% and 20% elongation.

5.1.2.1 Film Adherence Peel Testing Observations

Firstly, to get baseline performance, peel testing was done on both fresh aluminum and copper wire samples as seen in Figure 5.12 and Figure 5.13 respectively. A pull tab was able to be created on the fresh aluminum but not without damaging the underlying conductor and multiple failed attempts, Figure 5.12 (a-b). The insulation did not peel well, breaking off in thin layers and small chunks with remnants of insulation layers left behind on the conductor, Figure 5.12 (b-d). It was very difficult to remove any appreciable amount of insulation, demonstrating very good adhesion of the film insulation to the aluminum conductor.

Compared to fresh copper, the performance and behaviour was very similar. Pull tabs of insulation were difficult to create and left gouging on the wire surface during attempts, Figure 5.13 (b, e). When a pull tab could be created, it came off in more cohesive, slightly larger sections compared to aluminum and did not leave as many underlying layers of insulation behind, Figure 5.13 (d-f). Like fresh aluminum, it was very difficult to remove

any significant amount of insulation from the copper wire, demonstrating very good insulation adhesion strength. Comparing this to copper samples elongated to failure in Figure 5.6, behaviour is almost identical, illustrating no significant loss of adhesion from elongation testing.



Figure 5.12. Peel test results for fresh, untested, insulated aluminum wire establishing baseline insulation adhesion. (a) A pull tab was able to be created with significant effort and damage to underlying aluminum. (b-c) Insulation adhesion was too strong to remove any significant amount of insulation with only small pieces breaking off (d).

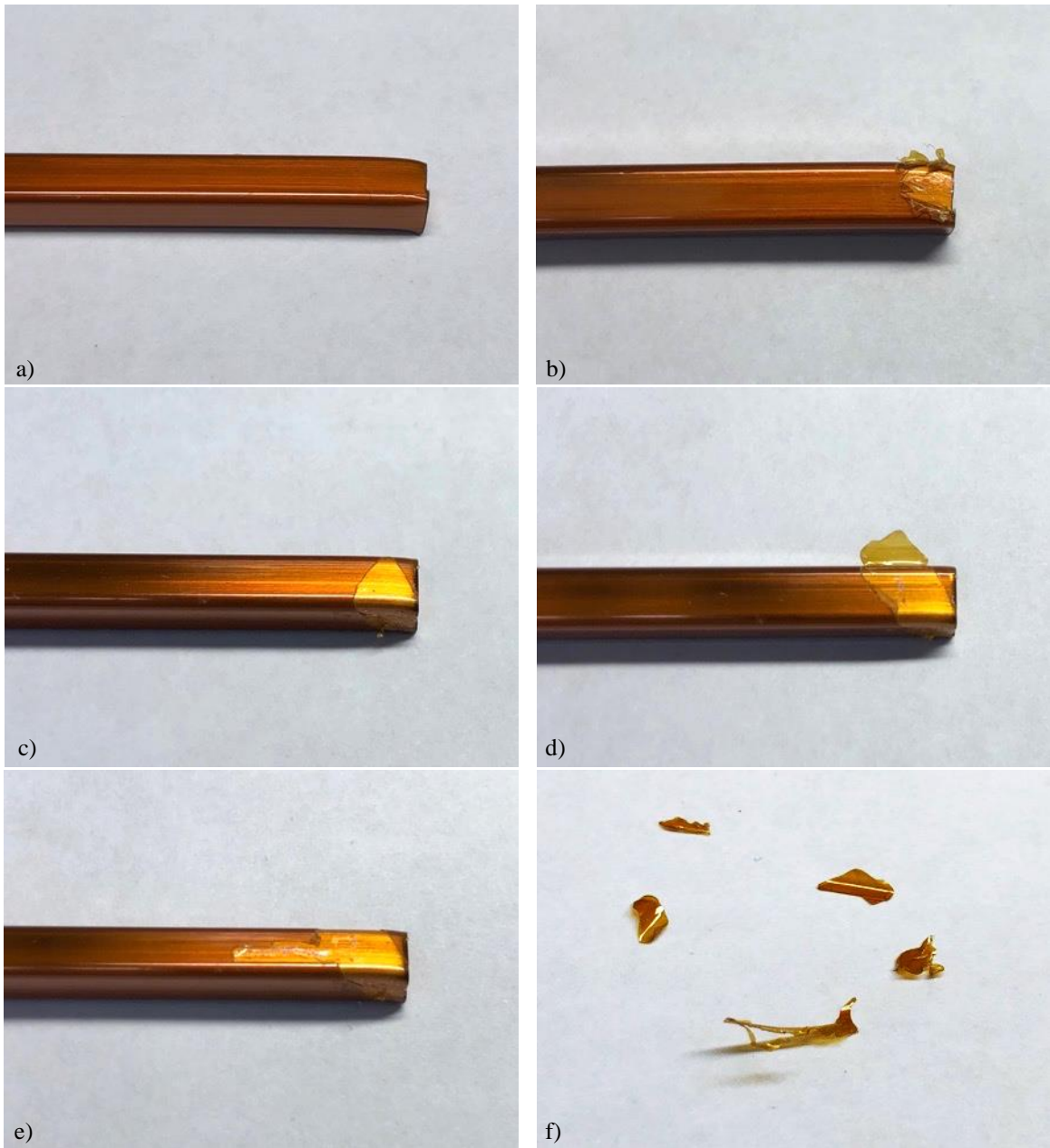


Figure 5.13. Peel test results for fresh, untested, insulated copper wire establishing baseline insulation adhesion. (a-e) Small pull tabs could be created but resulted in significant damage to underlying conductor and only small pieces of insulation breaking off (f).

Next, aluminum film adherence samples 5% through 20% underwent peel testing with results shown in Figure 5.14 and Figure 5.15. Incisions were made in the middle of the wires since there were no pre-existing delamination zones to start from. The sample elongated 5% performed identical to fresh aluminum. Significant effort was required to create a pull tab resulting in damage inflicted to the aluminum surface. Insulation pieces broke off in small chunks leaving layers of insulation behind, Figure 5.14 (a-b). The 10% sample also performed very similarly except less effort was required to create a pull tab and slightly larger pieces of insulation were able to be removed before they broke off, signifying slight reduction in adhesion strength, Figure 5.14 (c-e).

At 15% elongation, adherence significantly changed. About the same effort as the 10% sample was required to create a pull tab but multiple attempts were still required to start peeling the insulation from the wire. A base layer of insulation could still be left behind like with the previous samples, Figure 5.15 (a). However, once a good pull tab was created, the insulation started completely peeling off the conductor like seen with the elongation sample strained to failure. The insulation did not remove as easily though and great care was required to pull the insulation off without breaking it, Figure 5.15 (b-c). The insulation also felt stiffer and still slightly adhered to the aluminum surface unlike the wire elongated to failure where the insulation came off with little resistance. Despite this, total delamination was achieved, Figure 5.15 (d), but the removed insulation did not have the same coil shape as the wire elongated to failure, Figure 5.5 (g). Moving to the 20% sample, adhesion degraded even more with the peel test performing nearly identical to that of the wire elongated to failure.

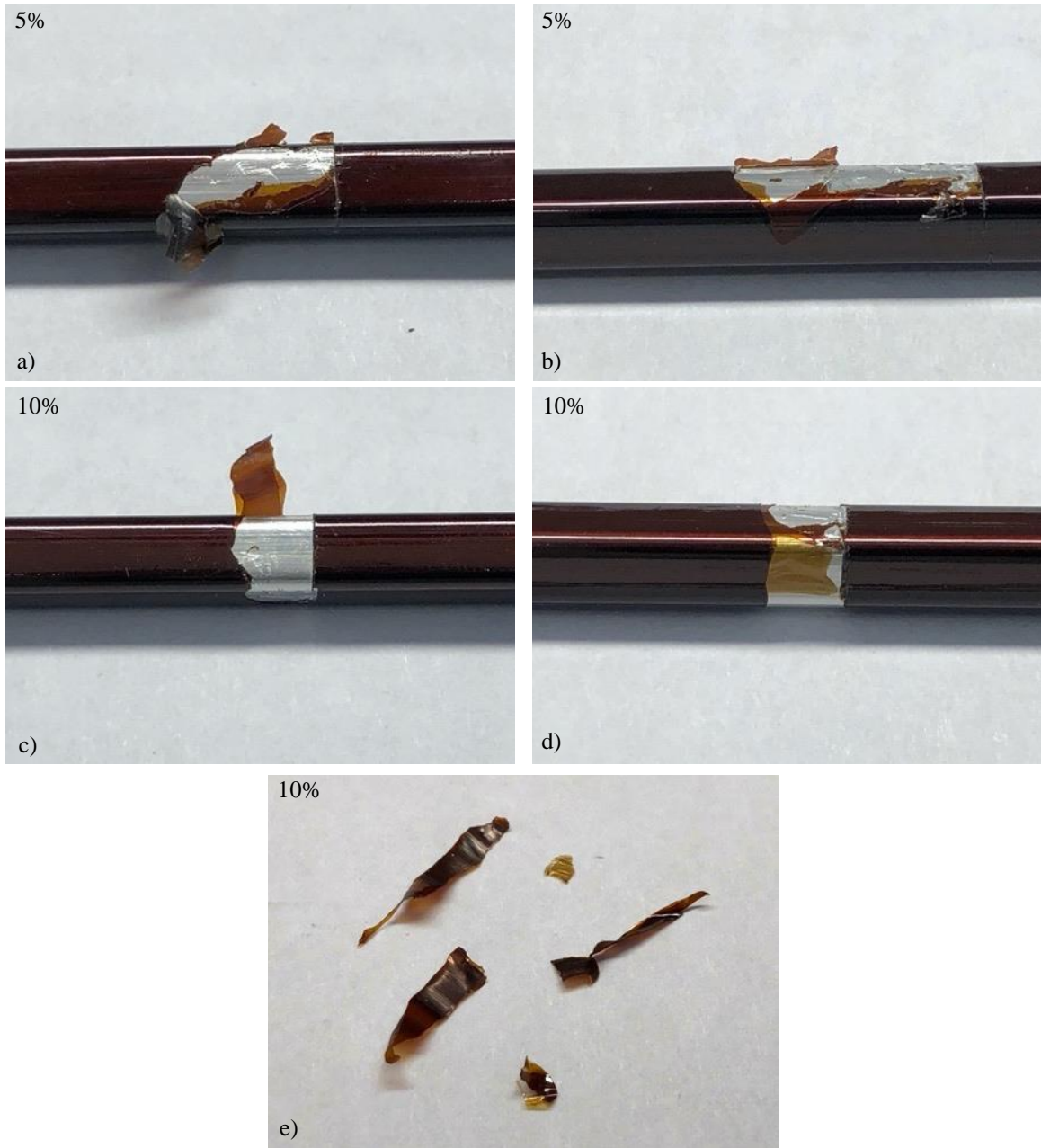


Figure 5.14. Peel test results for 5% (a-b) and 10% (c-e) film adherence samples. Insulation adhesion was almost identical to the fresh wire for both samples. Creating pull tabs was slightly easier for the 10% sample and larger pieces of insulation were able to be removed (e).

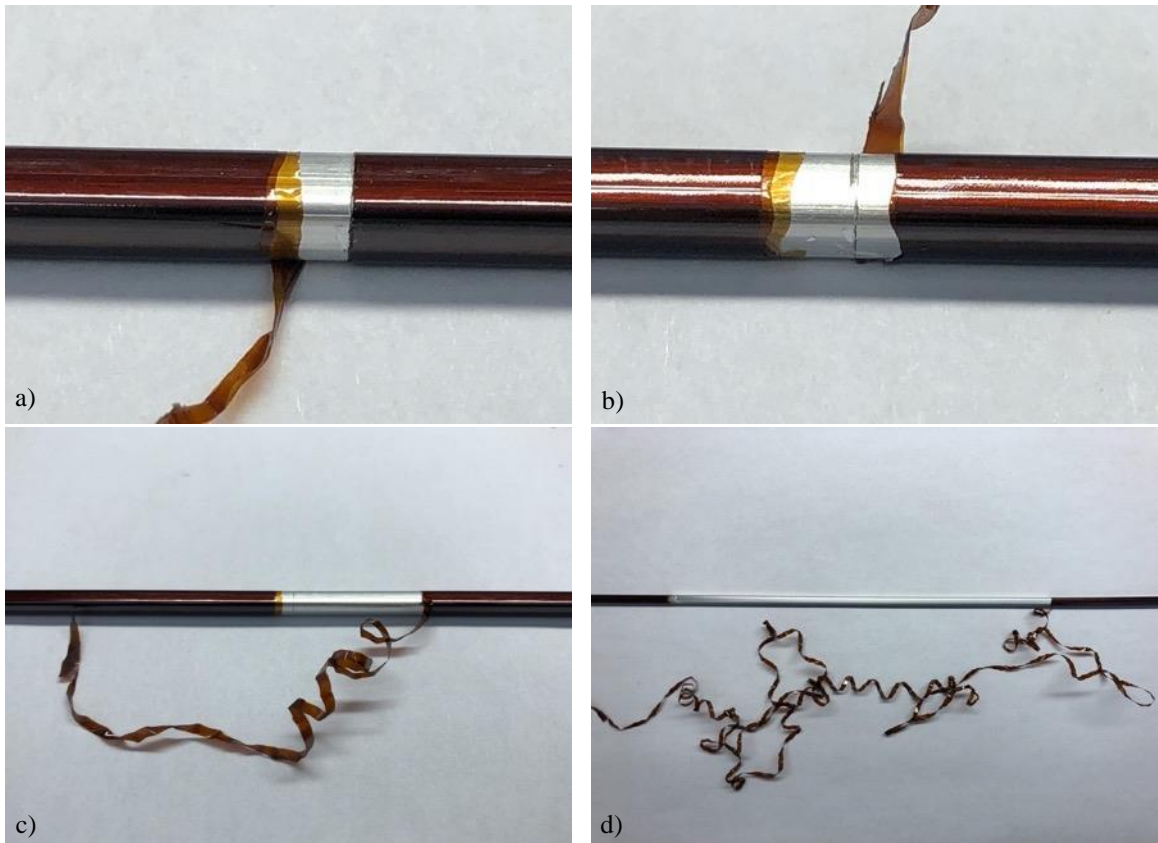


Figure 5.15. Peel test results for 15% film adherence sample. (a-b) Large pull tabs were easily created and used to peel insulation off the entire conductor in a spiral pattern (c-d) revealing significant loss of insulation adhesion.

5.1.2.2 Delamination Investigation

SEM and EDS analysis were used to analyze aluminum insulation delamination in more detail. Specifically, the delaminated tube of insulation was cut and mounted so the side in contact with aluminum could be observed. The aluminum surface that saw the insulation delaminate from it was also observed.

Firstly, looking at the underside of the insulation in Figure 5.16, the secondary electron (SE) image highlights 3 large particles imbedded in the insulation surface. The backscattered electron (BSE) image, showing elemental composition differences as a different brightness, reveals these large particles, along with many smaller particles not easily identified in the SE image, are not insulation material. Looking closer at these particles in Figure 5.17 shows they are well adhered to the insulation. This suggests the particles must be aluminum removed from the wire surface during delamination.

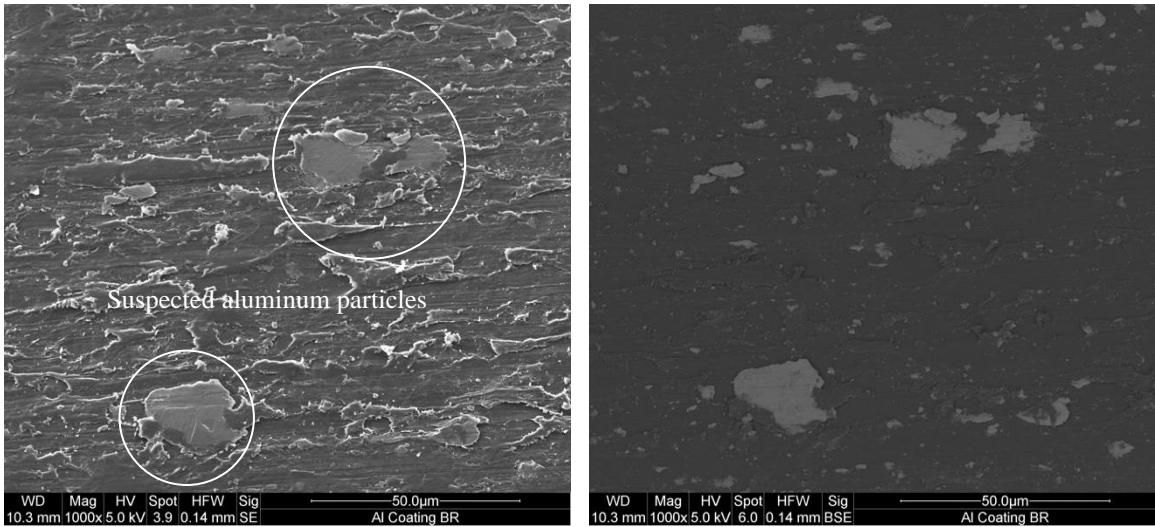


Figure 5.16. Secondary electron (left) and backscattered electron (right) SEM micrographs of underside of delaminated insulation tube highlighting suspected aluminum particles removed from the wire surface during delamination.

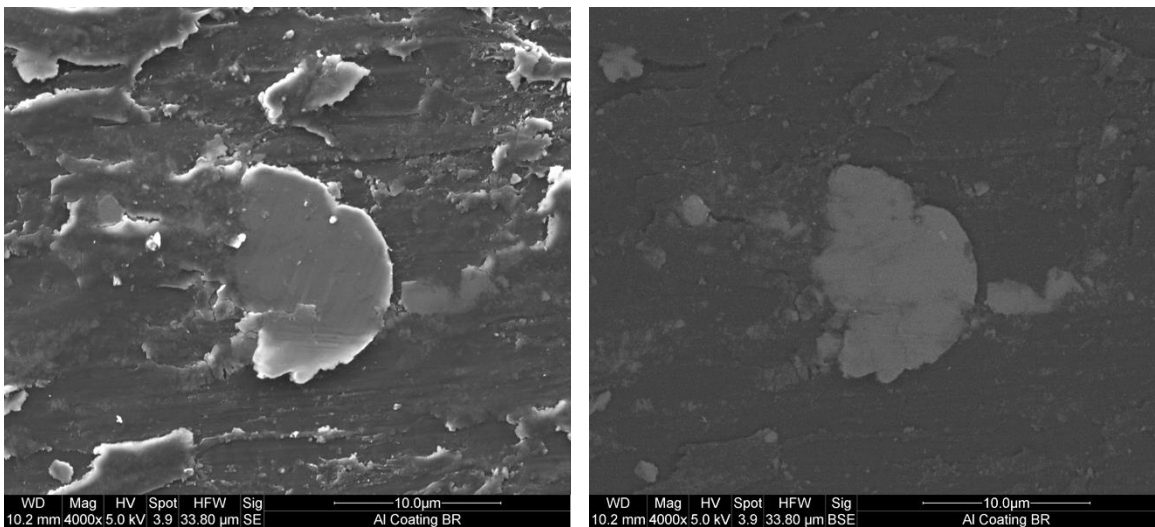


Figure 5.17. Higher magnification view of suspected aluminum particles imbedded in the underside of delaminated insulation.

EDS analysis was performed on the BSE image from Figure 5.16 with the mapping results displayed in Figure 5.18. The carbon map clearly shows the particles are not carbon based while the aluminum mapping matches perfectly with them confirming they are part of the conductor surface. The insulation composition is proprietary, but oxygen and nitrogen are suspected to be present. The nitrogen map reveals no counts on the aluminum particles while the oxygen map shows some presence on the aluminum particles which is most likely aluminum oxide. EDS analysis confirms particles of aluminum loosely bonded

to the aluminum surface are being removed with the insulation during delamination. These particles are most likely aluminum shingles created during manufacturing which are apparent on the aluminum cross section in Figure 4.2.

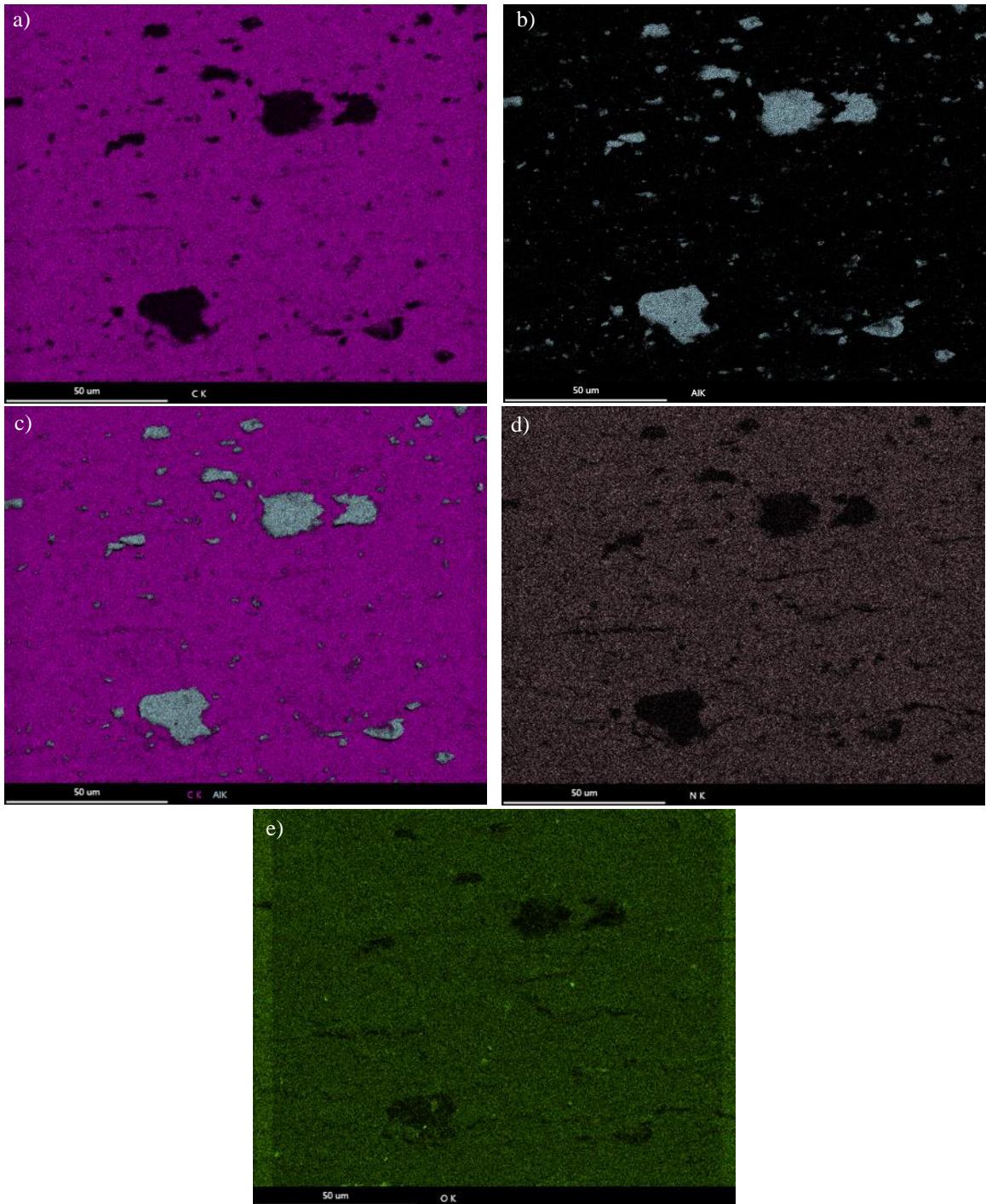


Figure 5.18. EDS mapping results of backscattered SEM image from Figure 5.16. The distribution of (a) carbon, (b) aluminum, (c) carbon & aluminum, (d) nitrogen and (e) oxygen establish imbedded particles in the underside of delaminated insulation are aluminum.

To study this further, the aluminum surface was also analyzed. The SE image in Figure 5.19 shows particles on the aluminum surface that are suspected to be insulation material. The associated BSE image shows an elemental composition difference for these particles. This same figure highlights an aluminum shingle like those seen imbedded in the delaminated insulation except this one was not detached from the conductor. Looking closer at the suspected insulation particles in Figure 5.20 shows they are adhered well to the surface. The BSE image highlights darker regions inside the cracks of the aluminum surface which may also be remnants of insulation.

EDS analysis was done on this same figure to determine what the adhered particles were with mapping results presented in Figure 5.21. The aluminum map clearly shows the particles are of a different composition while the carbon and nitrogen maps match the particle perfectly. This confirms the particles must be pieces of insulation left behind during delamination. The carbon and nitrogen maps also reveal the dark regions inside the aluminum cracks are indeed insulation that penetrated the cracks during manufacturing and remained post delamination. The oxygen map highlights a thin layer of what is most likely aluminum oxide covering the aluminum surface. This could have been present before the polymer was applied to the conductor or formed post delamination once exposed to air.

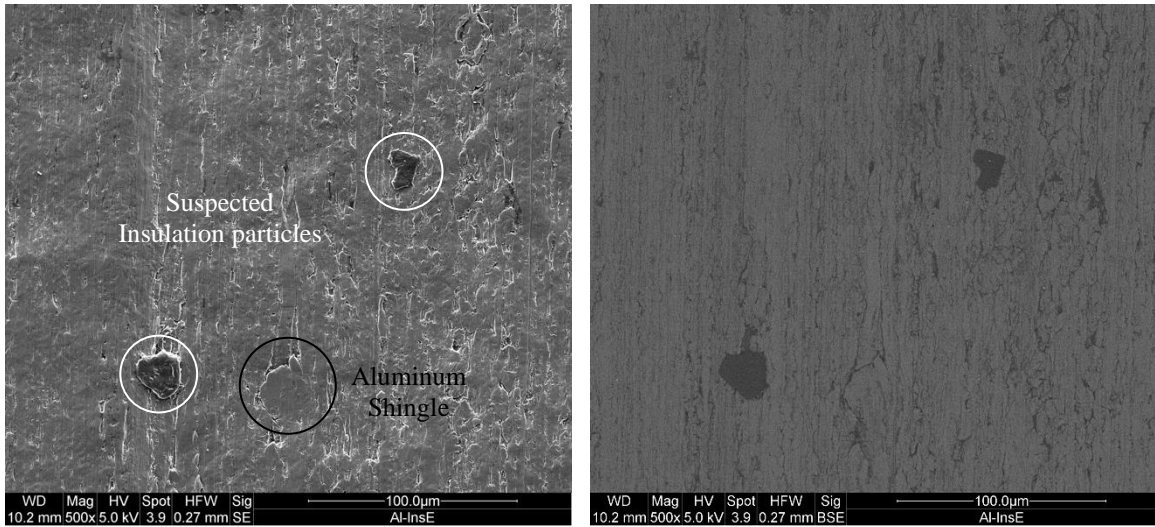


Figure 5.19. Secondary electron (left) and backscattered electron (right) SEM images of aluminum wire surface which experienced insulation delamination during elongation testing. SE image shows suspected insulation particles adhered to the surface left behind from delamination while the BSE image confirms they are of different composition to aluminum. Example of an aluminum shingle like those seen on the underside of delaminated insulation is also highlighted.

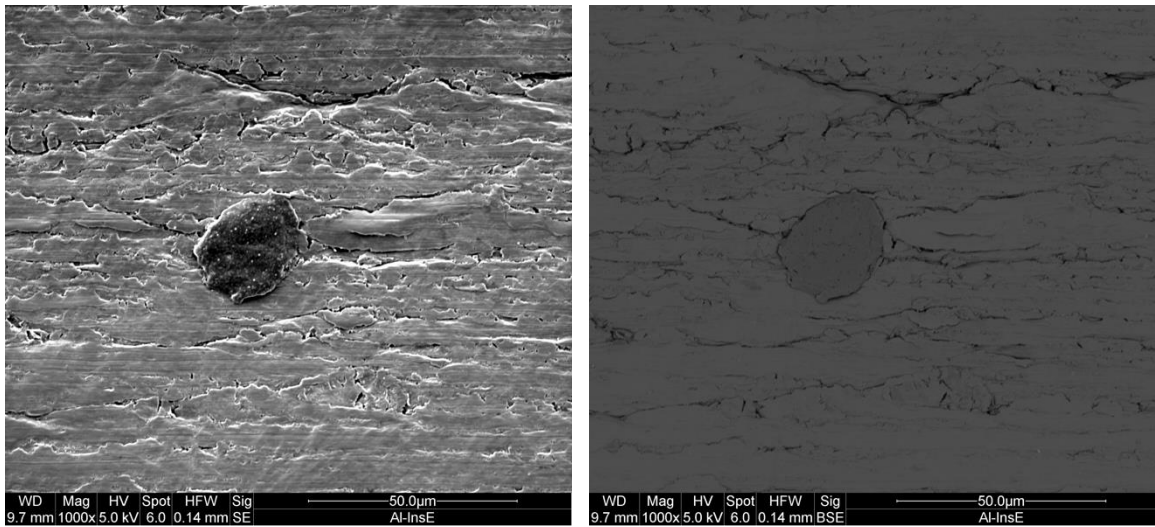


Figure 5.20. Higher magnification view of suspected insulation particle left behind on aluminum surface post insulation delamination.

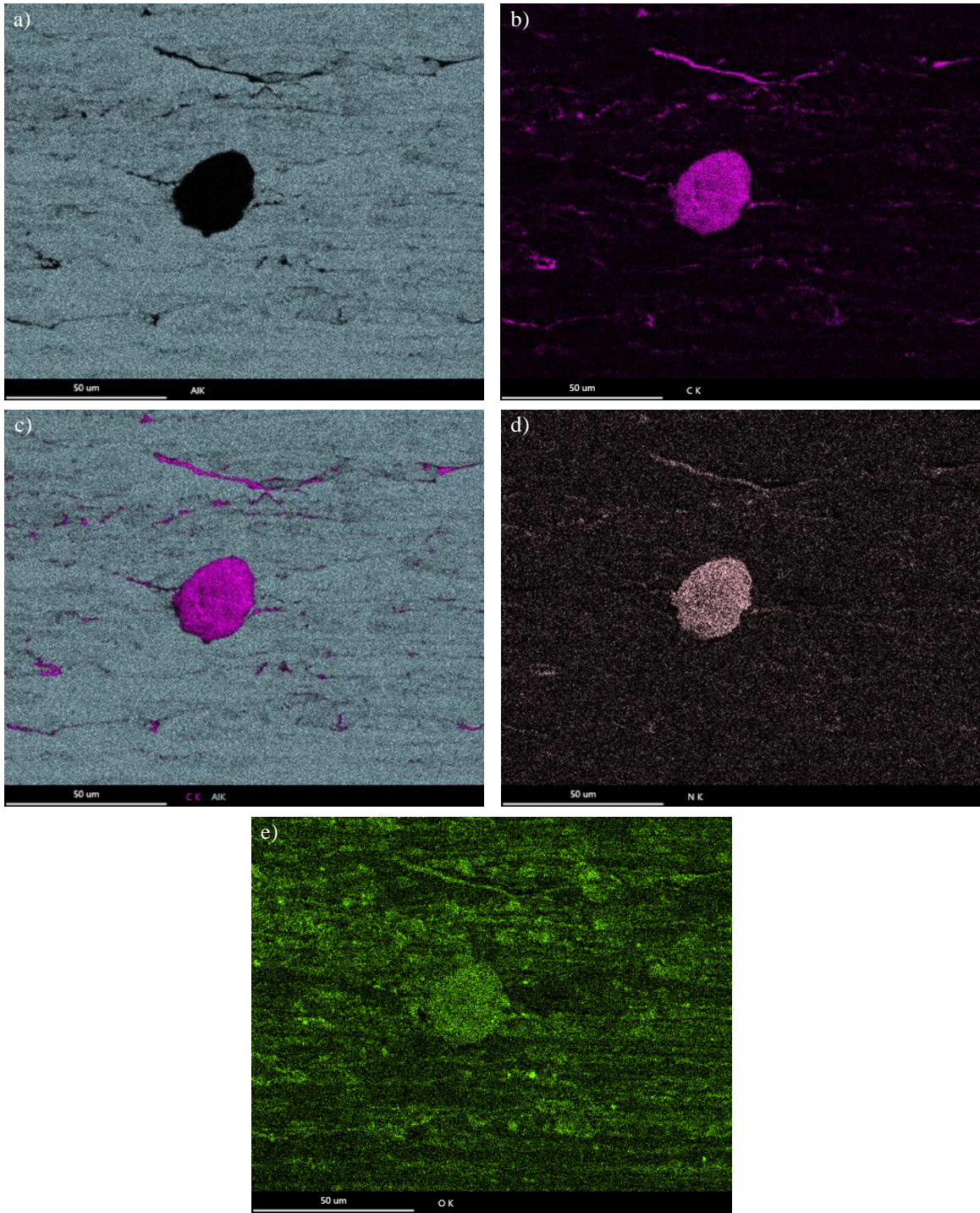


Figure 5.21. EDS mapping results of backscattered SEM image from Figure 5.20. The distribution of (a) aluminum, (b) carbon, (c) carbon & aluminum, (d) nitrogen and (e) oxygen establish adhered particle is insulation left behind post delamination. The carbon and nitrogen maps also reveal insulation remnants in the aluminum surface crevices.

5.1.2.3 Insulation Damage Observations

Part of film adherence and flexibility testing procedure requires analyzing wire insulation post testing for cracks or failures observable with the naked eye. Aluminum wire samples tested from 5-20% elongation did not experience any failures in the insulation, so they all passed this portion of the test. However, samples elongated to failure during elongation testing did experience cracks and fractures. This section characterizes the types of insulation fractures observed on both aluminum and copper wire samples elongated to failure.

Summarized in Section 5.1.1.1 and Figure 5.2, A. Demiri discussed large fractures in the copper insulation which corresponded to stress drops in the stress strain curve during elongation. These same types of failure were not observed on copper samples tested in this study, but other forms of fracture did occur which can be seen in Figure 5.22. Insulation failure mainly consisted of small splits and pinholes. Figure 5.22 (a) shows multiple tiny splits and pinholes grouped together on the edge of the wire sample while (b) the top view of a larger split and (c) the side view of the same large split.

These can be compared to the insulation failures found on aluminum samples elongated to failure in Figure 5.23. Aluminum samples also experience tiny split and pinhole type fractures as demonstrated in (a). However, aluminum seemed to occasionally experience much larger splits compared to those seen on the copper samples and in rare cases insulation fractures would span the width of the wire with a small delamination zone around them, Figure 5.23, (b-c). Although aluminum could see more gross insulation fractures, most failures found were very tiny splits and pinholes for both conductors.

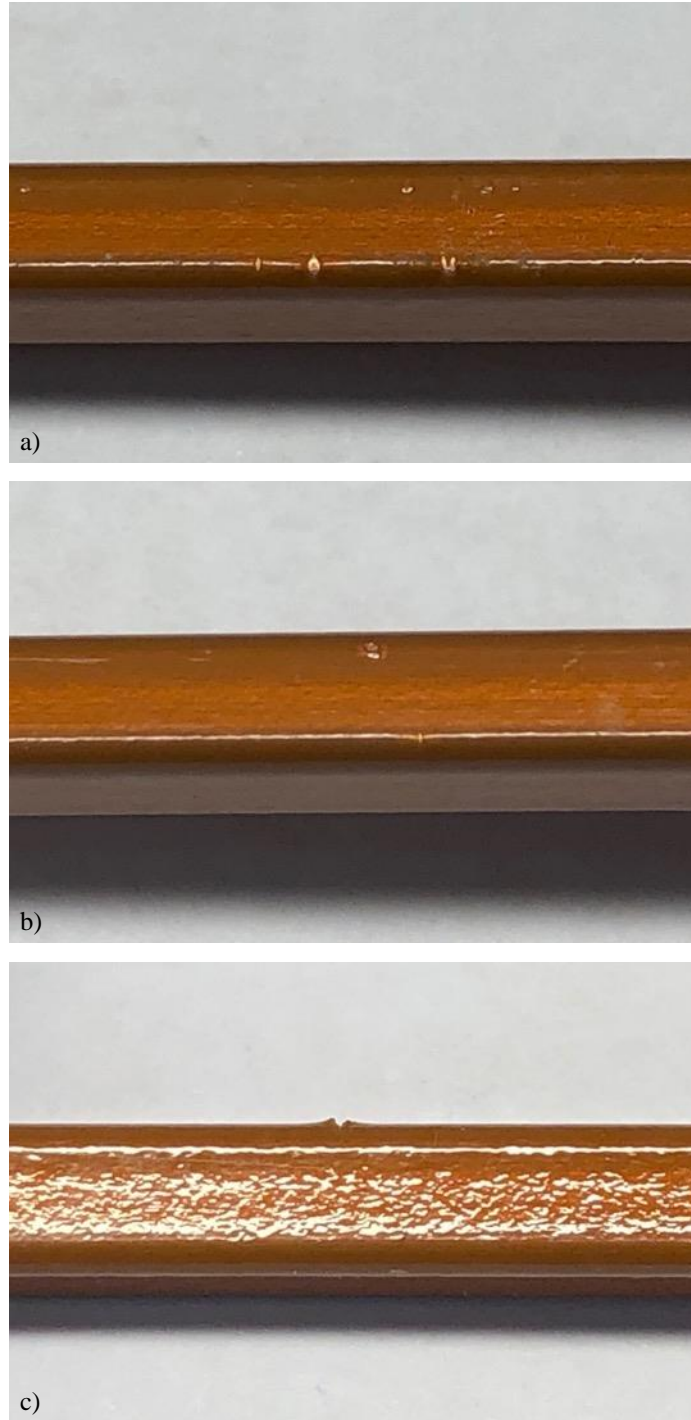


Figure 5.22. Copper insulation damage sustained during elongation to failure. (a) Small pin holes and splits in the insulation. (b) Larger, less common split in insulation with side view in (c).



Figure 5.23. Aluminum insulation damage sustained during elongation to failure. (a) Small pinhole failure of insulation. (b) Less common, large split revealing the underlying conductor. (c) Example of gross insulation failure consisting of insulation split the width of the conductor and delamination zone around the fracture.

5.1.3 Elastic Ratio Testing Results

Elongation testing and film adherence and flexibility testing provided a good look at both aluminum and copper insulation performance during elongation. Moving forward, the remaining formability and windability characterization tests from ASTM D1676 focus more on comparing conductor performance in manufacturing and winding operations. Elastic ratio testing was conducted for both aluminum and copper magnet wires according to the procedure outlined in Section 4.3.4. The same samples and data used for elongation testing were also used for the elastic ratio method since both tests require elongating the wire to failure with the only difference being how the data is analyzed. Results for both conductors are found in Table 5.2.

Aluminum saw an average elastic ratio of 165.5% meaning the average load at 5% elongation was 1.65x greater than the load at break. Copper saw a much higher elastic ratio with an average of 252% or 2.5x greater load at 5% elongation compared to load at break. Aluminum having the lower ratio suggests it can better accommodate elongation during winding at high speeds.

Table 5.2. Elastic ratio testing results for aluminum and copper magnet wire samples.

Aluminum			
Test #	Elastic Ratio (%)	AVG	STDEV
1	145.04	165.50	22.38
2	189.40		
3	162.08		
Copper			
Test #	Elastic Ratio (%)	AVG	STDEV
1	317.44	252.09	78.05
2	273.16		
3	165.67		

5.1.4 Low Stress Elongation Testing Results

Low stress elongation testing was conducted on both insulated aluminum and copper wire samples according to Section 4.3.5. Results can be found in Table 5.3 with stress versus strain curves shown in Figure 5.24. The average LSE for aluminum was 0.37% compared to copper at 0.87%. According to the standard, greater formability is attributed to the magnet wire with the larger LSE percentage. Therefore, the results suggest the copper magnet wire tested is more formable than aluminum. The stress strain curves corroborate this. Copper experiences greater permanent elongation and in turn has a larger LSE.

It is also important to note the higher standard deviation experienced for aluminum samples tested. This is easily illustrated with aluminum test #3 in Figure 5.24 which experiences greater elongation than the other two samples by a considerable amount. This is explained by the small gap between yield strength and ultimate tensile strength for aluminum, 27.5-48 MPa and 62-96.5 MPa respectively. The specified stress for testing aluminum was 55.2 MPa which is quite close to its tensile strength. Therefore, if too much plastic deformation is introduced into the wire before testing it can take longer to reach the specified stress during testing at slow speeds resulting in greater permanent elongation than expected. The specified stress for copper was 103.4 MPa where its yield and ultimate tensile strength are 62-83 MPa and 248-276 MPa respectively. Therefore, it does not experience the same elongation variability as aluminum.

Table 5.3. Low stress elongation testing results for aluminum and copper magnet wire samples

Aluminum			
Test #	LSE (%)	AVG	STDEV
1	0.31	0.37	0.16
2	0.25		
3	0.54		
Copper			
Test #	LSE (%)	AVG	STDEV
1	0.91	0.87	0.04
2	0.83		
3	0.86		

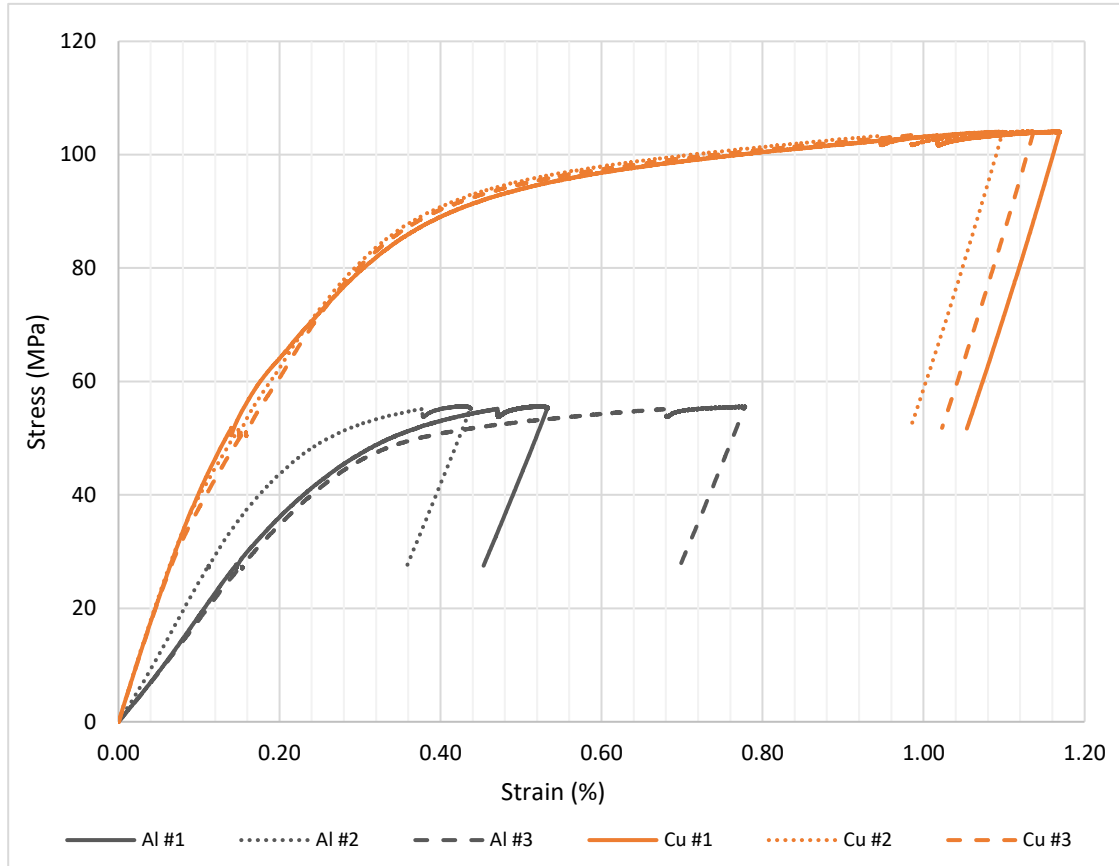


Figure 5.24. Low stress elongation stress vs strain curves for aluminum and copper wire samples.

5.1.5 Springback Testing Results

Springback testing was done on both bare and insulated aluminum wire samples as well as for both rectangular dimensions of the copper wire according to Section 4.3.6. Visual representation of the bending directions across each magnet wire cross section can be seen in Figure 5.25. Results from testing aluminum samples are found in Table 5.4 and copper samples in Table 5.5. A 0.25° difference in springback was found between insulated and bare aluminum samples. This can be attributed to bare aluminum being slightly softer with an average hardness of 17.7 HRB compared to insulated aluminum at 20.8 HRB. Copper wire showed little variation in springback across either rectangular dimension giving an overall average value of 3.67° . This is 1.25° greater springback than the average for insulated aluminum. This suggests aluminum has greater formability and windability than copper since it can maintain a desired shape better.

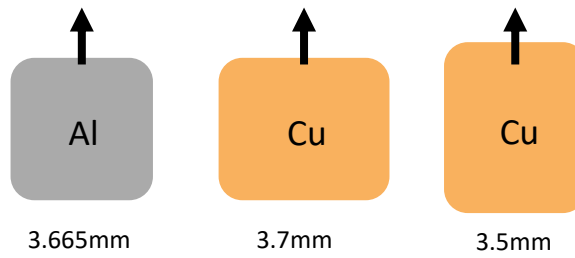


Figure 5.25. Bending direction for aluminum and copper magnet wire samples for springback testing.

Table 5.4. Springback testing results for aluminum magnet wire samples.

Insulated Aluminum			Overall AVG
Test #	Springback (deg)	AVG	
1	2.50	2.42	
2	2.50		
3	2.25		
Bare Aluminum			2.29
Test #	Springback (deg)	AVG	
1	2.25	2.17	
2	2.25		
3	2.00		

Table 5.5. Springback testing results for copper magnet wire samples.

Copper: 3.5mm Dimension			Overall AVG
Test #	Springback (deg)	AVG	
1	4.00	3.75	
2	3.75		
3	3.50		
Copper: 3.7mm Dimension			3.67
Test #	Springback (deg)	AVG	
1	3.50	3.58	
2	3.50		
3	3.75		

5.2 Wire Bending Simulation Testing Results

Concluding standardized formability and windability characterization for both conductors, the custom-built wire bending simulator discussed in Section 4.4.1 was then used to study formability and windability for a simulated die forming process used in hairpin conductor manufacture. The following sections outline the results from this testing as described in Section 4.4.

5.2.1 COF vs Normal Load Testing Results

Testing was conducted on both insulated aluminum and copper wires according to the procedure outlined in 4.4.2.1 with the following parameters:

- Applied normal load to aluminum of 7, 12, 17, 22, 27, 32, 37, 42 lbs
- Applied normal load to copper of 22, 42 lbs
- Both 3 mm and 24 mm radius support rollers for each load
- Sample contact length of 220 mm
- Constant speed and acceleration of 20 mm/s and 20 mm/s²
- Forming angle of 10°

Results for this testing are found in Table 5.6 and Table 5.7. Both tables outline individual and average COF values with associated standard deviation, individual and average standard deviation for each test and measured contact area with associated pressure exerted on the wire surface for each test. Average coefficient of friction values along with their standard deviation for each testing condition are plotted in Figure 5.26. Graph (a) best highlights the trend in COF as normal load increases while graph (b) better illustrates standard deviation for each test.

The variation of coefficient of friction was plotted along sample travel length for each test at the given normal load and support roller radius. Curves for aluminum wire samples are found from Figure 5.27 to Figure 5.42 while those for copper samples are found from Figure 5.43 to Figure 5.46. Each curve contains a section highlighted with a black line. This marks the portion of the test used for COF calculation. Only portions of the test under constant velocity were considered with the start and end acceleration phases

ignored. For the given speed and acceleration parameters, the constant speed portion of each test started at a travel length of 13 mm and ended at 209 mm. However, some tests experienced large spikes in COF at the start of a test which did not return to a steady state condition by the time 13 mm travel distance was reached. Other outlying tests experienced drastic changes in COF outside of normal test behaviour towards the end of the test. Therefore, in general, COF was measured only for the constant speed portion of a test, but some tests required adjustment of this calculation region to accommodate abnormalities in behavior according to individual judgement. For this reason, along with several tests displaying uncharacteristically high COF or STD, generally more than three samples were tested at a given normal load. This is especially true for aluminum between 22 lb and 32 lb for both rollers where higher average standard deviations between COF results were found.

Looking at the average COF curves for aluminum in Figure 5.26 (a), it can be seen for the 3 mm support roller, a large spike in COF occurs at 22 lb normal load followed by a sharp decrease and then a gradual increase up to 42 lbs. Similar behavior is seen for the 24 mm support roller as well but instead between 27 lbs and 32 lbs with a less drastic spike in COF. In general, the COF curve for the 24 mm support roller appears to be slightly lower and rightward shifted compared the that of the 3 mm support roller. This trend for aluminum wires is mirrored in Figure 5.26 (b) where the standard deviation for each test is better represented. This behavior suggests there is a deformation mechanism change at these normal loads for the respective support rollers that warrants further investigation.

Comparing the results for copper in the same figure shows very minimal change in COF occurs although standard deviation between tests is higher for 42 lbs applied normal load. Although A. Demiri in [14] did not exclusively tests the effects of normal load on COF for copper, two samples were compared at 40 lbs and 60 lbs. The results showed a 0.02 increase in COF from 40 lbs to 60 lbs which is a negligible change and consistent with results for copper in this study with both support rollers. Compared to the trends in COF seen for aluminum, this suggests applied normal load has negligible effect on COF for the copper wires tested.

Further comparing COF behavior between aluminum and copper wire samples shows that copper tends to experience lower standard deviation for individual tests. This is clear in the STDEV columns of Table 5.6 where individual standard deviation for

aluminum across all normal loads is generally higher than all copper tests. For the 3 mm support roller, copper samples at 22 lbs and 42 lbs saw an average STDEV of 0.0215 and 0.0180 which are lower than averages for all aluminum tests. This trend changes with the 24 mm radius support roller where individual and average standard deviations for aluminum and copper samples were closer. However, comparing COF curves shows aluminum generally behaves more sporadically while most copper curves are smoother and flat.

Copper testing in [14] used a standard normal load of 40 lbs to reproduce pressures seen during die forming operations. Aluminum was not used in the same operations so pressures for the procedure were not established, hence the COF vs normal load study results presented below. Therefore, a constant normal load to use for further testing needed to be established. Looking at the average COF results in Figure 5.26, tests with the 3 mm radius support roller saw fairly consistent COF and standard deviation up to 17 lbs where COF then rose rapidly. Tests with the 24 mm radius support roller also saw a rise in COF above 17 lbs normal load, although it was less severe. Next, contact area and associated pressure were analyzed. For both conductors, across all normal loads, contact area displayed no significant pattern with sporadic results across the testing range. However, as will be discussed in greater detail in Section 5.3.2, 7-17 lbs normal load only caused light scratching to the counterface while above this, there was large amounts of material transfer and smearing on the counterface surface. This limited the options for an appropriate normal load to 12-17 lbs. Since contact area, pressure, and wire surface damage were similar for both, it was decided to use 12 lbs as the standard normal load for testing moving forward to mitigate its influence on COF and keep the focus on affects from speed and forming angle.

Table 5.6. COF vs normal load testing results for 3 mm radius support roller.

Wire	Normal Load (lb)	COF	Avg COF	COF STDEV	STDEV	Avg STDEV	Contact Area (mm ²)	Pressure (MPa)
Al	7	0.2869	0.2590	0.0243	0.0307	0.0327	0.49	63.55
		0.2426			0.0295		0.74	42.08
		0.2474			0.0378		0.79	39.41
Al	12	0.2384	0.2651	0.0385	0.0327	0.0296	0.74	72.13
		0.2477			0.0271		0.93	57.40
		0.3093			0.0291		1.28	41.77
Al	17	0.3086	0.2694	0.0448	0.0503	0.0514	1.55	48.79
		0.3063			0.0595		1.02	74.14
		0.2210			0.0512		0.93	81.31
		0.2415			0.0445		1.87	40.44
Al	22	0.4281	0.3662	0.0570	0.0359	0.0409	2.72	35.98
		0.2862			0.0389		2.04	47.97
		0.3637			0.0419		4.61	21.23
		0.4123			0.0436		4.34	22.55
		0.3406			0.0443		2.69	36.38
Cu	22	0.2025	0.2053	0.0040	0.0244	0.0215	2.46	39.78
		0.2081			0.0185		2.36	41.47
Al	27	0.2138	0.2715	0.0453	0.0314	0.0429	3.17	37.89
		0.3052			0.0402		1.47	81.70
		0.2570			0.0448		4.51	26.63
		0.3100			0.0551		2.51	47.91
Al	32	0.2640	0.2752	0.0175	0.0412	0.0438	6.29	22.63
		0.2663			0.0465		5.66	25.15
		0.2954			0.0437		3.61	39.43
Al	37	0.2690	0.3053	0.0479	0.0615	0.0406	5.17	31.83
		0.2874			0.0329		4.17	39.47
		0.3596			0.0273		2.56	64.34
Al	42	0.3071	0.2975	0.0187	0.0381	0.0420	6.91	27.04
		0.2759			0.0681		6.43	29.06
		0.3094			0.0199		2.96	63.03
Cu	42	0.1462	0.2028	0.0507	0.0170	0.0180	3.12	59.88
		0.2440			0.0188		3.20	58.47
		0.2182			0.0182		2.55	73.26

Table 5.7. COF vs normal load testing results for 24 mm radius support roller.

Wire	Normal Load (lb)	COF	Avg COF	COF STDEV	STDEV	Avg STDEV	Contact Area (mm ²)	Pressure (MPa)
Al	7	0.2757	0.2888	0.0447	0.0302	0.0414	3.08	10.11
		0.2172			0.0196		2.14	14.55
		0.3037			0.0734		3.25	9.58
		0.3266			0.0415		0.39	79.84
		0.3209			0.0425		0.49	63.55
Al	12	0.2479	0.2194	0.0194	0.0380	0.0360	1.72	31.03
		0.2155			0.0439		2.05	26.04
		0.2060			0.0388		2.33	22.93
		0.2081			0.0232		4.38	12.18
Al	17	0.2695	0.2577	0.0130	0.0254	0.0304	3.51	21.54
		0.2437			0.0302		2.08	36.36
		0.2600			0.0357		2.35	32.18
Al	22	0.2656	0.2841	0.0496	0.0279	0.0422	6.94	14.10
		0.3411			0.0434		1.84	53.19
		0.2187			0.0427		3.18	30.75
		0.3258			0.0635		2.83	34.58
		0.2691			0.0333		2.04	47.97
Cu	22	0.1881	0.2149	0.0319	0.0263	0.0302	2.75	35.59
		0.2502			0.0152		1.60	61.16
		0.2063			0.0492		3.24	30.23
Al	27	0.2799	0.2816	0.0792	0.0395	0.0319	8.73	13.76
		0.1909			0.0224		9.16	13.11
		0.1813			0.0169		3.82	31.44
		0.4005			0.0520		2.79	43.05
		0.3772			0.0236		2.69	44.65
		0.3069			0.0324		3.57	33.64
		0.2758			0.0359		5.54	21.67
		0.2406			0.0325		5.10	23.57
Al	32	0.3094	0.3127	0.0449	0.0220	0.0385	5.11	27.86
		0.2452			0.0211		6.89	20.66
		0.2918			0.0599		3.53	40.32
		0.3061			0.0644		5.04	28.24
		0.3512			0.0271		3.06	46.52
		0.3724			0.0363		3.20	44.48
Al	37	0.2183	0.2333	0.0184	0.0222	0.0220	8.21	20.05
		0.2215			0.0218		8.64	19.05
		0.2346			0.0203			
		0.2587			0.0235		4.44	37.05
Al	42	0.2897	0.3148	0.0492	0.0301	0.0232	5.84	31.99
		0.2586			0.0290		8.36	22.35
		0.3459			0.0063		4.48	41.70
		0.3650			0.0272		4.66	40.13
Cu	42	0.2041	0.1909	0.0416	0.0424	0.0391	3.42	54.63
		0.2242			0.0302		5.39	34.66
		0.1443			0.0448		1.96	95.42

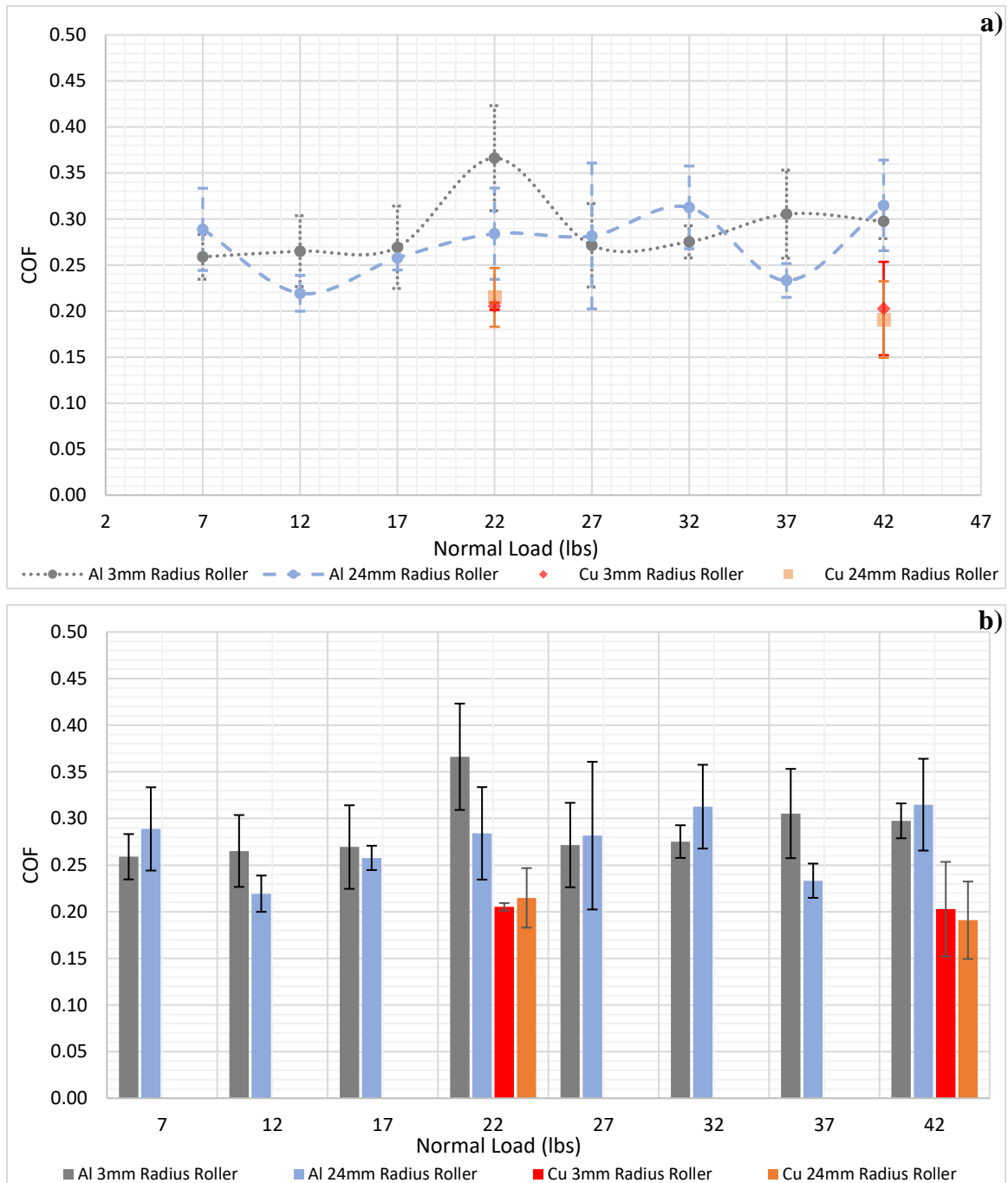


Figure 5.26. Average COF vs normal load testing results for aluminum and copper magnet wires. (a) Uses trend line to highlight change in COF for aluminum wire samples as normal load increases. (b) Highlights COF standard deviation for each testing condition.

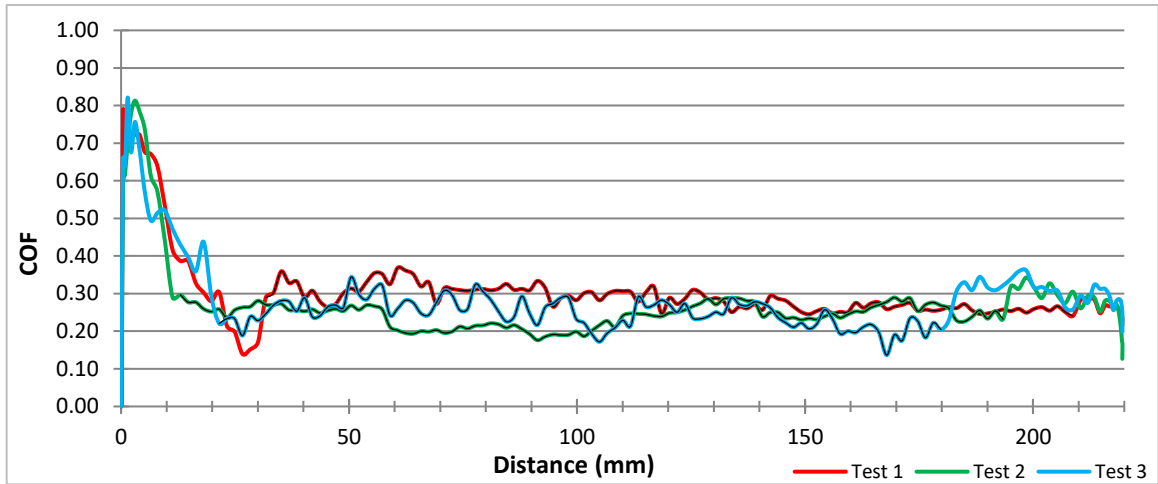


Figure 5.27. Variation of COF with aluminum wire travel length for normal load testing at 7 lbs with 3 mm radius support roller.

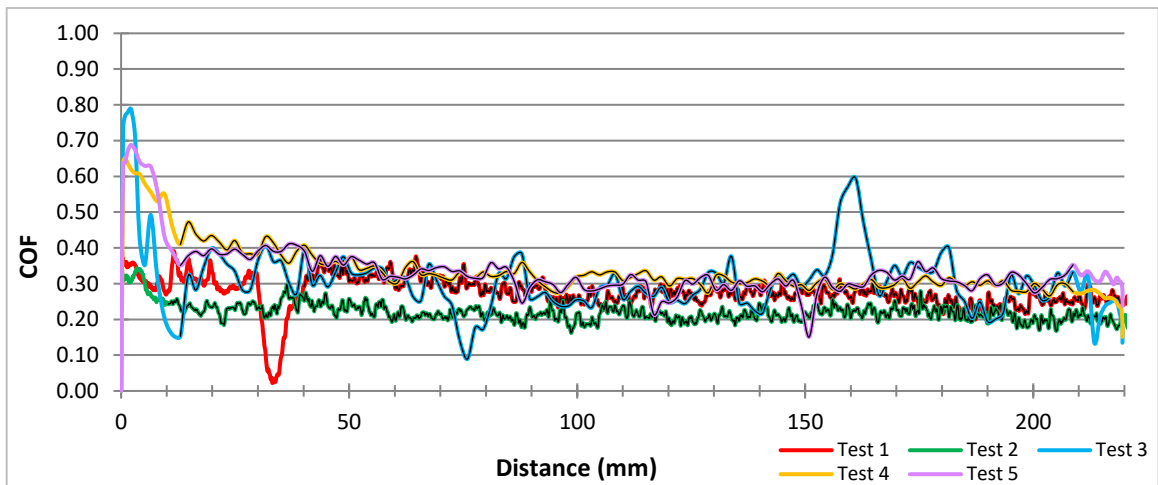


Figure 5.28. Variation of COF with aluminum wire travel length for normal load testing at 7 lbs with 24 mm radius support roller.

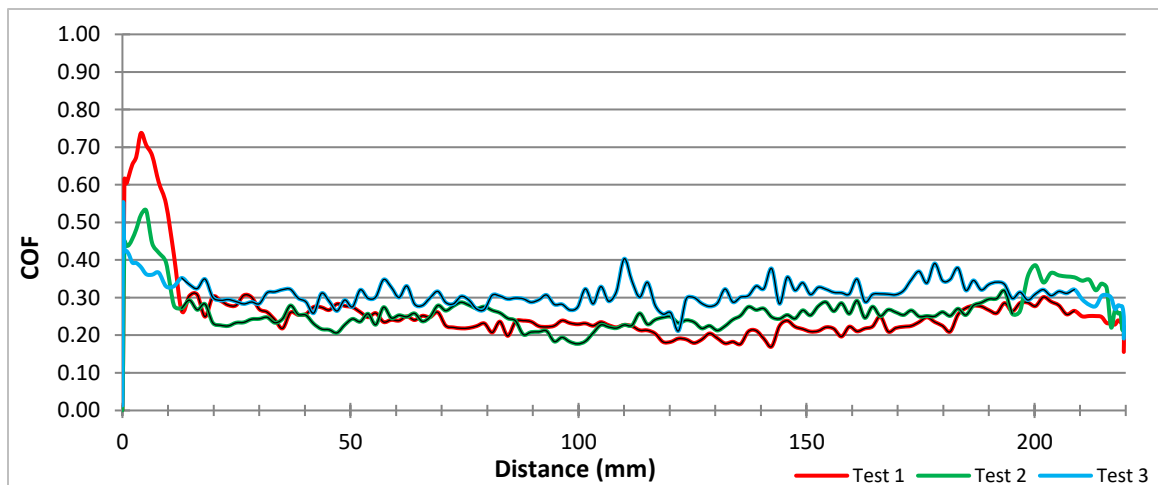


Figure 5.29. Variation of COF with aluminum wire travel length for normal load testing at 12 lbs with 3 mm radius support roller.

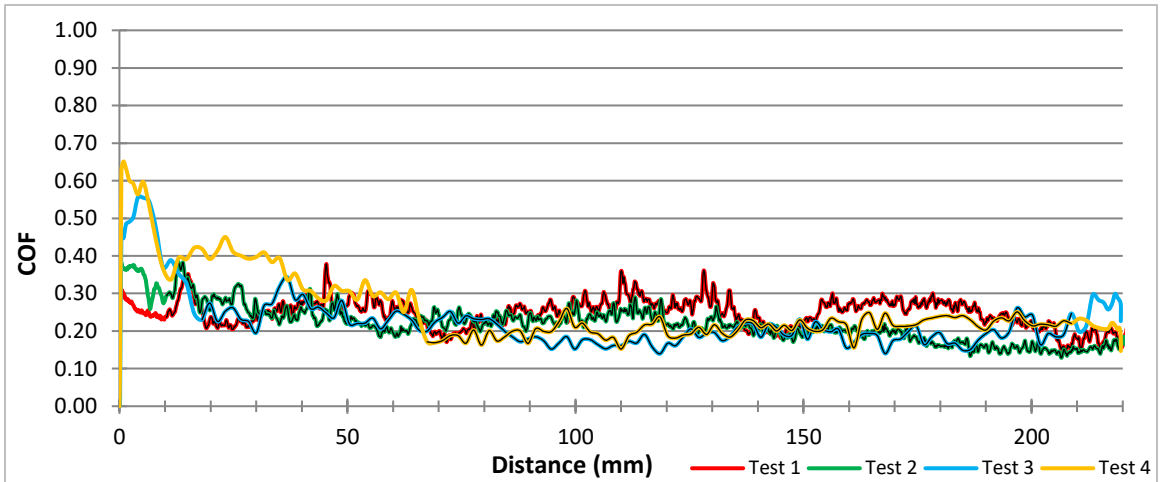


Figure 5.30. Variation of COF with aluminum wire travel length for normal load testing at 12 lbs with 24 mm radius support roller.

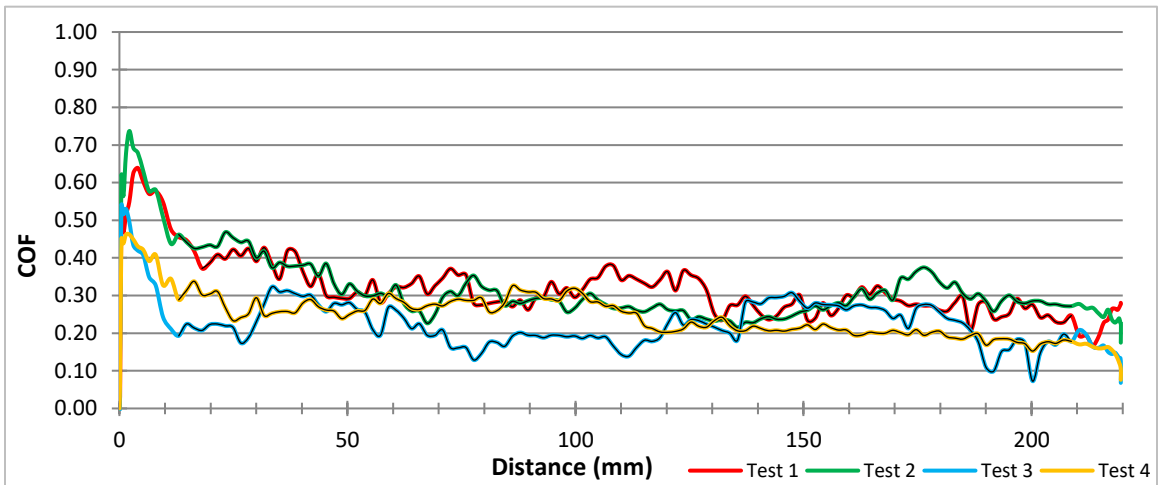


Figure 5.31. Variation of COF with aluminum wire travel length for normal load testing at 17 lbs with 3 mm radius support roller.

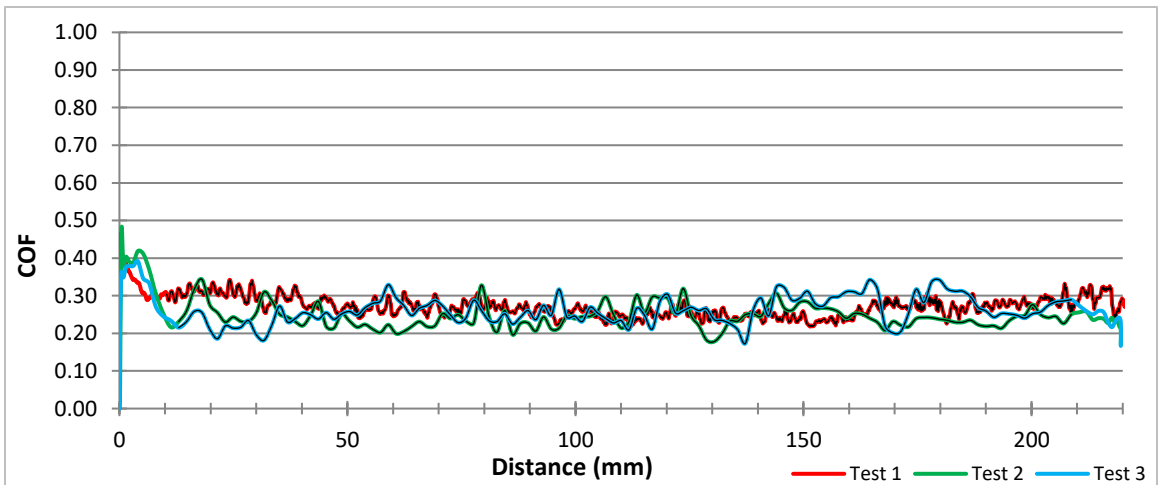


Figure 5.32. Variation of COF with aluminum wire travel length for normal load testing at 17 lbs with 24 mm radius support roller.

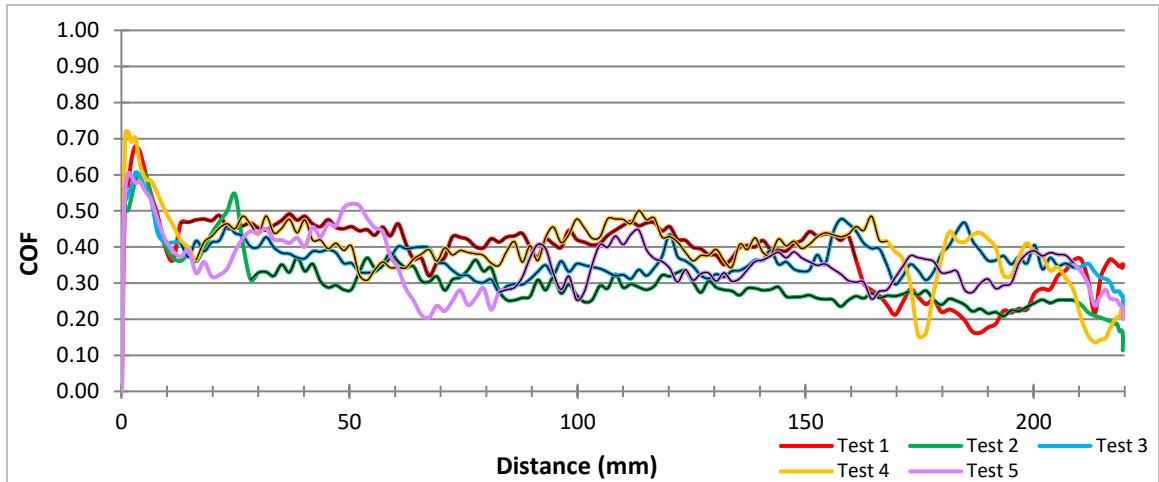


Figure 5.33. Variation of COF with aluminum wire travel length for normal load testing at 22 lbs with 3 mm radius support roller.

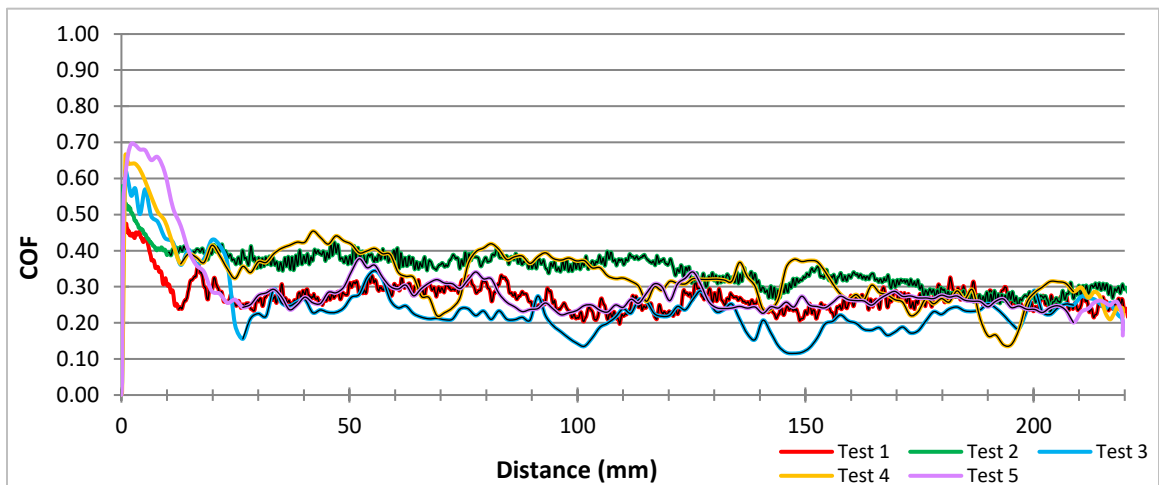


Figure 5.34. Variation of COF with aluminum wire travel length for normal load testing at 22 lbs with 24 mm radius support roller.

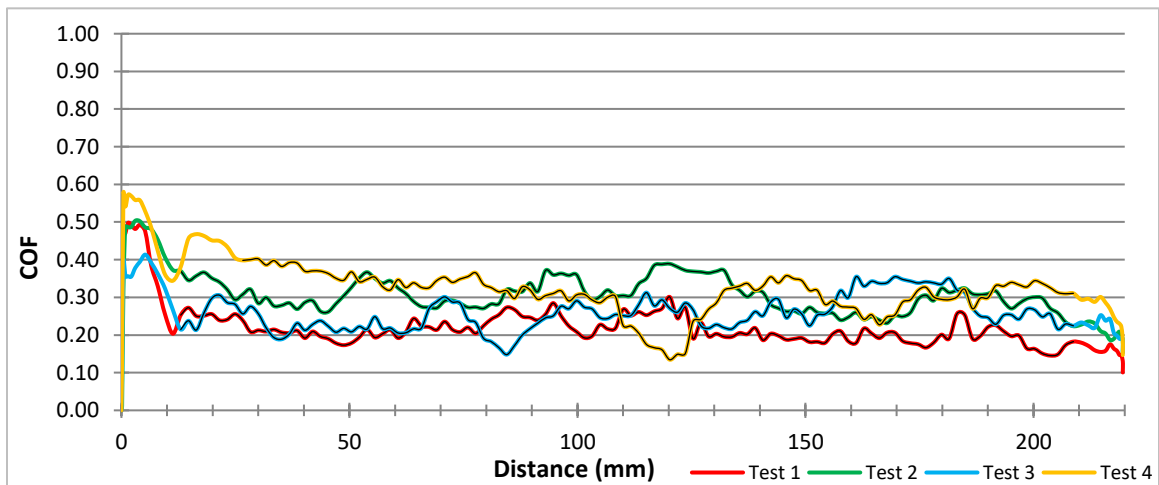


Figure 5.35. Variation of COF with aluminum wire travel length for normal load testing at 27 lbs with 3 mm radius support roller.

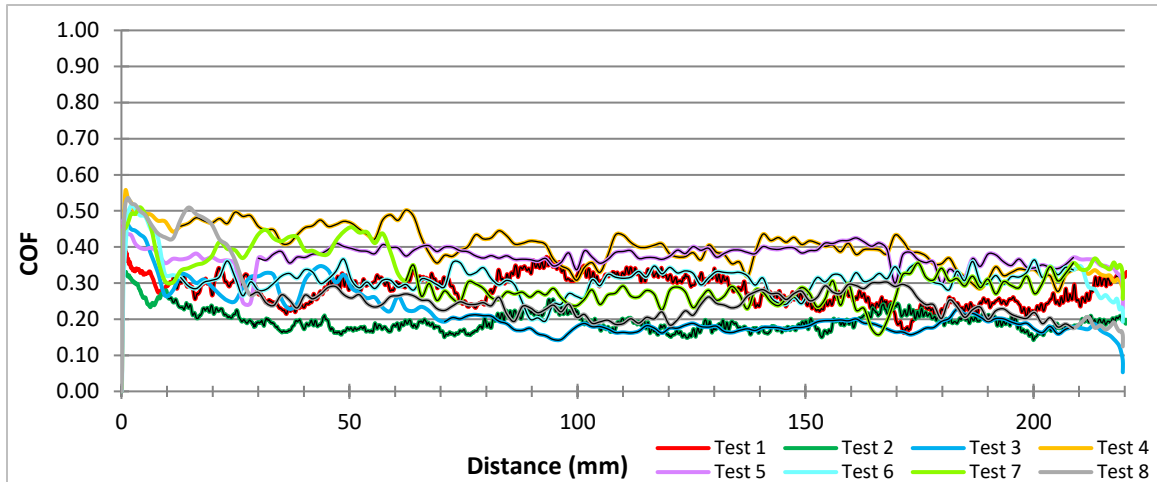


Figure 5.36. Variation of COF with aluminum wire travel length for normal load testing at 27 lbs with 24 mm radius support roller.

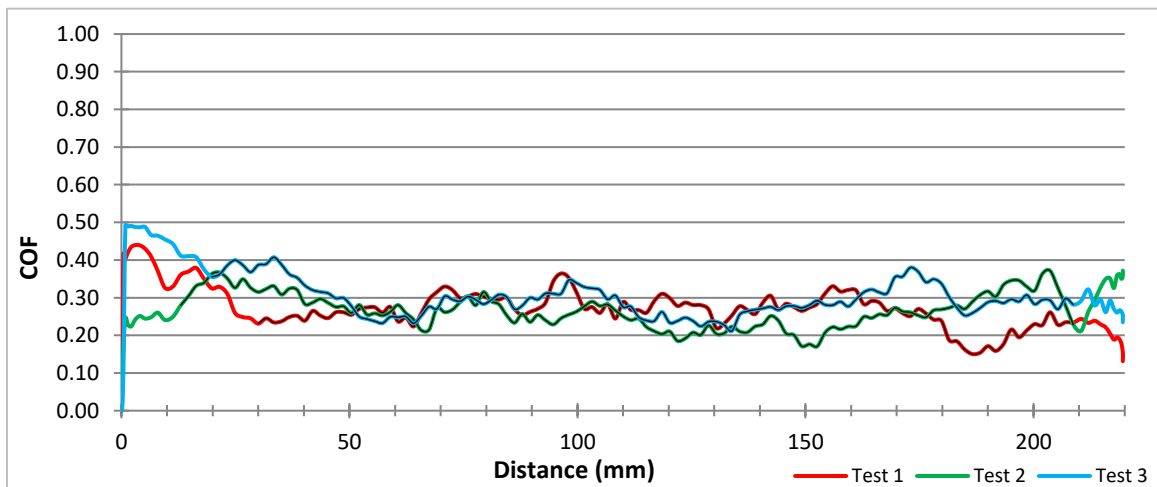


Figure 5.37. Variation of COF with aluminum wire travel length for normal load testing at 32 lbs with 3 mm radius support roller.

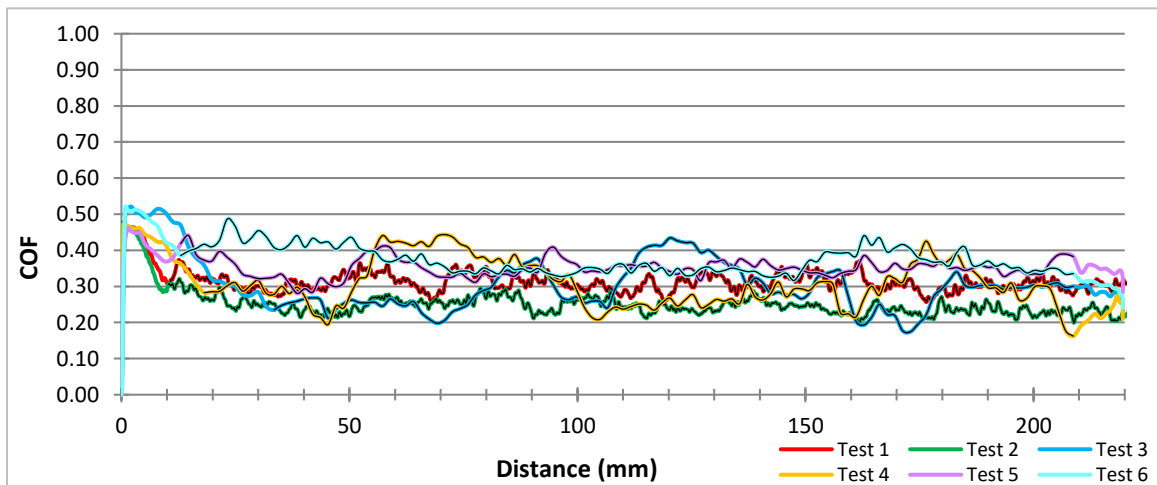


Figure 5.38. Variation of COF with aluminum wire travel length for normal load testing at 32 lbs with 24 mm radius support roller.

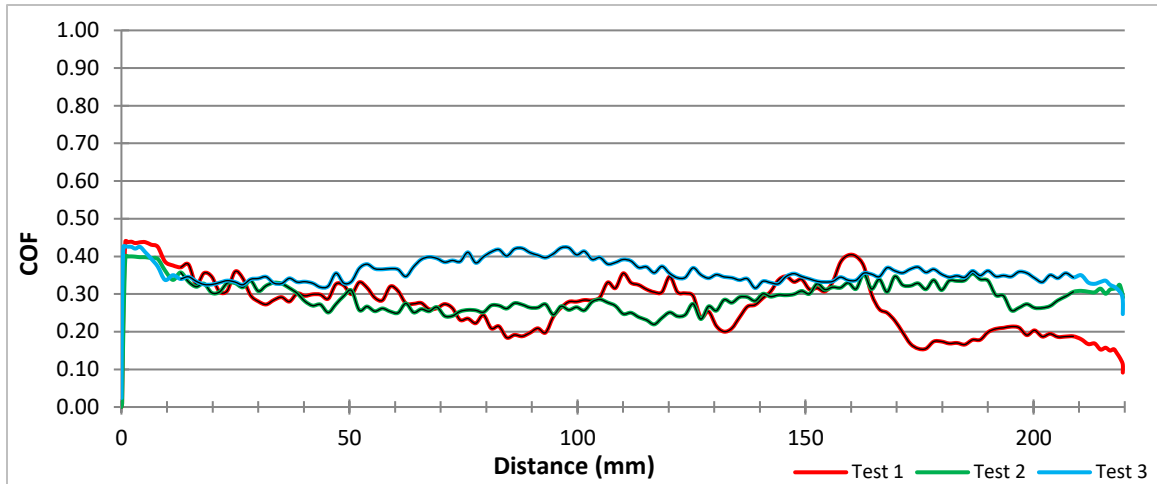


Figure 5.39. Variation of COF with aluminum wire travel length for normal load testing at 37 lbs with 3 mm radius support roller.

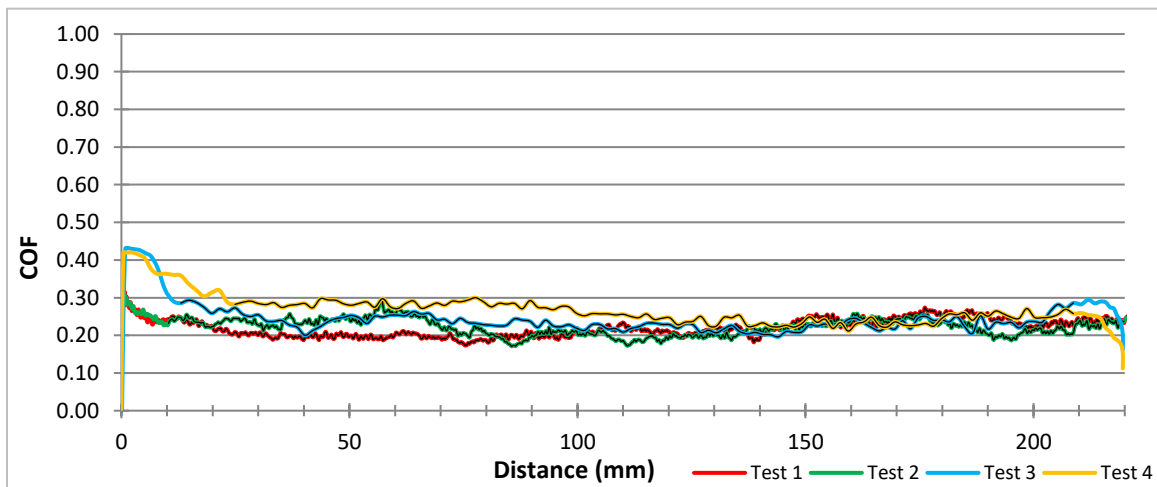


Figure 5.40. Variation of COF with aluminum wire travel length for normal load testing at 37 lbs with 24 mm radius support roller.

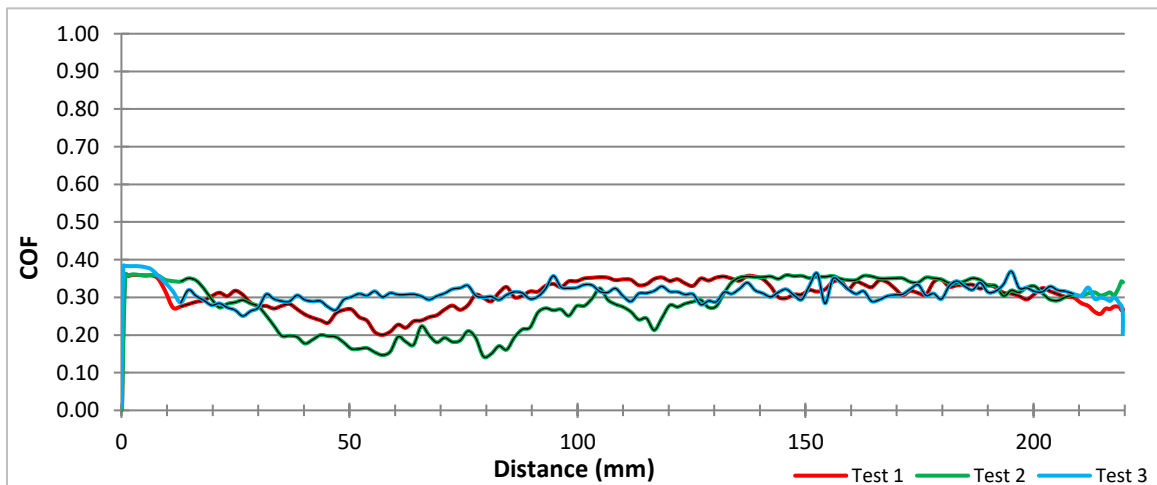


Figure 5.41. Variation of COF with aluminum wire travel length for normal load testing at 42 lbs with 3 mm radius support roller.

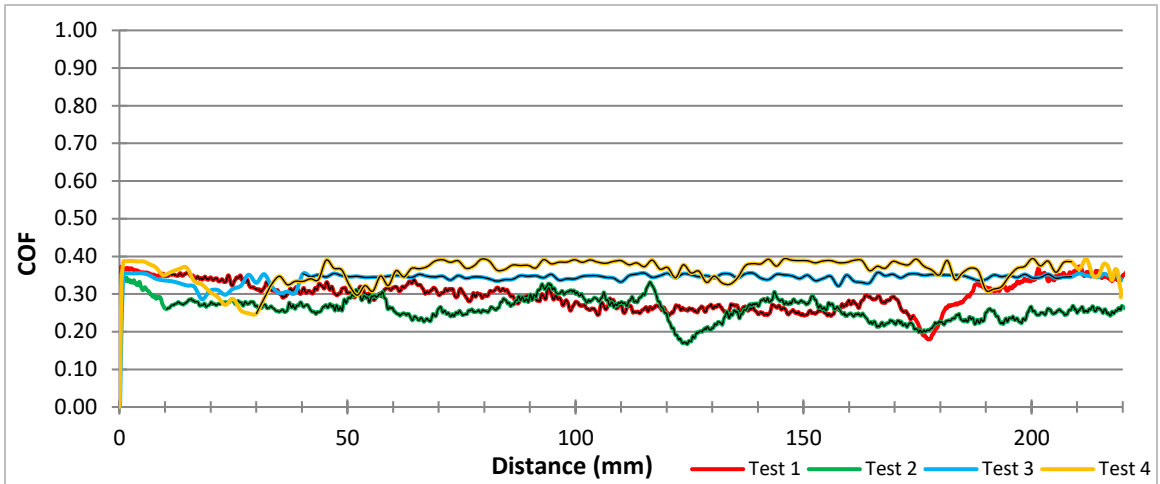


Figure 5.42. Variation of COF with aluminum wire travel length for normal load testing at 42 lbs with 24 mm radius support roller.

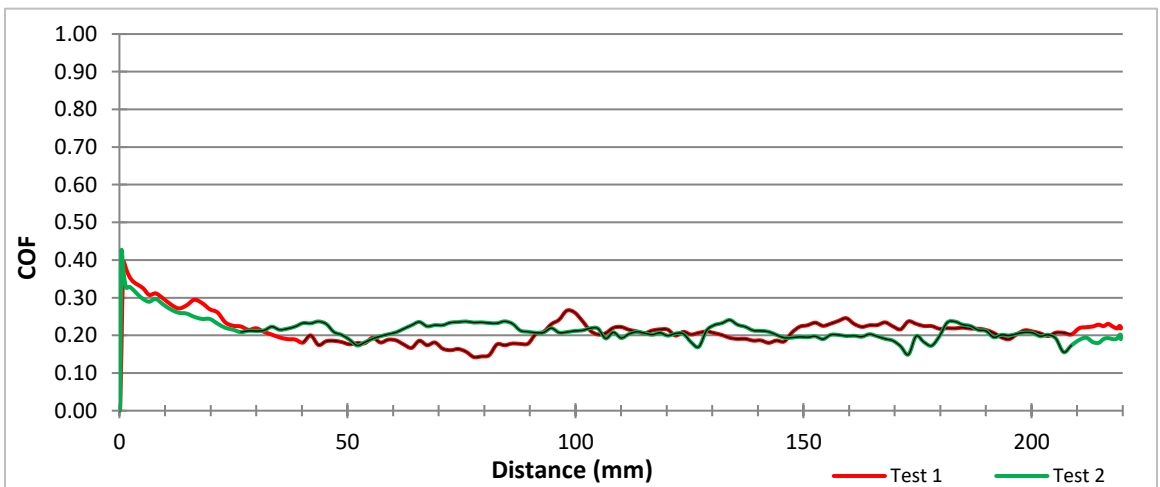


Figure 5.43. Variation of COF with copper wire travel length for normal load testing at 22 lbs with 3 mm radius support roller.

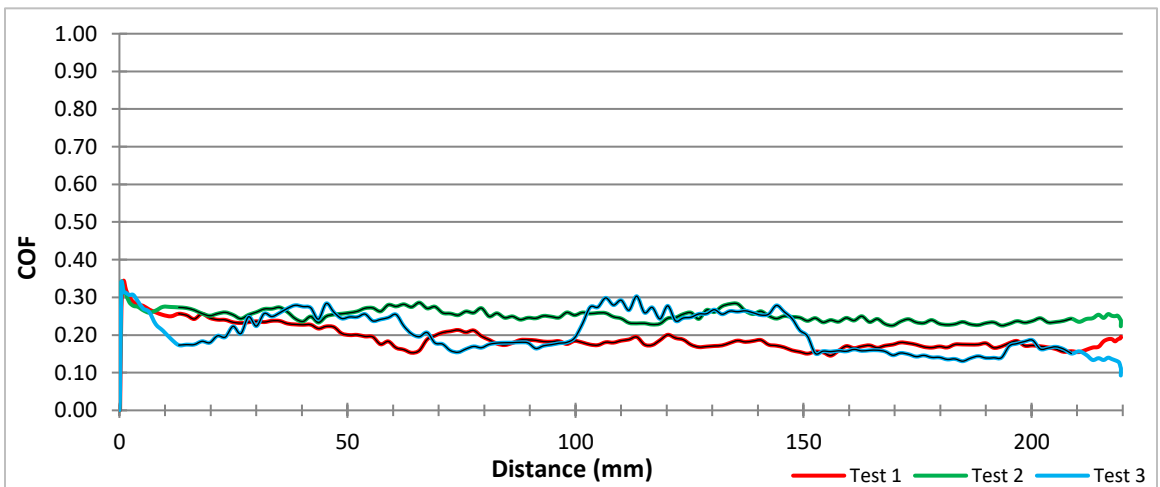


Figure 5.44. Variation of COF with copper wire travel length for normal load testing at 22 lbs with 24 mm radius support roller.

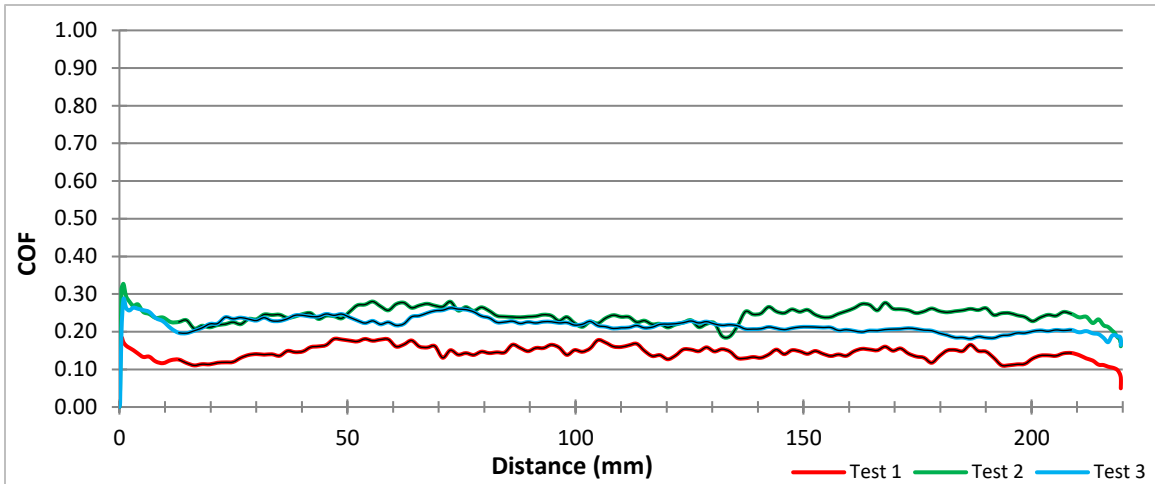


Figure 5.45. Variation of COF with copper wire travel length for normal load testing at 42 lbs with 3 mm radius support roller.

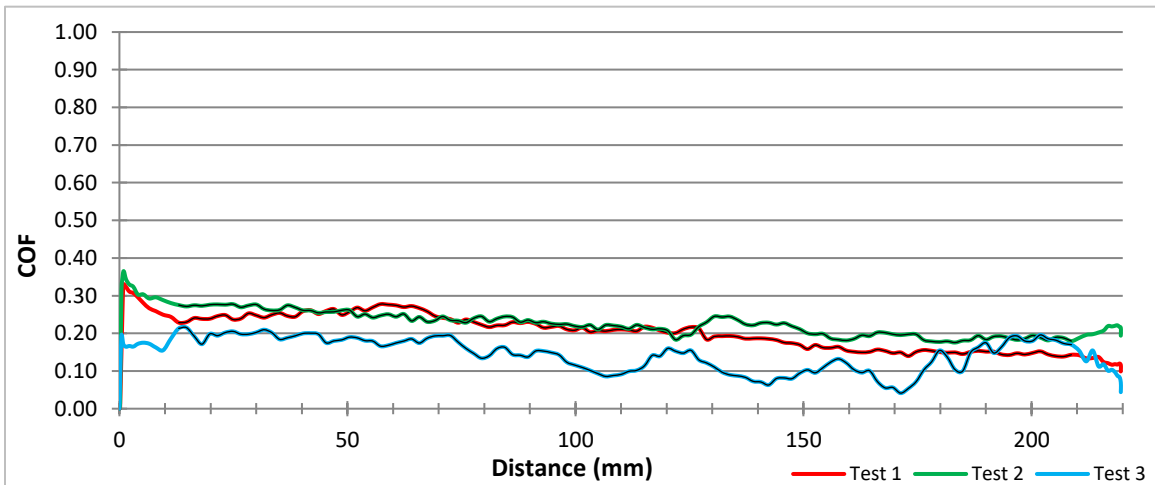


Figure 5.46. Variation of COF with copper wire travel length for normal load testing at 42 lbs with 24 mm radius support roller.

5.2.2 COF vs Travel Speed Testing Results

COF vs travel speed testing was only conducted on insulated aluminum wires according to the procedure outlined in 4.4.2.2 with the following parameters:

- Wire travel speed of 5, 10, 15, 20, 25, 30, 35 and 40 mm/s
- Constant applied normal load of 12 lb
- 3 mm radius support roller only
- Sample contact length of 220 mm
- Constant acceleration of 20 mm/s²
- Forming angle of 10°

Results for this testing are found in Table 5.8 which outlines individual and average COF values and associated standard deviation for each. Average coefficient of friction values along with their standard deviation are plotted in Figure 5.47. Graph (a) best highlights the trend in COF as wire travel speed increases while graph (b) better illustrates standard deviation for each test. The variation of coefficient of friction was plotted against aluminum wire travel length for each speed from Figure 5.48 to Figure 5.55. Each graph also contains the velocity profile for the test, represented by a dashed grey curve at the bottom of the plot, which highlights the acceleration and constant speed phases. Again, COF was only calculated with data from the constant speed section of each test which is highlighted by a black line on each curve. The same spikes in COF seen at test start in normal load testing are also present here so they were removed from the COF calculation range.

Looking at the plot of average COF for each speed in Figure 5.47, (a) shows a trend of increasing COF with increasing wire speed. The COF rose 0.1131 from 5-40 mm/s but the standard deviation between COF results was very high at both extremes. This trend can be compared to results found for copper wires tested by A. Demiri in [14]. Samples were tested at 1, 5, 10, 15, and 20 mm/s and saw a general rise in COF with wire speed as well but the relationship was weak.

Table 5.8. COF vs aluminum wire travel speed testing results for 3 mm radius support roller.

Speed (mm/s)	COF	Avg COF	COF STDEV	STDEV	Avg STDEV
5	0.0997 0.1490 0.2604	0.1697	0.0823	0.0254 0.0381 0.0616	0.0417
10	0.1675 0.1502 0.1184	0.1454	0.0249	0.0139 0.0259 0.0163	0.0187
15	0.1984 0.1406 0.2513	0.1968	0.0554	0.0168 0.0406 0.0218	0.0264
20	0.2384 0.2477 0.3093	0.2651	0.0385	0.0327 0.0271 0.0291	0.0296
25	0.2723 0.1696 0.2416	0.2278	0.0527	0.0287 0.0309 0.0396	0.0331
30	0.2755 0.2687 0.2274	0.2572	0.0260	0.0603 0.0400 0.0648	0.0550
35	0.1930 0.2340 0.2131	0.2134	0.0205	0.0202 0.0124 0.0501	0.0276
40	0.2034 0.3269 0.3181	0.2828	0.0689	0.0371 0.0223 0.0323	0.0306

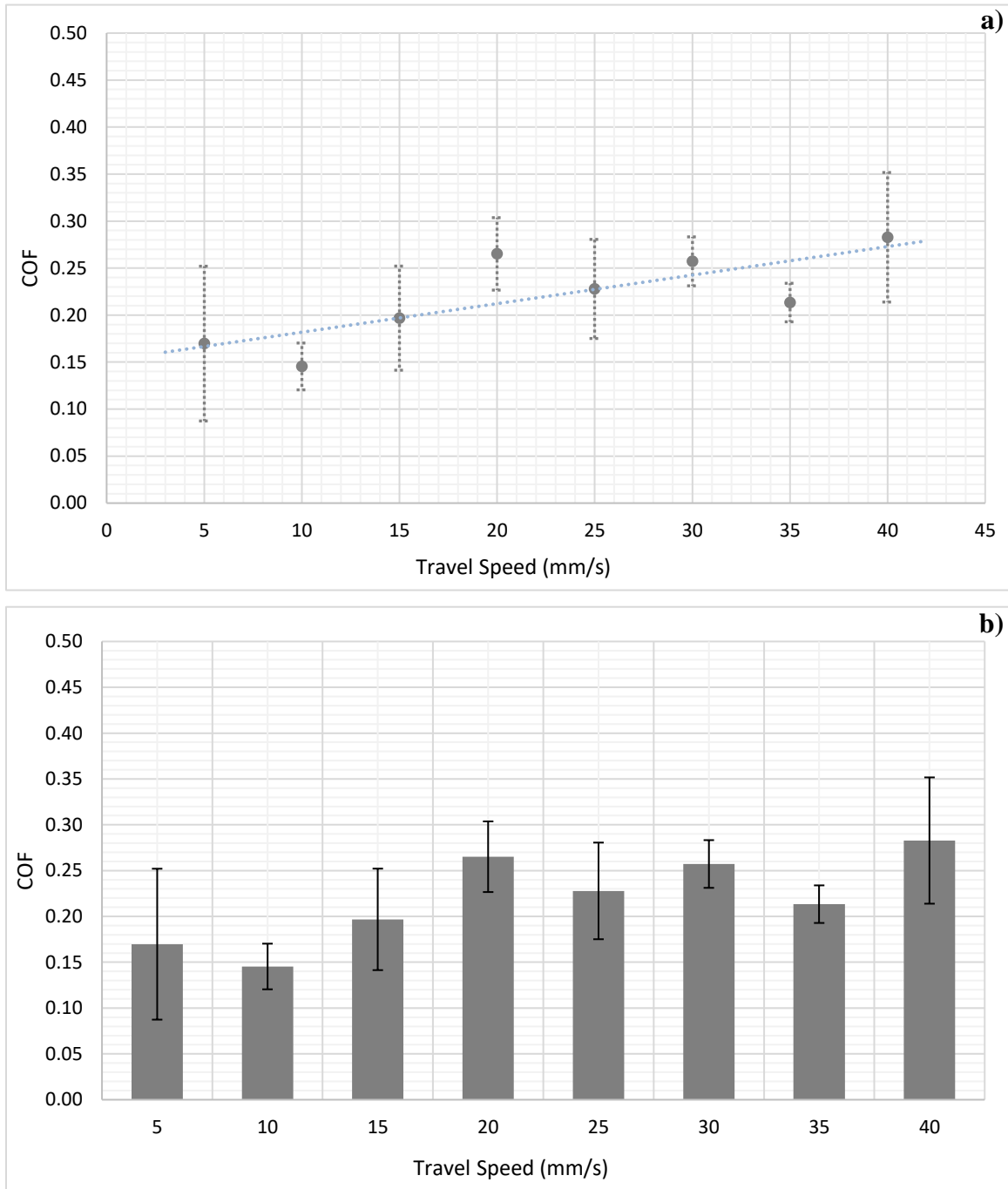


Figure 5.47. Average COF vs aluminum wire travel speed testing results. (a) Uses trend line to highlight change in COF as travel speed increases. (b) Highlights COF standard deviation for each wire speed.

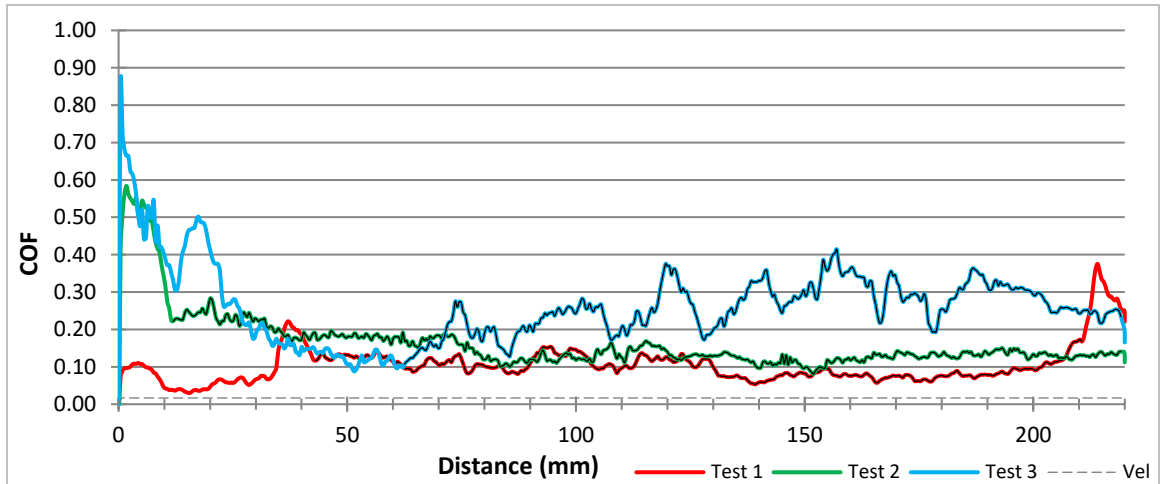


Figure 5.48. Variation of COF with aluminum wire travel length for travel speed testing at 5 mm/s.

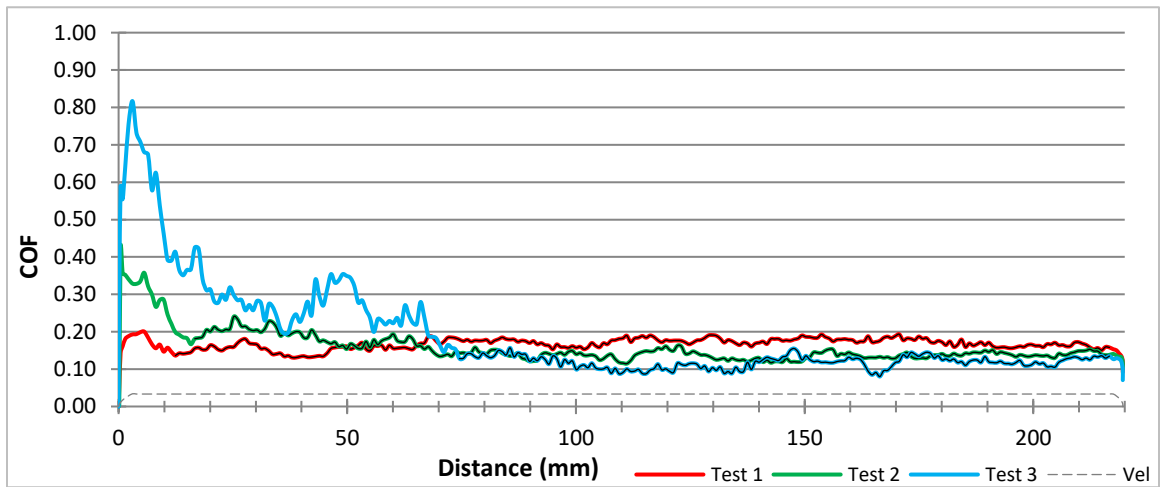


Figure 5.49. Variation of COF with aluminum wire travel length for travel speed testing at 10 mm/s.

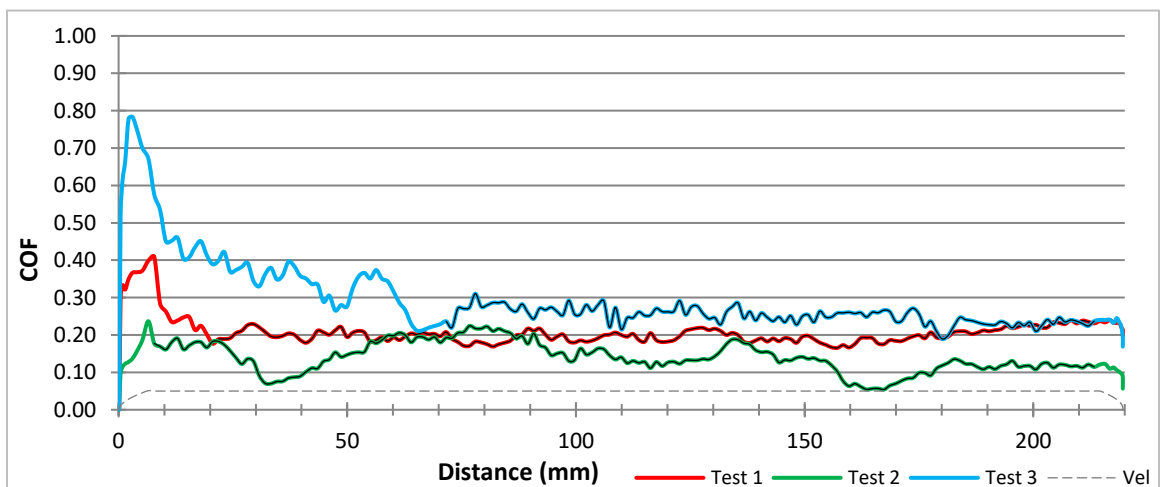


Figure 5.50. Variation of COF with aluminum wire travel length for travel speed testing at 15 mm/s.

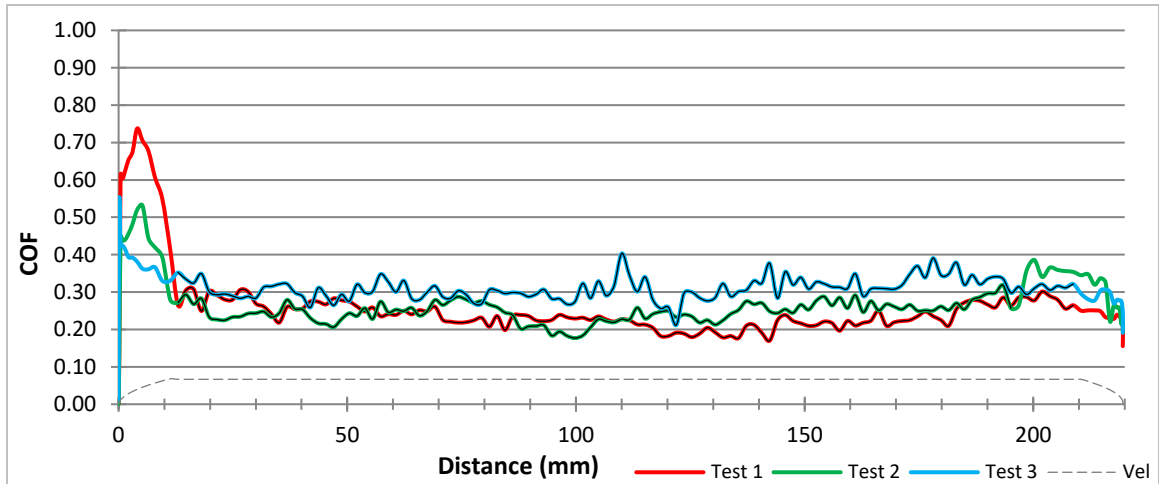


Figure 5.51. Variation of COF with aluminum wire travel length for travel speed testing at 20 mm/s.

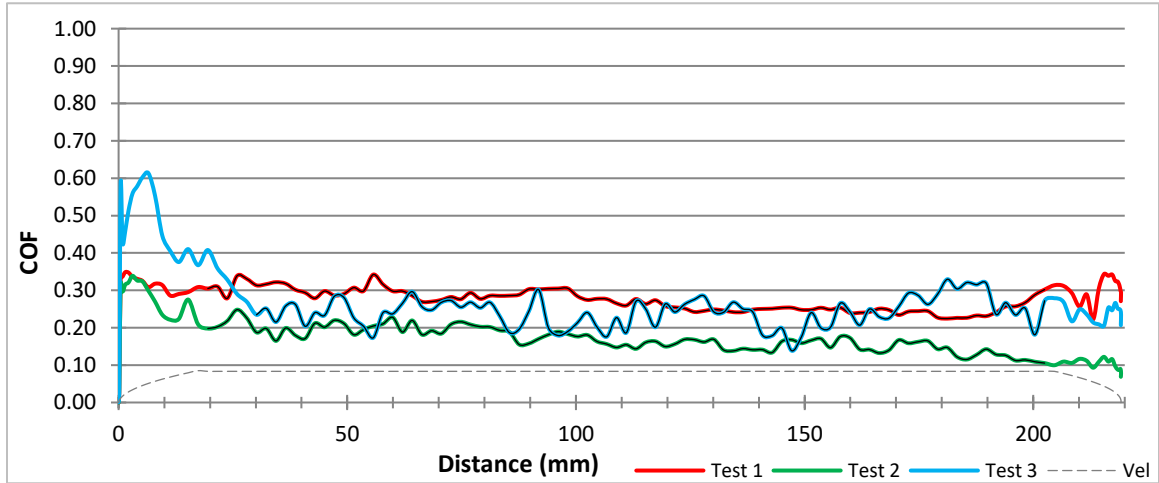


Figure 5.52. Variation of COF with aluminum wire travel length for travel speed testing at 25 mm/s.

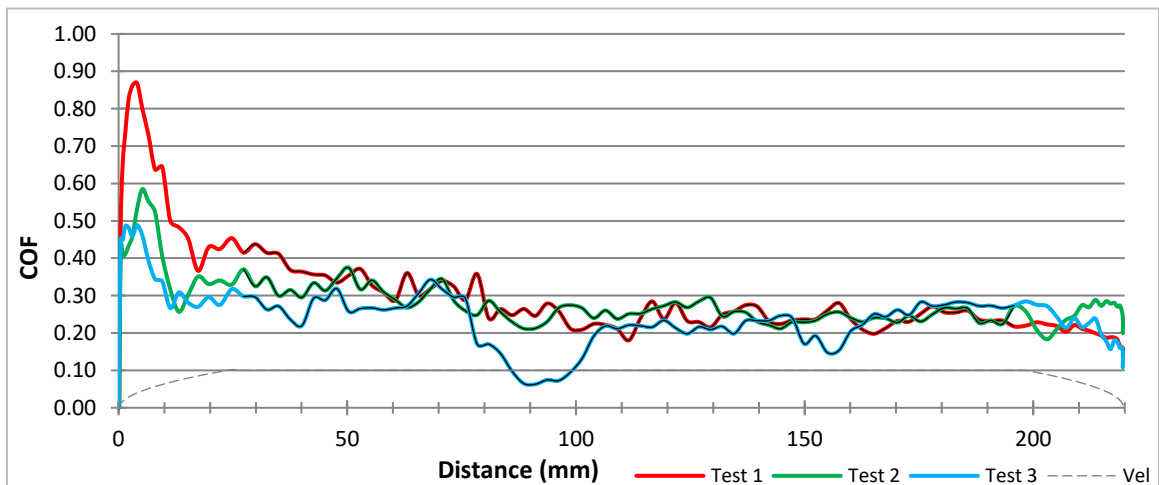


Figure 5.53. Variation of COF with aluminum wire travel length for travel speed testing at 30 mm/s.

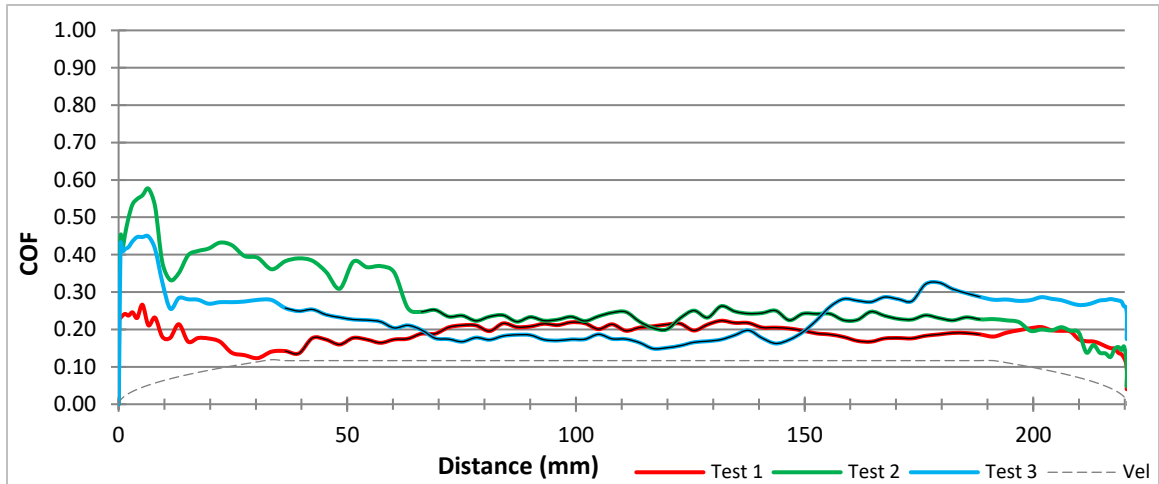


Figure 5.54. Variation of COF with aluminum wire travel length for travel speed testing at 35 mm/s.

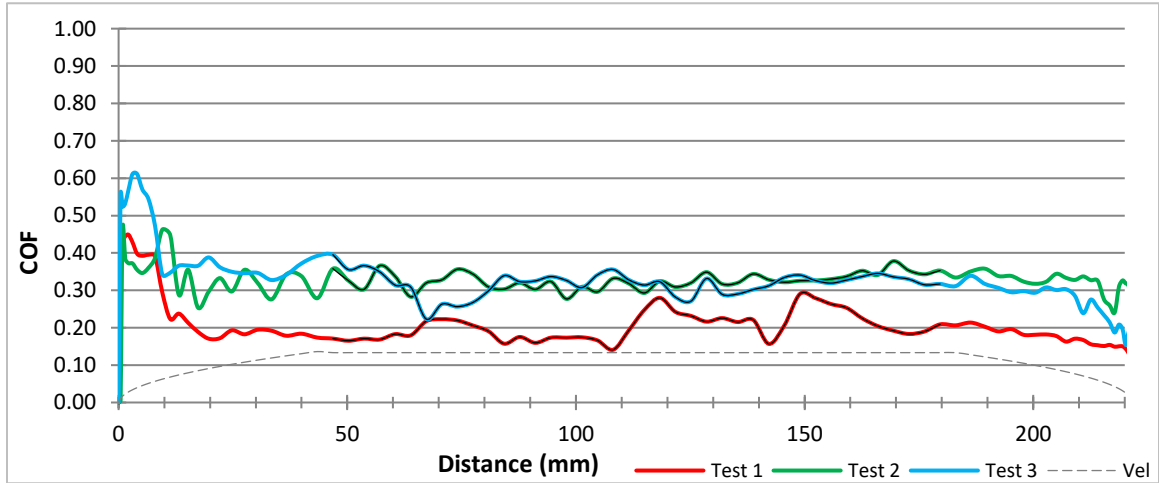


Figure 5.55. Variation of COF with aluminum wire travel length for travel speed testing at 40 mm/s.

5.2.3 COF vs Forming Angle Testing Results

COF vs wire forming angle testing was only conducted on insulated aluminum wires according to the procedure outlined in 4.4.2.3 with the following parameters:

- Forming angle of 10°, 30°, 60° and 90°
- Constant applied normal load of 12 lbs
- Both 3 mm and 24 mm radius support rollers
- Sample contact length of 220 mm
- Constant speed and acceleration of 20 mm/s and 20 mm/s²

Results for this testing are found in Table 5.9 for samples supported by the 3 mm radius roller and Table 5.10 for those supported by the 24 mm radius roller. Both tables outline individual coefficient of friction values and associated standard deviation for each test. Average coefficient of friction values along with their standard deviation for each testing condition are plotted in Figure 5.56. Graph (a) best highlights the trend in COF as aluminum wire forming angle increases while graph (b) better compares COF for each support roller. The variation of coefficient of friction was plotted against aluminum wire travel length for each angle from Figure 5.57 to Figure 5.63. Testing at 90° was not done for the 3 mm support roller due to limitations imposed by machine geometry.

Looking at the trend of COF with forming angle in Figure 5.56, (a) demonstrates a general increase in COF as forming angle increases for the 24 mm radius support roller. This trend is not as obviously mimicked with the 3 mm roller though since testing at 30° saw a significant decrease in COF compared to both 10° and 60°. However, COF at 60° is still increased over 10° suggesting it may follow the same trend as the 24 mm radius roller.

The results for aluminum can be compared to similar testing done for copper in [14], Section 4.7. It was found that as forming angle increased, COF experienced by copper decreased for both support roller sizes [14]. Section 4.8 analyzed the effects of surface strain on COF and saw a general decrease as surface strain increased as well [14]. This trend of decreasing COF with increased copper wire surface strain is opposite to that found for aluminum samples tested in this study.

Table 5.9. COF vs aluminum wire forming angle testing results for 3mm radius support roller.

Angle (deg)	COF	Avg COF	COF STDEV	STDEV	Avg STDEV
10	0.2384	0.2651	0.0385	0.0327	0.0296
	0.2477			0.0271	
	0.3093			0.0291	
30	0.1430	0.1835	0.0373	0.0261	0.0269
	0.1912			0.0290	
	0.2164			0.0255	
60	0.2947	0.2898	0.0057	0.0625	0.0600
	0.2910			0.0703	
	0.2836			0.0473	

Table 5.10. COF vs aluminum wire forming angle testing results for 24mm radius support roller.

Angle (deg)	COF	Avg COF	COF STDEV	STDEV	Avg STDEV
10	0.2479	0.2194	0.0194	0.0380	0.0360
	0.2155			0.0439	
	0.2060			0.0388	
	0.2081			0.0232	
30	0.2982	0.2976	0.0176	0.0279	0.0241
	0.3149			0.0208	
	0.2797			0.0237	
60	0.2924	0.3081	0.0233	0.0471	0.0410
	0.3349			0.0496	
	0.2971			0.0264	
90	0.3318	0.3598	0.0452	0.0349	0.0381
	0.4120			0.0357	
	0.3356			0.0438	

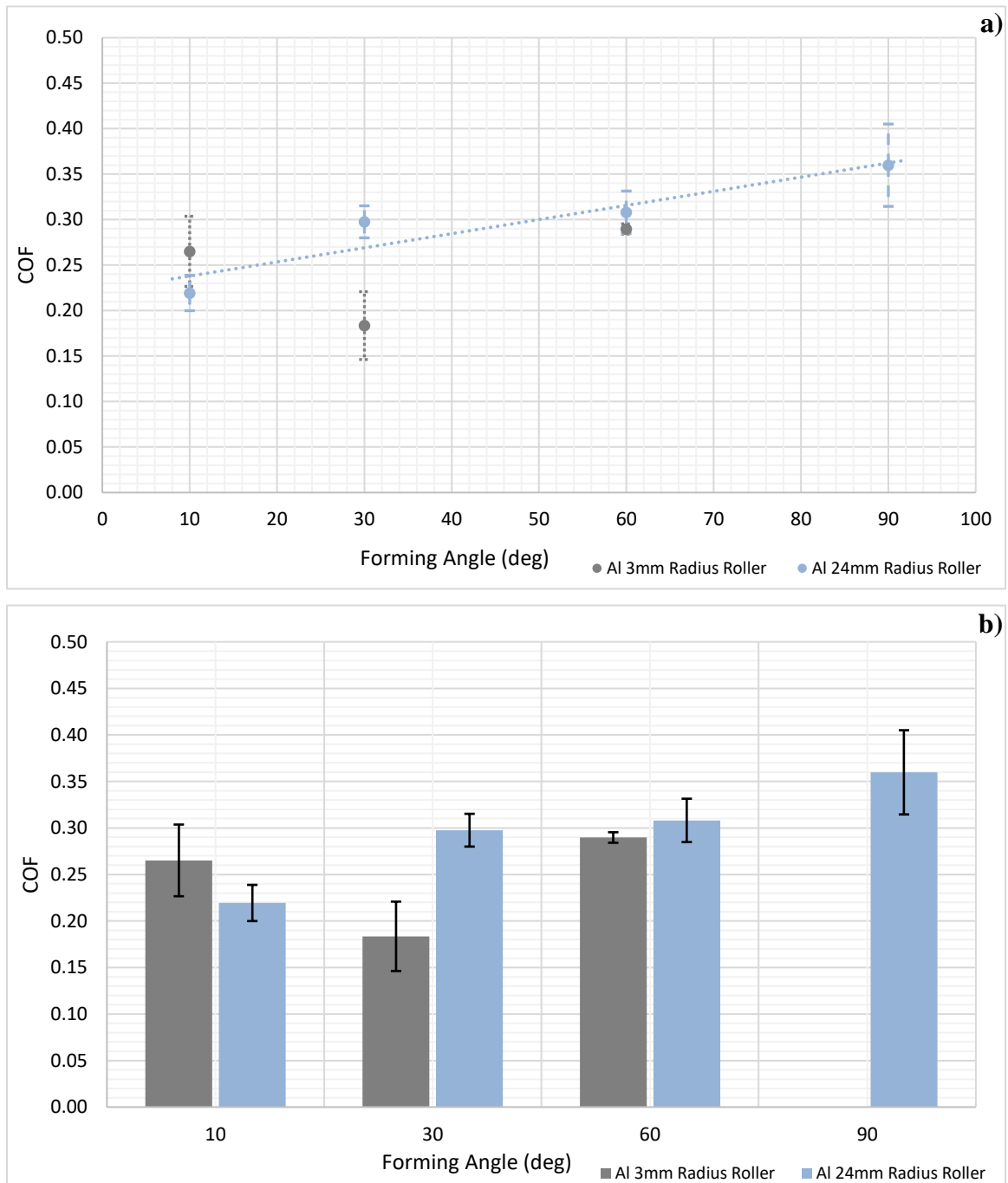


Figure 5.56. Average COF vs aluminum wire forming angle testing results. (a) Uses trend line to highlight change in COF for 24 mm radius support roller as forming angle increases. (b) Highlights COF standard deviation for each testing condition and better compares COF between support rollers for each forming angle.

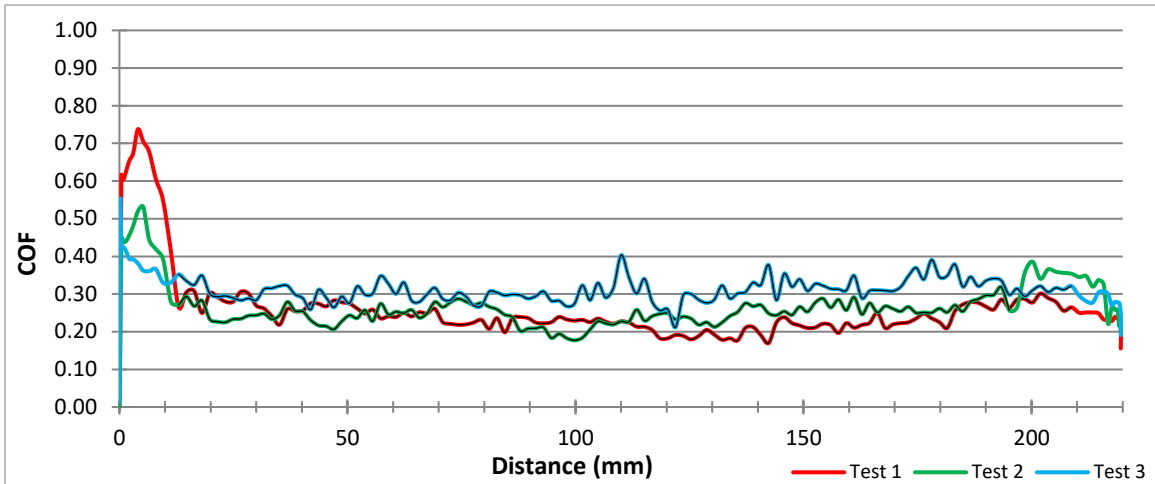


Figure 5.57. Variation of COF with aluminum wire travel length for forming angle testing at 10° with 3 mm radius support roller.

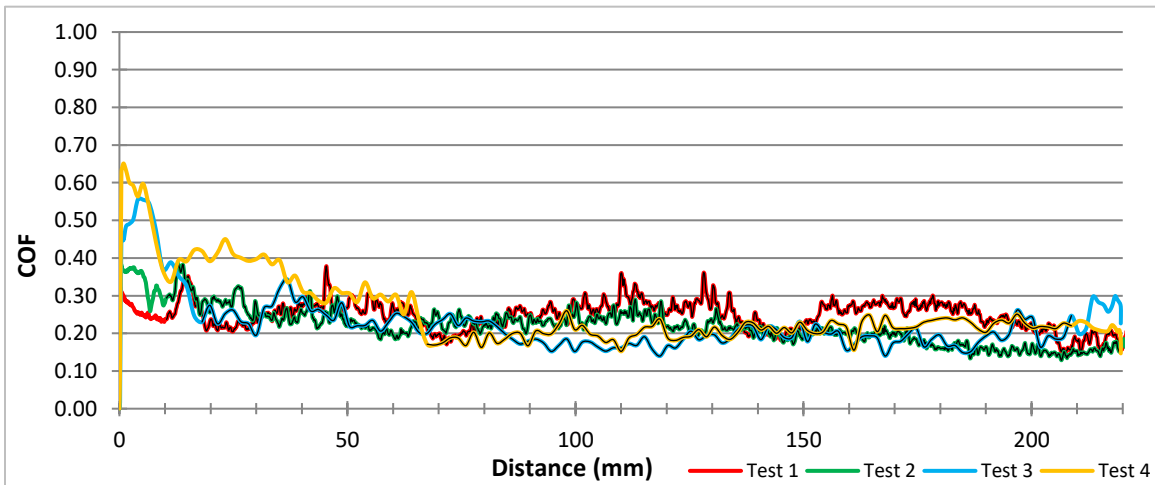


Figure 5.58. Variation of COF with aluminum wire travel length for forming angle testing at 10° with 24 mm radius support roller.

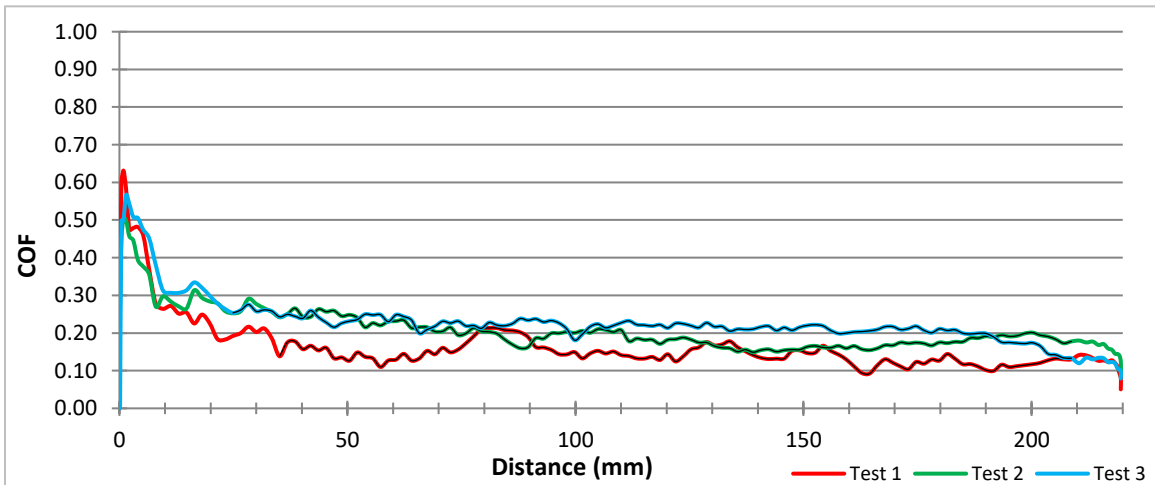


Figure 5.59. Variation of COF with aluminum wire travel length for forming angle testing at 30° with 3 mm radius support roller.

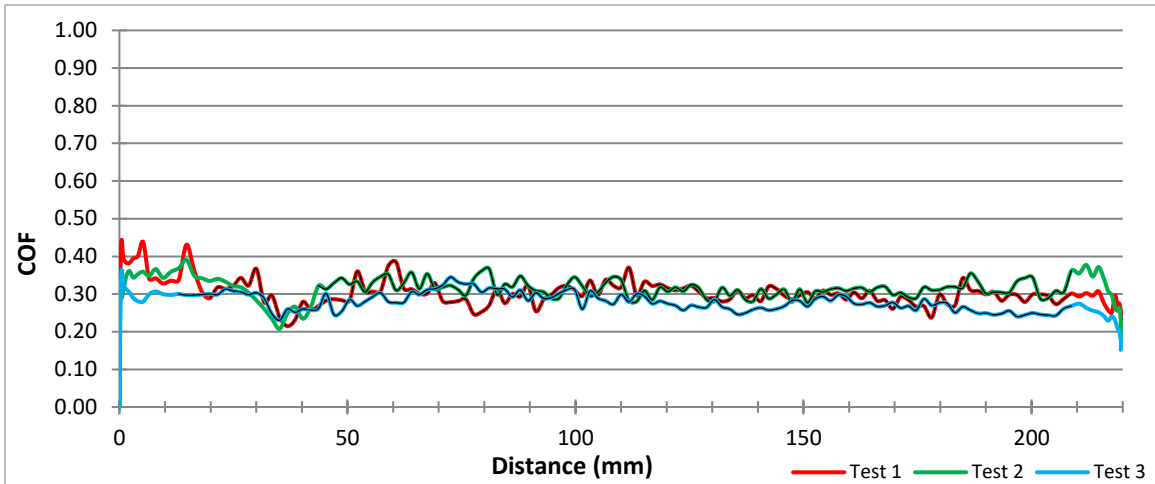


Figure 5.60. Variation of COF with aluminum wire travel length for forming angle testing at 30° with 24 mm radius support roller.

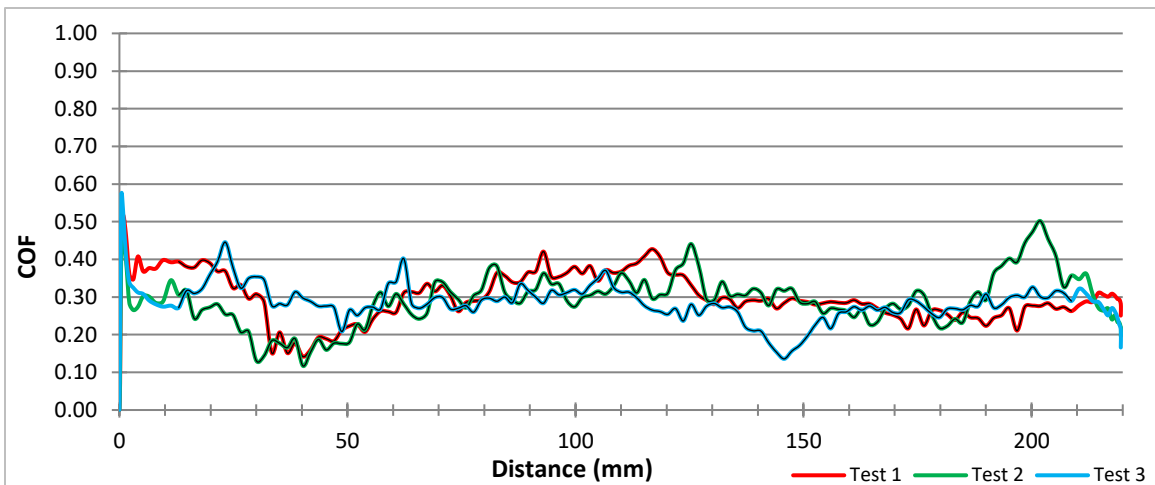


Figure 5.61. Variation of COF with aluminum wire travel length for forming angle testing at 60° with 3 mm radius support roller.

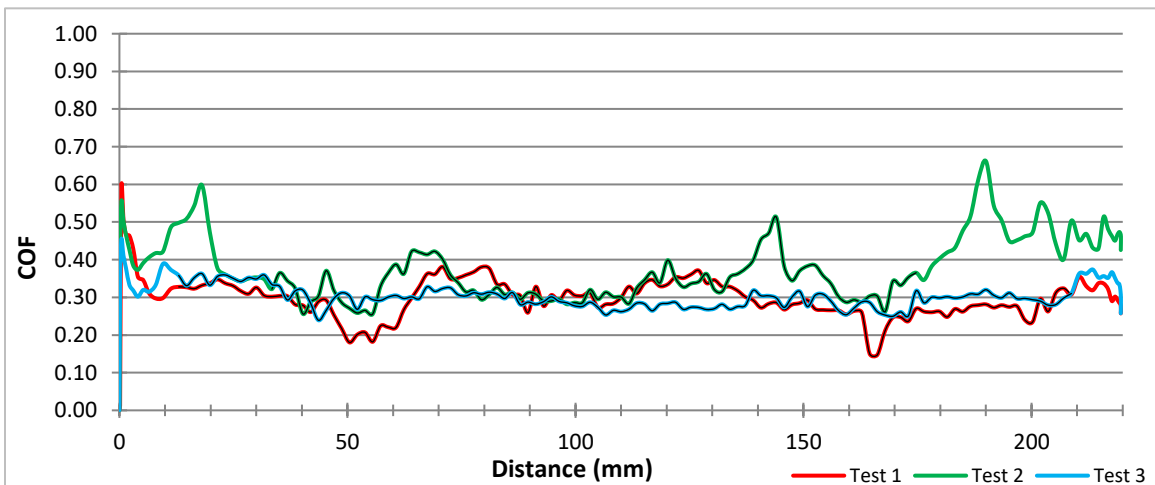


Figure 5.62. Variation of COF with aluminum wire travel length for forming angle testing at 60° with 24 mm radius support roller.

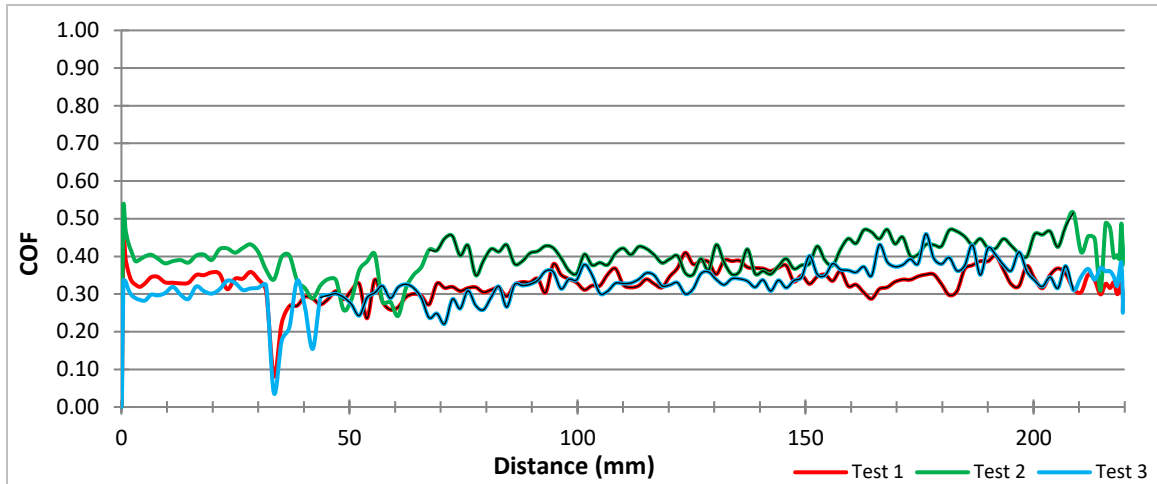


Figure 5.63. Variation of COF with aluminum wire travel length for forming angle testing at 90° with 24 mm radius support roller.

5.3 Wire Bending Simulator Testing Observations

The following section outlines observations made to tested aluminum and copper wire samples as well as the steel counterfaces to explain the COF behavior observed in normal load, travel speed, and forming angle testing results. For COF versus normal load testing, aluminum saw spikes in COF around 22 lbs for the 3 mm radius support roller and 27-32 lbs for the 24 mm radius support roller while copper saw negligible change. During forming angle testing, aluminum also saw opposite behavior to that of copper with an increase in COF as forming angle increased. The following observations seek to explain these behavior differences as well as characterize how aluminum wires behave during die forming operations compared to copper wires.

5.3.1 Thermal Imaging

The potential deformation mechanism change occurring where COF drastically increased and subsequently decreased during COF vs normal load testing of aluminum was thought to be thermally driven. With the large contact area and higher normal loads, it was suspected that local temperature spikes were forming underneath the counterface as COF and normal load increased until it was high enough to change the flow of the insulation, resulting in reducing COF. To test this theory, COF versus normal load testing was performed again for aluminum and copper while being observed with a thermal camera. Aluminum was tested with the 24 mm radius support roller at each region of the COF curves seen in Figure 5.26: 12 lbs where COF was low to start, 27 lbs where COF peaked, 37 lbs where it fell back to pre-spike levels and 42 lbs where it began to rise again. Copper was also tested at both 22 and 42 lbs to measure temperature changes even though influence of normal load on COF was negligible. A FLUKE TiX520 thermal imager was used to capture temperatures experienced at the counterface/wire interface for each test. Results of this testing are shown in Figure 5.64 through Figure 5.67.

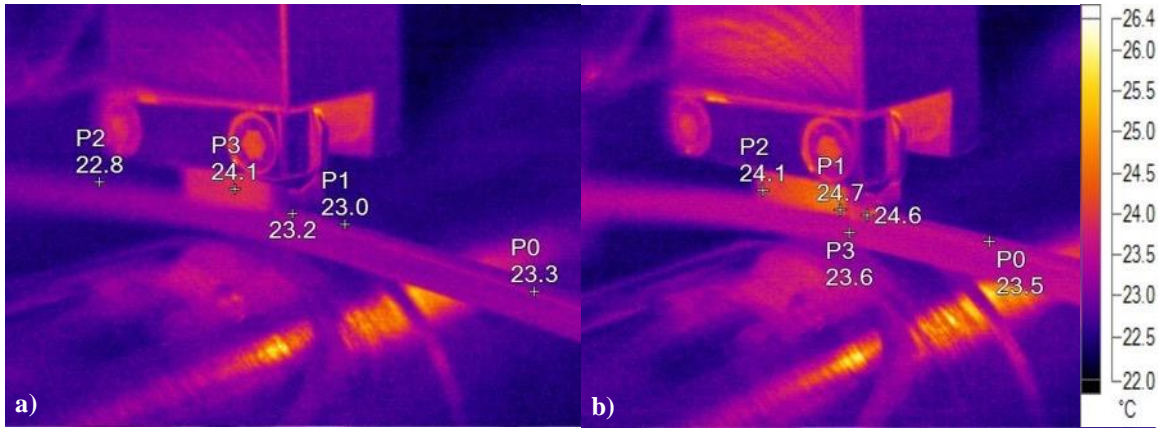


Figure 5.64. Thermal images of aluminum magnet wire tested at 12 lbs normal load. (a) Pre-test reference temperatures. (b) End of test temperatures.

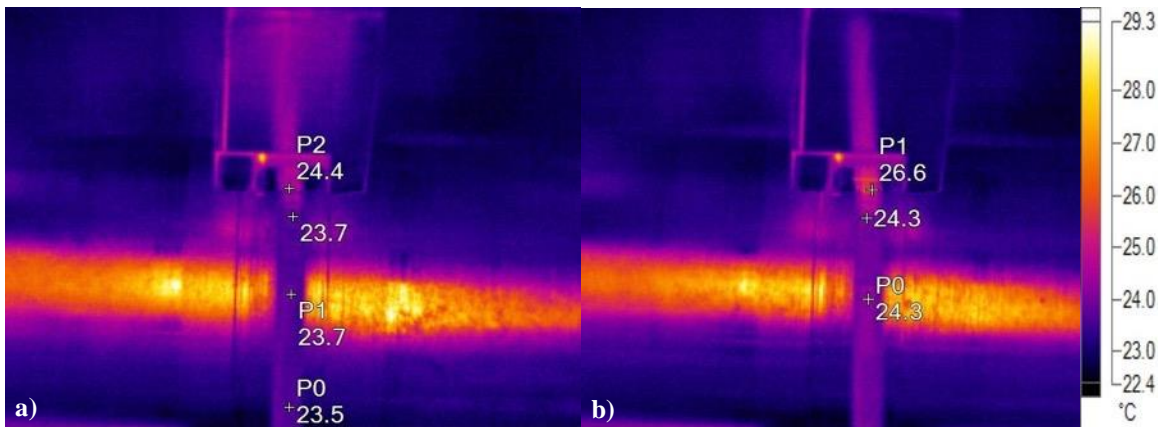


Figure 5.65. Thermal images of aluminum magnet wire tested at 27 lbs normal load. (a) Pre-test reference temperatures. (b) End of test temperatures.

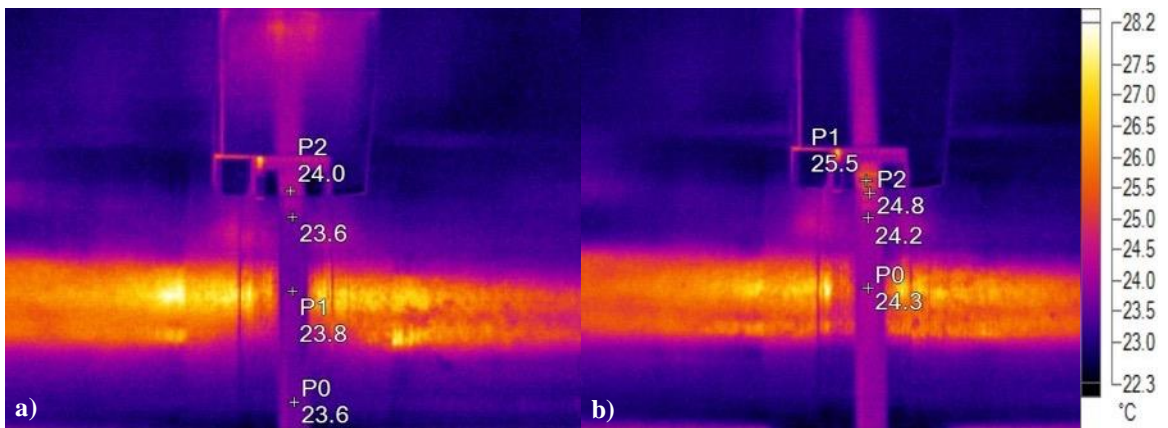


Figure 5.66. Thermal images of aluminum magnet wire tested at 37 lbs normal load. (a) Pre-test reference temperatures. (b) End of test temperatures.

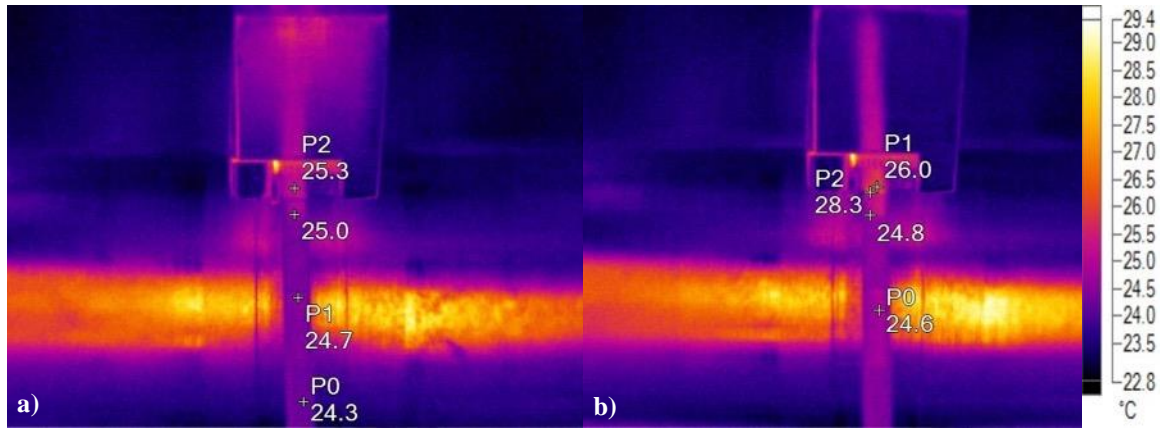


Figure 5.67. Thermal images of copper magnet wire tested at 22 lbs normal load. (a) Pre-test reference temperatures. (b) End of test temperatures.

Looking at the results for aluminum in Figure 5.64 to Figure 5.66, image (a) represents temperatures along the wire surface and the counterface prior to testing while image (b) is the resulting temperature change at test end. The wire is traveling from left to right in Figure 5.64 and top to bottom in Figure 5.65 through Figure 5.67. In general, there was no significant change in temperature to either the wire surface or the counterface at any normal load. The temperature of the counterface rose a maximum of 2°C with the highest temperature change registering at the trailing edge where contact seemed to be concentrated. The temperature of the wire surface rose less than 2°C during testing and very quickly dissipated, returning to pre-testing temperatures.

Comparing the results to copper wire tested in Figure 5.67, the behavior is the same. The only difference lies in the copper wire seems to experience contact only with the edges of the wire which concentrates the pressure in two localized regions. This is evident with the 3.3°C rise in temperature at one of these hot spots on the wire surface immediately after it passes the counterface. These temperature increases took the entire test to manifest and upon test conclusion returned to pre-test levels in a few seconds. Since copper and aluminum behave the same for all normal loads tested, it suggests temperature is not a factor in the spike in COF found with aluminum wires.

5.3.2 Counterface Contact Area Observations

The next area observed to help explain the COF behavior experienced by aluminum was the steel counterfaces contacting the wire during testing. Representative contact for aluminum wire samples tested at 12, 27, and 37 lbs is shown in Figure 5.68 through Figure 5.70. These figures first display total contact area macroscopically using a stereomicroscope. Light reflection in this view helps highlight scratches and smearing transfer on the counterfaces. An optical microscope was then used to get a more detailed view of scratching and transfer taking place in the contact area.

In general, for aluminum wires tested at low normal loads (7-17 lbs) contact was mainly concentrated at the edges of the counterface and consisting of scratching contact like that seen in Figure 5.68. As normal load increased past 17 lbs, contact started shifting more towards the centre of the counterface. Scratching contact was still present but material transfer from the wire surface also became very prevalent. This transfer generally consisted of decreasing size particles as contact progressed and a very fine layer of smearing seen as the blue streaks and burn like marks in Figure 5.69 (a) and (b) respectively. Further increasing the normal load past 32 lbs saw the contact remain towards the centre of the counterface with scratching and large amounts of material transfer but the smearing seen in Figure 5.69 ceased. An example of this contact is seen in Figure 5.70 where the various sized transferred particles are displayed more clearly. The increase in material transfer from the wire as normal load increases helps explain the spike in COF but there is still significant transfer at the highest normal loads where COF reduced to pre-peak values suggesting another deformation mechanism is occurring.

These results were compared to those of the copper wires with representative contact for both 22 and 42 lbs normal load depicted in Figure 5.71. Compared to aluminum, which saw a range of contact types, copper contact and material transfer was extremely consistent at both 22 and 42 lbs. It was noticed in thermal imaging testing that contact for copper was concentrated on the edges of the wire which is confirmed on the counterface with two distinct contact lines. The particles transferred to the counterface were very fine compared to those seen from aluminum and tended to form in dense layers instead. The consistency of contact for copper between both normal loads and support rollers corroborates the negligible change in COF with normal load.

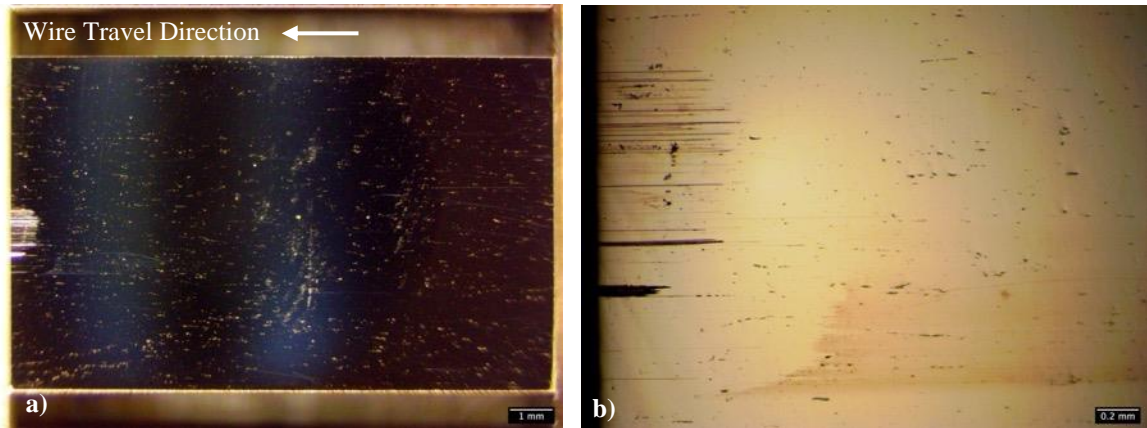


Figure 5.68. Counterface contact from testing aluminum at 12 lbs normal load with 3 mm radius support roller. (a) Macroscopic view of scratch contact at edge of counterface surface. (b) Higher magnification optical microscope image of scratch contact.

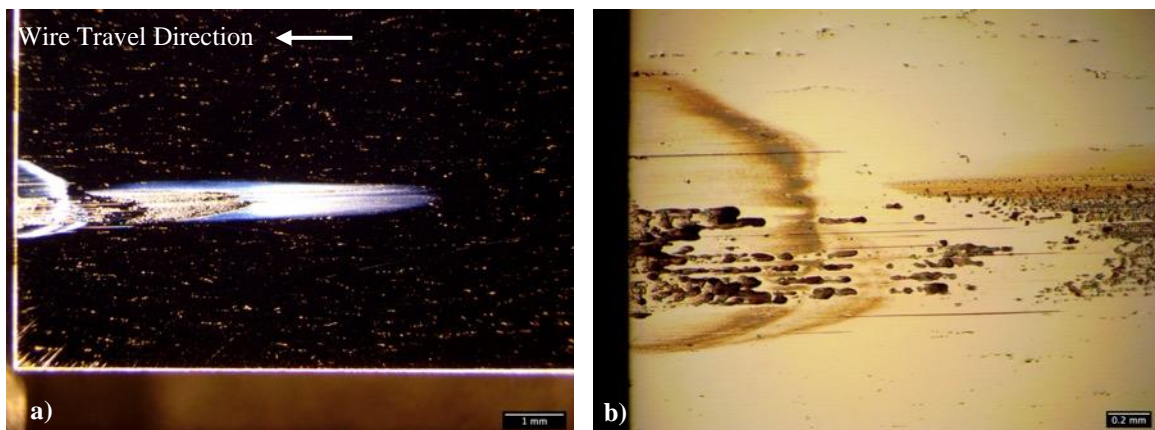


Figure 5.69. Counterface contact from testing aluminum at 27 lbs normal load with 24 mm radius support roller. (a) Macroscopic view of scratch contact and large amount of material transfer and smearing on counterface surface. (b) Higher magnification optical microscope image showing decreasing size particle transfer and smearing over scratching.

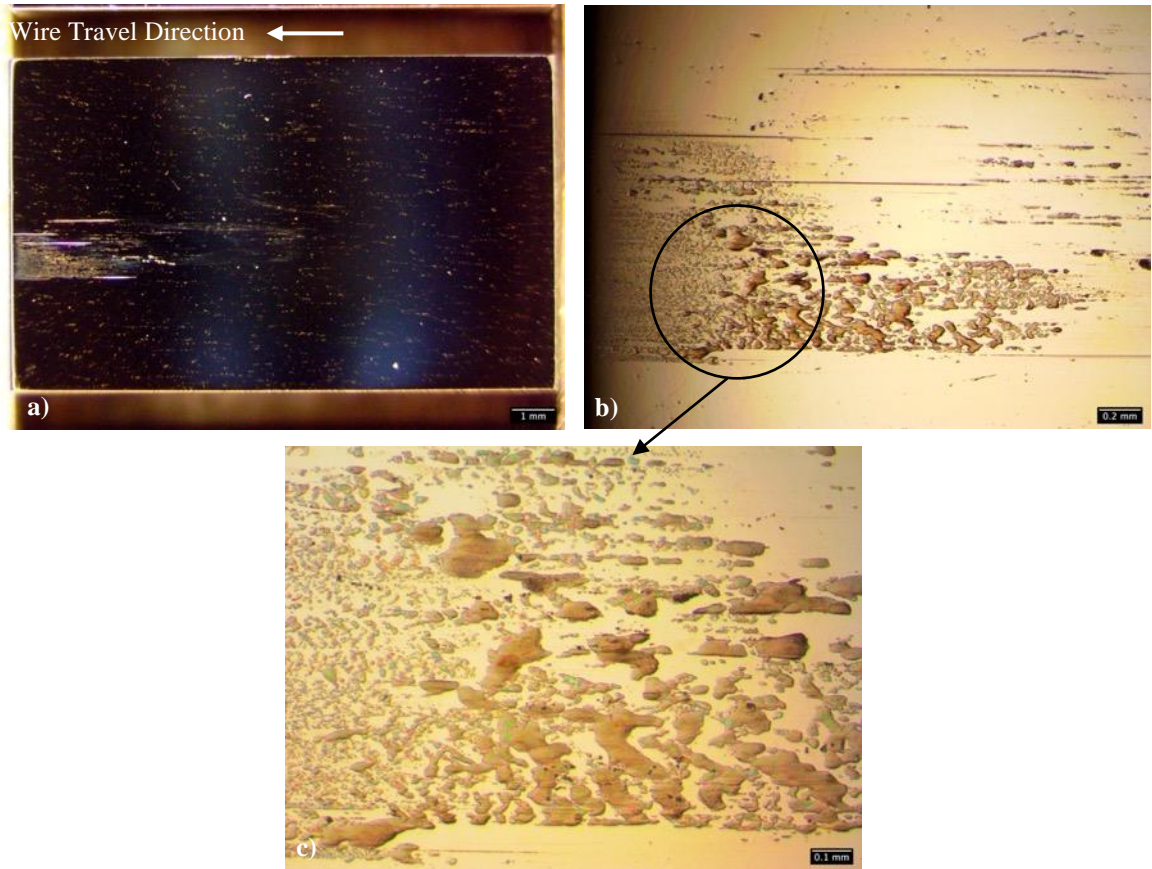


Figure 5.70. Counterface contact from testing aluminum at 37 lbs normal load with 3 mm radius support roller. (a) Macroscopic view of scratch contact and large amount of material transfer on counterface surface. (b) Higher magnification optical microscope image showing small particle transfer at counterface edge followed by larger particles over scratching. (c) Higher magnification optical microscope image of highlighted region showing small and large particle transfer on counterface surface.

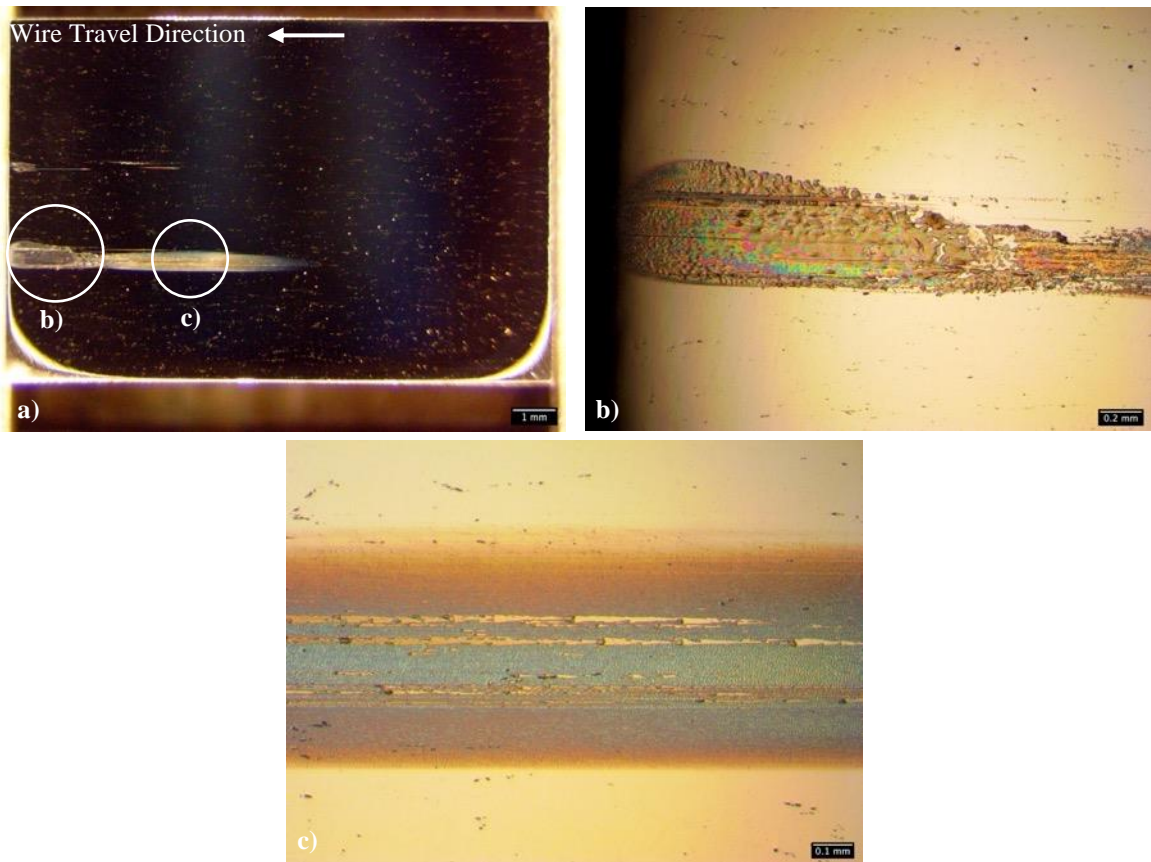


Figure 5.71. Counterface contact from testing copper at 42 lbs normal load with 3 mm radius support roller. (a) Macroscopic view of dual contact regions with light scratching and dense material transfer and smearing on counterface surface. (b) Higher magnification optical microscope image of larger particle transfer over light scratching at edge of counterface. (c) Higher magnification optical microscope image of very fine, dense, and layered material transfer making up most of the contact path.

5.3.2.1 Aluminum vs Copper Contact Transfer

It was noticed that the transfer mechanisms differ between aluminum and copper in the previous section. This was explored further by examining two counterfaces under SEM, one tested with aluminum and the other with copper. EDS analysis was also performed to confirm the observed particle and smearing transfer came from the wire insulation. The counterface used to represent aluminum contact was tested at 27 lbs normal load, showing scratching, particles and smearing transfer as seen on the left in Figure 5.72. The counterface on the right in the same figure is contact from copper wire tested at 42 lbs normal load showing the distinctive twin contact lines from edge contact with dense and layered material transfer.

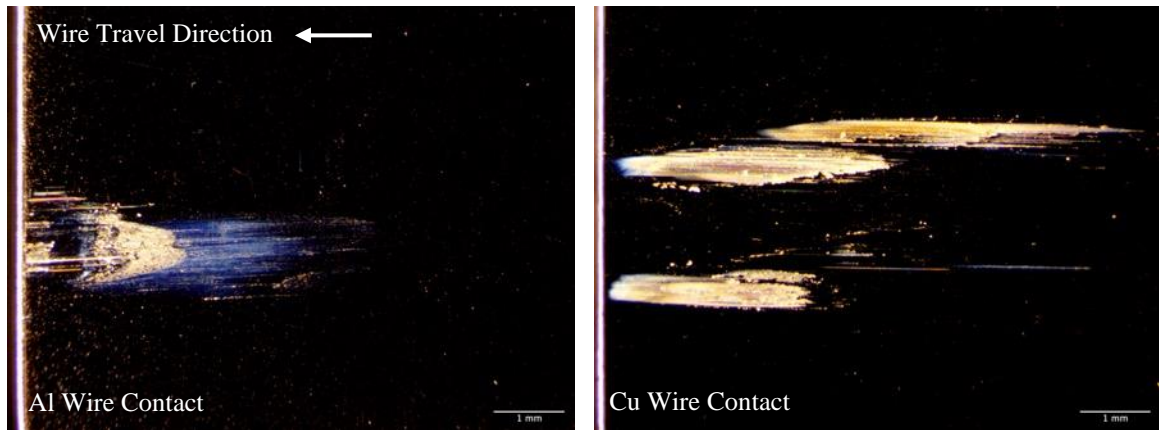


Figure 5.72. Counterfaces used to evaluate differing transfer mechanisms between aluminum wire (left) and copper wire (right). (left) Aluminum wire contact region from 27 lbs normal load on counterface consisting of scratching, material transfer, and smearing. (right) Copper wire contact region from 42 lbs normal load on counterface consisting of two contact regions from edges of the wire with light scratching and dense material transfer.

SEM images of both contact surfaces in Figure 5.73 further highlight the difference in material transfer between aluminum and copper wires. Aluminum generally transfers individual particles in decreasing size from contact start at the top of the figure where particles are quite large to contact end where a very fine film is deposited on the counterface. Copper on the other hand, clearly deposits a range of particle sizes in layers along the whole contact area. The base layer appears to be a fine film deposited in a wave like pattern where the underlying counterface can be seen. More layers appear to build on

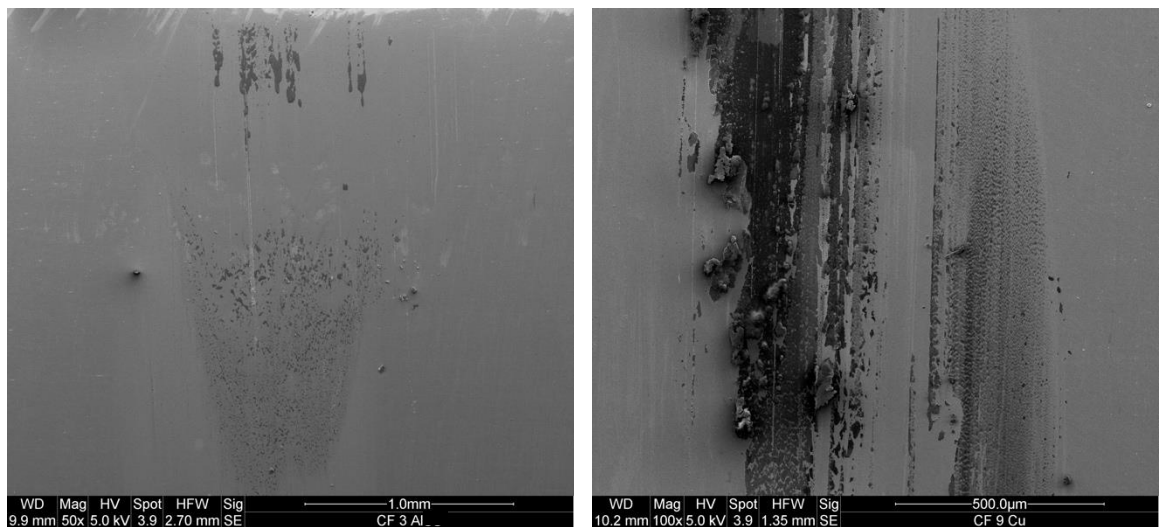


Figure 5.73. Secondary electron SEM images of aluminum (left) and copper (right) contact regions depicted in Figure 5.72. (left) Aluminum wire contact sees prominent scratching and decreasing size particle transfer from counterface edge (top) to middle. (right) Copper wire contact on counterface sees layered material transfer with larger particles on top of a dense film of fine particles.

top of this base layer, creating areas of much thicker and darker deposits. Larger particles adhere on top of these layers or as distinct particles. This is better illustrated in Figure 5.74 where the iron map shows thick layers as dark spots where iron is not registered and thinner layers where varying levels of iron are seen through the material transfer. This is opposed to aluminum transfer seen in more detail in Figure 5.75. Secondary electron and backscattered electron images show material transfer to be distinct particles which is corroborated by iron and carbon maps.

The BSE images in both figures illustrate the transferred particles are of different composition to the counterface while the carbon maps match them perfectly. This confirms the transfer to be electrical insulation of both conductors.

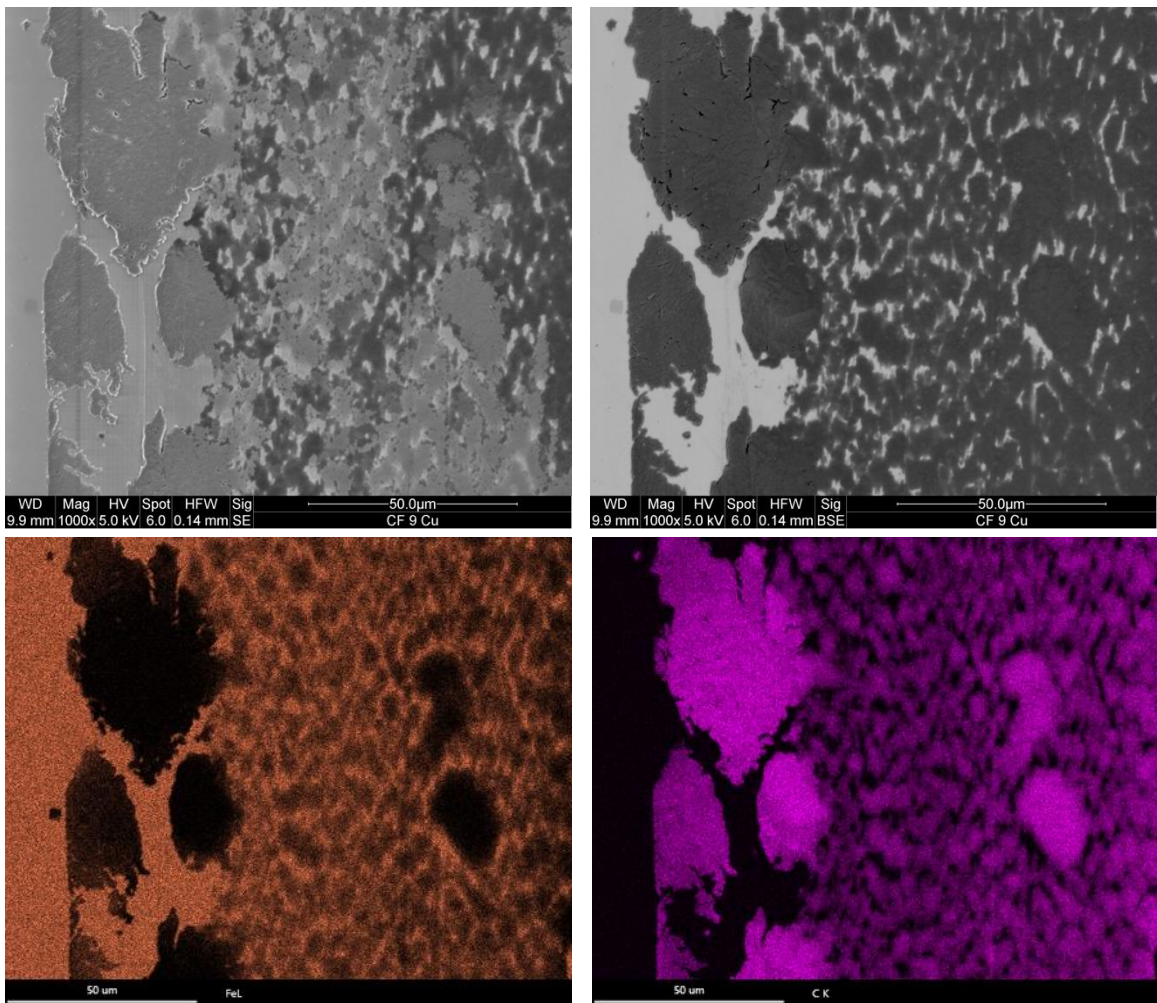


Figure 5.74. Secondary electron and backscattered electron SEM images of copper wire contact region on counterface with associated iron and carbon EDS maps for elemental analysis. SE image along with the iron map reveal varying levels of material transfer thickness while the carbon map indicates material transfer is copper wire electrical insulation.

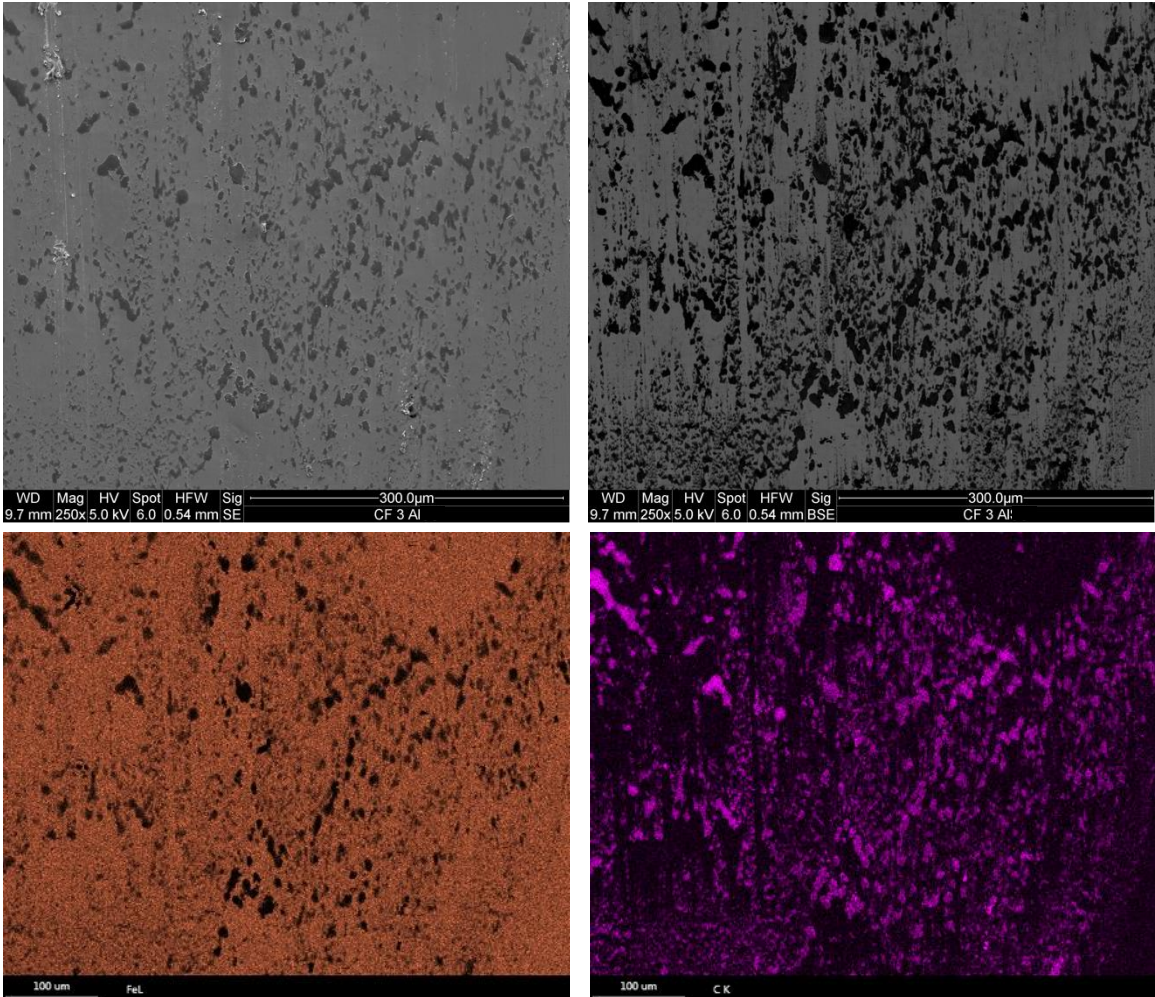


Figure 5.75. Secondary electron and backscattered electron SEM images of aluminum wire contact region on counterface with associated iron and carbon EDS maps for elemental analysis. Images reveal distinct particle transfer rather than layering as seen with copper transfer while iron and carbon maps indicate transfer is aluminum wire electrical insulation.

5.3.3 Wire Contact Surface Observations

Moving away from the counterface contact area, the damage inflicted on both aluminum and copper wire samples during testing was also analyzed. The top and bottom surfaces of aluminum samples were observed from testing at 12, 27, and 37 lbs for both 3 mm and 24 mm support rollers. The same was done for copper samples at both normal loads of 22 and 42 lbs and both support rollers. Both conductor insulations being semi-transparent meant imaging damage caused from testing was challenging. Using light reflections off the insulation surface with a stereo microscope proved to be the best method

to capture the deformation. A Keyence laser microscope was also used for greater detail and topography of surface features.

Aluminum wire contact surfaces are shown in Figure 5.76 to Figure 5.78. The top surface was in contact with the polished steel counterface while the bottom was contacting either the smooth 3 mm radius support roller or machined finish 24 mm radius support roller. Looking at the top surface first, the light reflections show the counterface ironed the insulation smooth. The images shown are of the very end of the contact region where the counterface left a small bump/step marking the transition between depressed and ironed smooth insulation and fresh wire. Across all normal loads, and illustrated with 12, 27, and 37 lbs, the severity of ironing did not appear to change. Since COF peaked around 22 lbs for the 3 mm roller and 27-32 lbs for the 24 mm roller it would be expected to see more severe contact damage at these loads, but this was not the case.

Looking at the bottom surfaces, there was significant difference in contact between support rollers. The smooth 3 mm support roller ironed the enamel just like the steel counterface but in a wavy pattern due to rolling contact. The 24 mm support roller was left with a machined surface containing very fine machine lines. These lines penetrated the surface of the insulation leaving gouge marks instead of ironing it smooth. Again though, severity of this contact did not appear to change with increasing normal load.

Comparing these results to those for copper shows very similar behavior. However, like mentioned before, contact on the copper wire was concentrated on the edges which is evident in Figure 5.79. Ironing on the top surface of the wire for most samples tested was extremely faint and did not change between 22 and 42 lbs. The figure only shows one obvious strip of ironed insulation where counterfaces clearly show two contact points. Most wires seemed to focus most contact on one edge with the other providing faint contact which explains the single visible ironed region on the wire surfaces. A small bump/step was left at the end of the test just like seen with aluminum wire however it was less prominent due to the much smaller contact region. Contact on the bottom of the wire was identical to that of aluminum but again, less severe since contact was concentrated on the edges only.

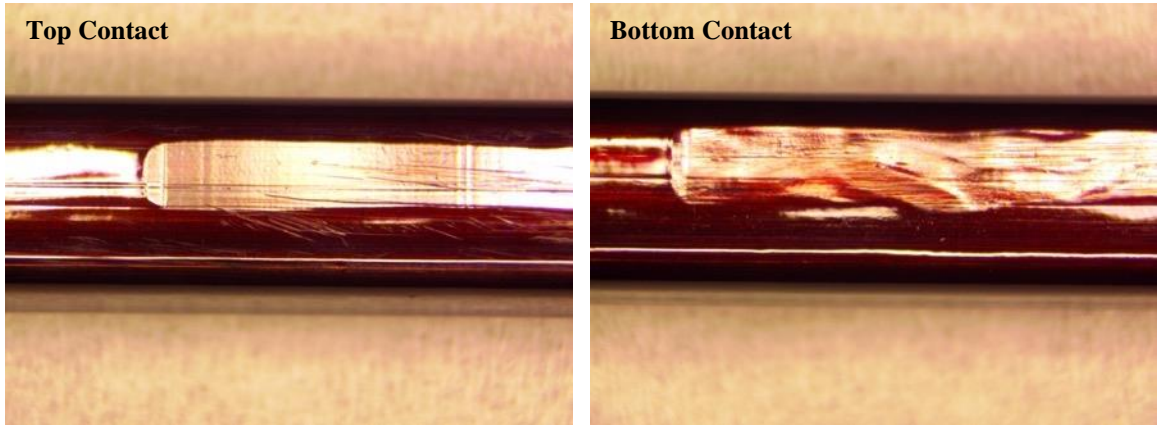


Figure 5.76. Top and bottom surface contact for aluminum magnet wire tested at 12 lbs normal load with 3 mm radius support roller.

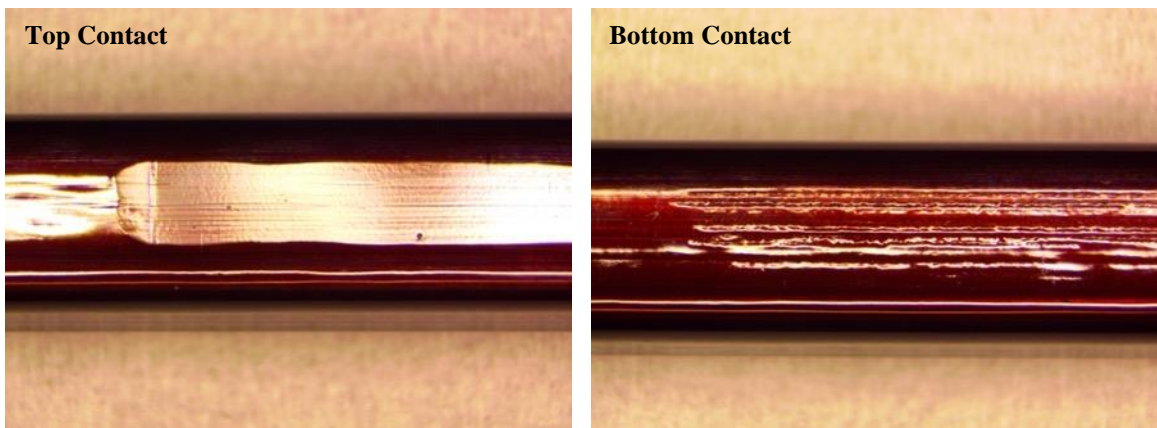


Figure 5.77. Top and bottom surface contact for aluminum wire tested at 27 lbs normal load with 24 mm radius support roller.

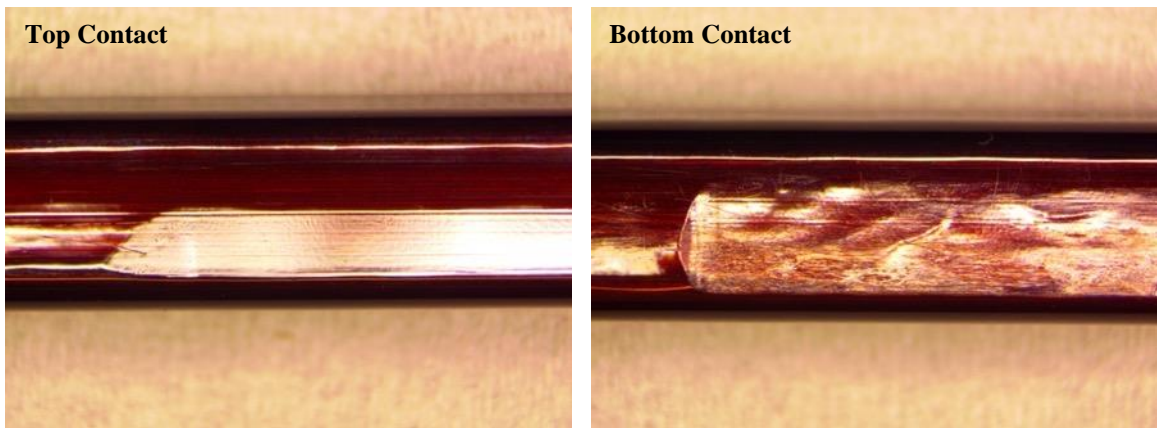


Figure 5.78. Top and bottom surface contact for aluminum wire tested at 37 lbs normal load with 3 mm radius support roller.

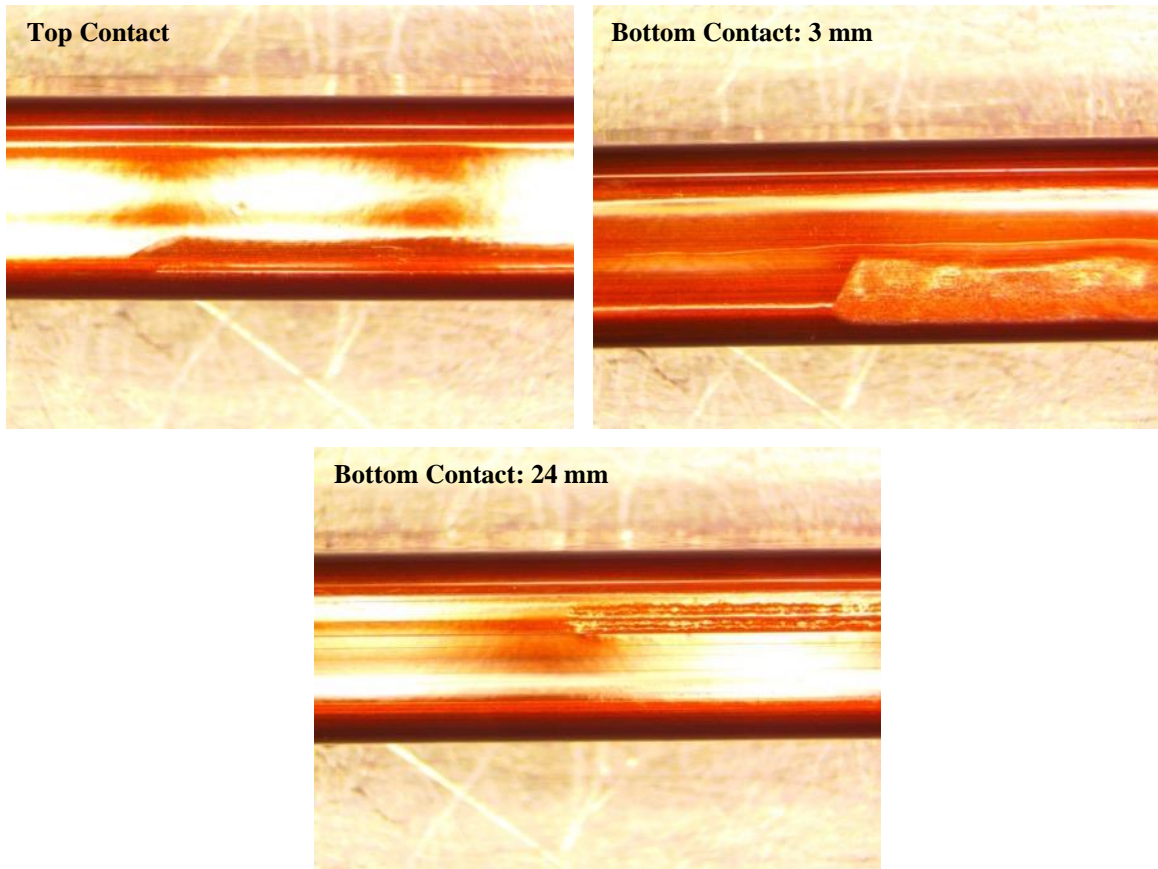


Figure 5.79. Representative top and bottom surface contact for copper wire tested at both 22 and 42 lbs with both support rollers.

Contact on the bottom of both aluminum and copper wires was the same with the 3 mm roller ironing the insulation while the 24 mm roller left gouge marks. Figure 5.80 explores this damage in greater detail. Wavy ironing caused by the 3 mm radius support roller is seen in (a) with the Keyence laser microscope image revealing light scratching not seen with the stereomicroscope. The 3 mm radius roller was sanded smooth but not polished so these scratch lines may be the imprint of the very finely sanded surface of the roller suggesting even seemingly smooth surfaces can lightly gouge the insulation, increasing sustained damage. Overall damage from the 3 mm radius support roller was minimal. The gouge marks created by the 24 mm radius support roller are shown in (b) and (c) where microcracking visible in the Keyence laser microscope image surrounds the gouge lines. Sustained damage appears the same for both aluminum and copper wires although aluminum experienced larger contact areas than copper.

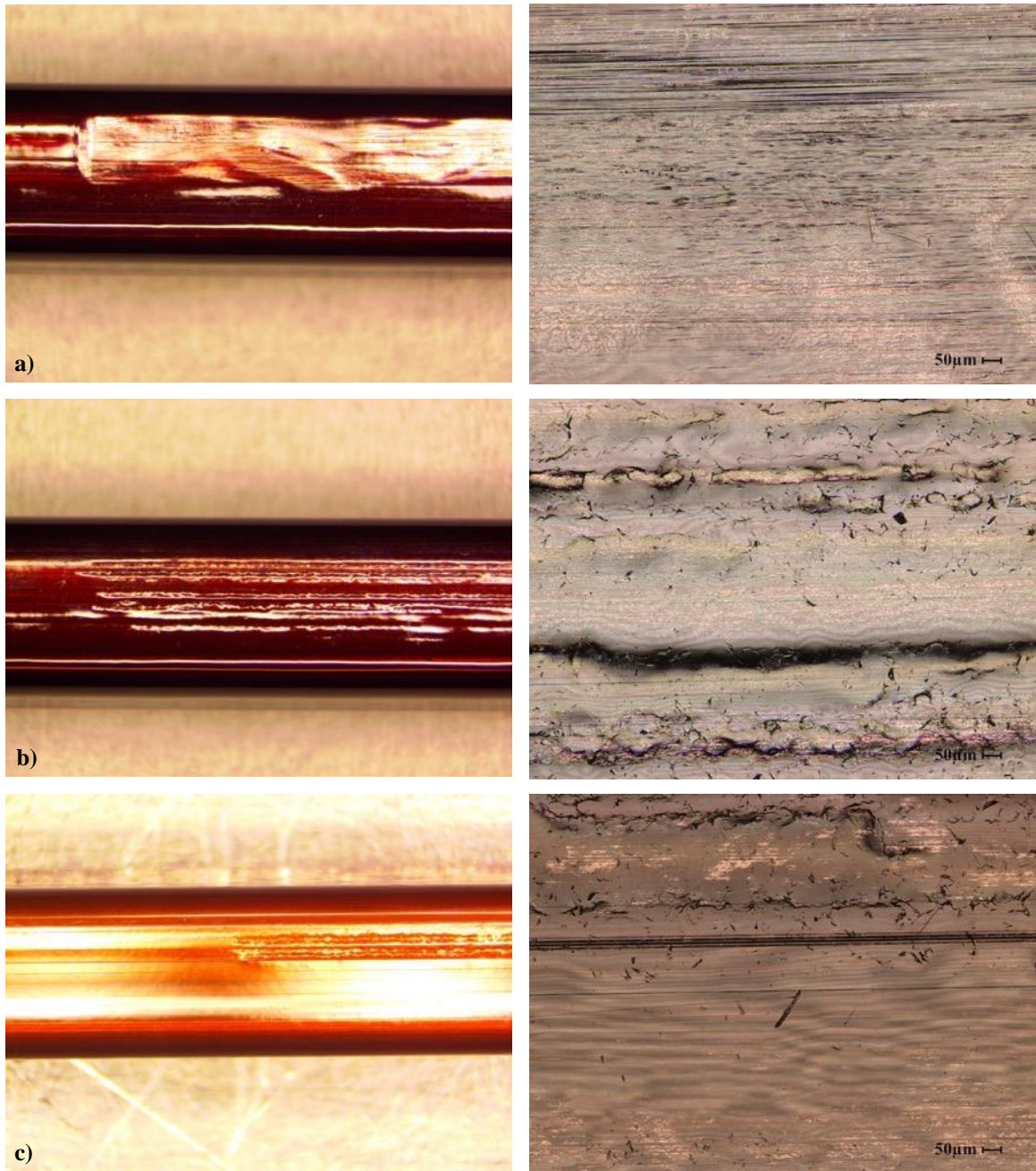


Figure 5.80. Macroscopic image (left) and Keyence laser microscope image (right) of damaged inflicted to aluminum and copper wire surface from smooth 3 mm radius support roller and 24 mm radius support roller with machined surface. (a) Aluminum against 3 mm radius support roller which causes ironing and light scratching. (b-c) Aluminum and copper against 24 mm radius support roller which caused gauging and associated cracking around gauge lines.

5.3.3.1 End of Test Bump Analysis

The ironed regions on the top surface of wires shown in the last section were at the very end of the testing length. Where the counterface stopped, a small bump/step was left behind, marking the transition between ironed smooth insulation and fresh wire. Figure 5.81 gives a better view of this bump using a Keyence laser microscope to analyze its topography. The sample shown was tested at 12 lbs normal load but is representative of behavior for both aluminum and copper wires at all normal loads. The topography map confirms the step is a change in insulation height rather than an artifact of light reflection from macroscopic observation. A line scan was performed across the middle of the step to get a better view of the change in height from the ironed region to fresh wire. The thickness of the ironed region measured around 47 μm while the peak was about 60 μm marking an increase of 13 μm . The thickness of the fresh region in the line scan shown measured about 50 μm . This suggests the ironed region was compressed about 3 μm during testing and ductile ploughing described in Section 3.2.1 occurred, creating the rising step at the end of the test.

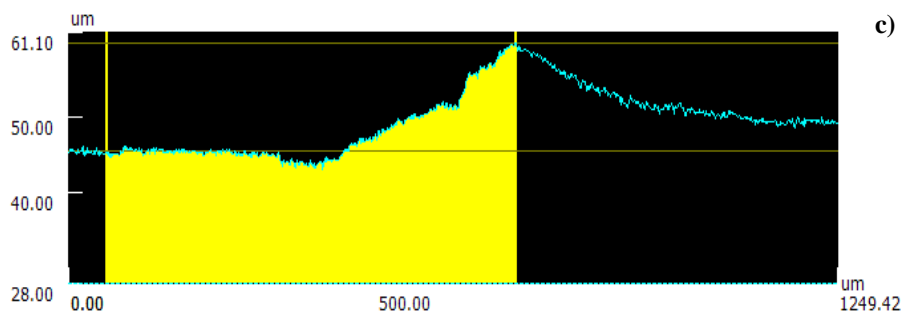
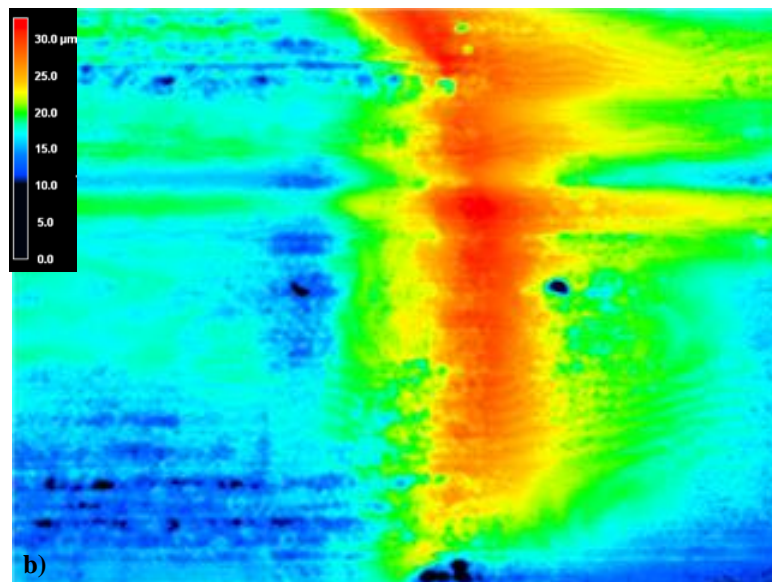
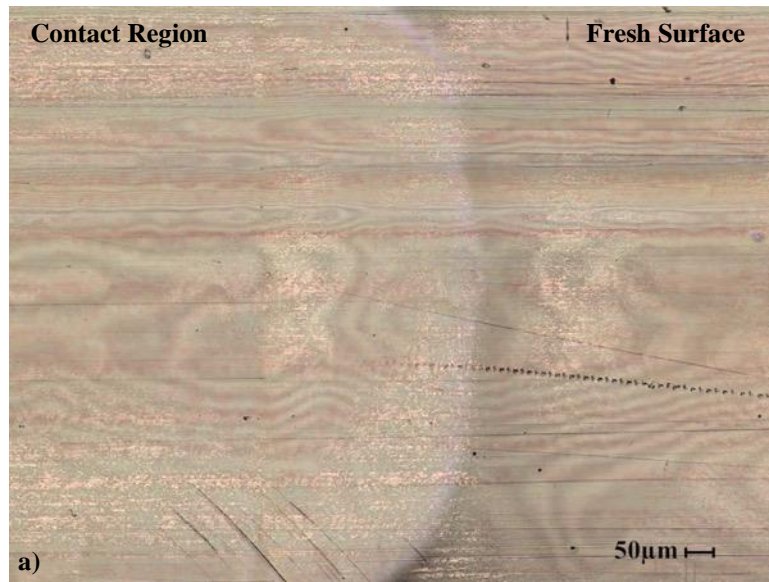


Figure 5.81. Aluminum wire top contact end of test transition between depressed and ironed insulation and fresh wire surface tested at 12 lbs normal load. (a) Keyence laser microscope image of transition zone. (b) Topography map highlighting raised region at bump peak. (c) End of test bump profile from line scan across transition zone.

5.4 Aluminum and Copper Cross-Sectional Analysis

Macroscopic observation of the counterface and wire contact surfaces did not explain the COF vs normal load behaviour observed for aluminum wires in Figure 5.26. Therefore, microscopic observations using SEM and EDS was performed on cut, mounted, and polished tested wire samples according to the procedure in Section 4.5.1. An example of this mounting is seen in Figure 5.82. The edgewise cross section allows for viewing around the whole perimeter of the wire at a given slice of the contact path. The lengthwise cross section gives a better view of the evolution of contact along a portion of the contact path. Combining these views gives a 3D representation of what is happening at the conductor/insulation interface. Aluminum samples tested at 12, 27 and 37 lbs along with copper samples tested at 22 and 42 lbs for both 3 mm and 24 mm support rollers were mounted and observed. The observations made from these samples were compared against mounted samples of fresh aluminum and copper. The following sections outline the results of these observations.

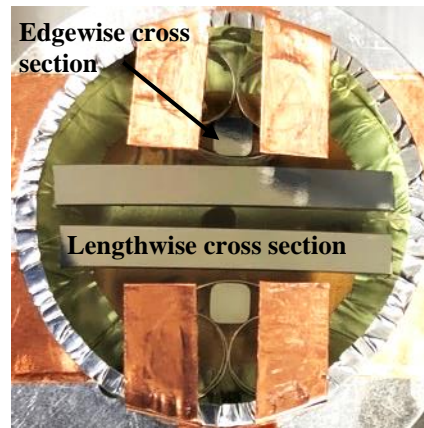


Figure 5.82. Mounted wire samples with both edgewise and lengthwise cross-sections for SEM analysis.

5.4.1 Fresh Aluminum and Copper Surface Features

Firstly, fresh aluminum and copper samples were analyzed to get a base line of surface features present at the conductor/insulation interface. Looking at aluminum in Figure 5.83, the light-coloured section is aluminum, with the insulation layer above it and the slightly darker mounting material above that. The area of interest is the boundary between the aluminum wire and insulation. Images (a-b), length wise and edgewise cross

section views illustrate complete penetration of insulation into crevices and voids between and around aluminum shingles suggesting good bonding with the aluminum conductor. This is important since the aluminum surface layer in (c) is populated with numerous shingles creating a non-uniform surface for bonding of insulation to aluminum conductor. Higher magnification BSE image (d) reveals a dark layer between shingles and bulk aluminum suggesting different elemental composition which could be a very thin layer of insulation.

To verify what was occurring at the shingle/aluminum boundary, EDS analysis was performed with the results presented in Figure 5.84. The aluminum mapping shows a very thin layer of reduced counts at the interface, but the carbon map shows no counts in the same spot. The phase map also shows a different phase where the dark line is. However, the oxygen mapping lines up well with this area suggesting the features are not cracks or a thin insulation layer but a layer of aluminum oxide between the shingles and bulk aluminum. It was discussed in Section 3.3 that cold and hot rolled aluminum sees delaminated surface material and delaminated flakes of the near-surface deformed layer which oxidize and get pressed back into the aluminum surface. This results in layers of aluminum oxide below the conductor surface explaining the observations made in Figure 5.83 and Figure 5.84.

The fresh copper surface seen in Figure 5.85 is much different than that of aluminum. The images shown represent surface features present on both the lengthwise and edgewise cross-sections. In general, the copper/insulation interface is very smooth and featureless with few defects. When flaws were found, they were usually small bumps or craters a few microns in height and width which were filled completely with insulation. Overall, the copper surface quality appeared far better than that of aluminum.

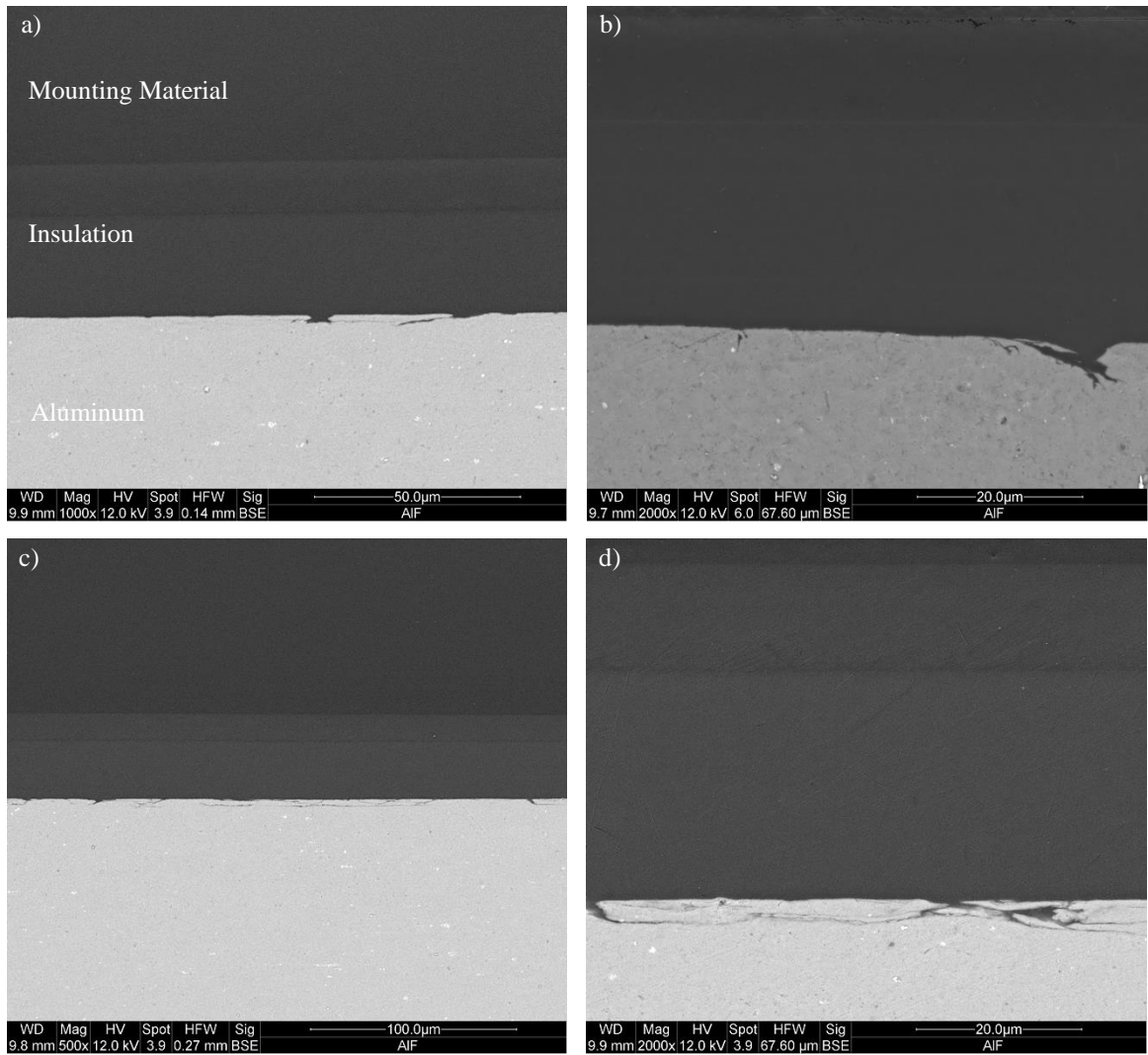


Figure 5.83. Backscattered electron SEM images of fresh insulated aluminum wire cross section. (a) Lengthwise and (b) edgewise cross section view showing complete insulation penetration into voids between and around aluminum shingles. (c) Numerous shingles a few microns in thickness populating the aluminum wire surface. (d) Darker lines between shingles and bulk aluminum suggesting different elemental composition or cracks.

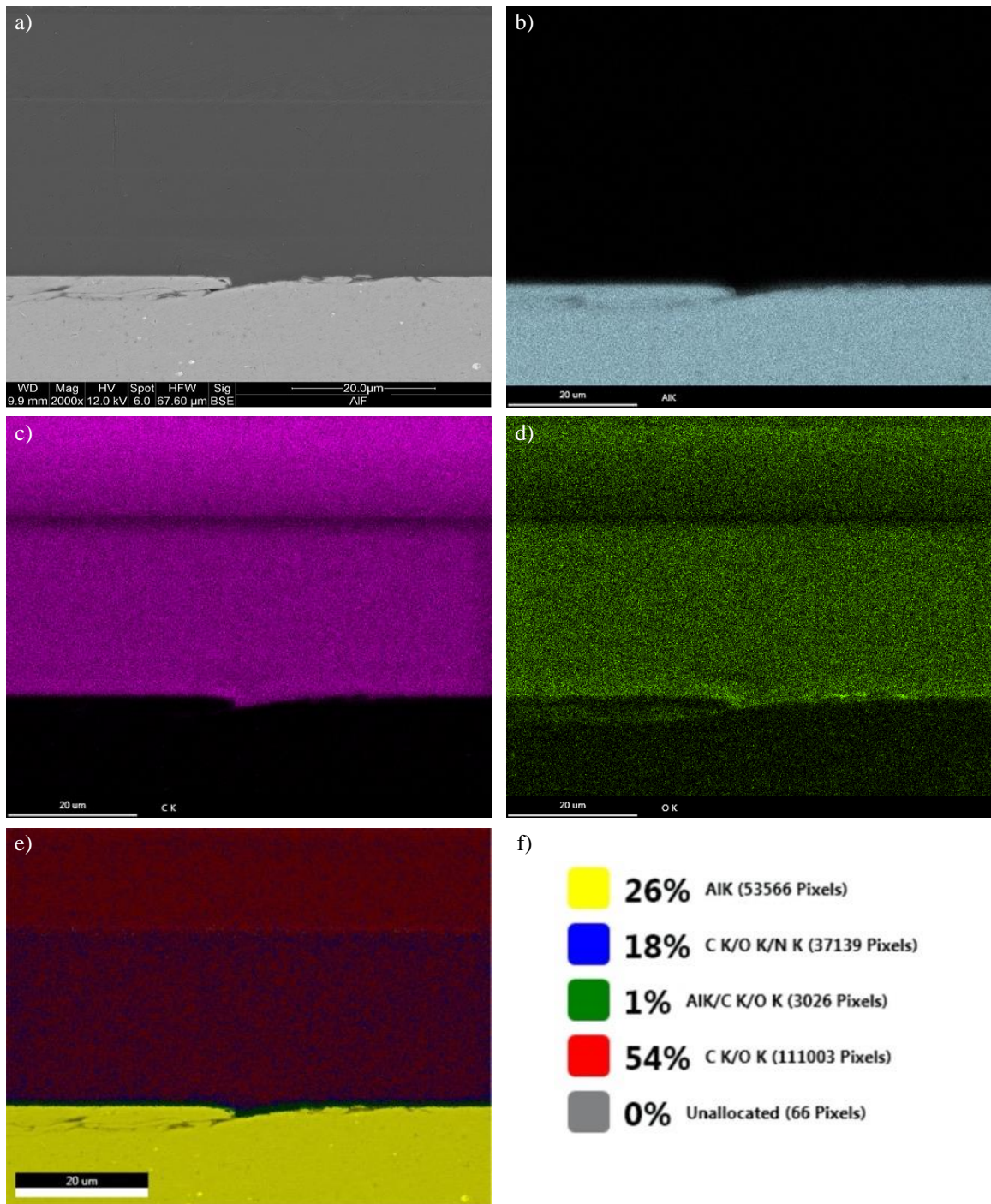


Figure 5.84. Backscattered electron SEM image of aluminum shingle and dark area at shingle/bulk aluminum boundary used for EDS mapping. Distribution of (b) aluminum, (c) carbon, (d) oxygen, with phase map (e) and phase composition (f). Oxygen map suggests shingle/bulk aluminum boundary contains oxides as no presence of elements composing electrical insulation were detected.

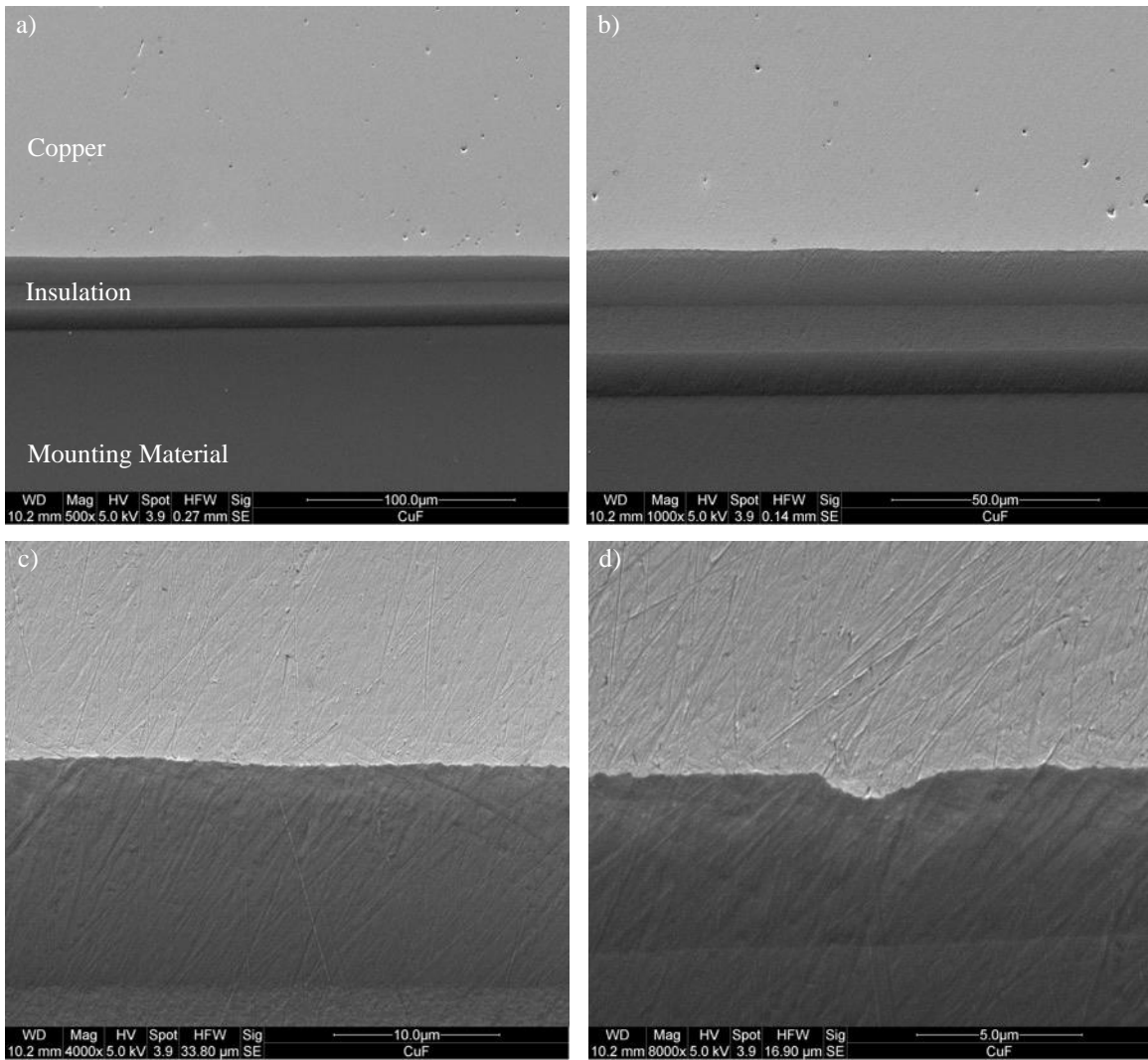


Figure 5.85. Secondary electron images of fresh insulated copper wire cross section. (a-c) Generally featureless, very smooth, and high-quality copper surface. (d) Example of surface defect consisting of bumps or crates a few microns in height and width.

5.4.2 Tested Wire Cross Section Observation

Both the edgewise and lengthwise cross-sections for tested aluminum and copper wires were observed with SEM and EDS. Results of these observations for aluminum wires are found in Figure 5.86 to Figure 5.91 and for copper wires in Figure 5.92. Samples tested at 12 lbs normal load saw no noticeable changes to the aluminum/insulation interface compared to the fresh aluminum sample. This was expected since the COF was at its lowest point for this load. Moving to the sample tested at 27 lbs, features at the aluminum/insulation boundary started to change as can be seen in Figure 5.86. Image (a) shows the edgewise view of a shingle with apparent crack propagation from the base of the shingle deeper into the aluminum surface. Looking at the lengthwise cross section images (b-d), sub-surface cracks appear to be forming. The BSE image (d) shows the crack is of different elemental composition than aluminum suggesting insulation may be present. Without obvious shingles present at the crack locations, a near-surface deformed layer as discussed in Section 3.3 may be present and acting as a favourable location for sub-surface crack initiation and propagation.

The aluminum sample tested at 37 lbs normal load was observed next with edgewise cross section surface features found in Figure 5.87. Observations of the edgewise cross section are found in Figure 5.87. Images (a-f) show crack propagation and associated insulation penetration around aluminum shingles. In the case of (c-d) the shingle appears separated from the bulk aluminum surface by a layer of insulation material. Images (e-f) highlight crack initiation and propagation deeper into the bulk aluminum surface underneath the shingle as well as lateral propagation, separating more surface material from the bulk conductor. A crater defect in the aluminum surface (g-h) also acts as a crack initiation site seeing propagation deeper into the surface. Compared to the aluminum samples tested at 27 lbs normal load, crack propagation is much more apparent and severe.

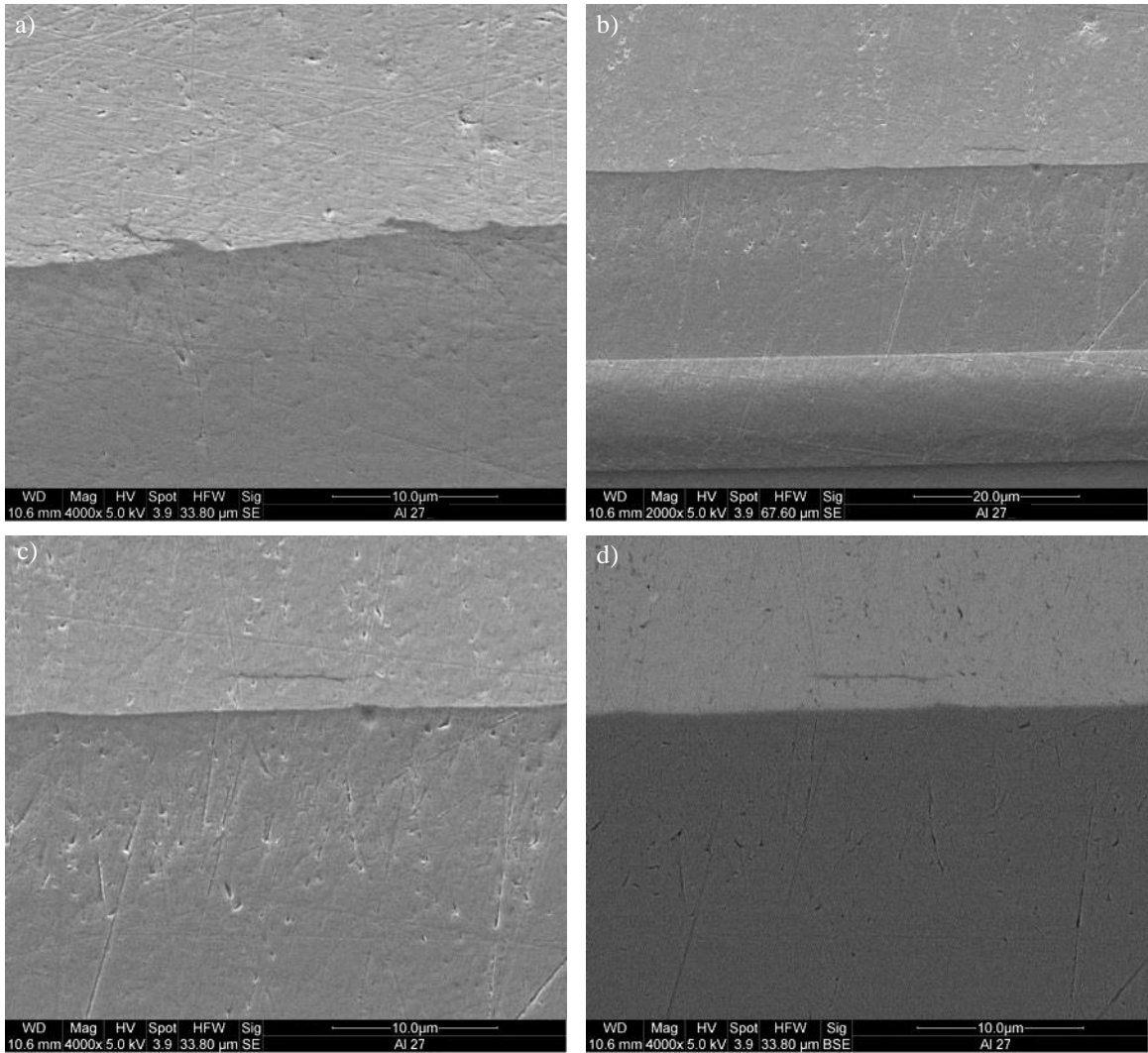
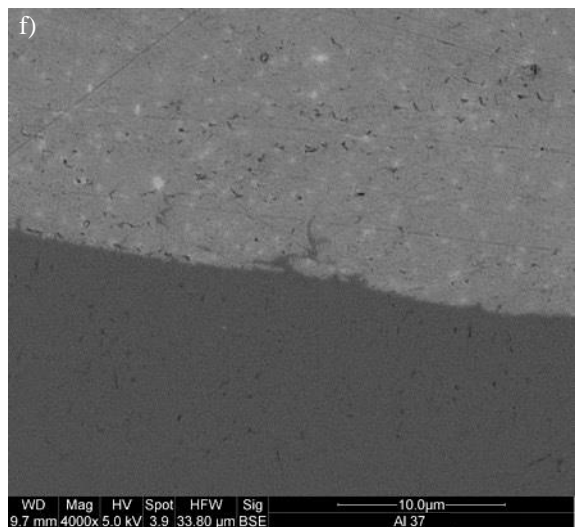
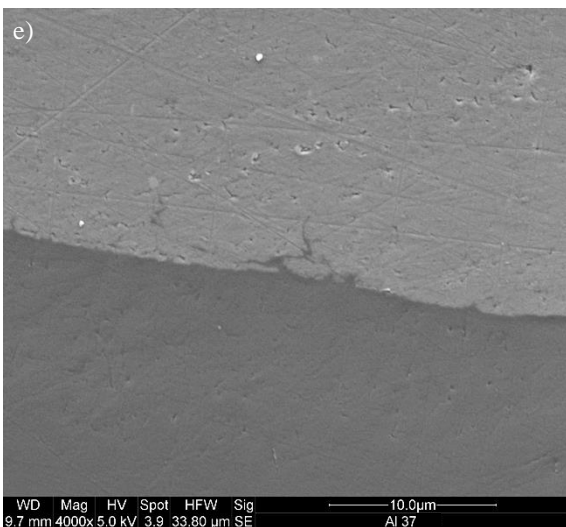
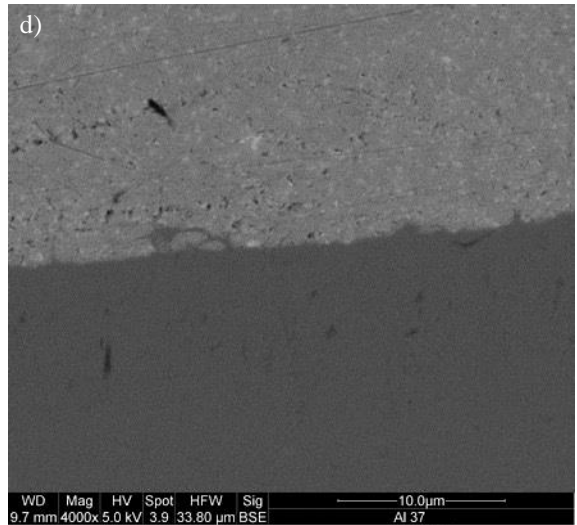
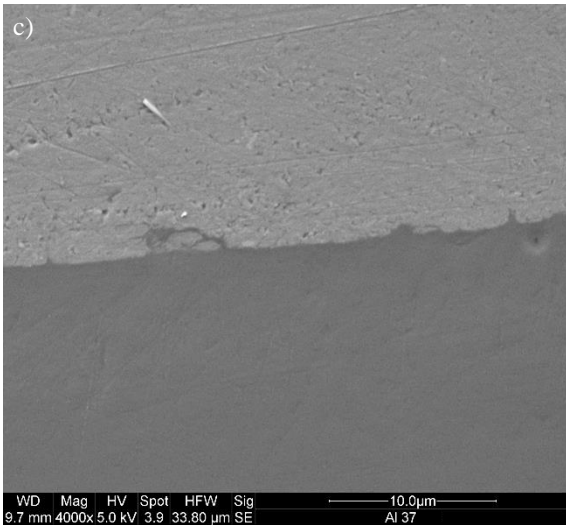
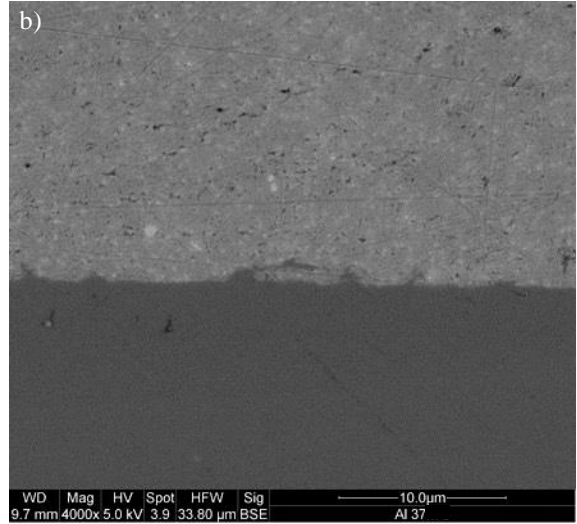
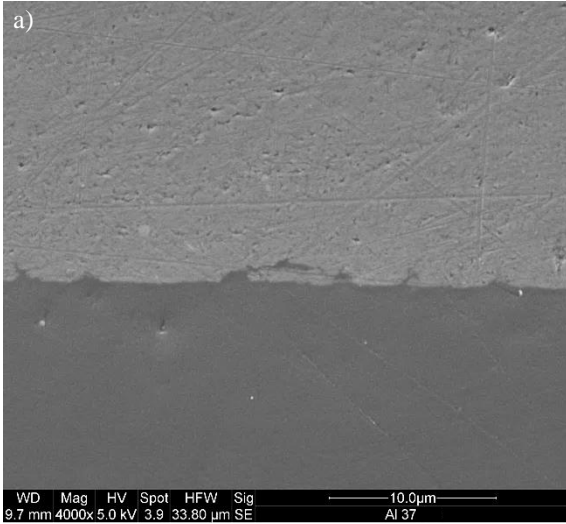


Figure 5.86. Surface features of aluminum sample tested at 27 lbs normal load. (a) Edgewise cross section showing deeper penetration of insulation into aluminum surface than seen on the fresh sample. (b) Lengthwise cross section highlighting formation of subsurface cracks from testing. (c) Higher magnification secondary electron SEM image of subsurface crack with backscattered electron SEM image (d) showing different elemental composition inside crack.



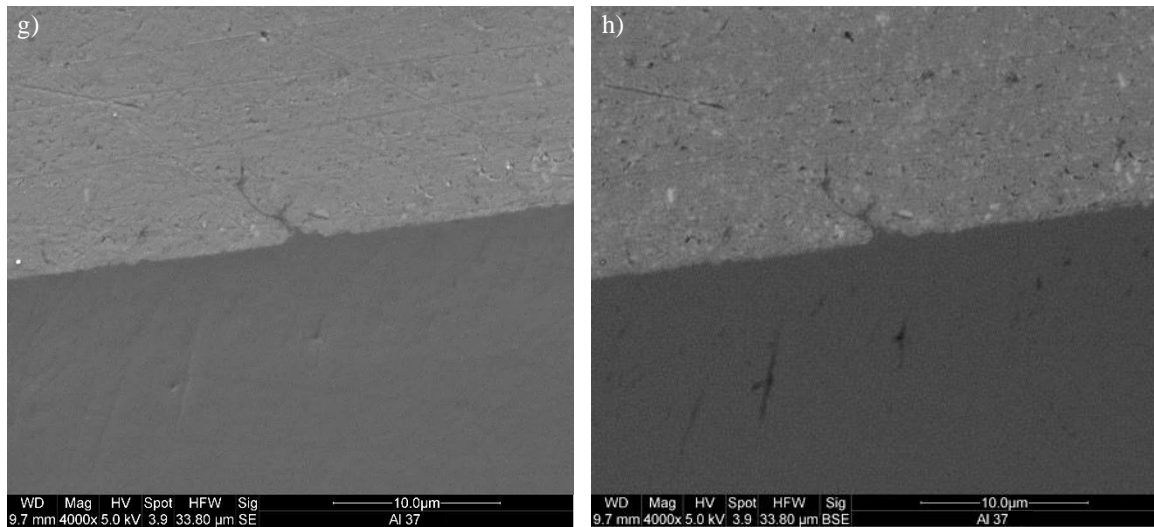


Figure 5.87. Secondary electron and associated backscattered electron SEM images of edgewise aluminum wire cross section tested at 37 lbs normal load. (a-f) Shows crack propagation around shingles, detaching or nearly detaching them from the bulk aluminum. (e-h) Show crack propagation deeper into the bulk aluminum surface than that seen for testing at 27 lbs normal load.

The lengthwise cross section surface features of aluminum sample tested at 37 lbs normal load are shown in Figure 5.88. It is more apparent in this figure that cracks are propagating into the previously coherent shingle/aluminum boundary causing separation from the bulk conductor by a layer of what is suspected to be insulation material. Images (a-d) also highlight lateral crack propagation from aluminum shingles along the surface causing further separation of the surface layer from the bulk aluminum. This behaviour is better illustrated in Figure 5.89 and Figure 5.90. A long subsurface crack is highlighted in Figure 5.89. The BSE image shows different elemental composition at the crack line and in large deposits along it, further suggesting it is filled with insulation material. A higher magnification image of subsurface cracking is show in Figure 5.90 where it also appears cracks are initiating in the absence of shingles and filling with insulation material. This means that most of the aluminum surface is susceptible to crack initiation and growth at the near-surface layer/bulk aluminum interface which would result in separation of the whole near-surface layer from the bulk conductor rather than just aluminum shingle defects.

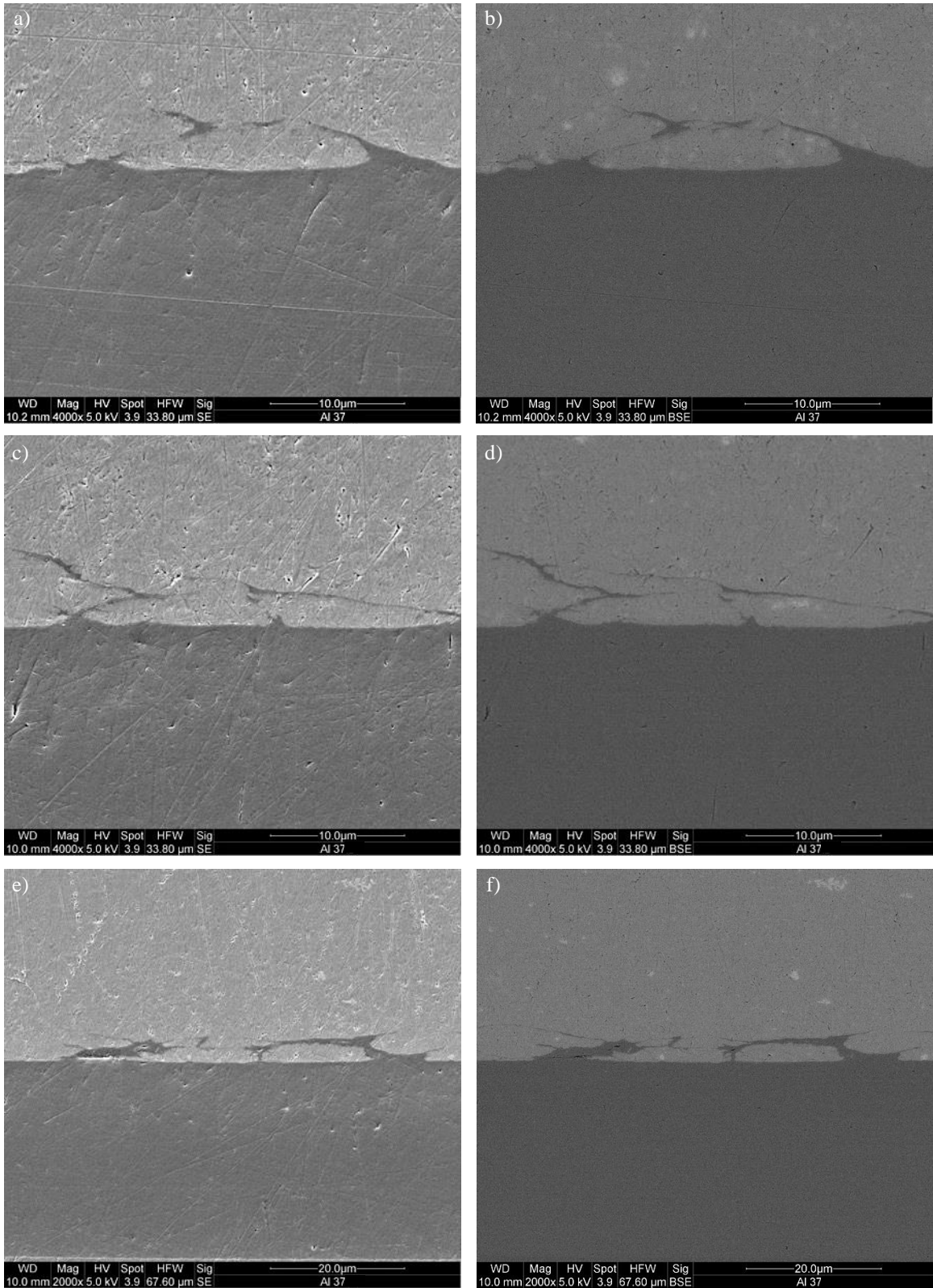


Figure 5.88. Secondary electron and associated backscattered electron SEM images of lengthwise aluminum wire cross section tested at 37 lbs normal load. Cracks propagate around and underneath shingles, detaching them and pushing them away from the bulk aluminum.

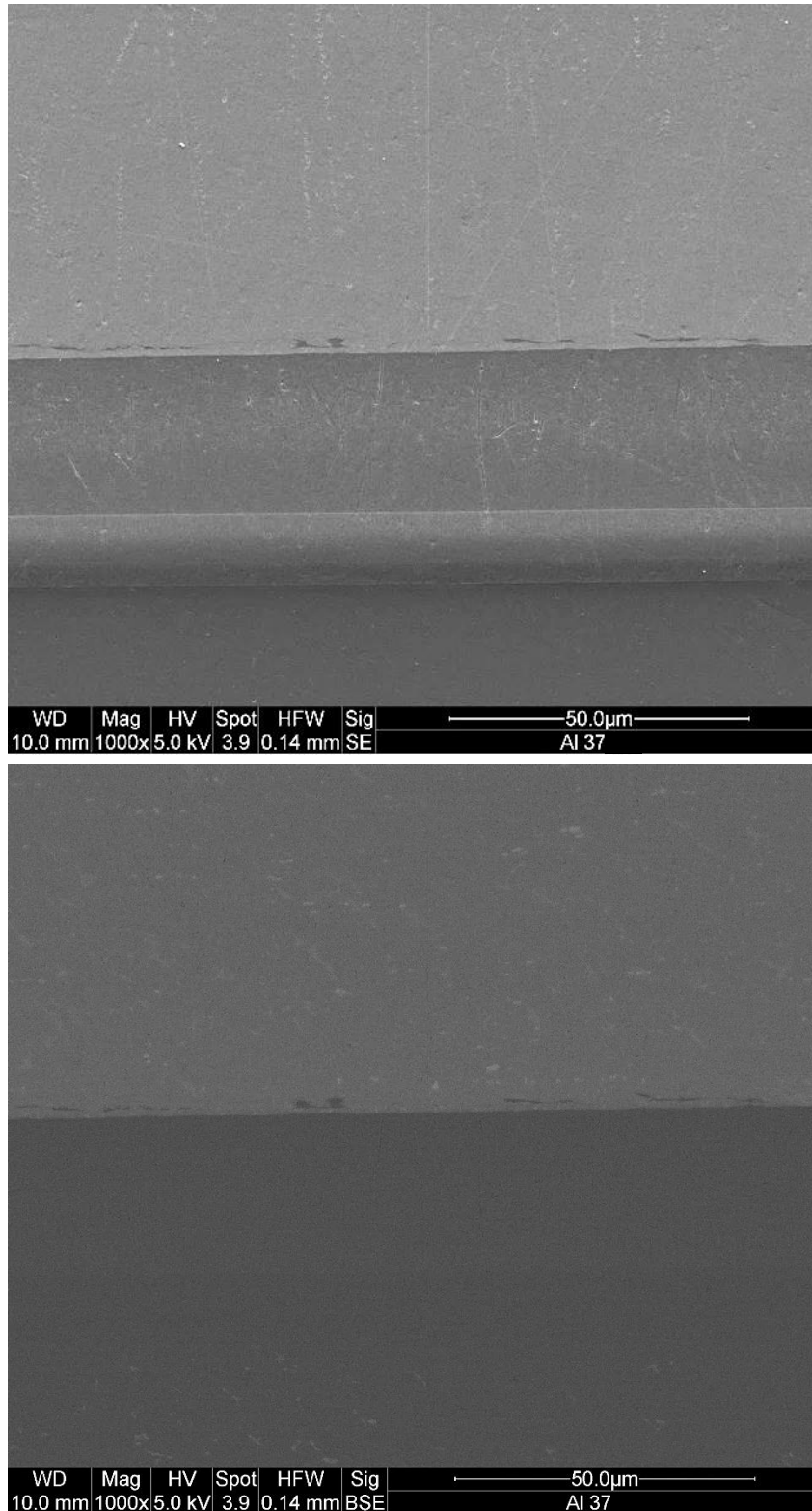


Figure 5.89. Secondary electron (top) and backscattered electron (bottom) SEM images of lengthwise aluminum wire cross section tested at 37 lbs normal load. Very long subsurface cracks suggest crack initiation and propagation at a suspected near-surface deformed layer, detaching it from the bulk aluminum. BSE images shows dark voids in subsurface cracks suggesting different elemental composition suspected to be electrical insulation.

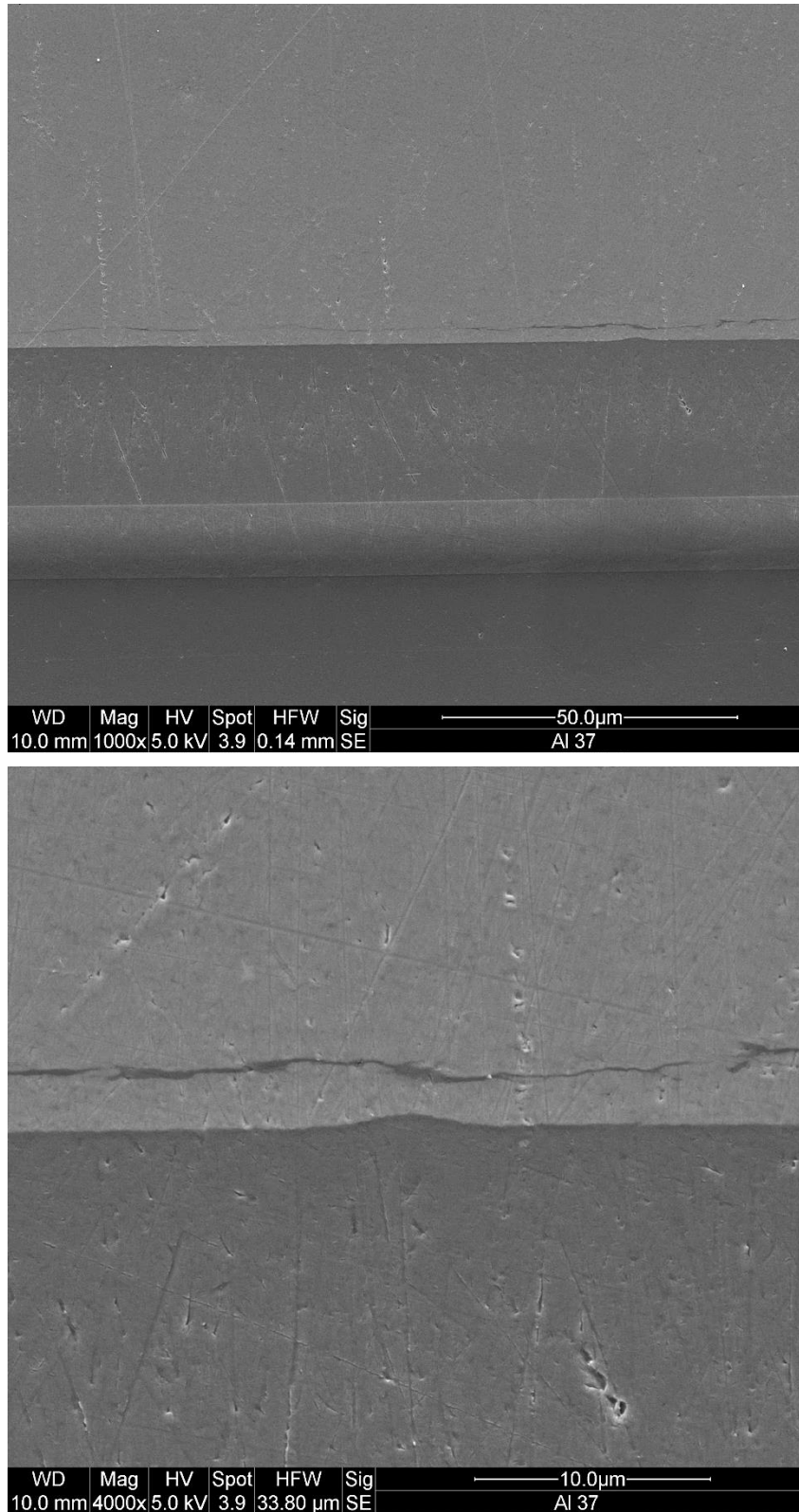


Figure 5.90. Higher magnification secondary electron SEM images of subsurface cracks in lengthwise aluminum wire cross section tested at 37 lbs normal load. Crack initiation and propagation along suspected near-surface deformed layer/bulk aluminum interface is highlighted resulting in separation of near surface layer from bulk aluminum.

To verify these subsurface cracks were filled with insulation as suspected, EDS analysis was performed on the same crack seen in Figure 5.90 with the results shown in Figure 5.91. The crack clearly shows an absence of aluminum, confirming the separation of the near surface layer from the bulk aluminum. Carbon and nitrogen match well with the crack which are both known elements in polyamide-imide electrical insulation. Further, the phase map shows the same phase as the insulation present in the crack, confirming aluminum electrical insulation present in the observed subsurface cracks and crack propagation around shingles. These EDS results can be compared to those of the suspected crack seen at the shingle/aluminum boundary for fresh aluminum in Figure 5.84. No phase change or carbon was present at this boundary. Therefore, as normal load increases, cracks initiate and grow at shingle/aluminum boundaries as well as in the suspected near-surface deformed layer with severity increasing with normal load. The viscoelastic insulation is forced into these cracks, causing further propagation and detachment of shingles and near-surface layer from the bulk aluminum. The energy associated with crack growth and insulation flow helps explain the COF behaviour observed for aluminum at higher normal loads in Figure 5.26.

Tested aluminum results are compared to the edgewise cross section of copper samples tested at 22 and 42 lbs. Surface features of the 42 lb sample are found in Figure 5.92. Compared to the observations made for fresh copper, there appears to be little to no change to the copper surface which is still smooth with minor flaws in quality being small bumps or craters that remain well bonded with the insulation. This lack of change reflects the negligible influence normal load had on COF for the copper wire samples tested.

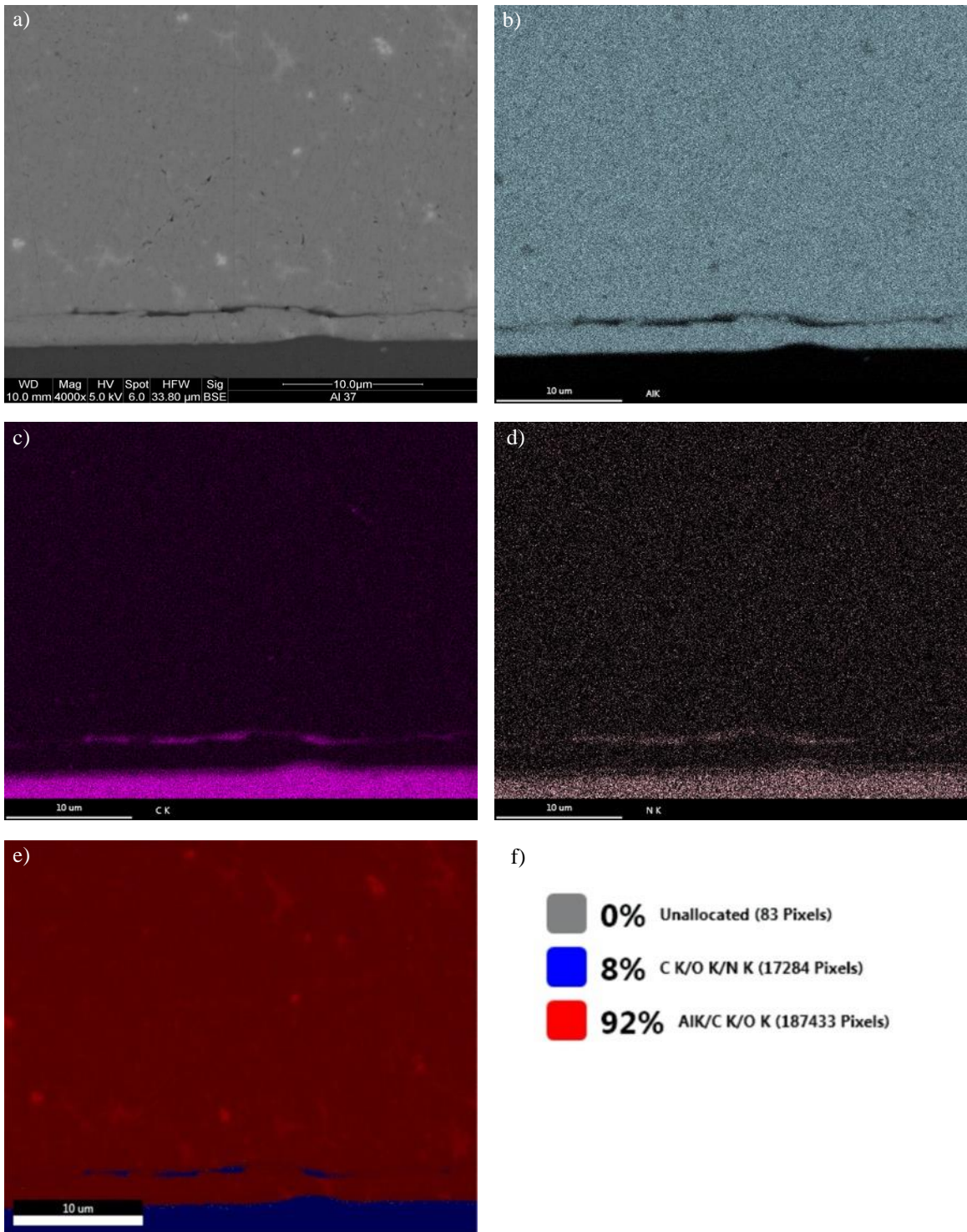


Figure 5.91. Backscattered electron SEM image of subsurface crack used for EDS mapping. Distribution of (b) aluminum, (c) carbon, (d) Nitrogen, with phase map (e) and phase composition (f). Carbon and nitrogen maps along with phase maps suggest subsurface crack is filled with electrical insulation.

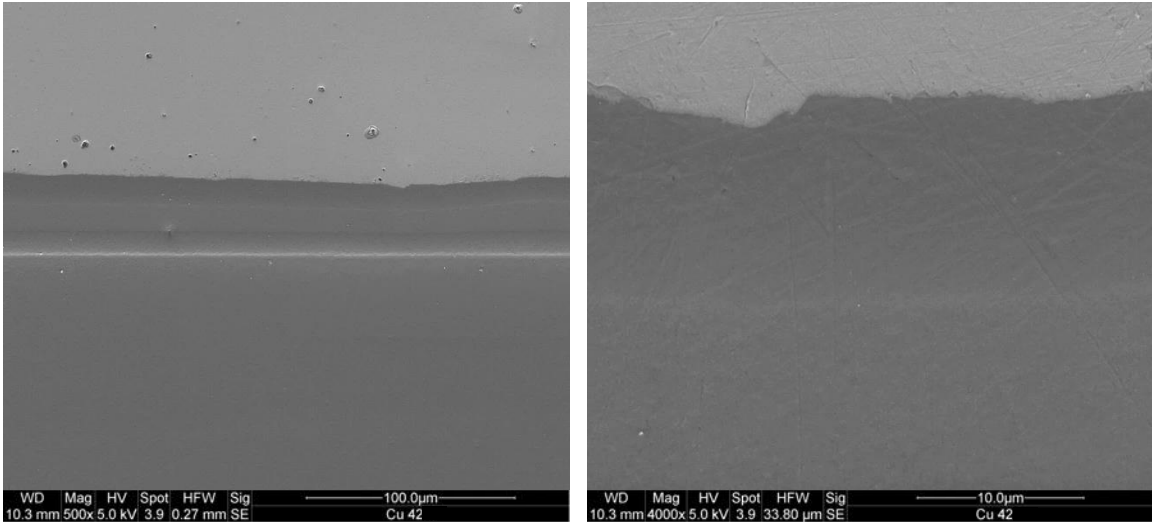


Figure 5.92. Secondary electron SEM images of edgewise copper wire cross section tested at 42 lbs normal load. Copper surface remains mostly featureless and smooth (left) with only surface defects being small bumps or craters a few microns in height and width (right).

5.4.2.1 Delamination Observation

The delamination observed in Section 5.1.2.2 was only found on wires elongated to failure. Looking at the underside of the delaminated insulation surface revealed imbedded shingles of aluminum. Observations made on the cross-sections of fresh and tested aluminum show these shingles are present from manufacturing but at 37 lbs normal load, start to become detached from the aluminum substrate due to crack propagation and insulation flow. Where these shingles start to detach, early signs of microscopic delamination were found with two examples shown in Figure 5.93. Images (a-b) highlight the formation of a void in the insulation between a detached shingle and bulk aluminum. This shingle may have already been semi-detached from manufacturing, but it is reasonable to suspect insulation flow and crack propagation from 37 lbs normal load testing caused further separation resulting in void formation. Another example in (c-d) shows two voids forming in the insulation region between neighbouring aluminum shingles. These voids could act as large scale delamination initiation zones causing reliability concerns, especially with stresses from further winding processes and motor assembly.

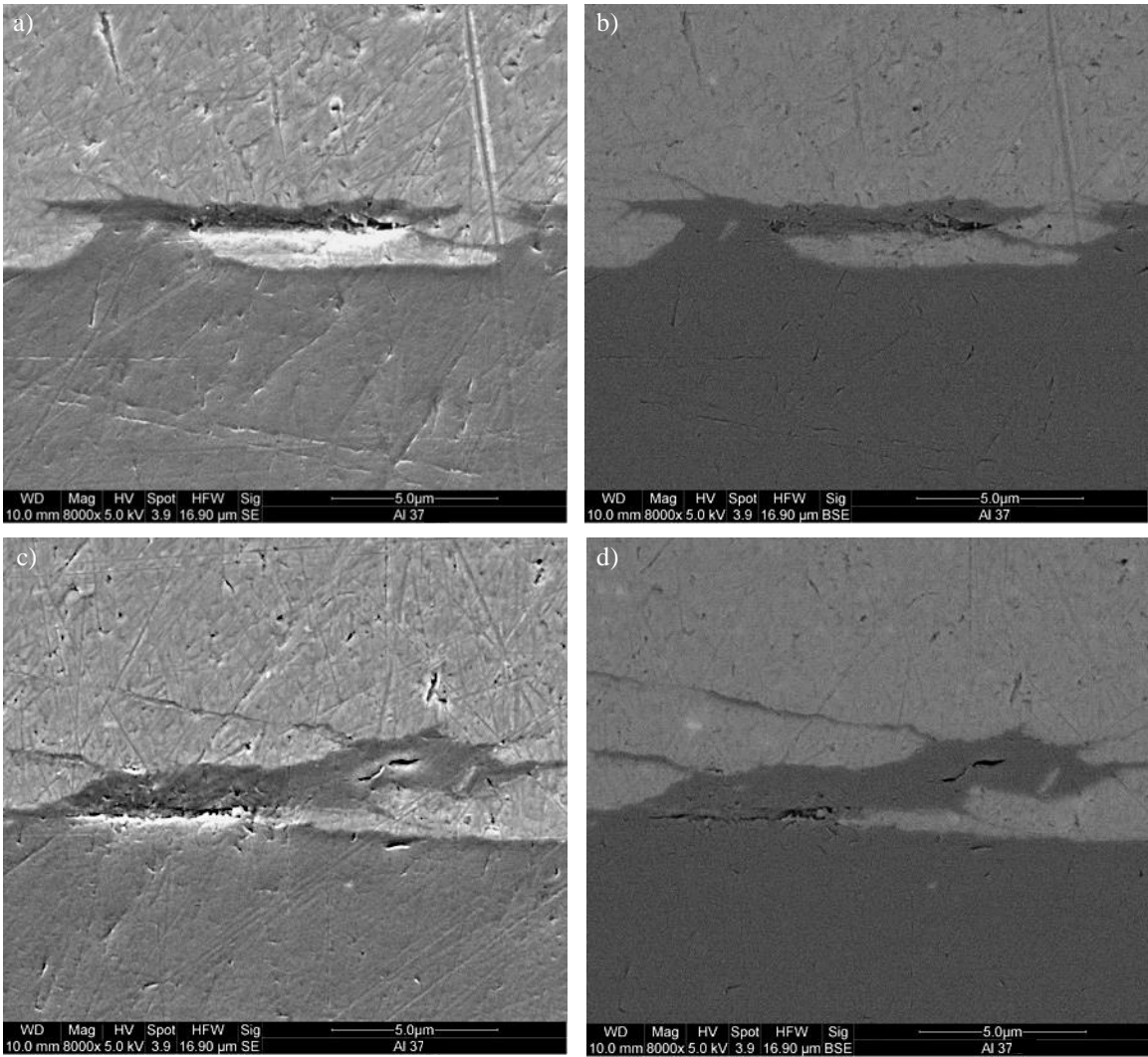


Figure 5.93. Secondary electron and associated backscattered electron SEM images of void formation in insulation surrounding and penetrating aluminum shingles from testing at 37 lbs normal load. (a-b) Void formation underneath shingle suggesting onset of delamination from bulk aluminum. (c-d) Void formation in insulation region between neighboring aluminum shingles.

There is an exception to this however, seen in Figure 5.94, where a delamination zone was found at the very end of the wire adjacent to the free end that was cut for mounting. The delamination found in this figure was only seen adjacent to the free end of the sample tested at 37 lbs, measuring 300-400 um long, and nowhere in the bulk of the wire sample. Therefore, the observed delamination was most likely caused from forces involved with cutting and mounting the sample. Although, sub-surface crack growth and separation of shingles from the aluminum surface by insulation penetration could have aided the delamination. This would explain why it was only seen on the sample tested at 37 lbs normal load where crack growth was most severe.

Figure 5.94 perfectly demonstrates insulation delamination behaviour observed on aluminum wire samples elongated to failure and explains why aluminum shingles were found imbedded in the delaminated insulation. The figure shows a large crack, originating from the free end of the mounted sample, traveling along the aluminum/insulation boundary. Image (c) highlights the crack traveling through the shingle/aluminum interfaces, separating them from the bulk conductor. The shingles remain adhered to the electrical insulation, suggesting the bond strength between insulation and aluminum shingle is stronger than that of interface between aluminum shingles and bulk aluminum. Image (e) shows a crack in the process of growing around a shingle while simultaneously fracturing the shingle/aluminum interface. Peel testing performed on all aluminum and copper wire samples from COF vs normal load testing revealed no loss of adhesion meaning this observed delamination behaviour is not representative insulation adhesion strength for these samples. However, it does raise concern for conductor reliability over its life if wire deformation greater than that analyzed in this study is experienced or electrically induced stresses are great enough to initiate delamination in formed hairpin conductors.

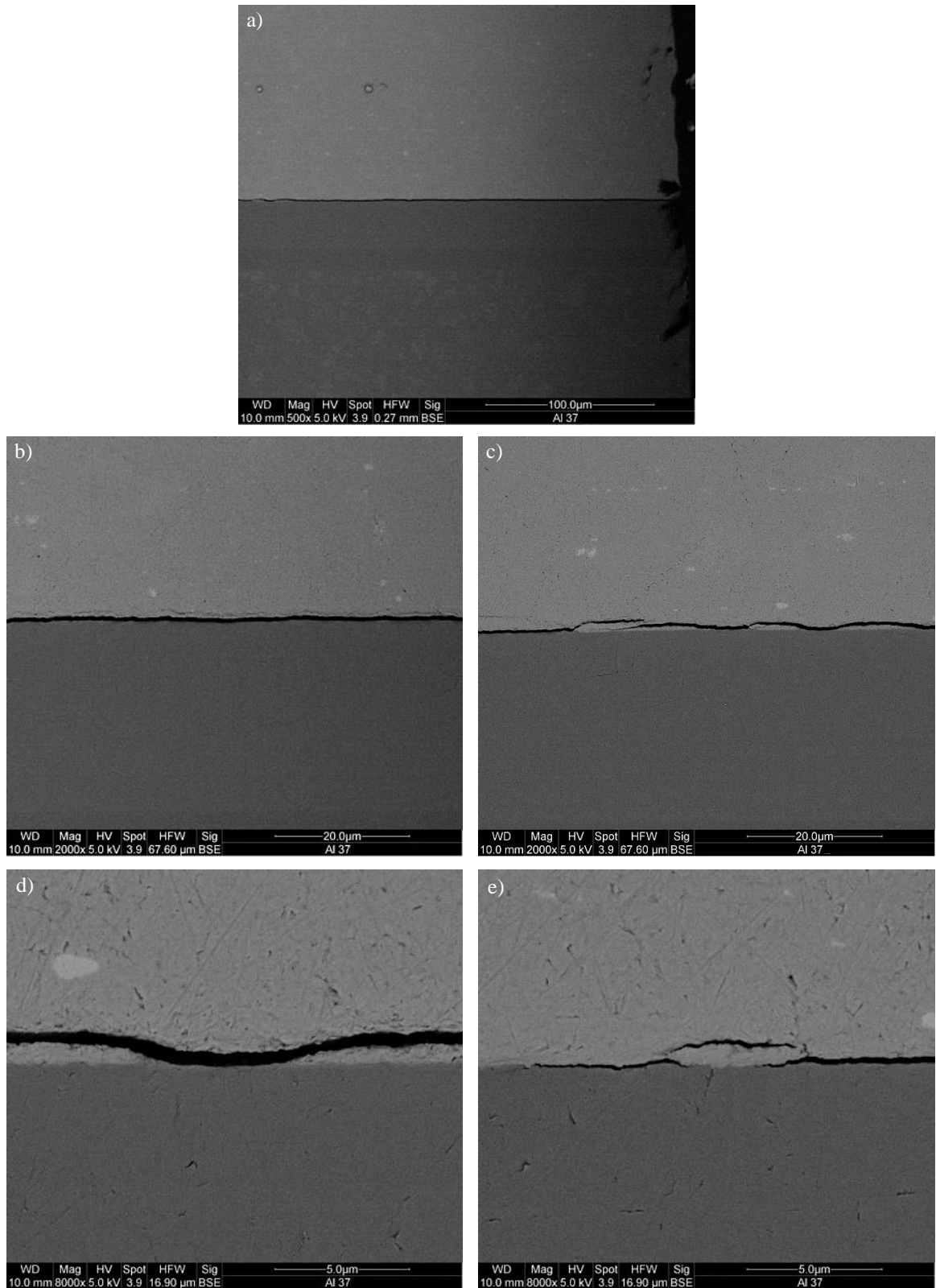


Figure 5.94. Backscattered electron SEM images of insulation delamination from bulk conductor at very edge of aluminum sample tested at 37 lbs normal load where it was sectioned from the larger wire sample. (c-e) Highlight crack propagation around aluminum shingles with some left imbedded in insulation accounting for observations made in Section 5.1.2.2.

Chapter 6

DISCUSSION

The main goal of this study was to determine the feasibility of effectively replacing copper with aluminum in manufacturing, winding and motor use. The following section discusses the results from the previous sections and how they pertain to this goal.

6.1 Formability and Windability of Aluminum and Copper

Standardized testing was conducted to characterize the formability and windability of both conductors studied according to testing outlined in ASTM D1676-17. Elongation testing results saw copper experiencing nearly twice the elongation of aluminum at 62.48% versus 32.80%. The stress versus strain curves for these samples seen in Figure 5.1 illustrate this elongation difference. It also highlights the copper curve rising sharply in the plastic region whereas the aluminum curve remains flat. This is due to aluminum having a much higher stacking fault energy than copper which means it does not cold work as easily or as much. The stacking fault energy of these conductors plays a large role in their performance during the remaining standardized tests.

With regards to elastic ratio testing, aluminum experiencing less cold work was advantageous. Copper strain hardened very quickly and saw a much higher load at 5% elongation compared to load at break resulting in a larger elastic ratio than aluminum. Since elongation up to 10% is common for high speed winding operations, the results suggest aluminum is more formable. The lower yield strength of aluminum ties in with its lower strain hardening rate, reducing the stress required for it to elongate so it can better accommodate high speed winding. This stress can remain more constant too since the aluminum curve is so flat. This means equipment used for winding aluminum does not need to be as robust and the winding forces can be reduced. Copper continuously gets stronger during elongation which requires increasing force to wind it and more robust machinery in general due to its higher yield strength.

The strength and cold working difference of the two conductors plays a role in low stress elongation testing as well. This test was designed to evaluate how well a conductor

can absorb bends and twists during winding operations by measuring their permanent deformation at low stresses. As seen in Table 5.3 and Figure 5.24, copper experienced greater permanent elongation with a LSE of 0.87% compared to 0.37% for aluminum. Knowing that copper cold works much more so than aluminum and therefore experiences almost double the elongation, these results make sense. However, low stress elongation is very sensitive to applied strain as can be seen in Figure 6.1 where LSE for copper wire decreases rapidly with only small amounts of applied strain [29]. Extrapolating from this, the softer the wire, and the softer it stays, the higher the LSE percentage [31].

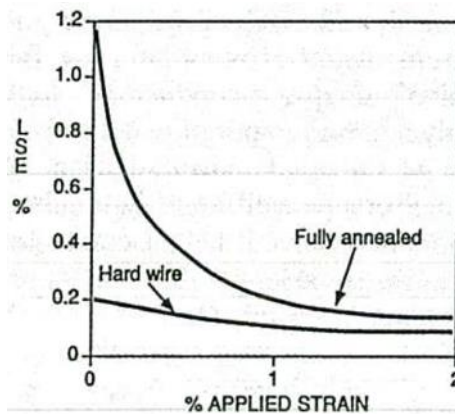


Figure 6.1. Effect of applied strain on LSE of copper wire [29].

For this reason, the higher stacking fault energy of aluminum may prove advantageous. Copper saw greater permanent elongation for samples only tested once. In practice though, during winding, a conductor may experience multiple bends and twists from the time of manufacture until it is inserted into the stator either by machine or by hand. To better account for this, the test could be run again with the same wires. Since aluminum experienced very little cold work, it would be expected to perform very similarly to the first test. Copper on the other hand, work hardened during the first test so it would be more likely to perform like the “Hard wire” in Figure 6.1 resulting in a lower LSE percentage. This could then give the advantage to aluminum allowing it to repeatedly absorb bends and twists during winding operations.

This can be further illustrated with sample Al #3 in Figure 5.24 which saw greater permanent elongation than the other two samples tested. For the low extension rates and stresses used for testing, this behaviour would occur if the aluminum wire experienced too

much plastic deformation from handling and straightening prior to testing. This is best illustrated with one test which resulted in failure due to never reaching the specified stress of 55.2 MPa. It experienced an elongation of 45 mm before it was stopped and marked as a failed test. This is compared to the less than 2 mm of elongation experienced by the successful tests. The ultimate tensile strength of aluminum ranges from 62-96.5 MPa which is very close to the specified stress used for testing. Coupled with the mild cold work experienced by the wire during handling, straightening, and mounting, along with the low extension rate of 5 mm/min, the gross elongation makes sense.

This helps corroborate the repeatability and potentially better formability of aluminum. The sample absorbed bending while being unspooled, cut and straightened, cold working mildly during the process. Its behaviour during testing was to continuously elongate, never reaching the specified stress. The limited cold working that occurred during handling and testing did not limit the elongation of the wire since the stresses used were so close to ultimate tensile strength. The greater permanent elongation then suggests it has better formability than the copper wire. This can also be disadvantageous though as more care would be required when handling the externally wound coils post winding. The copper coil would harden and become more resistant to bends and twists, maintaining the desired shape better but its stiffness would result in more springback, less compact coils, and lower slot fill factors. Aluminum would continue to absorb these bends and twists, deforming the wound coil.

The higher stacking fault energy and lower strength of aluminum tie in with its stiffness and ability to be formed into a desired shape. Springback testing evaluated this for both conductors. The results saw the insulated aluminum having 1.25° less springback than the copper wire suggesting it had greater formability and windability. In practice, this allows the aluminum wire to form more compact coils and therefore achieve higher slot fills. Tighter end turns can also be made resulting in more compact motors and less conductor material used. With the global effort to create more power dense and compact machines, this is very advantageous.

6.2 Die Forming Simulation of Aluminum and Copper

Square cross section conductors undergo die forming for shaping into hairpin style conductors. A. Demiri in [14] extensively studied how this operation affects copper wires in order to optimize operating conditions. The same investigation was performed in this study to determine the feasibility of effectively replacing copper with aluminum in this procedure. Results were presented for coefficient of friction experienced by aluminum wires tested against normal load, wire travel speed, and forming angle.

Normal load testing results seen in Figure 5.26, saw a spike in COF for aluminum supported by the 3 mm radius roller at 22 lbs followed by a sharp decrease then a slight rise up to 42 lbs normal load. Aluminum samples supported with the 24 mm radius roller did not see as drastic of a spike in COF, but it was shifted to 27-32 lbs. This was still followed by a sharp decrease but then saw another sharp increase at 42 lbs. Copper results presented in this study saw negligible increase in COF from 22 to 42 lbs which coincides with testing results at 40 and 60 lbs from [14]. The results still demonstrate a weak relationship between COF and normal load for copper but the same cannot be said for aluminum which saw drastic changes in COF as normal load increased.

Since aluminum sees a strong relationship between coefficient of friction and normal load, further analysis was required to determine an appropriate load to move forward with wire travel speed and forming angle testing. This is also required for determining an appropriate pressure to use for the actual die forming procedure should aluminum be used in place of copper. The goal was to minimize the coefficient of friction while also minimizing damage inflicted on the wire surface. Looking at Table 5.6, Table 5.7, and Figure 5.26, normal loads past 17 lbs for both support rollers were eliminated since coefficient of friction sharply rose past this point. COF did fall again around 32-37 lbs to nearly the same levels as 12 and 17 lbs but the spike experienced suggested a deformation mechanism change that could have damaged the wire, ruling out these loads as well. Looking at contact area on the steel counterfaces, 7-17 lbs generally saw the smallest contact areas although pressures experienced on the wire surface saw no specific relationship with normal load. In terms of the contact transfer itself, Figure 5.68 through Figure 5.70 illustrated mainly light scratching contact below 17 lbs with large amounts of material transfer experienced above this. Analyzing the wire surfaces in Section 5.3.3 saw

little variation in damage severity with increasing normal load. Combining all these observations together suggests an appropriate normal load to use for further testing and the actual die forming procedure is in the range of 12-17 lbs to minimize COF and mitigate wire damage. For these reasons, 12 lbs normal load was chosen for travel speed and forming angle testing.

COF versus wire travel speed testing was only performed on aluminum wires in this study with results compared to those for copper from [14]. Aluminum results in Figure 5.47 saw a general increase in COF as wire travel speed increased. Copper results from [14] also saw a general increase in COF as travel speed increased. This means both wires are experiencing similar behaviour and is beneficial for the aluminum versus copper debate since no modification would be required regarding die forming speed to substitute copper with aluminum.

However, aluminum did not see the same advantages with forming angle testing. Average COF versus forming angle plotted in Figure 5.56 shows an increasing trend as angle increases for the 24 mm radius roller. From 10° to 60° for the 3 mm radius roller there was an increasing trend as well but the 30° samples did see decreased COF. Copper results from [14] saw the opposite trend with decreasing COF as forming angle or surface strain increased. Like normal load testing, aluminum is experiencing a deformation mechanism that copper is not, resulting in differing coefficient of friction behaviour for the die forming procedure.

Combining the results from the suite of testing shows aluminum magnet wire cannot simply replace copper in the die forming process. Extra care needs to be taken regarding appropriate normal loads and contact pressures to minimize COF and mitigate excessive damage to the insulation. Copper on the other hand appeared largely unaffected by normal load with regards to coefficient of friction and wire damage giving it more flexibility during die forming. Hairpin style conductors made with this die forming process typically see very large forming angles which also poses a problem for aluminum wires. The increase in COF with increasing forming angle and surface strain needs to be addressed in order to optimize the forming process. Copper sees an advantage here as well as COF decreased with forming angle which would help mitigate damage sustained by the wire.

6.3 Aluminum Insulation Performance

Involved with determining the feasibility of replacing copper with aluminum is looking at the performance of the conductor during the suite of testing performed in this study. Delamination and adherence issues for aluminum magnet wire were discovered during standardized formability and windability testing where copper saw no problems. During wire bending simulation, potential deformation mechanism changes for aluminum were observed at higher normal loads where copper was largely unaffected. The following sections explore the performance of aluminum wire to help explain this behaviour.

6.3.1 Aluminum Insulation Flexibility

Elongation testing the aluminum magnet wire revealed issues with the properties of the insulation used. Figure 5.3 illustrated fracturing of the insulation prior to wire failure as well as shrinkage away from the fracture end. Figure 5.4 explored this in more detail revealing a long tube of delaminated insulation which indicates the aluminum insulation has flexibility issues and does not elongate at the same rate or to the same extent as aluminum. Conversely, the copper insulation remained adhered to the wire right up to the fracture end.

The delaminated tube of insulation was explored further to help explain the flexibility and delamination issues experienced. Sliding the tube back onto the conductor, it was found that it would not go past its initiation point, where the bubble is highlighted in the red circle in Figure 5.4. This means the cross section of the insulation tube reduced during elongation and is smaller than the cross section of the wire past this initiation point. It can then be inferred that the delamination zone is the size of the aluminum necking region. The insulation cross section reduced slightly to accommodate the aluminum cross section reduction, but it was not flexible enough to remain adhered to the conductor.

This suggests aluminum film insulation delamination is closely related to wire cross section reduction during elongation. Film adherence testing results presented in Section 5.1.2.1 further illustrate this. They saw a decrease in insulation adhesion with increased elongation. Adhesion reduced enough on the 15% sample to allow complete removal of the insulation with moderate effort. Past 15% elongation, minimal effort was required to

peel the insulation off the conductor. This then suggests that the wire cross section reduced enough above 10% elongation to surpass the insulation flexibility limit where it could no longer accommodate the area reduction of the aluminum wire. Considering wires typically see up to 10% elongation during winding [53], [54] this could be problematic for long term reliability of the square cross section aluminum wires analyzed in this study. If delamination were to initiate from elongation beyond 10% during manufacture and winding, or from electrical forces during machine operation, premature failure of the insulation could occur, resulting in short circuit conditions.

Aluminum insulation flexibility issues were also revealed in Section 5.1.1.5 where the insulated aluminum elongated to failure saw reduced orange peel texturing compared to the copper wire and bare aluminum wire also elongated to failure. The evolution of texture change on bare aluminum elongated to failure is illustrated in Figure 5.8 and Figure 5.9. The insulated aluminum elongated to failure in Figure 5.10 clearly shows a marked reduction in texture change. Both wires were strained to the same level with the only difference being the film insulation. This suggests that the insulation is partially inhabiting the texture change since it does not deform at the same rate as aluminum.

The incompatibility of aluminum insulation properties with EC aluminum are also seen in how the insulation fails. Section 5.1.2.3 compared the damage experienced on both insulated aluminum and copper conductors during elongation to failure. The most common form of failure to occur was very tiny pinholes or splits in the insulation. However, comparing the gross forms of insulation fracture further illustrates the flexibility and adherence issues with aluminum insulation. A. Demiri observed some large scale insulation fracture in [14], reviewed in Figure 5.2 in this study. The break in insulation revealed a lot of underlying conductor but all the insulation around the fracture appeared well adhered to the wire. In this study, copper experienced larger splits instead, as seen in Figure 5.22 (b-c), with the surrounding insulation also remaining adhered to the conductor. Comparing to aluminum insulation fracture in Figure 5.23 (b-c), it consists of large splits in the insulation with the surrounding area delaminated from the wire. Although no insulation failure was experienced for all wires tested in film adherence testing, the inflexibility and adherence issue of aluminum insulation can lead to more gross fracturing of the insulation.

6.3.2 Aluminum Insulation Adherence

Aluminum insulation flexibility issues relate closely with its adherence and in turn the surface quality of the aluminum wire. At elongation levels greater than 10%, it was found that insulation adhesion decreased to the point where it could be completely removed from the conductor. The underside of the tube of delaminated insulation, elongated wire surface and aluminum/insulation interface were all analyzed to help explain this. Section 5.1.2.2 investigated the insulation and elongated wire surfaces revealing pieces of aluminum imbedded in the underside of the insulation in Figure 5.16 and Figure 5.17. These pieces of aluminum were removed from the wire surface upon delamination.

Cross-sectional analysis of a fresh piece of aluminum in Figure 5.83 and Figure 5.84 highlighted shingles present on the aluminum surface but separated from the bulk aluminum by a layer of aluminum oxide. Aluminum shingles being present on the underside of the delaminated insulation suggests the bond strength between the shingles and base aluminum is weaker than the bond strength between the shingles and insulation. Fracturing and delamination of a near-surface deformed layer as depicted in Figure 3.8 could also result in aluminum present on the underside of the delaminated insulation. This is further corroborated by the delamination observations in Figure 5.94 where the insulation separates from the wire surface by cutting through these shingle/aluminum interfaces. Compared to the copper cross section in Figure 5.85, its surface was very smooth and coherent with no shingles present. Therefore, aluminum shingles appear to be a critical factor in insulation adherence since they are the key difference between aluminum and copper surface quality.

A thin layer of aluminum oxide present at the aluminum/insulation interface may also contribute to adhesion issues. It is well known that aluminum oxide forms nearly instantaneously when exposed to air. EDS analysis of the aluminum/insulation interface in Figure 5.84 sees higher concentrations of oxygen present than in the rest of the cross section. This suggests a very fine layer of aluminum oxide could be present at the boundary which may be affecting the chemical bonding of the insulation to the aluminum.

This also suggests that aluminum and copper insulation may in fact behave similarly but the poor surface quality of aluminum hinders the performance of its insulation. Chemical bonding may be affected from aluminum oxide and the mechanical

bond strength is degraded by the presence of aluminum shingles. During elongation, the shingles may start to detach from the bulk aluminum due to weak bonding at the shingle/aluminum interface. A near-surface deformed layer could also explain this behaviour since it is less ductile than the bulk aluminum and is a favorable location for crack propagation resulting in aluminum flake delamination. The insulation bonded to these shingles and surface layer would then start to lose adhesion with the bulk metal and fail to deform at the same rate as the aluminum wire ultimately leading to the flexibility and delamination issues observed. Poor surface quality in general as seen in Section 3.2 can cause insulation adhesion issues which would explain why copper did not suffer the same adhesion loss due to its good surface quality presented in Figure 5.85 and Figure 5.92.

6.3.3 Aluminum Insulation Long Term Performance

Square magnet wires undergo die forming to be shaped into hairpin style conductors for insertion into the motor stator. The forces experienced on the wire during this operation differ from those for conventional machine or hand wound conductors. During elongation aluminum saw adherence issues past 10% which could be problematic for the long-term performance of the wire during motor operation. Mechanical and electrical forces along with high temperatures during use combined with the observed adherence issues are something that needs to be considered when attempting to replace copper with aluminum.

During wire bending simulation, aluminum experienced a spike in COF at higher normal loads and elevated COF with increased forming angle which could pose problems with the longevity of the wire during operation. The previous section discussed shingles present on the aluminum surface which contribute to loss of adhesion for wires during elongation. Section 5.4.2 revealed that these shingles also pose problems for wires undergoing die forming. Samples tested at 12 lbs normal load saw no change from the fresh sample. However, at 27 lbs normal load, around where the spike in COF occurred, crack propagation and subsurface cracks were observed as seen in Figure 5.86. This deformation at the aluminum/insulation interface coupled with greater contact and material transfer experienced on the steel counterface help explain the rise in COF at this normal load.

At 37 lbs, this behaviour is amplified. Figure 5.87 though Figure 5.91 show more aggressive crack propagation and greater levels of sub surface cracking. Shingles were completely enveloped with insulation, detaching them from the aluminum surface while the insulation penetrated deeper into the bulk aluminum. Large subsurface cracks were also forming in absence of obvious shingles creating large sections of aluminum detached from the bulk wire. The cause of these very long cracks could be explained by the fracturing and delamination of a near-surface deformed layer from the bulk aluminum due to its much lower ductility. Wire surface contact and damage remained similar to samples tested at peak COF but the gross deformation occurring at the aluminum/insulation boundary decreased overall resistance to deformation and in turn decreased the experienced COF. This further confirms a deformation mechanism change did take place at peak and subsequent fall of COF explaining the behaviour observed in Figure 5.26.

This deformation behaviour of the aluminum surface could lead to longevity issues of the wire during motor operation. The detached shingles and near-surface layer of aluminum at high normal loads were enveloped with insulation which could see them act like sliver defects described in Section 3.2. The conductive aluminum now detached from the bulk wire, residing in the insulation could cause current leakage or sites for dielectric or continuity failure [6], [29]. This is especially important to consider for high frequency applications where current is concentrated on the surface of the conductor. These thin layers of insulation now residing between shingles and bulk wire could also cause adhesion issues. No bulk delamination was observed from testing or during the peel tests, but voids did start to appear in the sections of insulation between shingles and bulk wire.

Cross-sections of wires that underwent forming angle testing were not analyzed but they did experience a rise in COF where copper saw a decrease. It could then be assumed they are experiencing similar deformation behaviour to normal load testing wire samples. The normal load was 12 lbs for forming angle testing, but strain was induced into the wire surfaces due to increased forming angle. Combining deformation behaviour observed for elongation samples and normal load samples would then suggest large forming angles could cause longevity issues for aluminum wire as well.

Chapter 7

SUMMARY AND CONCLUSIONS

This study looked at the feasibility of replacing copper with aluminum magnet wires, specifically for use in high performance automotive scale electric motors. An extensive literature review on aluminum versus copper conductors covering more than 100 years of research was performed to effectively compare the advantages and disadvantages of replacing copper with aluminum. This review serves to create a unified source of all things aluminum versus copper for future research to draw on and advance the aluminum versus copper debate. A two-part formability and windability study on square cross section aluminum and copper magnet wires was also conducted. The first part characterized formability and windability for both conductors according to ASTM D1676. The second part used a novel wire bending simulator machine, which simulates the die forming procedure utilized in hairpin conductor formation, to compare formability and windability of both wires. The highlights of these results are presented below.

- Aluminum is a viable alternative to copper that has successfully been used in various applications for decades and can already provide significant cost and weight savings in electric machines with similar performance to copper. With further optimization of aluminum windings in high performance electric machines, especially those used for high frequency operation, the slight efficiency loss compared to copper could be eliminated making it a very attractive electrical conductor.
- Aluminum saw windability and formability advantages over copper. This was especially true for wire springback where aluminum saw 1.25° less springback than copper which allows for lower tensions during winding, formation of more compact coils that more efficiently utilize available space, and shorter end turns for lower losses, less waste heat production and more compact and cheaper motors.
- The higher stacking fault energy and lower strain hardening rate of aluminum offer general advantages to manufacturing, winding time and cost, and wire formability and windability. The lower elastic ratio of aluminum compared to copper allows it to better accommodate elongation during winding at high speeds. Copper saw higher low stress

elongation due to its greater cold workability but with repeated bends and twists during winding, aluminum would be more advantageous allowing for repeated absorption of the deformation with minimal cold working experienced.

- Insulation adherence and delamination issues occurred for aluminum wires with elongation greater than 10%. The suspected causes for this behaviour were poor aluminum surface quality and incompatibility of insulation elongation properties with those of aluminum. Further improvement of square cross section aluminum conductor surface quality as well as its electrical insulation properties is required to avoid these issues.
- Conductor surface analysis revealed aluminum experienced greater contact with forming equipment and therefore sustained more damage due to its low strength and softness. It was also found that rough, and poor-quality forming surface caused significantly more damage to the wire insulation making it particularly important to use polished die surfaces to form aluminum hairpin conductors.
- Microscopic cross-sectional analysis highlighted the deformation mechanism change aluminum experienced at higher normal loads and associated peak COF that copper did not. Aluminum shingle/bulk aluminum interfaces as well as a suspected near-surface deformed layer acted as favorable locations for crack initiation and propagation. The viscoelastic insulation under high normal load was forced into these cracks, causing further propagation and separation of shingles and the near-surface layer from the bulk aluminum by a layer of insulation material. This behaviour is not conducive to die forming square cross section aluminum conductors or their long-term reliability.
- To successfully use aluminum for hairpin conductors, the die forming process should be modified to accommodate its mechanical properties and deformation behaviour. Its lower yield strength required reducing tension during die forming simulation to 80 lbs compared to 200 lbs used for copper. To minimize COF and mitigate insulation and near-surface layer damage during die forming, an appropriate normal load for the procedure was established to be 12-17 lbs. This results in a forming pressure of around 50 MPa or less for aluminum compared to up to 500 MPa used for copper.

7.1 Suggestions for Future Research

This study characterized the formability and windability of square cross section aluminum and copper magnet wires according to standardized testing as well as die forming simulation. Adhesion and delamination issues were found for aluminum conductors as well as poor surface quality which resulted in subsurface crack propagation and surface layer detachment during wire forming at high normal loads. This section suggests future research to remedy these issues and expand upon the results presented.

- For equivalent conductivity, EC aluminum requires a 62% increase to cross-sectional area, but formability testing done in this study looked at equivalent sized aluminum and copper conductors. A larger aluminum wire would perform differently in some standardized tests as well as wire bending simulation. Therefore, it would be advantageous to compare formability and windability of equivalent conductivity conductors to get a clear understanding of real-world performance differences.
- The peel test used in this study was qualitative, not quantitative. Future work may wish to quantify adhesion strength to determine the precise level of elongation an aluminum wire can sustain before adhesion drops below an acceptable level for reliable use.
- General surface quality improvements are required for square cross section aluminum wire. In situ anodizing or plasma spray technology could be analyzed for their ability to create a uniform, high quality surface to improve adhesion with insulation and performance during die forming operations. Techniques to equalize material properties between the suspected near-surface deformed layer and bulk aluminum would also help mitigate deformation of this layer during high normal load die forming to reduce experienced COF and improve long term reliability.
- This near-surface deformed layer is known to form on cold and hot rolled aluminum and has a different microstructure and mechanical properties than the bulk aluminum. This layer was suspected to be present on square cross section samples analyzed in this study. Confirmation of its presence as well as determination of its presence on conventional round conductors could be advantageous for better understanding of deformation behaviour observed in this study.

- Separation of aluminum shingles and the near-surface layer from the bulk conductor by a layer of electrical insulation material may have negative effects of wire dielectric performance. It would be beneficial to study the impact this deformation has on dielectric properties, especially for high frequency operation, to better understand long term reliability of aluminum hairpin conductors.
- A solution for poor insulation performance on square cross section aluminum wires would be to explore the feasibility of anodized electrically insulative coatings. Aluminum hairpin conductors could be anodized post die forming to mitigate formability issues with the brittle coating while providing an extremely thin, abrasion resistant, and high temperature electrical insulation.

REFERENCES

- [1] IPCC 2014, *Climate Change 2014: Mitigation of Climate Change. Contribution of Working Group III to the Fifth Assessment Report of the Intergovernmental Panel on Climate Change*, O. Edenhofer, R. Pichs-Madruga, Y. Sokona, E. Farahani, S. Kadner, K. Seyboth, A. Adler, I. Baum, S. Brunner, P. Eickemeier, B. Kriemann, J. Savolainen, S. Schlömer and C. von Stechow, Eds., Cambridge, United Kingdom, and New York: Cambridge University Press, 2014.
- [2] BloombergNEF, *Electric Vehicle Outlook 2020: Executive Summary*, [Online]. Available: <https://bnef.turtil.co/story/evo-2020/?teaser=yes>. [Accessed 7 Aug. 2020].
- [3] L. Pryor, R. Schlobohm and B. Brownell, "A Comparison of Aluminum vs. Copper as Used in Electrical Equipment," GE Consumer and Industrial, 2008.
- [4] R. M. Valdes-Flores, "The use of Production Functions to Model Copper-Aluminum Substitution in the Electrical Conductor Industry," Ph.D. Thesis, Dept. of Mineral Economics., Penn State Univ., Pennsylvania, 1984.
- [5] D. Altenpohl and H. Witzig, "Aluminum Magnet Wire and Aluminum Foil Windings in Small Motors," in *10th Electrical Insulation Conference*, Chicago, USA, 1971. pp. 279-282.
- [6] H. Pops, "The Role of the Conductor in the Manufacture and Performance of Magnet Wire," *IEEE Electrical Insulation Magazine*, vol. 11, no. 5, pp. 17-23, Sept./Oct. 1995.
- [7] H. Pops, "Technology of Electrical Conductor Wires," *Technical Paper - Society of Manufacturing Engineers*, vol. 98, no. 347, pp. X1-18, 1998.
- [8] Commerce Department, National Institute of Standards and Technology (NIST), *Circular of the Bureau of Standards: Copper Wire Tables*, 3 ed., vol. 31, Washington Government Printing Office, 1914.
- [9] J. D. Widmer, C. M. Spargo, G. J. Atkinson and B. C. Mecrow, "Solar Plane Propulsion Motors With Precompressed Aluminum Stator Windings," *IEEE Transactions on Energy Conversion*, vol. 29, no. 3, pp. 681-688, Sept. 2014.
- [10] A. G. Craig, Jr., "Aluminum Alloys for Motor Windings," in *10th Electrical Insulation Conference*, Chicago, USA, 1971. pp. 49-53.
- [11] C. R. Sullivan, "Aluminum Windings and Other Strategies for High Frequency Magnetics Design in an Era of High Copper and Energy Costs," *IEEE Transactions on Power Electronics*, vol. 23, no. 4, pp. 2044-2051, Jul. 2008.
- [12] R. Yanniello, "Aluminum - The Other Conductor," Eaton Electrical Inc., Pennsylvania, USA, 2006.

- [13] R. Yanniello, P. Pollak and J. Rooks, "Technical and Economic Considerations of Aluminum Conductors," in *Conference Record of 2007 Annual Pulp and Paper Industry Technical Conference*, Williamsburg. pp. 63-67.
- [14] A. Demiri, "Enamel Insulated Copper Wire in Electric Motors: Sliding Behavior and Possible Damage Mechanisms During Die Bending," M.S. Thesis, Dept. of Mech. Auto. and Mats. Eng., Univ. of Windsor, Windsor, ON, 2014.
- [15] H. Pops, "Processing of Wire from Antiquity to Future," *Wire Journal International*, vol. 41, no. 6, pp. 58-66, Jun. 2008.
- [16] "The Electrical Conductivity of Aluminum," *Scientific American*, vol. 74, no. 17, p. 261, Apr. 1896.
- [17] "Aluminum vs. Copper for Electrical Conductors," *The Street Railway Review*, vol. 9, pp. 157-158, 1899.
- [18] "Aluminum vs. Copper Conductors," *Machinery*, vol. 17, p. 460, February 1911.
- [19] E. H. Chia and E. A. Starke, Jr., "Application of Subgrain Control to Aluminum Wire Products," *Metallurgical Transactions A*, vol. 8, no. 6, pp. 825-832, June 1977.
- [20] E. W. Tipton, "Experiences With the Use of Aluminum in Windings for Dry-Type Power Transformers," *Transactions of the American Institute of Electrical Engineers. Part III: Power Apparatus and Systems*, vol. 74, no. 3, pp. 1201-1204, Dec. 1955.
- [21] "Why Rock Island Uses Aluminum Wire for Dispatcher's Circuit," *Railway Signaling and Communications*, vol. 50, pp. 23-25, May 1957.
- [22] "Aluminum Strips Reduce Size of Transformer Windings," *Electrical Engineering*, vol. 74, no. 11, pp. 1024-1025, Nov. 1955.
- [23] N. Simon, "Copper vs. Aluminum Windings in Motors," *Air Conditioning, Heating & Refrigeration News*, vol. 212, no. 4, p. 26, 22 Jan. 2001.
- [24] Aluminum Association, *Aluminum Electrical Conductor Handbook*, 3 ed., L. Kirkpatrick, Ed., Washington, D.C.: Aluminum Association, 1989.
- [25] B. N. Bose, "Aluminum Foil for Electrical Windings," in *Symposium on Metallurgy of Substitute Ferrous & Non-Ferrous Alloys*, NML, Jamshedpur, 1966. pp. 205-209.
- [26] J. W. Dold, "Improved Aluminum Magnet Wires for Power & Distribution Transformers," in *10th Electrical Insulation Conference*, Chicago, USA, 1971. pp. 239-242.
- [27] J. H. Walker, "Aluminum Windings for Hydroelectric Generators: A Critical Analysis," *Proc. of IEE*, vol. 114, no. 10, pp. 1464-1470, Oct. 1967.

- [28] J. Olivares-Galván, F. de León, P. Georgilakis and R. Escarela-Pérez, "Selection of Copper Against Aluminium Windings for Distribution Transformers," *IET Electric Power Applications*, vol. 4, no. 6, pp. 474-485, Jul. 2010.
- [29] H. Pops, "Importance of the Conductor and Control of its Properties for Magnet Wire Application," *Wire Journal International*, vol. 26, no. 4, pp. 66-72, Apr. 1993.
- [30] X. Cui, Y. Wu, H. Cui, G. Zhang, B. Zhou and X. Liu, "The Improvement of Boron Treatment Efficiency and Electrical Conductivity of AA1070Al Achieved by Trace Ti Assistant," *Journal of Alloys and Compounds*, vol. 735, pp. 62-67, Feb. 2018.
- [31] H. Pops, "Factors Affecting the Annealing Behaviour of Aluminum Wire," *Wire Journal*, vol. 13, no. 2, pp. 72-76, Feb. 1980.
- [32] ASM International, "Properties of Wrought Aluminum and Aluminum Alloys," in *ASM Handbook, Volume 2: Properties and Selection: Nonferrous Alloys and Special-Purpose Materials, Specific Metals and Alloys*, ASM International, 1990, pp. 62-122.
- [33] M. A. Peralta, "High Conductivity Copper," *IEEE Potentials*, vol. 13, no. 5, pp. 39-41, Dec./Jan. 1994/1995.
- [34] *Historical Copper Prices and Price Chart*, [Online]. Available: <http://www.infomine.com/investment/metal-prices/copper/all/>. [Accessed 13 Jul. 2020].
- [35] *Historical Aluminum Prices and Price Chart*, [Online]. Available: <http://www.infomine.com/investment/metal-prices/aluminum/all/>. [Accessed 13 Jul. 2020].
- [36] B. Karlsson and J.-O. Järred, "Recycling of Electrical Motors by Automatic Disassembly," *Measurement Science and Technology*, vol. 11, no. 4, pp. 350-357, Apr. 2000.
- [37] ASM International, "Properties of Wrought Copper and Copper Alloys," in *ASM Handbook, Volume 2: Properties and Selection: Nonferrous Alloys and Special-Purpose Materials, Specific Metals and Alloys*, ASM International, 1990, pp. 265-345.
- [38] Essex Group Inc., "Magnet Wire / Winding Wire Engineering Data Handbook," 2009.
- [39] G. E. Dieter, *Mechanical Metallurgy*, McGraw Hill, 1986.
- [40] R. W. Hertzberg, *Deformation and Fracture Mechanics of Engineering Materials*, 4 ed., John Wiley & Sons, Inc., 1996.

- [41] L. J. Payette, "The Properties of a Universal Magnet Wire Enamel," *IEEE Electrical Insulation Magazine*, vol. 2, no. 5, pp. 40-43, Sept. 1986.
- [42] J. H. Thomas and J. F. Dexter, "Effect of Wire Metal on the Thermal Life of Enameled Magnet Wire," *Transactions of the American Institute of Electrical Engineers. Part III: Power Apparatus Systems*, vol. 76, no. 3, pp. 1009-1013, Apr. 1957.
- [43] J. W. Shearer, "Physical Stress Effects on Aluminum Magnet Wire," in *9th Electrical Insulation Conference*, Boston, USA, 1969. pp. 257-260.
- [44] S. Yasufuku, N. Okubo and H. Soejima, "Heat-Resistant Enameled Aluminum Alloy Magnet Wire," in *10th Electrical Insulation Conference*, Chicago, USA, 1971. pp. 262-266.
- [45] E. A. Goodman, "Magnet Wire Aluminum Alloy Conductors and Coil Winding," in *13th Electrical/Electronics Insulation Conference*, Chicago, USA, 1977. pp. 382-385.
- [46] A. Rassõlkin, A. Kallaste, S. Orlova, L. Gevorkov, T. Vaimann and A. Belahcen, "Re-Use and Recycling of Different Electrical Machines," *Latvian Journal of Physics and Technical Sciences*, vol. 55, no. 4, pp. 13-23, Aug. 2018.
- [47] A. Rassõlkin, A. Belahcen, A. Kallaste, T. Vaimann, D. V. Lukichev, S. Orlova, H. Heidari, B. Asad and J. P. Acedo, "Life Cycle Analysis of Electrical Motor-Drive System Based on Electrical Machine Type," *Proceedings of the Estonian Academy of Sciences*, vol. 69, no. 2, pp. 162-177, May 2020.
- [48] M. Alatalo, S. T. Lundmark and E. A. Grunditz, "Electric Machine Design for Traction Applications Considering Recycling Aspects - Review and New Solution," in *IECON 2011 - 37th Annual Conference of the IEEE Industrial Electronics Society*, Melbourne, Australia, 2011. pp. 1836-1841.
- [49] A. Allanore, "Electrochemical Engineering for Commodity Metals Extraction," *Electrochemical Society Interface*, vol. 26, no. 2, pp. 63-68, Summer 2017.
- [50] W. Bao, L. Lin, D. Song, H. Guo, L. Chen, L. Sun, M. Liu and J. Chen, "Comparative Study on Life Cycle Environmental Impact Assessment of Copper and Aluminum Cables," *IOP Conference Series: Earth and Environmental Science*, vol. 94, no. 1, p. 012166, Nov. 2017.
- [51] S. Kosh and H. Antrekowitsch, "Aluminum Alloys for Wire Harnesses in Automotive Engineering," *BHM Berg- und Hüttenmännische Monatshefte*, vol. 152, pp. 62-67, Mar. 2007.
- [52] J. Pyrhönen, J. Montonen, P. Lindh, J. Vauterin and M. J. Otto, "Replacing Copper with New Carbon Nanomaterials in Electrical Machine Windings," *International Review of Electrical Engineering, IREE*, vol. 10, no. 1, pp. 12-21, Feb. 2015.

- [53] T. J. Murray, "Poly(amide-imides): Wire Enamels with Excellent Thermal and Chemical Properties," *Macromolecular Materials and Engineering*, vol. 293, no. 5, pp. 350-360, May 2008.
- [54] M. G. Minnick, "The Effect of Winding Stresses on the Pulse Endurance of Corona Resistant Magnet Wire," in *Conference Record of the 2004 IEEE International Symposium on Electrical Insulation*, Indianapolis, USA. pp. 169-173.
- [55] J. L. Spears, "Reliability Testing of Aluminum Magnet Wire Connections for Hermetic Motors," in *11th Electrical Insulation Conference*, Chicago, USA, 1973. pp. 95-98.
- [56] R. Wrobel, D. Salt, N. Simpson and P. H. Mellor, "Comparative Study of Copper and Aluminium Conductors - Future Cost Effective PM Machines," in *7th IET International Conference on Power Electronics, Machines and Drives, PEMD 2014*, Manchester, UK. pp. 1-6.
- [57] J. D. Widmer, R. Martin and B. C. Mecrow, "Precompressed and Stranded Aluminum Motor Windings for Traction Motors," *IEEE Transactions on Industry Applications*, vol. 52, no. 3, pp. 2215-2223, May/Jun. 2016.
- [58] M. Kimiabeigi and J. D. Widmer, "On Winding Design of a High Performance Ferrite Motor for Traction Application," in *2016 XXII International Conference on Electrical Machines, ICEM*, Lausanne, Switzerland. pp. 1949-1956.
- [59] S. Ayat, R. Wrobel, J. Baker and D. Drury, "A Comparative Study Between Aluminium and Copper Windings for a Modular-Wound IPM Electric Machine," in *2017 IEEE International Electric Machines and Drives Conference, IEMDC*, Miami, USA, 2017. pp. 1-8.
- [60] S. Ayat, H. Liu, M. Kulan and R. Wrobel, "Estimation of Equivalent Thermal Conductivity for Electrical Windings with High Conductor Fill Factor," in *2018 IEEE Energy Conversion Congress and Exposition, ECCE*, Portland, USA, 2018. pp. 6529-6536.
- [61] D. Roger, V. Isov and S. Babicz, "Voltage Distribution in Inorganic Insulation Windings for High-Temperature Motors," *COMPEL - The International Journal for Computation and Mathematics in Electrical and Electronic Engineering*, vol. 35, no. 6, pp. 2074-2086, Nov. 2016.
- [62] G. W. Klein, "Mechanical Connections for Copper and Aluminum Magnet Wires in Hermetic Motors," in *10th Electrical Insulation Conference*, Chicago, USA, 1971. pp. 53-55.
- [63] M. Braunović, "Fretting in Ni-Coated Aluminum Conductors," *IEEE Transactions on Components, Hybrids, and Manufacturing Technology*, vol. 14, no. 2, pp. 327-336, June 1991.

- [64] J. P. Gourber and C. Wyss, "Anodized Aluminum Strip Excitation Coils for the Prototype LEP Quadrupole and Sextupole Magnets," *IEEE Transactions on Magnetics*, vol. 17, no. 5, pp. 1868-1871, Sept. 1981.
- [65] C. Araki and T. Taguchi, "Thermal Degradation of Polyesterimide Magnet Wire," in *Proc. of the IEEE Conference on Electrical Insulation and Dielectric Phenomena, CEIDP '93*, Pocono Manor, PA, USA, 1993. pp. 526-531.
- [66] W. G. Hamm and K. C. Heckeler, "Thermal Endurance Test for Insulating Varnishes," in *9th Electrical Insulation Conference*, Boston, USA, 1969. pp. 124-126.
- [67] E. A. Mol, "Windability and Performance Testing of Magnet Wire and NEMA MW-1000," in *6th Electrical/Electrical Insulation Conference*, Chicago, USA, 1983. pp. 114-118.
- [68] M. Popescu, J. Goss, D. A. Staton, D. Hawkins, Y. C. Chong and A. Boglietti, "Electrical Vehicles-Practical Solutions for Power Traction Motor Systems," *IEEE Transactions on Industry Applications*, vol. 54, no. 3, pp. 2751-2762, May/Jun. 2018.
- [69] W. R. Finley and M. M. Hodowanec, "Selection of Copper versus Aluminum Rotors for Induction Motors," *IEEE Transactions on Industry Applications*, vol. 37, no. 6, pp. 1563-1573, Nov./Dec. 2001.
- [70] R. L. Nailen, "Is There a Future for Cast Copper Rotors," *Electrical Apparatus*, vol. 54, no. 11, pp. 34-35, Nov. 2001.
- [71] A. M. Gazdac, S. C. Martis, A. M. Mabwe and K. Biro, "Analysis of Material Influence on the Performance of the Dual-Rotor Permanent Magnet Induction Machine," in *2012 13th International Conference on Optimization of Electrical and Electronic Equipment, OPTIM*, Brasov, Romania. pp. 453-459.
- [72] R. L. Nailen, "Developments in Cast Copper Rotors," *Electrical Apparatus*, vol. 72, no. 7, pp. 36-41, Jul. 2019.
- [73] S. Babicz, S. A.-A. Djennad and G. Vélú, "Preliminary Study of using Anodized Aluminum Strip for Electrical Motor Windings," in *2014 IEEE Conference on Electrical Insulation and Dielectric Phenomena, CEIDP*, Des Moines, USA. pp. 176-179.
- [74] S. Babicz, S. Ait-Amar and G. Vélú, "Evaluation of the Boron Oxide Healing Performance in the Case of Anodized Aluminum Strip Coils," in *2016 IEEE International Conference on Dielectrics, ICD*, Montpellier, France, 2016. pp. 983-986.
- [75] S. Babicz, S. Ati-Amar, G. Vélú, A. Cavallini and P. Mancinelli, "Behavior of Anodized Aluminum Strip under Sine and Square Wave Voltage," *IEEE Transactions on Dielectrics and Electrical Insulation*, vol. 24, no. 1, pp. 39-46, Feb. 2017.

- [76] S. Babicz, S. Ait-Amar and G. Vélú, "Temperature and Humidity Dependence of Anodized Aluminum Strip," in *2016 IEEE International Conference on Dielectrics, ICD*, Montpellier, France, 2016. pp. 979-982.
- [77] *Copper-clad aluminum wire*, [Online]. Available: https://en.wikipedia.org/wiki/Copper-clad_aluminium_wire. [Accessed 21 Jul. 2020].
- [78] ELEKTRISOLA Enamelled Copper Wire, *Copper Clad Aluminum - CCA10%*, [Online]. Available: <https://www.elektrisola.com/conductor-materials/aluminum-copper-clad-aluminum/cca10.html>. [Accessed 13 Jul. 2020].
- [79] MWS Wire Industries, Inc., *Copper Clad Aluminum*, [Online]. Available: <https://mwswire.com/copper-clad-aluminum/>. [Accessed 20 Jul. 2020].
- [80] V. Rallabandi, N. Taran, D. M. Ionel and J. F. Eastham, "Coreless Multidisc Axial Flux PM Machine with Carbon Nanotube Windings," *IEEE Transactions on Magnetics*, vol. 53, no. 6, p. 8102904, Jun. 2017.
- [81] W. Li, D. Li, Q. Fu and C. Pan, "Conductive Enhancement of Copper/Graphene Composites Based on High-Quality Graphene," *RSC Advances*, vol. 5, no. 98, pp. 80428-80433, Sept. 2015.
- [82] M. Li, H. Gao, J. Liang, S. Gu, W. You, D. Shu, J. Wang and B. Sun, "Microstructure Evolution and Properties of Graphene Nanoplatelets Reinforced Aluminum Matrix Composites," *Materials Characterization*, vol. 140, pp. 172-178, Jun. 2018.
- [83] J. Tokutomi, T. Uemura, S. Sugiyama, J. Shiomi and J. Yanagimoto, "Hot Extrusion to Manufacture the Metal Matrix Composite of Carbon Nanotube and Aluminum with Excellent Electrical Conductivities and Mechanical Properties," *CIRP Annals - Manufacturing Technology*, vol. 64, no. 1, pp. 257-260, 2015.
- [84] L. Lu, Y. Shen, X. Chen, L. Qian and K. Lu, "Ultrahigh Strength and High Electrical Conductivity in Copper," *Science*, vol. 304, no. 5669, pp. 422-426, Apr. 2004.
- [85] S. Karabay, "Modification of AA-6201 Alloy for Manufacturing of High Conductivity and Extra High Conductivity Wires with Property of High Tensile Stress after Artificial Aging Heat Treatment for All-Aluminum Alloy Conductors," *Materials and Design*, vol. 27, no. 10, pp. 821-832, 2006.
- [86] J. P. Hou, R. Li, Q. Wang, H. Y. Yu, Z. J. Zhang, Q. Y. Chen, H. Ma, X. M. Wu, X. W. Li and Z. F. Zhang, "Breaking the Trade-Off Relation of Strength and Electrical Conductivity in Pure Al Wire by Controlling Texture and Grain Boundary," *Journal of Alloys and Compounds*, vol. 769, pp. 96-109, Nov. 2018.
- [87] W. W. Wareham, "Magnet Wire for 600 C Temperature Transformers," *Transactions of the American Institute of Electrical Engineers, Part I: Communication and Electronics*, vol. 78, no. 1, pp. 66-70, Mar. 1959.

- [88] L. Del Ferraro and F. G. Capponi, "Aluminum Multi-Wire for High-Frequency Electric Machines," in *2007 IEEE Industry Applications Annual Meeting*, New Orleans, USA. pp. 89-93.
- [89] P. Melendez-Vega and G. Venkataramanan, "Aluminum Foil Coils for Human Scale Wind Turbines," in *2012 IEEE Global Humanitarian Technology Conference*, Seattle, USA. pp. 1-5.
- [90] L. Reißweber, A. Stadler, J. v. Lidenfels and J. Franke, "Improved Thermal Behavior of an Electromagnetic Linear Actuator with Different Winding Types and the Influence on the Complex Impedance," in *2019 9th International Electric Drives Production Conference, EDPC*, Esslingen, Germany. pp. 1-6.
- [91] M. A. Green, "Use of Aluminum Coils Instead of Copper Coils in Accelerator Magnet Systems," *IEEE Transactions on Nuclear Science*, vol. 14, no. 3, pp. 398-404, Jun. 1967.
- [92] P. Paul, M. Sacotte and F. Walter, "Large Aluminium Distribution Transformer," in *2012 1st International Conference on Power and Energy in NERIST, ICPEN*, Nirjuli, India, 2012. pp. 1-5.
- [93] N. S. Beniwal, H. O. Gupta and D. K. Dwivedi, "Effect of Creep on Failure of Distribution Transformers: An Experimental Evaluation," *International Journal of Performability Engineering*, vol. 6, no. 2, pp. 171-179, Mar. 2010.
- [94] N. S. Beniwal, D. K. Dwivedi and H. O. Gupta, "Creep Life Assessment of Distribution Transformers," *Engineering Failure Analysis*, vol. 17, no. 5, pp. 1077-1085, Jul. 2010.
- [95] J. C. Olivares-Galvan, R. Escarela-Perez, S. Maximov, S. Magdaleno-Adame and P. S. Georgilakis, "Cost Reduction by Interchanging the Location of the Windings in Distribution Transformers with HV Copper Winding and LV Aluminum Winding," *International Transactions on Electrical Energy Systems*, vol. 25, no. 11, pp. 2685-2695, Nov. 2015.
- [96] G. Volpe, M. Popescu, I. Foley and J. Goss, "Winding Material Effect on High Speed Brushless Permanent Magnet Machines," in *2019 IEEE Energy Conversion Congress and Exposition, ECCE*, Baltimore, USA. pp. 3144-3149.
- [97] M. Kimiabeigi, J. D. Widmer, R. S. Sheridan, A. Walton and R. Harris, "Design of High Performance Traction Motors Using Cheaper Grade of Materials," in *8th IET International Conference on Power Electronics, Machines and Drives, PEMD 2016*, Glasgow, UK. pp. 1-7.
- [98] H. Dhulipati, S. Mukundan, L. Chauvin, C. Riczu, A. Edrissy, M. Kozdras, J. Bauman, S. Habibi, J. Tjong and N. C. Kar, "Investigation of Aluminium and Copper Wound PMSM for Direct-drive Electric Vehicle Application," *IOP Conference Series: Materials Science and Engineering*, vol. 654, no. 1, p. 012002, Oct. 2019.

- [99] S. Mukundan, H. Dhulipati, L. Chauvin, B. D. S. Guruwatta Vidanalage, A. Edrisky, J. Tjong and N. C. Kar, "Comparative Performance Analysis of Copper and Aluminum Wound Fractional-Slot PMSMs for High-Speed Traction Application," in *2019 22nd International Conference on Electrical Machines and Systems, ICEMS*, Harbin, China, 2019. pp. 1-6.
- [100] S. Ullah, M. Kimiabeigi, B. Scholes, A. Steven, R. Wrobel, W. Davis and J. Widmer, "Optimisation of Permanent Magnet Machine Topologies Suitable for Solar Powered Aircraft," in *2018 XIII International Conference on Electrical Machines, ICEM*, Alexandroupoli, Greece. pp. 332-338.
- [101] P.-W. Han, Y.-D. Chun, J.-h. Choi, M.-J. Kim, D.-H. Koo and J. Lee, "The Study to Substitute Aluminum for Copper as a Winding Material in Induction Machine," in *31st International Telecommunications Energy Conference, INTELEC 2009*, Incheon, South Korea. pp. 1-3.
- [102] M. Ayaz, "Design and Cost Analysis of Permanent Magnet Synchronous Motor with Aluminum Winding for Gearless Elevator Systems," *Düzce Üniversitesi Bilim ve Teknoloji Dergisi*, vol. 7, no. 1, pp. 115-123, Jan. 2019.
- [103] M. M. Islam, M. N. Islam and M. A. Taleb, "Replacing Copper Winding to Aluminium Winding of Refrigerator Compressor Motor for Cost Saving and Performance Analysis Using ANSYS Electronics Desktop," in *2019 4th International Conference on Electrical Information and Communication Technology, EICT*, Khulna, Bangladesh. pp. 1-5.
- [104] M. Iorgulescu, "Study of Single Phase Induction Motor with Aluminium Versus Copper Stator Winding," in *2016 International Conference on Applied and Theoretical Electricity, ICATE*, Craiova, Romania, 2016. p. RS 5.5.
- [105] D. Choi, T.-J. Kang, S. B. Lee, J. Kim and J. Kim, "Stator Insulation Testing for Appliance Motors with Aluminum Windings: Applying Solutions to Root Causes of Failure," *IEEE Industry Applications Magazine*, vol. 24, no. 6, pp. 14-24, Nov./Dec. 2018.
- [106] R. Wrobel, N. Simpson, P. H. Mellor, J. Goss and D. A. Staton, "Design of a Brushless PM Starter Generator for Low-Cost Manufacture and High-Aspect-Ratio Mechanical Space Envelope," *IEEE Transactions on Industry Applications*, vol. 53, no. 2, pp. 1038-1048, Mar./Apr. 2017.
- [107] J.-H. Choi, Y.-D. Chun, P.-W. Han, M.-J. Kim, D.-H. Koo, J. Lee and J.-S. Chun, "Design of High Power Permanent Magnet Motor with Segment Rectangular Copper Wire and Closed Slot Opening on Electric Vehicles*," *IEEE Transactions on Magnetics*, vol. 46, no. 9, pp. 3701-3704, Spet. 2010.
- [108] N. Bianchi and G. Berardi, "Analytical Approach to Design Hairpin Windings in High Performance Electric Vehicle Motors," in *2018 IEEE Energy Conversion Congress and Exposition, ECCE*, Portland, USA. pp. 4398-4405.

- [109] Remy Electric Motors, "Inside the HVH Hybrid Motor," Remy International Inc., 2009.
- [110] K. Rahman, M. Anwar, S. Schulz, E. Kaiser, P. Turnbull, S. Glaeson, B. Given and M. Grimmer, "The Voltec 4ET50 Electric Drive System," *SAE International Journal of Engines*, vol. 4, no. 1, pp. 323-337, Apr. 2011.
- [111] *Chevrolet Showcases Spark EV Electric Motor*, 26 10 2011. [Online]. Available: https://media.gm.com/media/us/en/gm/news.detail.html/content/Pages/news/us/en/2011/Oct/1026_spark_elec_mtr.html. [Accessed 7 Aug. 2020].
- [112] X. Fan, D. Li, R. Qu, C. Wang and J. Li, "Hybrid Rectangular Bar Wave Windings to Minimize Winding Losses of Permanent Magnet Machines for EV/HEVs over a Driving Cycle," in *2018 IEEE International Magnetics Conference. INTERMAG*, Singapore, Singapore. pp. 1-2.
- [113] S. Jurkovic, K. Rahman, B. Bae, N. Patel and P. Savagian, "Next Generation Chevy Volt Electric Machines; Design, Optimization and Control for Performance and Rare-Earth Mitigation," in *2015 IEEE Energy Conversion Congress and Exposition, ECCE*, Montreal, Canada. pp. 5219-5226.
- [114] J. Fleischer, S. Haag and J. Hofmann, "Quo Vadis Winding Technology?," Institute of Production Science (wbk), Karlsruhe Institute of Technology (KIT), 2017.
- [115] J. Hagedorn, F. Sell-Le Blanc and J. Fleischer, Eds., *Handbook of Coil Winding, Technologies for efficient electrical wound products and their automated production*, Springer Vieweg, 2018.
- [116] A. Kuehl, A. Riedel, A. Vogel, S. Hartl, T. Glaessel, M. Masuch and J. Franke, "Robot-based Production of Electric Motors with Hairpin Winding Technology," in *2019 World Congress on Engineering and Computer Science, WCECS 2019*, San Francisco, USA. pp. 257-262.
- [117] A. Riedel, M. Masuch, M. Weigelt, T. Gläbel, A. Kühl, S. Reinstein and J. Franke, "Challenges of the Hairpin Technology for Production Techniques," in *2018 21st International Conference on Electrical Machines and Systems, ICEMS*, Jeju, South Korea. pp. 2471-2476.
- [118] M. Weigelt, A. Riedel, M. Masuch, A. Mahr, T. Gläbel and J. Franke, "Potentials of an Explicit Finite Element Analysis of the Bending Processes for Coated Copper Wires," in *2017 7th International Electric Drives Production Conference, EDPC*, Würzburg, Germany. pp. 1-5.
- [119] T. Glaessel, D. B. Pinhal, M. Masuch, D. Gerling and J. Franke, "Manufacturing Influences on the Motor Performance of Traction Drives with Hairpin Winding," in *2019 9th International Electric Drives Production Conference, EDPC*, Esslingen, Germany. pp. 1-8.

- [120] BMW Group Corporate Communications, *BMW Group Prototype Production E-Drivetrains: Scene 1 of 6: E-Drive Component*, [Online]. Available: <https://www.press.bmwgroup.com/global/tv-footage/detail/PF0005720/bmw-group-prototype-production-e-drivetrains/5>. [Accessed 25 Jun. 2020].
- [121] R. Obika, Y. Tatematsu, M. Mesaki and A. Higashiura, "Development of Magnet Wire Having Excellent Windability," in *Proc. of the Electrical Insulation Conference and Electrical Manufacturing and Coil Winding Conference*, Cincinnati, USA, 1999. pp. 479-483.
- [122] J. A. Whitney and R. B. Duke, "Why Test Magnet Wire?," in *Proc. of the Electrical Insulation Conference and Electrical Manufacturing and Coil Winding Conference*, Cincinnati, USA, 2001. pp. 281-283.
- [123] B. Moharana and B. K. Kushwaha, "Breakage Analysis of Aluminum Wire Rod in Drawing Operation," *International Research Journal of Engineering and Technology*, IRJET, vol. 4, no. 12, pp. 971-981, Dec. 2017.
- [124] B. J. Briscoe, "Isolated Contact Stress Deformations of Polymers: The Basis for Interpreting Polymer Tribology," *Tribology International*, vol. 31, no. 1-3, pp. 121-126, Jan. 1998.
- [125] X. Zhou, Y. Liu, G. E. Thompson, G. M. Scamans, P. Skeldon and J. A. Hunter, "Near-Surface Deformed Layers on Rolled Aluminum Alloys," *Metallurgical and Materials Transactions A: Physical Metallurgy and Materials Science*, vol. 42, no. 5, pp. 1373-1385, May 2011.
- [126] J. Wang, X. Zhou, G. E. Thompson, J. A. Hunter and Y. Yuan, "Delamination of Near-Surface Layer on Cold Rolled AlFeSi Alloy During Sheet Forming," *Materials Characterization*, vol. 99, pp. 109-117, Jan. 2015.
- [127] Y. Liu, M. F. Frolich, W. M. Rainforth, X. Zhou, G. E. Thompson, G. M. Scamans and J. A. Hunter, "Evolution of Near-Surface Deformed Layers During Hot Rolling of AA3104 Aluminum Alloy," *Surface and Interface Analysis*, vol. 42, no. 4, pp. 180-184, Apr. 2010.
- [128] *Standard Test Methods for Film-Insulated Magnet Wire*, ASTM D1676-17, 2017.
- [129] M. S. Gadd, "Tensile Testing Clamp". United States of America Patent 3,528,283, 15 Sept. 1970.

VITAAUCTORIS

NAME: Lucas Chauvin

PLACE OF BIRTH: Windsor, ON

YEAR OF BIRTH: 1994

EDUCATION: Kingsville District High School
Kingsville, ON,
2008-2013

Bachelor of Applied Science
Honours Mechanical Engineering-Materials Option
University of Windsor,
Windsor, ON,
2013-2017

Master of Applied Science
Engineering Materials
University of Windsor,
Windsor, ON,
2018-2020